



University of
Stavanger

FACULTY OF SCIENCE AND TECHNOLOGY

MASTER'S THESIS

Study program/specialization: Petroleum Geosciences Engineering	Spring semester, 2018 Open
Author: Emilie Aasen Kavli (signature of author)
Programme coordinator: Nestor Cardozo Supervisor: Dr. rer. nat. Udo Zimmermann	
Title of master's thesis: Characterization of Nannofacies in Upper Cretaceous Chalks used in IOR Research	
Credits: 30	
Keywords: Chalk Increased Oil Recovery, IOR Enhanced Oil Recovery, EOR Nannofacies Calcareous Nannofossils Micropaleontology Biostratigraphy Optical Light Microscope Field Emission Gun Scanning Electron Microscope, FEG-SEM	Number of pages: + supplemental material/other: Stavanger, date/year

Copyright

by

Emilie Aasen Kavli

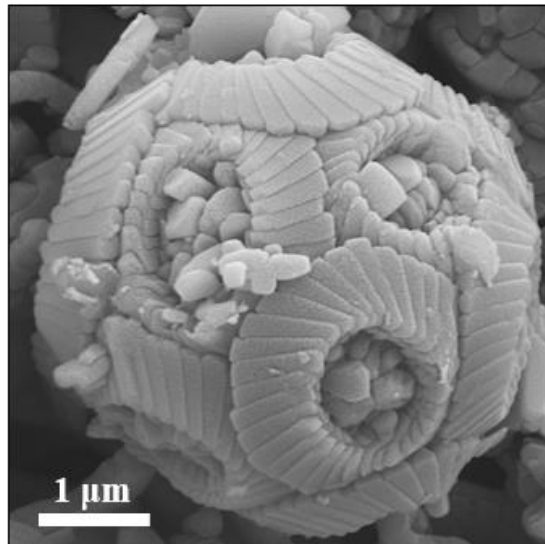
2018

Master's Thesis

Characterization of Nannofacies in Upper Cretaceous Chalks used in IOR Research

By

Emilie Aasen Kavli



MSc Thesis

Petroleum Geosciences Engineering
The Faculty of Science and Technology
The University of Stavanger
Norway

The University of Stavanger

July 2018

Acknowledgement

I would like to thank my supervisor Dr. Udo Zimmermann, for letting me write this thesis on a subject of my interest. Thank you for your help and guidance, as well as reviewing my thesis and giving valuable feedback along the way. Thank you for encouraging and supporting discussions throughout this thesis.

Dr. Zimmermann arranged contact with the University of Milan (UNIMI). A great thank you to professor Elisabetta Erba at the UNIMI, who welcomed me so warmly to Milan and took her time introducing me to the field of micropaleontology. Thank you for your assistance and for letting me use UNIMI's laboratories and equipment. I would also like to thank Dr. Cinzia Bottini for help and guidance with biostratigraphic work and for her patience with me in the microscope. *Grazie mille* to Matteo and Christian for preparing my samples, and to Carla and Francesco for our discussions. It was truly a pleasure to stay in Milan.

In need of acknowledgement is also Mona Wettrhus Minde. Thank you for giving me your time, opinions and availability, and for assisting me with the Scanning Electron Microscope. As well, Emanuela I. Kallestén - thank you for letting me borrow your samples, and for being available when I had questions.

I would like to recognize the National IOR Centre of Norway for their financial support to this thesis.

A big thanks to colleagues and friends at the University of Stavanger. A special *merci beaucoup* to A for surviving with me during this thesis and for all your support.

Finally, I wish to thank my family. Thank you for putting that first dinosaur movie on the TV when I was only a few years old, and for all the prehistoric books you read to me. It led me to write this master's thesis. I am lucky to have a personal motivation for this thesis, as I feel a thrill of excitement every time I put a new sample under the microscope. When I realized that micropaleontology not only opens the door to a whole new (microscopic) world, but also to a world of research in so many important disciplines; petroleum, deep-ocean drilling, oceanography and climate change – I was sold. I hope my joy for my work shines through this thesis, and that it can be a contribution to the world of research.

Abstract

The aim of this thesis is to contribute to enhanced oil recovery (EOR) research by characterizing nanofacies in chalk samples used in increased oil recovery (IOR) flooding experiments with a $MgCl_2$ brine at reservoir conditions. The objectives were achieved by combining optical light microscopy (OLM) with field emission gun scanning electron microscopy (FEG-SEM). The studied samples are of Cretaceous age and from onshore Denmark, Belgium and USA, as well as an offshore section from the Tor field in the North Sea. Five flooded equivalents of the onshore samples were analysed to determine how the nanofacies are both influenced by flooding and controlling it.

Calcareous nanofossil biostratigraphic analyses of the samples proved that some of the presumed ages were improper and in need of adjustments, especially the sample from Stevns Klint. General age data from open pit quarries might not be accurate and can be a pitfall when using onshore chinks as analogues to real reservoir chinks in EOR research. The samples displayed different calcareous nanofossil preservations and assemblages. The preservation level typically decreased one to two levels at the inlet position (closest to injection) after flooding. During flooding, certain species proved to be dissolution-resistant and others dissolution-susceptible. However, the assemblage composition could not predict MgO wt% after flooding. What might be able to predict it is total calculated nanofossil abundance from random settling smear slides, as well as estimated nanofossil versus micarbs ratios. Higher nanofossil abundance and lower micarb content in the original unflooded core yielded higher MgO wt% after flooding. More data is needed to verify this correlation. Results suggest that estimates of nanofossil versus micarb ratios from random settling smear slides trended to be 10-15% higher than estimates from the FEG-SEM. This might indicate that micarbs get dissolved during the random settling technique and hence, this technique might alter the sample - which should be taken into consideration when using this methodology.

The samples contained various paleoecological index nanofossils (indices). Paleoecological indices from all onshore samples except Aalborg point towards warmer waters with lower nutrient levels. In addition, evidence of the K/T extinction event might be observable in the offshore section. By combining changes in species diversity, nanofossil abundance and assemblage composition – it could be possible to indicate if the onshore samples have been sampled horizontally or vertically through the stratigraphy.

The methodologies and results described in this thesis proved to be of importance for the chalk characterization and might even to some extent be used to predict how chalk samples will react to IOR flooding experiments. These applied calcareous nanofossil methodologies should not be neglected but be included in future EOR research. This thesis' work should be continued in the future, to further improve the methodologies and gain additional data to strengthen the results.

Table of Contents

Acknowledgement.....	i
Abstract	ii
Table of Contents	iii
List of Figures	vi
List of Tables.....	ix
List of Appendices	x
List of Commonly Used Abbreviations	x
1. Introduction	1
1.1. Motivation for the Thesis	1
1.2. Structure and Objectives of the Thesis	1
2. Theoretical Background	4
2.1. Chalk.....	4
2.1.1. Introduction	4
2.1.2. Classification.....	5
2.1.3. Depositional Controls.....	6
2.1.4. Calcareous Ooze Composition	8
2.2. Biostratigraphy	9
2.2.1. Introduction	9
2.2.2. Unbiased Approach	10
2.2.3. Biozones	10
2.2.4. Upper Cretaceous Biozonation.....	12
2.3. Calcareous Nannofossils.....	13
2.3.1. Introduction	13
2.3.2. Coccolith Function and Morphology	16
2.3.3. Nannolith Morphology	20
2.3.4. Paleocological Implications.....	21
2.4. Calcareous Nannofossil Evolution	23
2.4.1. Triassic	23
2.4.2. Jurassic	24
2.4.3. Lower Cretaceous.....	25
2.4.4. Upper Cretaceous	26
2.4.5. Cenozoic.....	27
2.5. Optical light microscopy (OLM).....	27
2.5.1. Components of the Light Microscope	27
2.5.2. Oil Immersion Technique.....	30

2.5.3.	Optical Properties of Calcareous Nannofossils	31
2.5.4.	Polarized Light	32
2.5.5.	Birefringence, Interference Colour and Gypsum Plate	34
2.6.	Field Emission Gun Scanning Electron Microscope (FEG-SEM)	37
2.6.1.	Introduction	37
2.6.2.	Components of the FEG-SEM	38
2.7.	IOR Flooding Experiment	40
3.	Sample Preparation and Methodology	42
3.1.	Sample Preparation and Sample ID	42
3.2.	Optical Light Microscopy (OLM)	45
3.2.1.	Simple Smear Slides of Dry and Wet Powder	45
3.2.2.	Simple Smear Slides using the Random Settling Technique	47
3.2.3.	Calcareous Nannofossil Preservation	49
3.2.4.	Calcareous Nannofossil Abundance and Diversity	53
3.2.5.	Identification of Taxa	54
3.2.6.	Range Chart and Biostratigraphy	54
3.2.7.	Point Counting.....	57
3.2.8.	Paleoecology	58
3.2.9.	Calcareous Nannofossil versus Micarb Ratios	59
3.3.	Field Emission Gun Scanning Electron Microscopy (FEG-SEM)	60
3.3.1.	FEG-SEM Sample Preparation	60
3.3.2.	Examination and Micrography	61
3.3.3.	Calcareous Nannofossil Preservation	65
3.3.4.	Calcareous Nannofossil versus Micarb Ratios	67
4.	Results	69
4.1.	Optical Light Microscopy (OLM)	69
4.1.1.	Calcareous Nannofossil Preservation	69
4.1.2.	Calcareous Nannofossil Abundance and Diversity	70
4.1.3.	Range Chart and Biostratigraphy	73
4.1.4.	Point Counting.....	81
4.1.5.	Paleoecology	86
4.1.6.	Calcareous Nannofossil versus Micarb Ratios	87
4.1.7.	Special Observations	88
4.2.	Scanning Emission Gun Scanning Electron Microscopy (FEG-SEM)	90
4.2.1.	Calcareous Nannofossil Preservation	90
4.2.2.	Calcareous Nannofossil versus Micarb Ratios	94
5.	Discussion	95
5.1.	Calcareous Nannofossil Preservation in OLM and FEG-SEM	95

5.2.	Calcareous Nannofossil Abundance and Species Diversity	97
5.3.	Biostratigraphic Analyses	99
5.4.	Point Count: Calcareous Nannofossil Assemblages and Implications	102
5.5.	Paleoecology.....	107
5.6.	Nannofossil versus Micarb Ratios	108
5.7.	Special Observations	110
5.8.	IOR Flooding Experiment	110
6.	Conclusion.....	114
7.	Recommendations for Future Work	115
8.	References	116
9.	Appendices	128
9.1.	Appendix 1: Offshore Chalk Reservoir Samples	128
9.2.	Appendix 2: Sample Weight in Random Settling Smear Slides	129
9.3.	Appendix 3: Taxonomic Description	130
9.3.1.	Heterococcoliths	131
9.3.2.	Holococcoliths.....	160
9.3.3.	Nannoliths	162
9.4.	Appendix 4: Plates.....	170
9.5.	Appendix 5: Percentage Estimation chart	182
9.6.	Appendix 6: Point Counting Chart	183
9.7.	Appendix 7: Calcareous Nannofossil Assemblages, Species and Genera in % of Total Count	184

List of Figures

Figure 1: Chalk (sample K, see Table 1 in Chapter 3.1) seen in the field emission gun scanning electron microscope (FEG-SEM), displaying a high content of calcareous nannofossils.	2
Figure 2: The Seven Sisters cliffs cutting into chalk in south England (James and Jones, 2016).	4
Figure 3: Map showing distribution of continents, mountains, shallow seas and deep ocean basins during the Late Cretaceous Period (94 ma.) (Scotese, 2002).	6
Figure 4: The different zones of carbonate dissolution and precipitation. CCD: Carbonate compensation depth. From James and Jones (2016).	8
Figure 5: Figure displaying various types of biozones with delimiting species that are used in this thesis. The left side displays the timescale of Campanian to Maastrichtian and the species are named below the figure and visualized by sketches. The black line that goes through a species represents the lifespan of the species, with first occurrence as a dot and last occurrence as an arrow. If a species had its first occurrence earlier than Campanian, it will not have a dot, for example for <i>A. confusa</i> . The green/yellow boxes are establishing the age range of the biozone from bottom to top, and the corresponding species' events from left to right. 1a: Local range biozone; 1b: Concurrent interval biozone; 1c: Successive last appearance zone; 1d: Consecutive range biozone (type 1); 1e: Consecutive range biozone (type 2); 2: Acme biozone and 3: Assemblage biozone.	11
Figure 6: Sketches showing the three main nannofossil groups, not in scale. From the left: coccoliths forming a coccolithophore (based on personal observation), <i>discoaster</i> (based on photograph by Young (1998)) and nannoconid (based on personal observation).	13
Figure 7: Various Nannoconus species. A: <i>Nannoconus globulus</i> , B: <i>Nannoconus circularis</i> , C: <i>Nannoconus truitti</i> , D: <i>Nannoconus bermudezii</i> , E: <i>Nannoconus elongatus</i> , F: <i>Nannoconus minutus</i> , G: <i>Nannoconus kamptneri</i> , H: <i>Nannoconus colomii</i> and I: <i>Nannoconus steinmannii</i>	15
Figure 8: <i>Nannoconus colomii</i> forming a rosette based on reported observation by Tréjo (1960).	15
Figure 9: A complete coccolithophore in sample SK1. The shields that protect the single cell in the center are called coccoliths.	17
Figure 10: Coccolith terminology, redrawn and modified from Young et al. (2016).	19
Figure 11: R- and V-units and segment. Redrawn and modified from Young et al. (2016). ...	19
Figure 12: From left to right: 3D sketch, simplified cross-section without spine and cross-section with spine. A: murolith, B: placolith. Redrawn and modified after Young et al. (2016).	20
Figure 13: Various nannoliths with different shapes. a: <i>Braarudosphaera bigelowii</i> small in sample L5; b: <i>Lithraphidites</i> sp. in sample A5; c: <i>Microrhabdulus decoratus</i> in sample MS1; d: <i>Eprolithus moratus</i> in sample K1; e: <i>Lithastrinus grillii</i> in sample MOV1; f: <i>Quadrum gartneri</i> in sample MS1 and g: <i>Micula staurophora</i> in sample MS1. White scale bar = 2 μ m.	21
Figure 14: Illustrative sketch of the main components of a light microscope. Modified from Murphy (2001).	29
Figure 15: Sketch displaying how the system of lenses are producing a virtual image of a specimen in the light microscope. Modified from Murphy (2001).	30
Figure 16: Oil drop between the objective and the smear slide to increase the numerical aperture and the resolution.	31
Figure 17: Typical extinction pattern for a: A placolith seen on a <i>Watznaueria fossacincta</i> in sample MT1, and b: A murolith seen on <i>Reinhardtites anthophorus</i> in sample MON1. White scale bar = 2 μ m.	33

Figure 18: Nannoliths with different extinction-patterns. a: <i>Braarudosphaera bigelowii</i> with one-to-two plaquettes close to extinction and b: <i>Microrhabdulus decoratus</i> with chequerboard extinction-pattern. White scale bar = 2 μm	34
Figure 19: Calcite crystals showing interference colors, while the background composed of glass appears black due to its isotropic nature.	35
Figure 20: Different species show different interference colors. a: <i>Micula staurophora</i> with stronger interference colors than <i>Quadrum gartneri</i> in sample MS1 and b: <i>Zeugrhabdotus embergeri</i> in sample K5 with its typical strong interference colors. White scale bar = 2 μm	36
Figure 21: <i>Watznaueria fossacineta</i> in sample MT1 under a: crossed nicols and b: crossed nicols combined with gypsum plate. The gypsum plate makes it easier to distinguish the different cycles. White scale bar = 2 μm	36
Figure 22: a: When looking under crossed nicols, one might be in doubt if the object in the circle is a calcareous nannofossil or inorganic calcite crystals. b: The gypsum plate can show if there is a consistency of optical orientation of the elements, such as in this case, where two elements are blue and two yellow, in diagonal patterns – in favor to interpret it as a calcareous nannofossil, here in sample MS1. White scale bar = 2 μm	37
Figure 23: A field emission gun scanning electron microscope (Zeiss Supra 35-VP FE-SEM) at the University of Stavanger with the main components.	38
Figure 24: Simplified sketch showing how the electron beam is focused by a set of magnetic lenses, before it scans the surface of the specimen.	39
Figure 25: Five cylindrical onshore chalk cores were divided as displayed in this figure. a: First the core was cut in three pieces, where only the central core was used for flooding. b: The central core was divided into seven slices after flooding, with slice number 1 being closest to inlet and slice number 7 being closest to outlet. Modified after Andersen et al. (2017).	41
Figure 26: Eight cores cut in five slices and a sixth, thinner slice. a: L; b: K; c: A; d: SK; e: MOV; f: MON; g: MT and h: MS. For sample IDs, see Table 1 on the next page.....	43
Figure 27: Each slice was cut in half, and then one half was cut in half again.....	44
Figure 28: The different steps in simple smear slide production using dry and wet powder... ..	47
Figure 29: Photos showing the methodology of preparing random settling smear slides.....	49
Figure 30: Photos illustrating the different degrees of preservation using three different genera: Left column: <i>Watznaueria</i> ; middle column: <i>Eiffellithus</i> and right column: <i>Reinhardtites</i> . White scale bar = 2 μm	52
Figure 31: UC biozonation scheme after Burnett (1998), modified by Erba, Miniati, Bottini, Russo in prep. (unpublished data).	56
Figure 32: One “FOV” from sample A5, estimated to have a NvsM-ratio of 5:95.	59
Figure 33: One “FOV” from sample K1, estimated to have a NvsM-ratio of 70:30.	60
Figure 34: Photographs displaying the different steps of preparing chalk samples for the FEG-SEM: a: Hammer and chisel cleaned with ethanol between each sample were used to cut off a small piece of each sample; b: A small piece of each sample was picked with tweezers and glued on a FEG-SEM sample mount with the fresh surface upwards; c: The glued samples were put under ventilation to dry overnight; d: The samples were put on a rotating stage to ensure even coating of palladium; e: Coating of palladium lasted for 2.5 minutes and f: The samples were ready to be put into the sample chamber in the FEG-SEM.	61
Figure 35: Joystick to move samples up or down, and various rotating knobs to adjust the stigmator alignment, aperture alignment, magnification and focus.	62
Figure 36: FEG-SEM micrograph with magnification x5000, displaying an overview of species in sample MOV5.	63
Figure 37: FEG-SEM micrograph with magnification x10.000, displaying a coccolithophore in sample MT1.....	63

Figure 38: FEG-SEM micrograph with magnification x25.000, displaying an <i>Arkhangelskiella cymbiformis</i> in sample A5.....	64
Figure 39: FEG-SEM micrograph with magnification x30.000, displaying a <i>Micula sp.</i> in sample MS1.....	64
Figure 40: FEG-SEM micrographs illustrating the different degrees of preservation using several different genera: Left column: <i>Tranolithus</i> ; middle column: <i>Prediscosphaera</i> and right column: Various genera. White scale bar = 2 μ m.	66
Figure 41: Sample A5, estimated to have a NvsM-ratio of 10:90.....	68
Figure 42: Sample K1, estimated to have a NvsM-ratio of 70:30.....	68
Figure 43: Preservation levels of the various samples, from youngest to oldest (left to right). VP: very poor; P: poor; P-M: poor to moderate and M: moderate.	69
Figure 44: Abundance results from all samples, as abundance in nannofossils per FOV [n/FOV] and total calculated abundance of nannofossils per gram of sample [n/g] 10^3	70
Figure 45: Species and genera diversity in the offshore samples are presented as an average, and the onshore samples are presented from both ends of the core (1 and 5), as well as their flooded inlet position equivalents. Listed from youngest to oldest (left to right).	72
Figure 46: Species and genera diversity in the offshore TOR sequence, from oldest to youngest (bottom to top).....	73
Figure 47: Range chart for offshore samples.	75
Figure 48: Range chart for onshore samples.	76
Figure 49: Biostratigraphic chart for the offshore samples.....	77
Figure 50: Biostratigraphic chart for the onshore samples.....	78
Figure 51: Conclusion of biostratigraphy for the offshore and onshore samples, represented by colored lines corresponding to the age span of the samples.	79
Figure 52: Coccoliths contained in the flooded SK6 core, at inlet position: sample SK_inlet. a: Reniform coccolith resembling <i>Nephrolithus frequens</i> and b: <i>Arkhangelskiella maastrichtiensis</i> . White scale bar = 5 μ m.	81
Figure 53: Assemblage composition in the offshore samples listed from youngest to oldest (left to right), represented by genera and species as percentages of total assemblage that are constituting more than 3 % of the total assemblage.....	82
Figure 54: Assemblage composition in the various samples listed from youngest to oldest (left to right), represented by genera and species counts constituting more than 3 % of the total assemblage.	84
Figure 55: Comparison of assemblage compositions from unflooded to flooded samples at inlet position, as counts per sample.....	85
Figure 56: Change of assemblage compositions from unflooded to flooded samples at inlet position, as species or genus percentages of the total assemblage.....	86
Figure 57: Various paleoecological indices in the offshore and onshore samples in percentage of total assemblage, from youngest to oldest (left to right). The combined percentages go above 100% for some samples due to that certain species are used as several paleoecological indices.	87
Figure 58: Nannofossil versus micarb ratios for the various samples estimated in the OLM, listed from youngest to oldest (left to right).....	88
Figure 59: Small versions of calcareous nannofossil species. a-d: Small <i>Micula sp.</i> , e-h: small <i>Braarudosphaera bigelowii</i> . White scale bar = 2 μ m.....	89
Figure 60: Counts of dwarf-species in the various offshore and onshore samples, from youngest to oldest (left to right).....	89
Figure 61: FEG-SEM micrograph of sample MT1, displaying poor-moderate preservation. .	91
Figure 62: FEG-SEM micrograph of sample MT_inlet, displaying poor preservation.	91

Figure 63: FEG-SEM micrographs of sample K1, displaying moderate preservation, as opposed to poor-moderate as determined using the OLM.....	92
Figure 64: FEG-SEM micrographs of sample K_inlet, displaying very poor preservation.....	92
Figure 65: FEG-SEM micrograph of sample A1, displaying poor preservation.....	93
Figure 66: FEG-SEM micrograph of sample A_inlet, displaying very poor preservation.	93
Figure 67: Nannofossil versus micarb ratios for the various samples estimated in the FEG-SEM, listed from youngest to oldest (left to right).....	94
Figure 68: Stevns Klint onshore chalk quarry with different lithostratigraphic sections, photographed by Pedersen (2013).	101
Figure 69: Comparison of estimation of % nannofossils versus micarbs in the onshore samples.	109
Figure 70: MgO wt% after flooding plotted against % nannofossils versus micarbs in the unflooded equivalent core. Blue line shows linear trend for samples L, MT and A which were flooded for 60-65 days.	112
Figure 71: MgO wt% after flooding plotted against % nannofossils versus micarbs in the unflooded equivalent core. Blue line shows linear trend for all samples.	112
Figure 72: MgO wt% after flooding plotted against average total calculated nannofossil abundance in the unflooded equivalent core. Blue line shows linear trend for samples L, MT and A which were flooded for 60-65 days.	113
Figure 73: MgO wt% after flooding plotted against average total calculated nannofossil abundance in the unflooded equivalent core. Blue line shows linear trend for all samples... ..	113

List of Tables

Table 1: Overview of the original core IDs and the sample IDs used in this thesis.....	44
Table 2: Nannofossil preservation levels used in OLM, based on Lees (2002) and Tremolada (2002).	50
Table 3: Species used as paleoecological indices.	58
Table 4: Nannofossil preservation levels used in FEG-SEM, based on Lees (2002) and Tremolada (2002).	65
Table 5: Species and genera diversity in the studied samples, listed from youngest to oldest (left to right, top to bottom).	71
Table 6: Presumed ages for the samples (for references, see Chapter 5.3), and the results for new determined ages from this thesis' biostratigraphic analyses.	80
Table 7: Comparison of preservation levels determined from the OLM and FEG-SEM, and final determination by combining them. The preservation levels are assigned a colour range depending on the level: from dark grey (very poor) to white (moderate).	96
Table 8: Comparison of preservation level and duration of flooding (d = day). Duration data from Andersen et al. (2017). The preservation levels are assigned a colour depending on the level: from dark grey (very poor) to white (moderate).	97
Table 9: Rank of species or genera from dissolution-resistant (negative decrease, top) to dissolution-susceptible (positive decrease, bottom), based on average data from four unflooded samples with their flooded equivalents.	106
Table 10: Flooded samples at inlet position different data: MgO wt% after flooding, data from Andersen et al. (2017); average NvsM-ratios in % nannofossils in the unflooded sample equivalent (Unfl. NvsM); average NvsM-ratios in % nannofossils in the flooded samples (F. NvsM); the difference between Unfl. NvsM and F. NvsM, giving the % nannofossils which were lost during flooding; average total calculated nannofossil abundance of the original unflooded core (O. Tot. C. N. A.); and duration of the flooding in days (T(d)).	111

List of Appendices

Appendix 1: Offshore chalk reservoir samples with additional data.	128
Appendix 2: Sample weight in random settling slides with calculations for total nannofossil abundances. After Williams and Bralower (1995): X = particles per gram of sediment [n/g], N = number of particles counted, V = volume of water used for dilution [ml], M = grams of sediment added [g], F = number of fields of view observed, A = surface area of one FOV [cm ²] and H = height of water column above slide [cm].	129
Appendix 3: Taxonomic descriptions: This appendix presents short taxonomic descriptions of every genus and species encountered in this thesis, followed with simplified sketches and photos from the light microscope and/or the FEG-SEM. The descriptions are based on various authors, which will be referenced accordingly.	130
Appendix 4: Plates with photographs taken in the light microscope or the FEG-SEM. First line below each photograph specifies the genus or species name, and the second line specifies in which sample the photograph was taken.	170
Appendix 5: Percentage estimation chart from Baccelle and Bosellini (1965).	182
Appendix 6: Point counting chart.	183
Appendix 7: Calcareous nannofossil assemblages, species and genera in % of total count. .	184

List of Commonly Used Abbreviations

IOR	= Increased Oil Recovery
EOR	= Enhanced Oil Recovery
FEG-SEM	= Field Emission Gun Scanning Electron Microscopy
OLM	= Optical Light Microscopy
Ky	= Thousand years
Ma	= Million years
CCD	= Calcite Compensation Depth
FOV	= Field of view
OAE	= Oceanic Anoxic Event
SE	= Secondary electrons
BSE	= Backscattered electrons
UC	= Upper Cretaceous
[n]	= number of nannofossils
A	= Aalborg
MS	= Mons Spiennes
SK	= Stevns Klint
MT	= Mons Trivières
MON	= Mons Limit Obourg Nouvelles
L	= Liège
MOV	= Mons Obourg Saint Vaast
K	= Kansas
wt%	= weight percent
n:m-ratio	= Nannofossil versus micarb ratio
k	= Thousand
K/T boundary	= Cretaceous/Cenozoic boundary

1. Introduction

1.1. Motivation for the Thesis

This thesis came to be from the necessity of adding paleontological reservoir characterization to IOR research on chalks. The abundance and origin of paleontological material plays a role in which way a fluid propagates throughout cores used for flooding experiments related to increased oil recovery (IOR) research (Minde et al., 2016) (U. Zimmermann, personal communication, 2018). Moreover, it is important to identify the stratigraphic level and the nanofacies. Any data enhancing the knowledge of the tested samples is of uttermost importance for future IOR purposes and the paleontological material is one of the keys in understanding the depositional environments of the chalks. In turn, this also controls the mineralogical changes and may be interpreted as decisive for changes of rock mechanical parameters.

1.2. Structure and Objectives of the Thesis

Carbonate hydrocarbon reservoirs have been estimated to trap more than 60 % of the world's oil and 40 % of the world's gas reserves (*World Energy Outlook 2006*, International Energy Agency). These reservoirs constitute a remarkable amount of the hydrocarbon reserves in the world. In the North Sea, an important amount of the oil production comes from chalk reservoirs, with the giant Ekofisk field being the ground-breaking example that positioned Norway on the map as a petroleum nation in 1969. Chalk reservoirs are subjects of experimentation in enhanced oil recovery (EOR) research to improve oil recovery.

The chalk reservoirs are often stratigraphically controlled, which means that biostratigraphic data are an essential part of the reservoir characterization. These analyses are performed to assign relative ages to the rock strata based on the contained fossil assemblages to correlate them. In the exploration phase, petroleum geologists will search for rocks of a certain age that has the highest potential of possessing hydrocarbons. In the drilling phase, it is necessary to have a continuous control that the drilling stays within the reservoir successions of the aimed age, for example through biosteering. A mistake in stratigraphy can be extremely expensive.

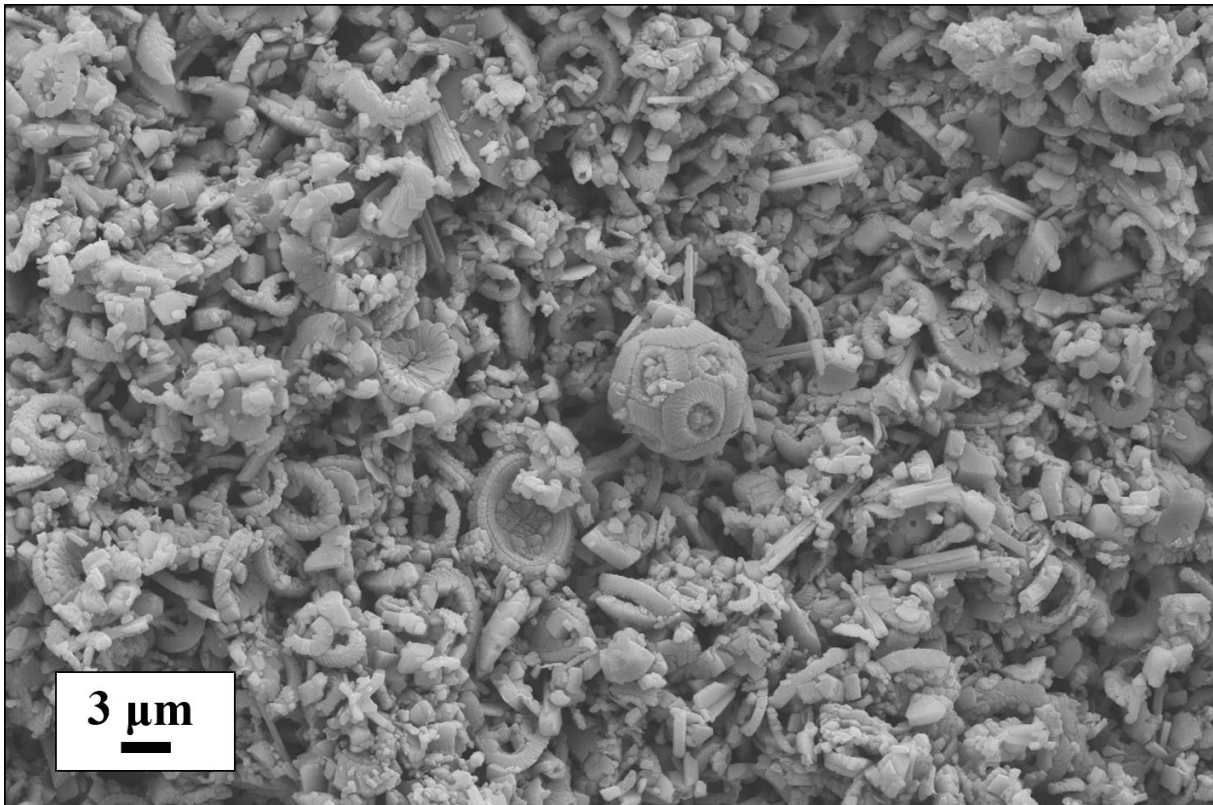


Figure 1: Chalk (sample K, see Table 1 in Chapter 3.1) seen in the field emission gun scanning electron microscope (FEG-SEM), displaying a high content of calcareous nanofossils.

Chalk is a highly fossiliferous rock, with calcareous nanofossils being the main constituent (Figure 1). These nanofossils are less than 30 μm in diameter, and the type, the amount and the form of these nanofossils will significantly affect the fluid flow in chalk, which again affects the production of these reservoirs. These three parameters are dependent on the nanofacies, which often is unknown and not tackled in chalk-related IOR-research. Indeed, the quantity of different taxa, their forms, orientations and degree of diagenesis control the porosity and density of chalk reservoirs and therefore control fluid flow.

This thesis executes a combination of optical light microscopy (OLM) with field emission gun scanning electron microscopy (FEG-SEM) to characterize the calcareous nanofossils, by describing the nanofacies of both onshore outcrop- and offshore reservoir-chalks. In the search for the best analogues for reservoir chalk, it is preferable to find onshore chalk with similar mineralogy, depositional environment, age, nanofacies, permeability and porosity, hence rock mechanical characteristics. Differences in how various chalk samples react to flooding might be due to differences in their paleoecological conditions, hence their calcareous nanofossil abundances and assemblages. By going back to the most basic constituent of the chalk - the

nannoplankton that deposited on the ancient ocean floors and formed the chalk – this thesis intends to contribute to EOR chalk-research.

The focus of the thesis is twofold. One objective is to characterize nannofacies in both onshore- and offshore chalk samples. This objective can be broken down into the following key issues:

- (1) Calcareous nannofossil **preservation** using OLM and FEG-SEM
- (2) Calcareous nannofossil **abundance**, both total abundance and abundance of certain taxa and **species diversity**
- (3) Calcareous nannofossil **biostratigraphy** using OLM
- (4) Simple relative abundance **counting** of calcareous nannofossil genera and species using OLM giving **quantitative data**
- (5) Describing calcareous nannofossil **assemblages**
- (6) and their implications in terms of interpreting **paleoecology**
- (7) Estimating calcareous **nannofossil versus micarb ratios** using OLM and FEG-SEM for a quick assessment of the nannofacies

Secondly, the thesis aims to compare the results from above with flooded versions of the onshore chalk samples. At the National IOR centre of Norway at the University of Stavanger, it is routine since decades to flood onshore chalk samples with various fluids to observe the mineralogical changes, which in turn affect rock mechanics (Andersen et al., 2017). This thesis aims to present a dataset useful for evaluation of the effect paleontological material has on flooding experiments.

2. Theoretical Background

2.1. Chalk

2.1.1. Introduction



Figure 2: The Seven Sisters cliffs cutting into chalk in south England (James and Jones, 2016).

The magnificent White Cliffs of Dover (Figure 2), extending 16 km along the coast of South England, can be an impressive sight. The cliffs have formed the background for several dramatic moments in British history, from the first invasion by Caesar in 55 BC to the return of British forces during World War II (Winterman, 2012). On a less dramatic note, the White Cliffs of Dover also stands as one of the most reachable and complete records of the history of chalk. This chalk was deposited during the Upper Cretaceous and got uplifted about 30 million years ago. The same chalk group extends eastwards and constitute the important petroleum reservoirs in the North Sea Central Graben, such as the Ekofisk field.

Chalk was recognized for its properties as excellent grapevine-soil by the Romans even before the science of geology had been established. The Cretaceous Period is named after the Roman word for chalk, *Creta*. The Latin name of England, *Albion*, from Latin *alba* meaning white, is possibly derived from the white colour of the chalk that raised above them as the Roman Empire encountered England for the first time: The White Cliffs of Dover (Winterman, 2012). Chalk is an interesting and important rock in many aspects.

2.1.2. Classification

Chalk is a white and soft sedimentary carbonate rock, which is composed of calcium carbonate, mostly the mineral calcite in the remains of calcareous organisms. It can also be interbedded or intermixed with siliciclastics or clay. Usually, chalk displays an absence of terrigenous material, due to the depositional environment being distal from the continent and the influence of clastic deposition. Chert bands are commonly found parallel to bedding, or as embedded nodules within the chalk. Classification of chalk can be done based on texture - referring to the size, shape and arrangement of the grains, or fabric; describing the orientation of the grains, crystals and cement.

Dunham (1962)'s classification classifies chalk as a mudstone and occasionally as a wackestone, based on its fine-grained depositional texture, and the nature of the supporting framework between particles, being mud supported. The differentiation between mudstone and wackestone is determined based on grain content; >10% and <10% respectively. Folk's (1959, 1962) classification on the other hand is based on the type of allochems (particles), and if they are embedded in micrite matrix or calcite cement. Chalk is a fossiliferous micrite (1-10% allochems) according to this classification.

2.1.3. Depositional Controls

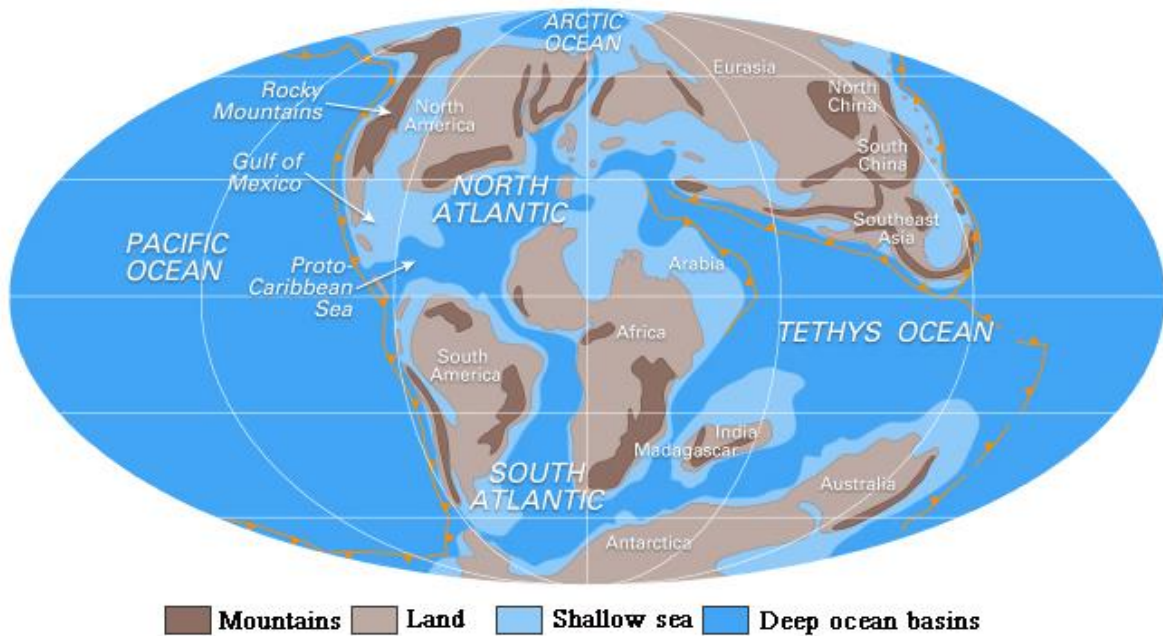


Figure 3: Map showing distribution of continents, mountains, shallow seas and deep ocean basins during the Late Cretaceous Period (94 ma.) (Scotese, 2002).

The Cretaceous Period was characterized by warmer climate, and rising sea levels resulted in shallow seas covering large areas of the continents (Figure 3). These seas were ideal for accumulating and preserving chalk and lasted for approximately 30 million years (Wicander and Monroe, 2004).

Chalk is generally deposited in a low-energy environment, such as in a hemipelagic setting, which on a larger scale gives it layered, homogenous and pelagic autochthonous facies. Its brittle nature commonly results in reworking. Tectonics might increase instability and faulting of previously deposited sediments. Heterogeneous, brecciated and allochthonous chalk facies are typically found more basinwards, because of syn- and post-depositional gravitational movements, such as slides, slumps, debris-flows and turbidites. Even though the deep seafloor is below influence from tides and surface waves, the carbonate sediments can be reworked and sorted by submarine currents. The chalk-reservoirs of the Ekofisk field are excellent examples of re-deposited chalk (Ramberg, 2008). Especially during icehouse times, contour currents along continental margins are active and easily capable of eroding and removing fine-grained sediments, resulting in hiatuses. During greenhouse times, high sea level can be associated to erosion of the seafloor (James and Jones, 2016).

Chalk is deposited in the deep-water pelagic basin environments. The generation of sediments takes place in the photic zone water column (0-200 metres) by swimming and floating phyto- and zooplankton: the most important being the unicellular algae coccolithophorids and the planktic foraminifers. There are several critical controlling factors for the pelagic carbonate factory: light, salinity, oxygen, nutrients and temperature. In general, the calcareous plankton organisms thrive in tropical and warm equatorial regions, with light waters, upwelling, moderate nutrient levels and in areas where oceanic currents diverge. Siliceous plankton are more commonly found in cooler surface waters (James and Jones, 2016).

According to James and Jones (2016), the pelagic carbonate accumulates on the seafloor deeper than 200 meters, often down to several kilometres. The particles making up the sediment is minute calcite shells (coccoliths) which are shed from microorganisms when they die. They can be extremely abundant, up to 50.000-500.000 per litre of seawater. The remains sink slowly to the ocean floor, and depending on their sizes, it can take from a few days (planktonic foraminifers) to 100 years (coccoliths) to reach the bottom. Accumulation rates in general uncompacted Mesozoic-Cenozoic pelagic sediments were around 3 cm ky⁻¹, but in the North Sea Basin they could be as high as 15 to 25 cm ky⁻¹ (James and Jones, 2016). Recently deposited, the accumulated carbonate ooze (deep sea soft mud deposits consisting of at least 30 % skeletal remains of microscopic floating organisms) range in porosity from 60 to 80%. After burial, porosity is lost by mechanical compaction, recrystallization, pressure dissolution and cementation. Finally, porosity might be reduced to less than 20% (Fabricius, 2003). To conclude, it takes time to accumulate sediments to form chalk. A few meters of chalk might represent millions of years in time.

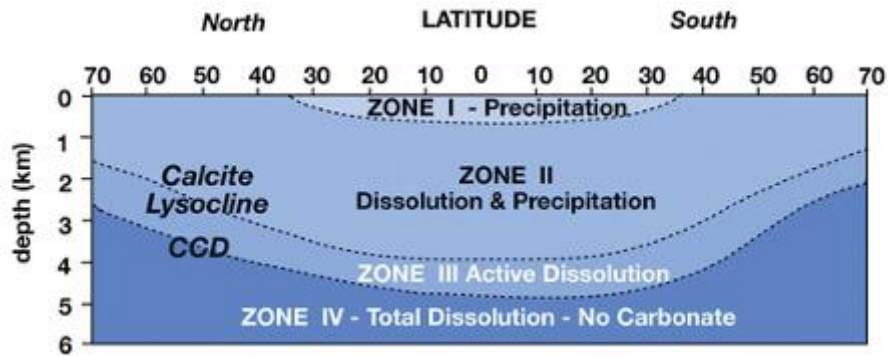


Figure 4: The different zones of carbonate dissolution and precipitation. CCD: Carbonate compensation depth. From James and Jones (2016).

Another important controlling factor for preservation of calcareous sediment is dissolution. There is a balance between the rate of supply of the calcareous sediment, and the rate of dissolution. This is called the calcite compensation depth (CCD) (Figure 4), where the supply of calcite is much slower than the rate of dissolution, such that no calcite is preserved. Dissolution is varying depending on several different factors, such as temperature, hydrostatic pressure, depth and CO₂ content of the water. Below the CCD in the modern oceans, there is no carbonate. The seafloor is instead covered in red clay and biosiliceous ooze. Underwater hills that come through to the CCD might be covered in calcareous ooze, giving them the name “snow-capped mountains of the deep sea” (James and Jones, 2016). The depth where dissolution begins is called the lysocline and is much shallower than the CCD (Figure 4). The depth of the CCD has varied through time and is dependent on how nutritious the shallow waters are, which again controls the rate of carbonate production. The nutrient level is controlled by temperatures and salinities, which on their side is regulated by plate tectonics. For example, in the Atlantic Ocean, the CCD is found around 5500 meters, because the pelagic productivity is high. In the Pacific Ocean, the CCD lies around 3500 meters, and indicates surface waters with nutrient starvation (Gornitz, 2009).

2.1.4. Calcareous Ooze Composition

Calcareous ooze is a deep-sea deposit which consists of at least 30% calcareous skeletal remains, from calcareous nannoplankton, planktonic foraminifers and radiolarians. Modern oozes may have water content as high as 80%, and the textural feeling may range from soup to pudding (Feazel and Farrell, 1998). They are mostly made up of coccolithophores and pelagic gastropods. There are different grain sizes, with the majority around 0.5 μm, which are calcite laths from broken calcareous nannofossils. Integrated calcareous nannofossils might range from 1-

20 µm, while whole foraminifers have sizes ranging from 25-64 µm. Calcispheres, sponges and microfossils such as bivalve fragments, echinoid plates and bryozoans also constitutes the chalk (Flügel, 2004).

2.2. Biostratigraphy

2.2.1. Introduction

Biostratigraphy is the branch of stratigraphy which uses fossils and their abundances to determine the relative ages of strata subdivisions. The fossil record of species appearing and species going extinct, combined with numerical dates from radioactive decay or information about geomagnetic changes as well as stable isotope data through time builds up an important part of the modern geochronology. Micropaleontology is the branch of paleontology concerning micro- and nanofossils, and sometimes it is required to use a microscope to determine essential morphologies. Fossils can be grouped together into assemblages based on the identification of taxa and tracing their lateral and vertical extent. This is done with the aim of zonation and correlation. Zonation is performed by dividing the strata into bodies of rock based on how the species ranges overlap between inception and extinction.

The basic concept of biostratigraphy is that if two rocks at different locations contain the same type of fossil (same species), then the rocks are time-equivalent, meaning that they were deposited at about the same time. Fossil species might appear in a series of environmental settings or have restricted geographical extent, their evolution might have been slow or rapid and their biology can be complicated and dependant on life-stages or cycles. Finally, the preservation potential of different species might vary, leading to different probabilities to be discovered and observed by the biostratigrapher. All this combined gives an intricate picture to interpret and must be accounted for.

The best fossil species in biostratigraphy is therefore those which were the fastest evolving and lived the shortest, ranging the widest in terms of environmental and geographic extent and being resistant enough to survive the geological record and to sustain severe etching (dissolution) and overgrowth. If a fossil species fulfils these criteria, it can be called an index fossil/marker species. Ideally if such a fossil is encountered in a rock, the age of the rock would be constrained to a very specific time interval reflecting the marker species' lifespan, or a combination of species' first and last occurrences.

Microfossils can be extremely abundant in rocks and especially in chalk. They are geographically widespread, and most of them evolved very fast, which means they naturally divided the rock record in a high stratigraphic resolution. Fossilized calcareous nannoplankton that built up chalk lived in open waters and were free-floating, meaning they widely inhabited the paleoceans. They evolved rapidly and since they were so small, they were prone to be well-preserved in the geological record and can be found in vast numbers today. This basis makes *calcareous nannofossils* some of the best fossils to use in biostratigraphy (Armstrong and Brasier, 2005).

2.2.2. Unbiased Approach

As in most sciences, it is extremely important to be unbiased when performing biostratigraphic analyses. In biostratigraphy, being unbiased means to not have information about the samples prior to the analyses, so that they can be analysed without having for example an age or a depositional system already in mind affecting the studies. The samples should be assessed with all options open.

2.2.3. Biozones

A biozone, or a biostratigraphic unit, is an interval of rock strata that is defined by its characteristic fossil taxa. If the length of time represented by a biozone is known, this is called a biochron. A biozone might be defined based on a single species, a combination or an abundance period (acme) of certain species. Broadly, biozones can be divided into three types: interval, acme and assemblage biozones, and they are visualized in Figure 5.

(1) **Interval** biozones are the best defined of the three and reflect actual ranges of one or several species and is based on species' first occurrences (FO) and last occurrences (LO). This biozone can be subdivided into five types: (a) local range biozone, when a biozone is limited by a single taxon's range, from FO to LO, (b) concurrent interval biozone, limited by the FO of one taxon and the LO of another taxon, (c) successive last appearance zone, which is limited by two successive LOs and is much applied in the petroleum industry to determine biostratigraphy of borehole cuttings where FOs are easily contaminated, (d) consecutive range biozone (type 1) based on the interval between two FOs and (e) consecutive range biozone (type 2) based on two LOs.

(2) **Acme** biozones represent a time when a certain taxon was superabundant. Acme episodes are often related to local nutrient influxes, and therefore it may not be applicable to a large geographical area. Acme biozones might be difficult to correlate on a global scale.

(3) **Assemblage** biozones are characterized by three or more species that are significantly different than the surrounding assemblages. Such a biozone will be strongly controlled by environmental constraints and can also be difficult to correlate on a global scale. It is best suited to be applied to a local or basinal level. However, if the evolution of the species involved is slow, the biozone might be widely recognizable (Armstrong and Brasier, 2005).

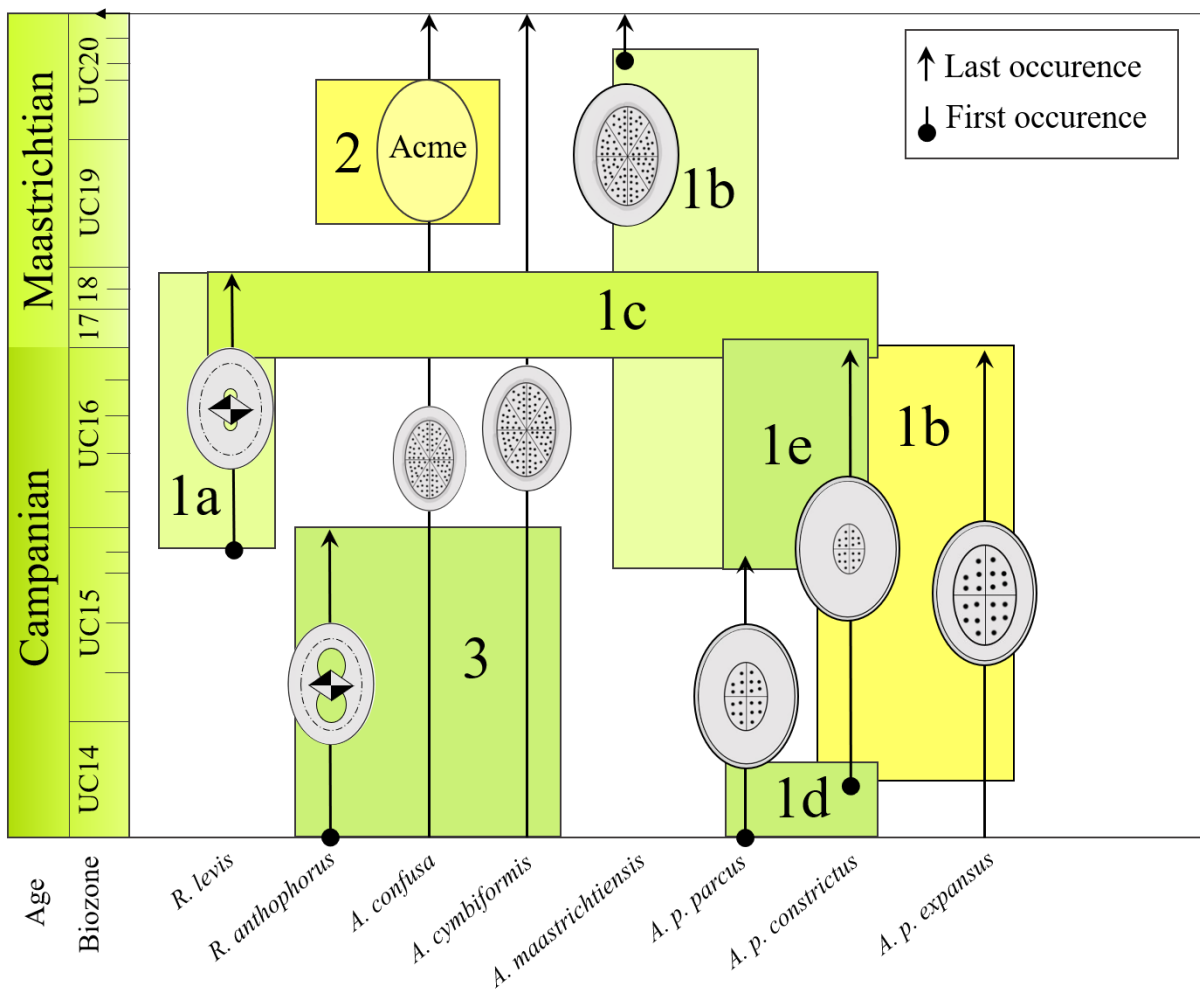


Figure 5: Figure displaying various types of biozones with delimiting species that are used in this thesis. The left side displays the timescale of Campanian to Maastrichtian and the species are named below the figure and visualized by sketches. The black line that goes through a species represents the lifespan of the species, with first occurrence as a dot and last occurrence as an arrow. If a species had its first occurrence earlier than Campanian, it will not have a dot,

for example for *A. confusa*. The green/yellow boxes are establishing the age range of the biozone from bottom to top, and the corresponding species' events from left to right. 1a: Local range biozone; 1b: Concurrent interval biozone; 1c: Successive last appearance zone; 1d: Consecutive range biozone (type 1); 1e: Consecutive range biozone (type 2); 2: Acme biozone and 3: Assemblage biozone.

2.2.4. Upper Cretaceous Biozonation

The development of biozones based on calcareous nannofossils have been performed by numerous authors (Sissingh and Prins, 1977; Roth, 1978; Sissingh, 1978; Perch-Nielsen, 1979, 1983, 1985; Bralower et al., 1995; Burnett, 1998). Since the authors have worked on sections from different localities in the world with both offshore and onshore samples, different biozonation schemes have been proposed and it can be difficult to correlate them. For the Upper Cretaceous, there are four available biozonation schemes using calcareous nannofossils: (1) CC biozonation of Sissingh and Prins (1977); (Sissingh, 1978), as modified by Perch-Nielsen (1979); (Perch-Nielsen, 1983, 1985), (2) NC zonation by Roth (1978), (3) Bralower et al. (1995) and (4) Upper Cretaceous UC biozonation of Burnett (1998). In this thesis, the UC biozonation of Burnett (1998) will be used as the base and is therefore the only one that will be discussed further.

According to Burnett (1998), the Sissingh and Prins (1977); (Sissingh, 1978) and Perch-Nielsen (1979); (Perch-Nielsen, 1983, 1985) CC biozonation scheme based too many critical intervals on low-latitude bioevents and cannot be applied at a global level. Burnett (1998) developed her UC biozonation by combining “old and new bioevent data, from a range of paleolatitudes and biogeographic provinces, and from both oceanic and shelf palaeoenvironments” (Burnett, 1998). The biozones are alphanumeric and correlated with macrofossil events onshore. The UC biozonation was also the first one to be correlated with stage-boundary events. The species chosen as biozonal marker species are robust and believed to have marked bioevents that can be correlated over a wide area and be applied to most geographic situations (Burnett, 1998).

For the Cenomanian to Santonian, the marker species are reliable and globally distributed. However, it is evident that for the subzonation there are some paleoenvironmental constraints, so they cannot necessarily be applied to all paleoceanographic localities. During Campanian to Maastrichtian, nannoflora became more provincial, as the separation of paleobiogeographic areas became more apparent. This means that correlation on a global scale is difficult, resulting in the Campanian to Maastrichtian having the lowest correlation resolution in the Upper

Cretaceous. Biozones are still globally correlatable, but subzones are not. To come by this issue, three different regions have been created with their own subzones: “a ‘boreal’ province (broadly, northern high-palaeolatitudes), an intermediate-‘tethyan’ province (broadly, moderate- to low palaeolatitudes), and an ‘austral’ province (southern high-palaeolatitudes)” (Burnett, 1998).

2.3. Calcareous Nannofossils

2.3.1. Introduction

Nannofossils are fossils defined to be smaller than 30 μm , which also includes a diverse range of fossils like spicules, calcispheres and juvenile foraminifers. However, the predominant group are the remains of marine phytoplankton (algae) with the following taxonomic rank:

Domain: **EUKARYOTE** (Chatton, 1925) Whittaker and Margulis, 1978

Kingdom: **CHROMISTA** Cavalier-Smith, 1981

Phylum: **HAPTOPHYTA** Cavalier-Smith, 1986

Class: **PRYMNESIOPHYCEAE** Hibberd, 1976

Calcareous nannofossils are made of calcium carbonate and include three forms: coccoliths, discoasters and nannoconids (Figure 6).

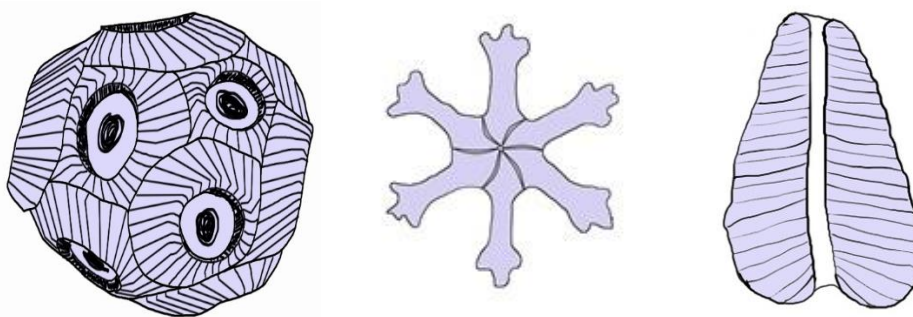


Figure 6: Sketches showing the three main nannofossil groups, not in scale. From the left: coccoliths forming a coccolithophore (based on personal observation), *discoaster* (based on photograph by Young (1998)) and nannoconid (based on personal observation).

Their size range is approximately 0.25-30 μm . They can be found in fine-grained pelagic sediments, and if they are sufficiently abundant, they can become rock forming as chalk. The

systematic classification of calcareous nanofossils is challenging because of their small sizes and poor preservation in deep water sediments.

Discoasters and nannoconids were not encountered in the studied samples and will therefore only be discussed briefly in this thesis. Coccoliths and nannoliths will be discussed in detail in Chapters 2.3.2-2.3.3.

Discoasters are an extinct group of marine algae with a radiating, star-shaped form of which their numbers of rays and details build up their taxonomy. Discoasters are more abundant in tropical ocean sediments, where they often can be the dominant nanofossil. Their temporal range is from Paleocene to Pleistocene. For biostratigraphy, they are especially useful in the timespan from Paleogene to Neogene (Armstrong and Brasier, 2005). However, since this thesis do not include samples of these ages, discoasters will not be discussed further.

The nannoconids are of uncertain affinities and belong to the informal group of nannoliths – calcareous nanofossils that neither show the rim structure of heterococcoliths nor the microcrystal structure of holococcoliths (hetero- and holococcoliths will be explained in the next chapter). They are cone-shaped and constructed of triangular calcite plates packed tightly together with their points towards an axis, creating a spiral. A canal perforates the axis, with opening on both ends. Their overall sizes, wall and canal thicknesses distinguish them into different species (Figure 7).

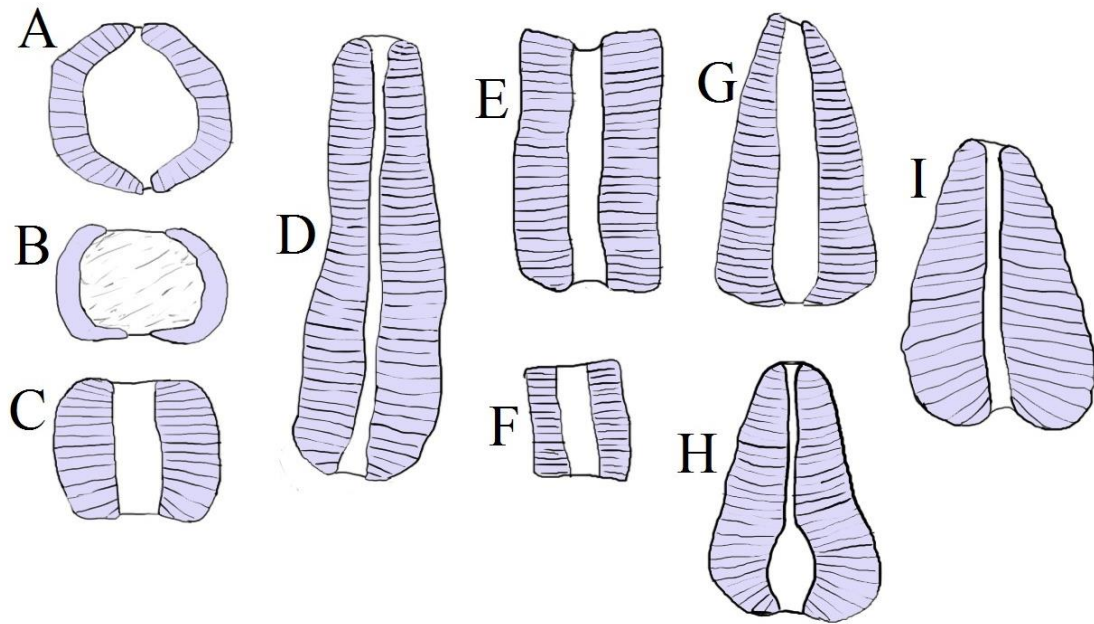


Figure 7: Various *Nannoconus* species. A: *Nannoconus globulus*, B: *Nannoconus circularis*, C: *Nannoconus truitti*, D: *Nannoconus bermudezii*, E: *Nannoconus elongatus*, F: *Nannoconus minutus*, G: *Nannoconus kamptneri*, H: *Nannoconus colomii* and I: *Nannoconus steinmannii*.

They can be roughly divided into *Nannoconus* with wide axial canal ($> 2 \mu\text{m}$, Figure 7: A, B, C, E, F and G) and *Nannoconus* with narrow axial canal ($< 2 \mu\text{m}$, Figure 7: D, H and I). It remains unknown until today which organism produced *Nannoconus*. However, discoveries of nannoconids grouped together as rosettes were reported by Tréjo (1960), raising the question if they could represent individual skeletons of a colonial Protozoan (Figure 8).

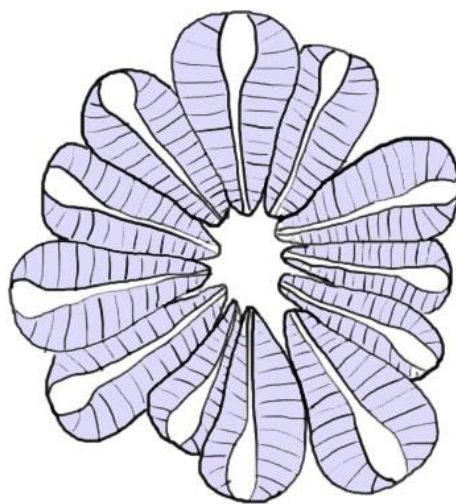


Figure 8: *Nannoconus colomii* forming a rosette based on reported observation by Tréjo (1960).

Nannoconids can be a good biostratigraphic tool if coccoliths are lacking or are poorly preserved. Their temporal range is from Tithonian to Campanian (Deres and Achéritéguy, 1980), but the ranges of the different species are distinct and overlapping. The *Nannoconus* species with narrow axial canals appeared first. Then, during the early Aptian, an event called ‘The *Nannoconus* crisis’ happened simultaneously as the Oceanic Anoxic Event 1 (OEA1) (Silva et al., 1999). Interestingly, the *Nannoconus* crisis seems to have happened synchronously with large scaled volcanic eruptions in the Pacific Ocean during the early Aptian (Erba, 1994). A theory proposes that higher CO₂ levels developed in the atmosphere due to the eruptions and possibly joined with changes in nutrient levels in the surface waters caused the *Nannoconus* crisis (Erba, 1994).

During this crisis, the narrow axial canal-species faded out and got extinct, and the wide axial canal-species evolved and took over. This created an interesting and overlapping interval for biostratigraphy in the Lower Cretaceous. Since the studied samples in this thesis are of Upper Cretaceous age, *Nannoconus* is not used for biostratigraphy, and will not be discussed further.

2.3.2. Coccolith Function and Morphology

Generally, most calcareous nanofossils are clear analogues to the living haptophyte algae of the sub-group coccolithophores. A coccolithophore (Figure 9) is a single-celled golden-brown marine alga, which is protected by calcareous plates (3-15 µm in diameter) called coccoliths (Figure 9) (Armstrong and Brasier, 2005). The cell is round to oval and ranges from 10-50 µm in diameter. The cell wall has pectin structures (polysaccharides) that form a hard layer on the outside. This layer has 10 to 30 coccoliths embedded in it (if it is thick) or resting on its surface (if it is thin) (Bigot, 1985). The coccoliths may be somewhat separated or adjoining. If they touch, they are either united or partially imbricating. The coccoliths that connect are called a coccosphere. The function of the coccoliths is still uncertain. Theories include protection of the cell from zooplankton, virus and bacteria as well as flotation- and light-regulation.

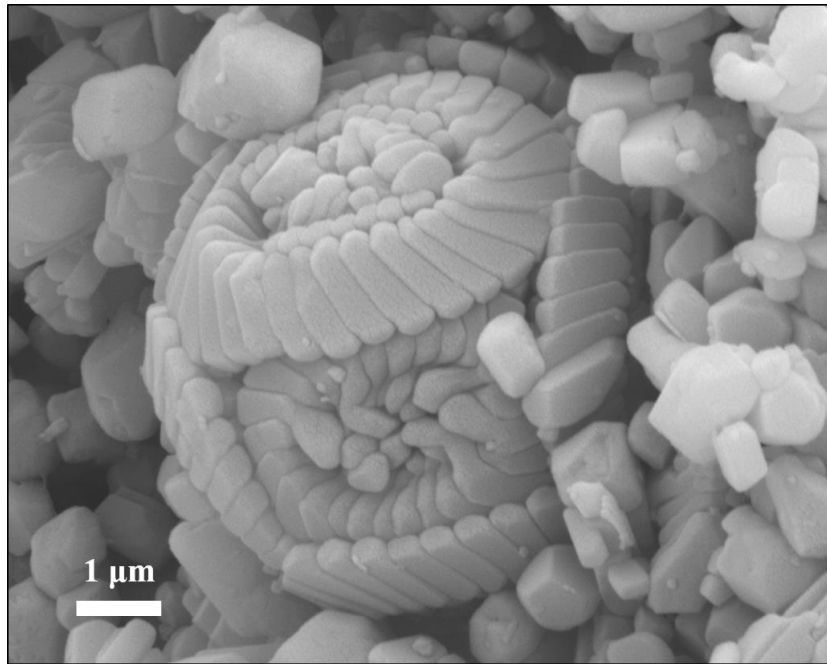


Figure 9: A complete coccolithophore in sample SK1. The shields that protect the single cell in the center are called coccoliths.

Coccolithophores are phytoplankton that require sunlight for their photosynthesis and are therefore found in the photic zone/surface waters (0-200 meters depth, but usually 0-80 meters). The assemblage of coccolithophores at various depths is therefore corresponding to the climate. Water stratification, salinity and variation in nutrients (such as upwellings) also heavily influence the assemblage composition. Various species of living coccolithophores have been proven to have very different temperature tolerance ranges, from 1-31° C for the most tolerant, to 20-30° C for the least tolerant (McIntyre et al., 1970).

Generally, the lighter species live in the upper photic zone and the heavier in the lower photic zone, based on their size and weight (Erba, 2004). The depth of the nutricline (layer in the ocean where the nutrient levels rapidly decrease with increasing depth) might therefore favour certain species over others, and a shift of the nutricline might alter the assemblage composition, as proposed by (Erba, 2004). Different nutrient conditions; oligotrophic (low), mesotrophic (moderate) or eutrophic (high) benefit different species. The majority of species live in marine oceans, although a few are adapted to fresh or brackish waters (Armstrong and Brasier, 2005).

When a coccolithophore dies, the coccoliths fall off and start to sink towards the ocean bottom. With depth, the coccoliths tend to break into finer pieces or dissolve. The calcite-compensation depth (CCD) combined with the water composition will largely control how well preserved the

coccoliths are when they reach the bottom. Until ~1000 metres depth, the coccoliths are generally well-preserved. If sinking deeper than this, the delicate nannofossils will start to break and dissolve, and the recognizable assemblage at the bottom will not reflect the true original nannoflora (Armstrong and Brasier, 2005). This is a crucial fact to keep in mind when interpreting assemblages in terms of paleoecology and paleoceanography – the calcareous nannofossils that are found in chalk samples are the robust ones that survived the way down the ocean column. Less robust species might have been lost, but nevertheless have been very important constituents of the original nannoflora. Other challenges are overgrowth and recrystallization of calcareous nannofossils, which might conceal important morphological details and make certain species unrecognizable.

The taxonomic division of calcareous nannofossils is based on the morphology of the coccoliths that protected the cell. Two basic ways of how a coccolith is constructed are known today, which can divide them into two main types: the heterococcoliths and the holococcoliths. Holococcoliths are formed from calcite crystals of uniform sizes and forms, while the crystals of the heterococcolith are of different sizes and forms. These structures can be distinguished using an electron microscope. In the samples studied in this thesis, only two genera of holococcoliths were encountered (*Calculites* and *Lucianorhabdus*), and since they are of less importance in terms of biostratigraphy and paleoecology – the construction of holococcoliths will not be discussed further. However, an interesting note is that studies (Parke and Adams, 1960; Geisen et al., 2002; Houdan et al., 2003) indicate that holococcolithophores might in fact be a stage-form in the life of heterococcolithophores, and not individual organisms, as previously thought.

To presume with a different type of shape-classification of heterococcoliths, some coccolith terms must be explained. The coccolith is composed of an outer and an inner part, whereas the inner part is somewhat immersed. The outer part is called *the rim*, and the inner part is called *the central-area* (Figure 10). A ring of crystals is called a *cycle*. The rim is characterized by regular cycles formed by outward and upward growth, while the central-area is formed by inward growth and is enclosed by the rim but has less regular cycles. A coccolith can have several well-developed shields. The *proximal* shield is directed towards the centre of the cell, while the *distal* shield is directed towards the outer surface (Figure 10).

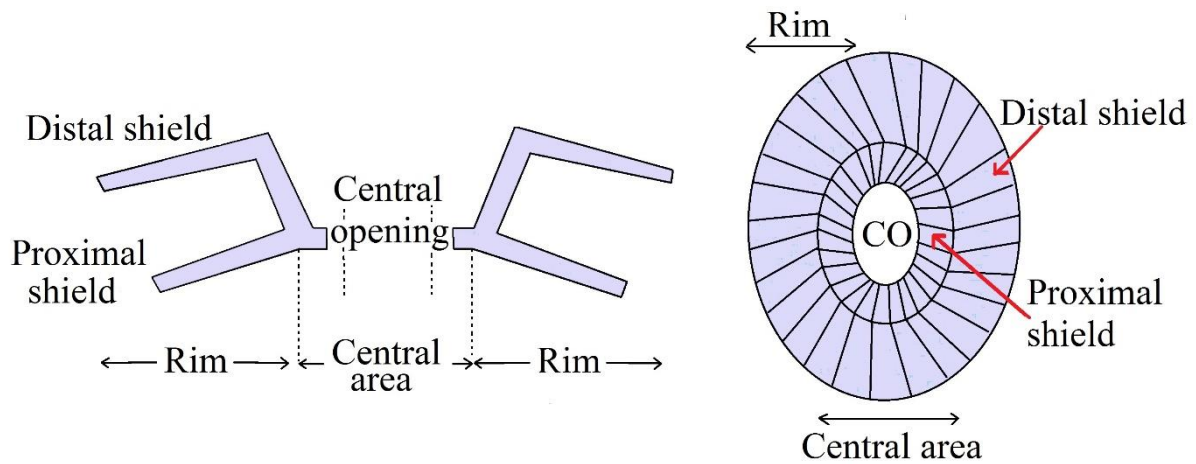


Figure 10: Coccolith terminology, redrawn and modified from Young et al. (2016).

Coccoliths consist of crystal units that can be divided into two groups: *V-units* (vertical-units) and *R-units* (radial-units) (Figure 11). They are groups of elements “from different cycles in crystallographic continuity” (Young et al., 2016). These are important components of a coccolith and can be a strong pointer for further identification. When one V-unit and one R-unit are put together, the complete piece is called a *segment*. The segment can be divided into different elements; the mid tube element, the distal shield element, the inner tube element and the proximal shield element. The taxonomic descriptions of coccoliths in Appendix 3 rely on these terms.

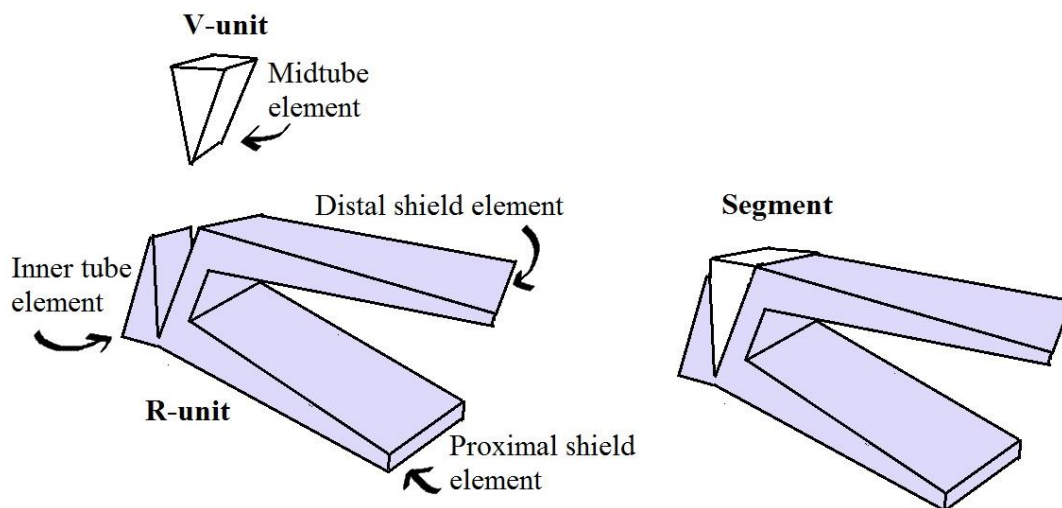


Figure 11: R- and V-units and segment. Redrawn and modified from Young et al. (2016).

In the polarization microscope, it is possible to distinguish between a *placolith* and a *murolith*. A *murolith* is a heterococcolith with an elevated rim but without well-developed shields (Figure

12A), while a placolith is a heterococcolith with two or more well-developed shields (Figure 12B).

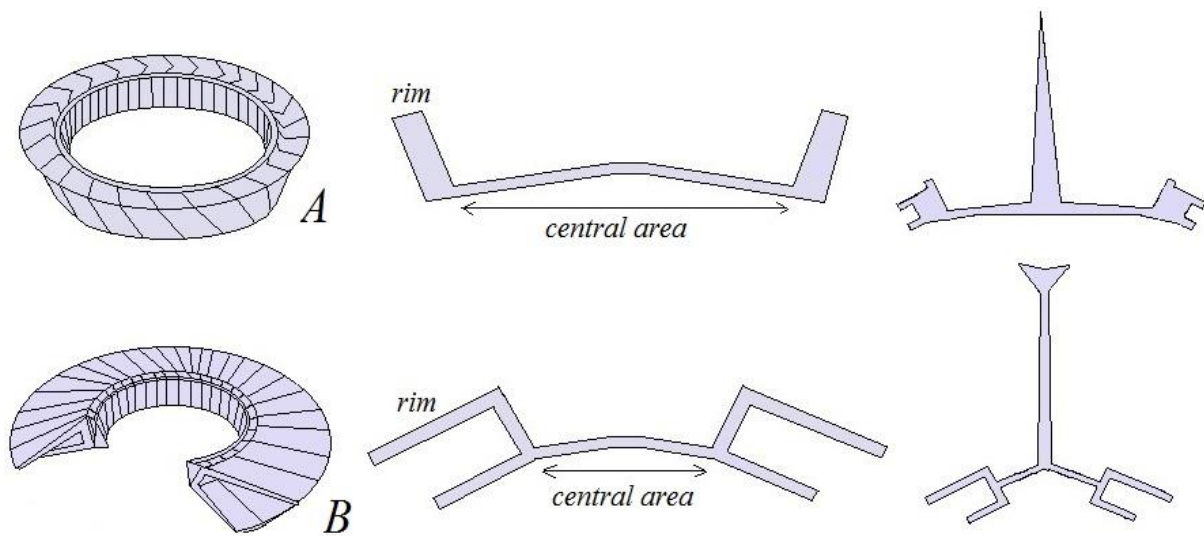


Figure 12: From left to right: 3D sketch, simplified cross-section without spine and cross-section with spine. A: murolith, B: placolith. Redrawn and modified after Young et al. (2016).

2.3.3. Nannolith Morphology

Nannoliths are calcareous nannofossils of unknown affinity that do not resemble heterococcoliths or holococcoliths. Their morphologies vary significantly from family to family, and includes shapes such as: rods, rays, arrowheads, horseshoes, stars, pentagons and rosettes to name a few. The taxonomy of nannoliths are based on their shapes, number of elements and their arrangement. Some examples are pentagonal-shaped *Braarudosphaera* (Figure 13a), rod-shaped *Lithraphidites* (Figure 13b), rod-shaped and chequered extinction-patterned (explained in Chapter 2.5.3) *Microrhabdulus* (Figure 13c), rosette-shaped *Eprolithus* (Figure 13d), rosette-shaped *Lithastrinus* (Figure 13e), stellate to cubic-shaped *Quadrum* (Figure 13f) and cubic-to-flower-shaped *Micula* (Figure 13g).

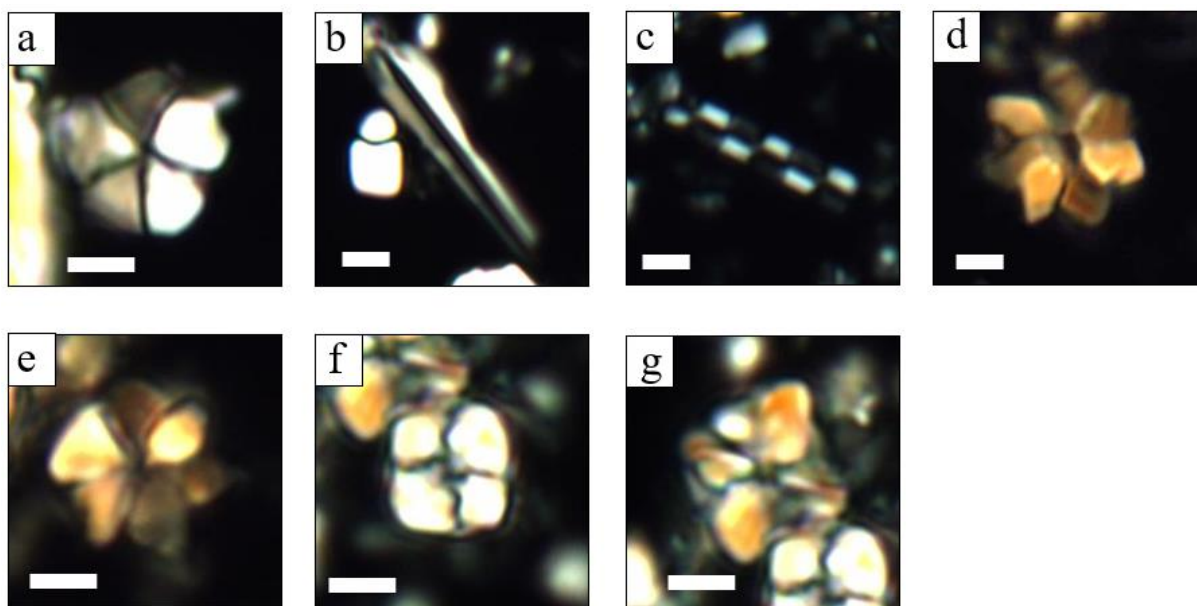


Figure 13: Various nannoliths with different shapes. a: *Braarudosphaera bigelowii* small in sample L5; b: *Lithraphidites* sp. in sample A5; c: *Microrhabdulus decoratus* in sample MS1; d: *Eprolithus moratus* in sample K1; e: *Lithastrinus grillii* in sample MOV1; f: *Quadrum gartneri* in sample MS1 and g: *Micula staurophora* in sample MS1. White scale bar = 2 μ m.

2.3.4. Paleocological Implications

The evolution of calcareous nannofossils and their assemblages at different localities in the world at different times rely on the three main autoecological factors: light, nutrient availability and temperature. Some species might be favoured to others depending on these factors. For example, if one species thrives in cold and nutrient-rich waters, it might not be able to survive if an influx of warmer waters with fewer nutrients proceeds. If the temperature rises in the surface waters, the calcareous nannofossil assemblage in this location would change. Therefore, changes in the assemblage compositions can be studied to highlight changes in paleoecology, paleoceanography and paleoclimate in the past (Mutterlose et al., 2005). However, it is important to consider the preservation state of the chalk sample, as a poor preservation means that the calcareous nannofossil assemblage will not reflect the true original nannoflora and will have a limited usage as a paleoecological indicator of the paleoceanic conditions.

Some calcareous nannofossil species are cosmopolitan, meaning that they can be found in habitats globally. One example is *Watznaueria barnesiae*, that must have handled a broad temperature range since it has been found in both low and high paleolatitudes. Cosmopolitan species allow global correlation and are the best biostratigraphic marker species. Other

calcareous nannofossils might be endemic, which means that they are limited to certain geographical regions. One example of an endemic species is *Kamptnerius magnificus*, that typically inhabited high latitude, cold waters (Lees, 2003).

Ecologically stable ocean conditions today, for example warm oligotrophic surface waters in low latitudes, typically generate a nannoflora with a high diversity (McIntyre and Bé, 1967; McIntyre et al., 1970; Brand, 1994). Contrarily; unstable and stressed ecological conditions, such as cold surface water with high nutrient levels in high latitudes, favour low diversity assemblages (Okada and Honjo, 1973; Brand, 1994). If today's nannoflora is an analogue for the Mesozoic nannoflora, it can be assumed that the same trends were likely during the Mesozoic.

Nutrient supply is another factor that might be reflected from calcareous nannofossil assemblages. Certain species, such as *Biscutum constans* and *Zeughrabdotos* species (especially the smaller forms), indicate high nutrient levels according to some authors, such as an upwelling of cold nutrient-rich water to the surface (Roth and Bowdler, 1981; Roth and Krumbach, 1986; Watkins, 1986; Erba, 1987; Watkins, 1989; Erba, 1992; Erba et al., 1992; Corbett and Watkins, 2013). *Watznaueria barnesiae*, even though it could survive in both high and low nutrient levels, seems to have preferred lower nutrient levels (Herrle, 2003; Watkins et al., 2005; Hardas and Mutterlose, 2007). Other low-fertility preferring species might have been *Eiffellithus* sp., *Prediscosphaera* sp. (excluding *Prediscosphaera stoveri*) and *Lithraphidites* sp. (Erba et al., 1995; Linnert and Mutterlose, 2013; Mandur, 2016).

Temperature is closely connected to latitudes, and various species have been proposed as temperature indices. Species that have been associated to high latitudes and cold waters are *Lucianorhabdus cayeuxii*, *Lithraphidites carniolensis*, *Staurolithites stradneri*, *Eprolithus floralis*, *Repagulum parvidentatum*, *Microrhabdulus decoratus*, *Reinhardtites levis*, *Arkhangelskiella cymbiformis* and *Prediscosphaera spinosa* (Roth and Krumbach, 1986; Bralower, 1988; Wise Jr, 1988; Erba, 1992; Erba et al., 1992; Herrle and Mutterlose, 2003; Herrle et al., 2003; Thibault and Gardin, 2007; Tiraboschi et al., 2009; Mandur and El Ashwah, 2015). Species associated to lower latitudes and warmer waters are *Watznaueria barnesiae* and *Braarudosphaera bigelowii* (Thibault and Gardin, 2007). *Braarudosphaera bigelowii* has also been reported as an indicator of lower salinity, as it is one of the most dominant Holocene coccoliths in the Black Sea (Bukry, 1974).

If a sample has a dominance of dissolution-resistant species, such as *Watznaueria barnesiae* and *Micula staurophora* – it might be an indicator of poor nannofossil preservation and diagenetic alteration (Thierstein, 1981; Roth, 1983; Moshkovitz and Eshet, 1989; Eshet et al., 1992; Eshet and Almogi-Labin, 1996; Faris and Abu Shama, 2006; Mandur and El Ashwah, 2015).

Micula staurophora has been reported to have been significant in Coniacian to Maastrichtian assemblages, even overriding *Watznaueria barnesiae* in abundance in some locations (Eshet and Almogi-Labin, 1996), and during the Maastrichtian the species diversified. Lees et al. (2005) suggested that there likely were environmental changes responsible for these blooming-episodes and the diversification during the Maastrichtian. A predominance of *Micula sp.* must be a response to certain paleoecological conditions, and might have paleoecological value, but so far these conditions favoring *Micula sp.* have not been detected.

Some authors are critical to expanding certain nannofossil proxy measures of paleoecology to be valid for a variety of paleoenvironments and to assume that what works as a proxy during one time-interval can also be applied without problems to another time-interval (Lees et al., 2005). It is important to be aware of pitfalls of paleoecological proxies – what might seem to be an obvious response in one species to a paleoenvironmental change, might have other plausible paleoecological explanations.

The next big step in achieving a better understanding with more precise measures for paleoecological nannofossil indices is to be able to geochemically characterize individual taxa, and to hopefully discover new nannofossil indices. This frontier-work has been designed by Lees et al. (2005). However, until this new program has been developed and proven useful, the current knowledge of paleoecological indices is the only approach for interpreting assemblages in terms of paleoecology.

2.4. Calcareous Nannofossil Evolution

2.4.1. Triassic

Triassic nannofossils were first well-documented and published by Moshkovitz (1982). Triassic nannofossil-like objects had been reported prior to Moshkovitz' publication, for example by Gumbel (1870), but were highly doubtful and had different measurement, structures and compositions and therefore unlikely to be familial to species in the Jurassic (Bown, 1998).

Nannofossils have also been proven to easily contaminate older sediments (Bown, 1998), for example Jurassic coccoliths sourcing sediments of Devonian- and Pennsylvanian ages (Nöel, 1965).

After Moshkovitz' report from 1982 followed several reports that assured the existence of Triassic nannofossils, such as the earliest very small coccoliths ($< 2 \mu\text{m}$), diverse calcispheres and nannoliths. The Triassic nannoflora is characterized by low diversity but abundant assemblages, from low paleolatitude sites of Upper Triassic age. Bown (1998) observed no nannofossils in high paleolatitudes and concluded that they did not migrate north until the Jurassic. Except for an important bioevent at the Triassic/Jurassic boundary, where all but a few species got extinct, Triassic nannofossils have not proven to be of high biostratigraphical value yet. This might be due to the lack of rich Triassic nannofossil sites, meaning that there is still potential to yield new insight if richer sites are discovered. The Triassic has so far been divided into two biozones by Bralower et al. (1991) (Bown, 1998).

Erba et al. (2013) investigated samples from China (Wusha samples) and documented what is believed to be the oldest calcareous nannofossils: Middle Triassic. They conclude that further analyses are necessary.

2.4.2. Jurassic

The Jurassic period was the first to be described and divided stratigraphically (d'Orbigny, 1842-1951; Opperl, 1856-1858). Although ammonites still provide the best biostratigraphic resolution of the Jurassic, calcareous nannofossils are useful where ammonites are lacking.

After the extinction event at the Triassic/Jurassic boundary, calcareous nannofossils inhabited all open-marine environments, as well as higher paleolatitudes. Only one coccolith species is known to have survived the extinction event, and nannoliths were therefore dominating lower Jurassic successions. In the Pliensbachian stage, coccoliths diversified and new coccolith morphologies evolved and started to dominate the assemblages. The family *Watznaueriaceae* evolved in the Late Pliensbachian and rapidly started to dominate assemblages. In the Callovian age, the genus *Watznaueria* became the most dominant, and kept its dominance into the Cretaceous (Bown, 1998).

During the Jurassic, coccolithophores evolved into the most abundant calcareous nannofossil group, and towards the end of the period, calcareous nanнопlankton produced “biogenic carbonate in rock-forming proportions” (Bown et al., 1992; Bown, 1998).

Various environmental perturbations severely affect and disturb calcareous nanнопlankton communities. OAEs are global events characterized by deposition of organic material and less carbonates. Since calcareous nanнопlankton were so abundant and widespread in the Jurassic and Cretaceous oceans, the characterization of the calcareous nannofossil assemblages in OAE intervals can provide important insight into how the marine ecosystem and biological processes responded to such perturbations (Erba, 2004). One such event, which might be considered as one of the most dramatic of the Mesozoic era, is the early Toarcian Oceanic Anoxic event (T-OAE) that lasted 500 ky (Hesselbo et al., 2000). This OAE is characterized by a negative $\delta^{13}\text{C}$ shift and the deposition of carbon-rich black shales. The negative $\delta^{13}\text{C}$ shift has been interpreted to be due to greenhouse climatic conditions and the consecutive release of methane (Hesselbo et al., 2000; Beerling et al., 2002). The T-OAE resulted in a speciation of species, and according to Erba (2004), it favored lighter coccoliths living in surface waters over deeper species living in the photic and oligotrophic zone, such as the nannolith *Schizosphaerella*, which experienced a decrease in abundance. Erba (2004) suggested that during the T-OAE, a change in the depth of the nutricline from deep to shallower induced the decrease of nanнопlankton living in the photic zone and increased the abundance of nannofossils living in the euphotic zone. This could explain why coccolithophores diversified and established themselves as the dominant nannofossil group during the Jurassic (Bown, 1998).

2.4.3. Lower Cretaceous

Early Cretaceous followed the same trend as the late Jurassic, with evolution of new coccoliths and nannoliths. Nannofossils continued to populate larger areas geographically, and there was a steadily diversity increase throughout the Cretaceous. Common early Cretaceous nannolith groups, such as *Nannoconus*, *Braarudosphaera*, *Lithraphidites*, and *Polycyclolithaceae* (*Micula*) were first thought to have appeared in the beginning of the early Cretaceous, but a study by Bralower et al. (1989) indicated they in fact probably appeared during the Tithonian. Rarer families or families that had been near extinct from the Jurassic suddenly bloomed and became more dominant in the Cretaceous, but with uncertain exact timing. *Watznaueria* continued to be the dominant genus, but there was a transition from *Watznaueria britannica* to *Watznaueria barnesiae* being the most abundant species of the genus (Bown, 1998).

The early Cretaceous experienced two OAEs with global consequences for the nannoflora. The first one happened in the early Aptian (OAE1a) and coincides with the onset of the middle Cretaceous greenhouse climate, and the latest Cenomanian (OAE2) coincides with the climax of this climate, which is the warmest for the last 150 million years (Erba, 2004).

During the OAE1a, one genus was particularly affected. The “Nannoconid crisis” has been documented to have happened simultaneously worldwide (Bralower et al., 1993; Bralower et al., 1994; Erba, 1994; Bralower et al., 1999; Erba, 2004; Erba and Tremolada, 2004), as described in Chapter 2.3.1. Before the crisis, the conditions favoured narrow-canal Nannoconids, due to a deeper nutricline. During the OAE, the deposition of black shale led to a decrease in the overall abundance of *Nannoconus*. After the crisis, the nutricline rose, favouring wide-canal *Nannoconus* and coccoliths. There were no extinctions due to the OAE1a, but the change in environmental parameters led to a speciation of species and changes in morphologies (Erba, 2004).

The beginning of OAE2 activated a decrease in total abundances and species richness, as well as a decrease in fertility indicative species. Cooler oceans followed in the late OAE2 due to a reversed greenhouse effect (Clarke and Jenkyns, 1999; Jenkyns, 1999), leading to a period following with low species richness (Erba, 2004).

2.4.4. Upper Cretaceous

The upper Cretaceous lithologies, with chalks and marls being the most characteristic, are the most widespread geographically and the best-preserved lithologies of the Mesozoic. High sea-levels provided ocean pathways, giving the calcareous nannofossil taxa access to flourish and spread globally. Due to its high porosity, chalk can be excellent petroleum reservoirs, and therefore the petroleum industry (especially with the upper Cretaceous Norwegian chalk reservoirs in thought) has pushed research on the biostratigraphic value of calcareous nannofossils (Bown, 1998).

Upper Cretaceous followed the same trend as the late Albian had seen, with diversity increase. *Arkhangelskiales* and *Prediscosphaera* became more diverse and abundant and are characteristic of upper Cretaceous assemblages. During the Coniacian, *Micula* had its first occurrence and evolved and eventually even became more abundant than *Watznaueria* which had dominated assemblages since the Jurassic. *Zeugrhabdotus* and *Rhagodiscus* declined in abundances. During Santonian, *Calculites* became a significant constituent of assemblages.

Campanian saw many first occurrences, but few last occurrences of species, with an exception of *Nannoconus* that got extinct. During Maastrichtian, *Reinhardtites* and several *Biscutum* species got extinct (Bown, 1998).

2.4.5. Cenozoic

The Mesozoic/Cenozoic boundary is the most severe and global event in the history of calcareous nannofossils, as the extinction event caused a reduction of 92 % in diversity (Bown et al., 1991) and 99 % in abundances (Pospichal, 1994). This extreme reduction left only a few Mesozoic survivors, such as *Braarudosphaera*, *Biscutum* and *Watznaueria* (Bown, 1998).

Following the extinction event, the diversity rose again and reached a maximum in the Eocene. New groups, such as the radiate nannolith *Discoaster* had their first occurrences. Towards Pliocene, both coccoliths and *Discoaster* decreased in numbers, and at the end of the Eocene, *Discoaster* got extinct. (Bown, 1998).

Quaternary calcareous nannofossils reached a maximum again and provided a high biostratigraphic resolution due to several first and last occurrences of species. The Quaternary experienced several episodes where one species flourished and constituted up to 90 % of the total nannoflora (acme episode). One example is the domination of *Emiliana huxleyi*, which started its last acme episode eight thousand years ago, and is still dominating today's nanoplankton assemblages (Bown, 1998).

2.5. Optical light microscopy (OLM)

2.5.1. Components of the Light Microscope

A light microscope is a type of microscope that utilises visible light and a system of lenses to project a magnified image of a specimen onto the eye, or if connected with a digital camera – onto a computer screen. The most important components of a light microscope are the objective lens (above the specimen) and the condenser lens. The condenser lens focuses the light from the illuminator source onto an area of the specimen, while the objective lens collects the light diffracted by the specimen and magnifies it into a visual image at the oculars. Most light microscopes have several objective lenses on a thumb-wheel that can be rotated to give different magnifications.

Other components are oculars/eyepiece (lens near the eyes of the observer), rotational stage with lock control, slide holder with graduated locator markings, lamp collector and socket, filters and polarizers (Figure 14). The microscope components are complex, and the optical path must be very precisely set up and controlled for the microscope to work the best.

The light microscope is a compound microscope, which means that it uses at least two lenses to produce the magnified image. Each of these lenses might be made up of several lenses again. It is the combination of magnification of the objective lens and the eyepiece oculars that gives the final magnification, given as:

$$M_{\text{final}} = M_{\text{objective}} \times M_{\text{oculars}}$$

Common eyepiece oculars might have a magnification of 10x or 12.5x, while the objective lenses could be 5x, 10x, 20x, 40x and even 100x – giving final magnifications up to 1250x, which is close to the maximum resolution of light microscopy, being half of the wavelength of the visible light (0.390-0.700 μm). When objects smaller than 0.26 μm (theoretical limit for green light) must be observed, light microscopy cannot be used anymore. Then wavelength smaller than 390 nm is needed, and the electron microscope takes over.

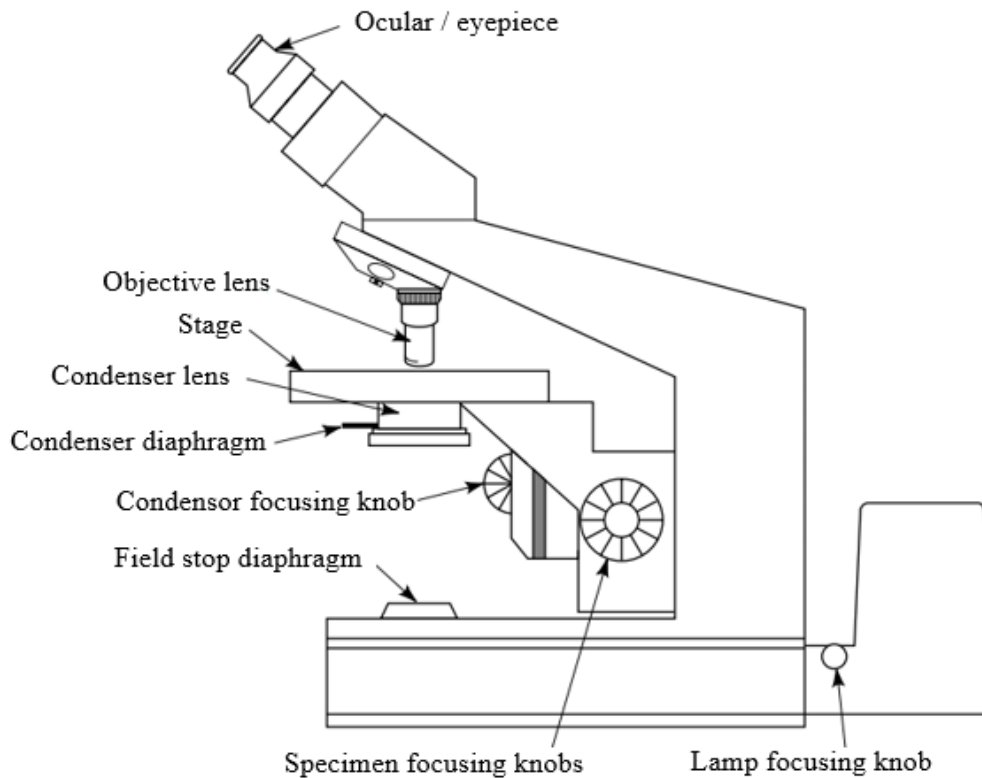


Figure 14: Illustrative sketch of the main components of a light microscope. Modified from Murphy (2001).

Figure 15 illustrates how the oculars and the objective are producing a magnified image of the specimen that is perceived by the eye. To put it simply, the objective lens works as a magnifying glass with a very short focal length, giving it greater optical power. The objective is placed so close to the specimen, that the light from the specimen comes to focus inside the microscope tube and produce a magnified real intermediate image of the specimen in the oculars. To bring the specimen to focus, the stage is moved up or down by turning a thumb wheel (for an inverted microscope, the stage is fixed and the objective is moved up or down). The lenses focus the minutely separated light rays from the small specimen and spread them apart, so they appear as an enlarged image. If a digital camera is connected to the light microscope – the magnified real intermediate image of the specimen is recorded directly onto a computer screen. If the specimen is observed by the eyes, the oculars together with the eyes project a second real image, called the real final image, onto the retina (the back of the eye on the inside) to be interpreted by the observer. The virtual image is formed due to perspective and is the observer's brain's interpreted image in front of the eye.

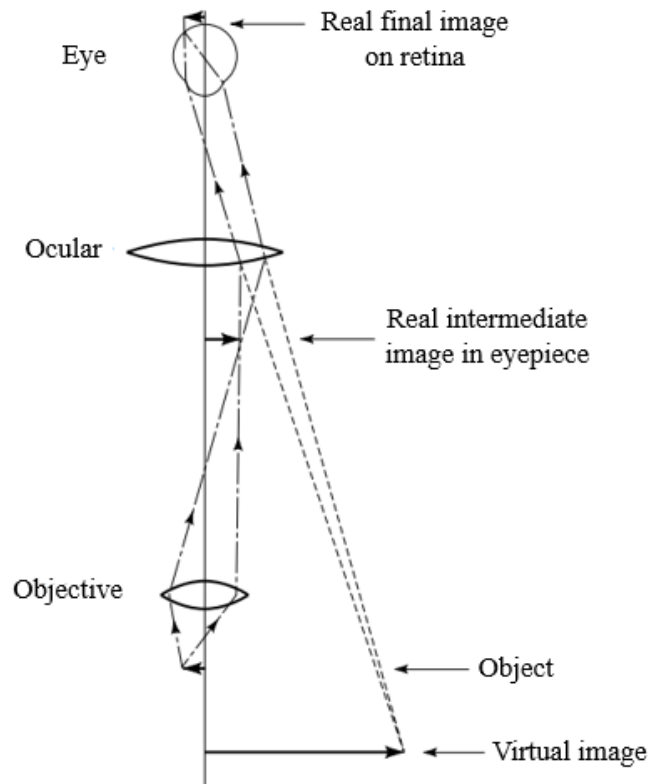


Figure 15: Sketch displaying how the system of lenses are producing a virtual image of a specimen in the light microscope. Modified from Murphy (2001).

2.5.2. Oil Immersion Technique

The oil immersion technique is used to increase the numerical aperture of the objective and the resolution. The smear slide is placed in the mechanical stage, and a drop of immersion oil is carefully placed on an area of interest in the slide. The objective lens is set directly above the oil drop and lowered until the oil drop is immersing both the lens and slide (Figure 16). When observing the sample through the oculars and using the fine focus control, the specimen can be brought to focus.



Figure 16: Oil drop between the objective and the smear slide to increase the numerical aperture and the resolution.

In microscopy, numerical aperture (NA) describes the acceptance cone of an objective, which means the amount of reflected light rays it can gather. The formula is:

$$NA = n \sin \theta$$

where n is the index of refraction, and θ is the half-angle of the maximum cone of light that can enter or exit the objective lens.

The index of refraction is the amount of diffraction of the light and depends on the physical properties of the medium that the light passes through. For dry objectives, this means that the light needs to pass through an air gap before reaching the specimen. Most microscope slides have a refractive index of 1.5, whereas air has a refractive index of 1.0. Since light refracts (bends and scatter) when passing from one medium to another, this means that some of the light will undergo refraction in the air-smear slide interface, and some rays of light will miss the objective and this information will be lost. By replacing the air gap with immersion oil with a refractive index of around 1.52 (similar as glass and therefore optically very similar), the refraction will be lowered. The resolution of the objective and its numerical aperture will be improved, and it can be possible to identify calcareous nannofossils.

2.5.3. Optical Properties of Calcareous Nannofossils

In the light microscope, structural and crystallographic information about the calcareous nannofossils can be obtained. Even though the electron microscope with its high-resolution revolutionized the way calcareous nannofossils were studied in the 1950s, the light microscope

remains the most useful observational instrument for routine studies and industrial work. With the correct settings, it can be possible to observe morphological features that allow identification down to a species level. Since the nannofossils are so small that they are close to the limit of light microscope resolution, it is important to have high quality optics. A x100 oil-immersion objective lens is essential together with a good condenser and cross-polarization illumination (Bown, 1998).

A mechanical stage is needed when working with a x100 lens, so that the slide movement can be controlled mechanically, and the covered length can be noted. The stage must be rotatable to allow observation of extinction patterns. The eyepiece oculars should preferably be x12.5 to allow combined magnification of x1250 to gain the optimal nannofossil observation (Bown, 1998).

The most useful transmitted light techniques are plane-polarized light (for crystallographic and morphological features and for low birefringence nannofossils), cross-polarized light (essential for identifying many nannofossils using extinction patterns and birefringence) and cross-polarized light with a gypsum plate (further crystallographic orientation information) (Bown, 1998).

2.5.4. Polarized Light

Polarized light is light waves that have a specific geometrical orientation of the oscillations. Most microscopes have an illuminator source with unpolarized light, meaning that the light waves from this source vibrate in all possible angles with respect to the axis of wave propagation. When a polarizing filter is slot in front of the illuminator source, only the light waves with one specific vibration angle can pass through the filter, and all the other waves are blocked. Crossed-polarized light is produced when the polarizing filter is inserted 90 degrees in respect of the analyser, which is another polarizing filter that is normally fixed in place between objective lens and oculars.

Calcareous nannofossils are composed of calcite crystals that have optical axes that are oriented differently. The crystals are arranged in cycles. Because of this organization of crystals, crossed-polarized light is very useful when studying calcareous nannofossils. When a crystal's optical axis is oriented parallel to the oscillation direction of the polarized light and they coincide – the crystal will appear isotropic (extinct) and be dark. When rotating the stage 360 degrees, each crystal will become extinct four times, with 90 degrees increments. This causes

different calcareous nanofossils to have distinct *extinction-patterns* consisting of dark lines (*isogyres*) or areas, where placoliths and muroliths show different patterns.

The extinction-figure consist of dark lines (*isogyres*) caused by elements being extinct. Both placoliths and muroliths have four of these lines, creating a cross. When rotating the stage, the cross will rotate simultaneously. The typical extinction-figure for a placolith has curved isogyres as shown in Figure 17a, while for a murolith the isogyres are often less curved as shown in Figure 17b. The smallest angle between two extinction arms will typically be wider and more curved for a placolith than for a murolith. Placoliths can have angles up to 90 °.

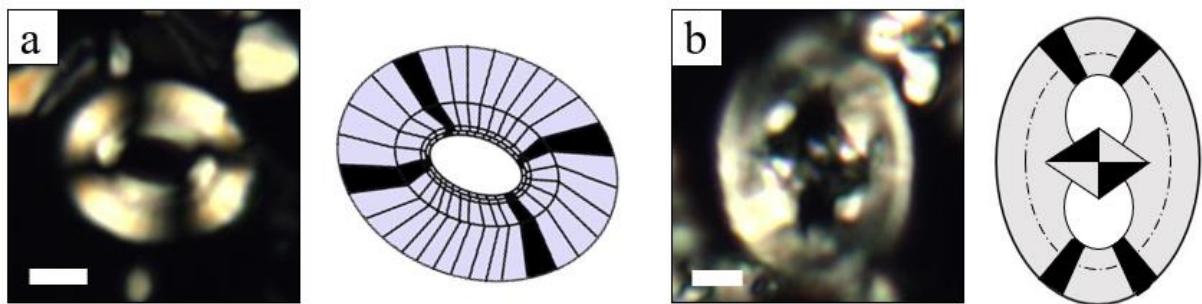


Figure 17: Typical extinction pattern for a: A placolith seen on a *Watznaueria fossacineta* in sample MT1, and b: A murolith seen on *Reinhardtites anthophorus* in sample MON1. White scale bar = 2 μm .

For nannoliths, the extinction-figures can be quite variable. For nannoliths with simpler structures, for example the pentagonal *Braarudosphaera bigelowii*, one-to-two triangular plaquette go extinct at a time, while the more complex species *Microrhabdulus decoratus* displays a chequerboard extinction-pattern (Figure 18).

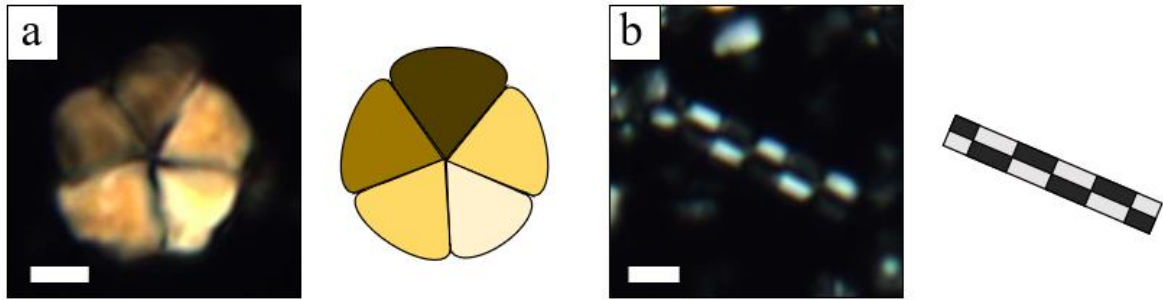


Figure 18: Nannoliths with different extinction-patterns. a: *Braarudosphaera bigelowii* with one-to-two plaquettes close to extinction and b: *Microrhabdulus decoratus* with chequerboard extinction-pattern. White scale bar = 2 μm .

2.5.5. Birefringence, Interference Colour and Gypsum Plate

All anisotropic crystals display birefringence or different refraction indices to some degree. Calcite has different refraction indices depending on the orientation, because the crystal is composed internally of arrays of calcium and carbonate ions in different directions in the 3D structure. This causes the anisotropic crystals to display interference colours under crossed-polarized light (Figure 19).

An isotropic crystal, for example sodium chloride, has a perfectly cubic structure giving equal crystallographic axes and the same refraction index in all orientations – and would show zero birefringence and appear black under crossed-polarized light throughout the 360 degrees rotation. The same is valid for glass and causes a black appearing background of smear slides under crossed nicols (Figure 19).

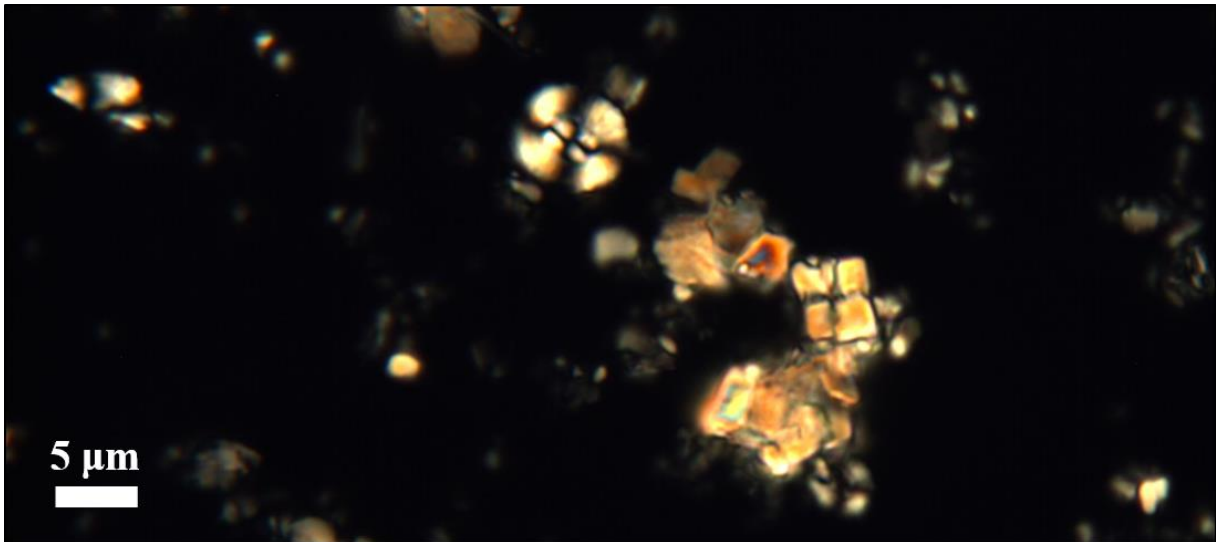


Figure 19: Calcite crystals showing interference colors, while the background composed of glass appears black due to its isotropic nature.

The interference colour depends on the thickness of the crystal, and the amount of birefringence in its specific orientation. Very thin calcite crystals ($< 0.1 \mu\text{m}$) will therefore not display birefringence no matter the orientation. For calcareous nannofossils, interference colours can be used in identification. Some species might show higher birefringence than others, due to certain parts being thicker. For example, one way to quickly distinguish between a *Quadrum* and a *Micula* is to look at the interference colours. *Quadrum* is thinner and therefore appears white-grey, while *Micula* is thicker and displays yellow-orange interference colours (Figure 20a). The thick murolith *Zeugrhabdotus embergeri* is also easily recognized by its extremely strong interference colours (Figure 20b).

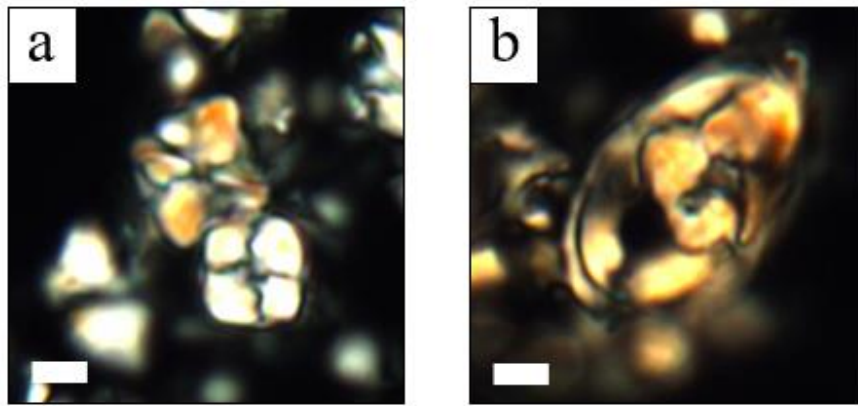


Figure 20: Different species show different interference colors. a: *Micula staurophora* with stronger interference colors than *Quadrum gartneri* in sample MS1 and b: *Zeugrhabdotus embergeri* in sample K5 with its typical strong interference colors. White scale bar = 2 μm .

A gypsum plate can be inserted at an angle of 45 degrees with the polarizing directions, to produce constructive or destructive interference, meaning an increase or a decrease in birefringence colours. Since the gypsum plate retards one wavelength of red light (1λ), first order grey colours produce blue interference colours when constructive, and destructive produces yellows and oranges (Bown, 1998).

Nannofossils will show sectors defined by their extinction lines under the gypsum plate. Elements that belong to the same cycles will display the same colours, which makes it possible to distinguish the narrowest cycles (Figure 21).

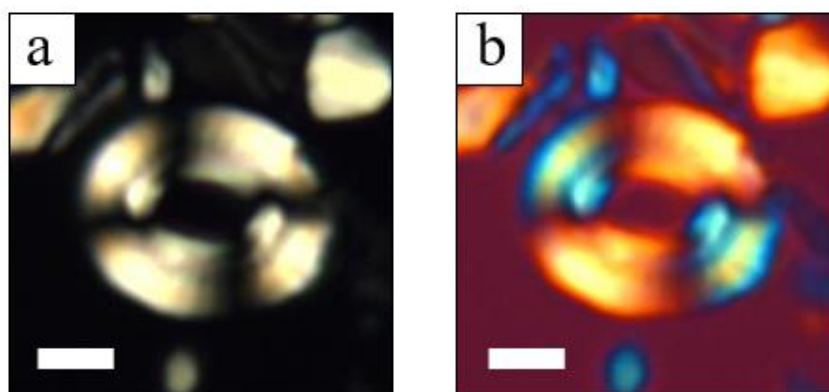


Figure 21: *Watznaueria fossacincta* in sample MT1 under a: crossed nicols and b: crossed nicols combined with gypsum plate. The gypsum plate makes it easier to distinguish the different cycles. White scale bar = 2 μm .

For nannoliths with very simple structures, the gypsum plate can be used to control if there is a consistency of optical orientation of the elements, which allows to differentiate them from inorganic calcite crystals (Figure 22). Inorganic calcite crystals would display random optical orientations of the elements.

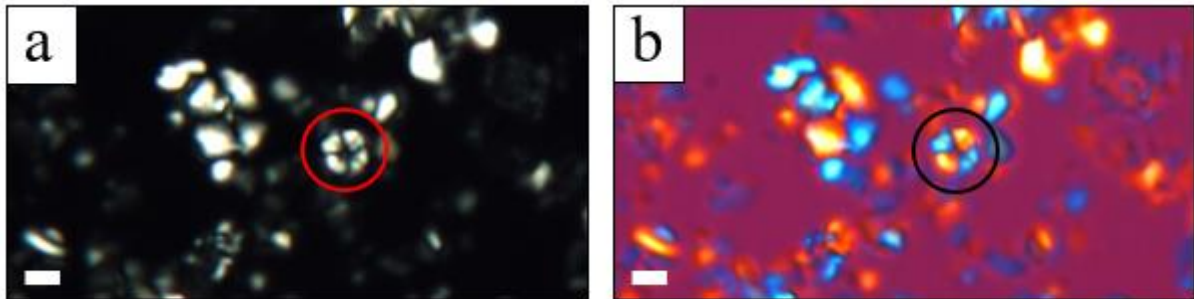


Figure 22: a: When looking under crossed nicols, one might be in doubt if the object in the circle is a calcareous nannofossil or inorganic calcite crystals. b: The gypsum plate can show if there is a consistency of optical orientation of the elements, such as in this case, where two elements are blue and two yellow, in diagonal patterns – in favor to interpret it as a calcareous nannofossil, here in sample MS1. White scale bar = 2 μm .

2.6. Field Emission Gun Scanning Electron Microscope (FEG-SEM)

2.6.1. Introduction

When studying objects that are smaller than the wavelength of visible light, that means smaller than 0.26 μm , the light microscope cannot be used anymore. The light source must be replaced with something else that has a smaller wavelength. The field emission gun scanning electron microscope (FEG-SEM) (Figure 23) is a valuable instrument that uses an electron beam as the “light source” to produce high-resolution images of the surface topography on a micron-scale. The electrons interact with the surface of the sample and produce an image with magnifications as high as up to x100.000. The FEG-SEM is also highly advantageous when studying fresh samples’ surfaces which may not be flat. The depth of field, defined as the distance between the nearest point in focus to the furthest point in focus, is much higher in a FEG-SEM, allowing the high-resolution micrographs. Figure 23 illustrates the main components of the FEG-SEM, and the methodology to use them will be discussed further in Chapter 3.3.

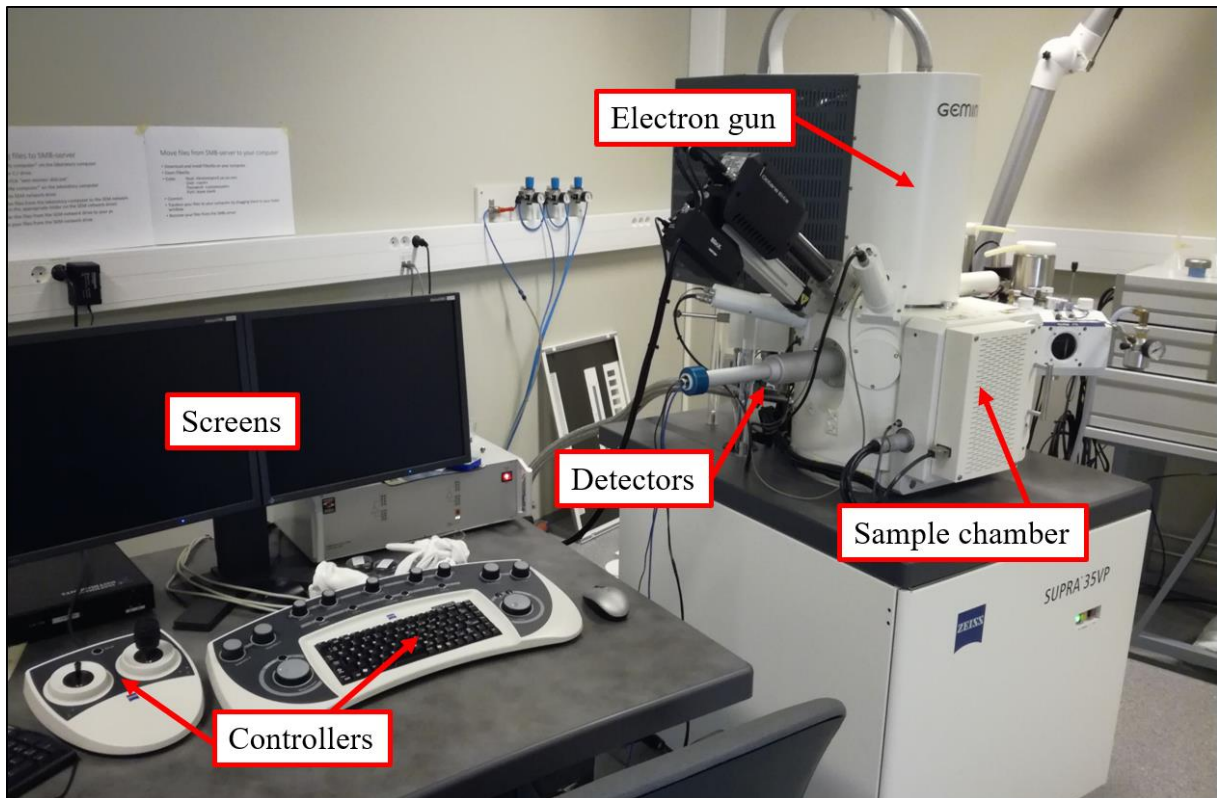


Figure 23: A field emission gun scanning electron microscope (Zeiss Supra 35-VP FE-SEM) at the University of Stavanger with the main components.

Before a sample can be inserted into the FEG-SEM, it must be coated with an electrically conductive material such as gold, carbon or palladium – to avoid overcharging and to ensure a stable flux of electrons. The coating also increases the emission of secondary electrons – which leads to higher image resolution. The procedure of coating is described in Chapter 3.3.1.

2.6.2. Components of the FEG-SEM

When the samples are placed in the FEG-SEM, they get enclosed in a vacuum chamber, because electrons cannot travel far in air. Electrons are accelerated in the electron gun through a potential field and travel through a column of several magnetic lenses (condenser lenses and objective lenses). The lenses focus the thin electron beam before it scans a raster of the sample's surface. A simple sketch of how the scanning electron microscope works is shown in Figure 24:

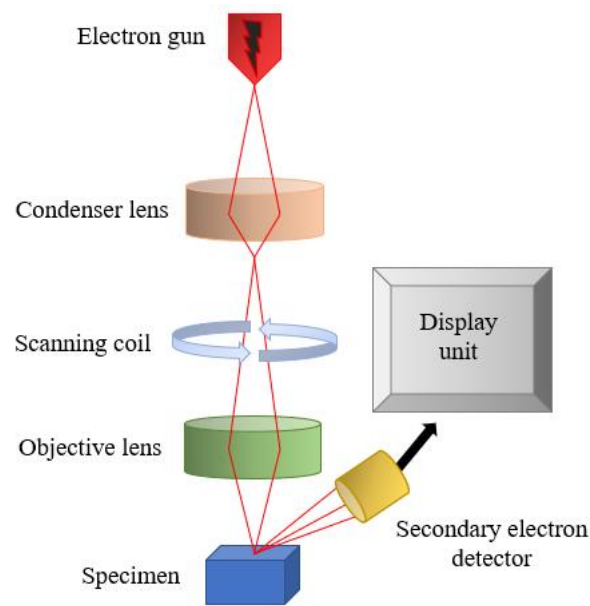


Figure 24: Simplified sketch showing how the electron beam is focused by a set of magnetic lenses, before it scans the surface of the specimen.

When the focused electron beam hits the surface of the sample, several interactions happen which give rise to various signals that can be detected, such as: low-energy ($< 50\text{eV}$) secondary electrons (SE), high-energy backscattered electrons (BSE), x-ray emission, Auger electrons and light of different energies (Hjelen, 1989). Since only the signals from the secondary electrons were used to generate the FEG-SEM-micrographs in this thesis, the other signals will not be discussed further.

The secondary electrons get knocked out of the sample surface by the electrons in the electron beam. When the electrons from the beam reached the atoms in the sample surface, the electrons in the atoms get unstable and might get emitted as secondary electrons. These have lower energy than the electrons in the beam and are a result of inelastic scattering. The depth of how deep the electron beam penetrates the sample and secondary electrons are emitted is dependent on the sample material and how high the acceleration voltage is.

The intensity of secondary electrons varies with the angle that the electrons from the beam hits the surface of the sample. When the sample is tilted (or has a topography), the emission of secondary electrons will be higher. Some of these secondary electrons will be detected and amplified to create the FEG-SEM-micrographs. The micrographs show the samples' topography, based on the detected signal strengths of the secondary electrons.

2.7. IOR Flooding Experiment

Since subsidence due to chalk compaction was discovered in the Ekofisk field during the 1980s (Wiborg and Jewhurst, 1986), the correlation between reservoir chalk properties and pore fluid composition has been of great interest both in academic research and industry (Hermansen et al., 1997; Risnes and Flaageng, 1999; Hermansen et al., 2000; Nagel, 2001; Risnes et al., 2005; Fabricius and Borre, 2007; Wang et al., 2016; Andersen et al., 2017). Flooding experiments with various brines have been carried out on chalks to understand chalk strength and deformation, which changes due to interactions between the chalk and brine and is dependent on the type of chalk and the chemical composition of the brine (Newman, 1983; Hellmann et al., 2002; Madland, 2005; Korsnes et al., 2006; Korsnes, 2007; Korsnes et al., 2008; Madland et al., 2008; Madland and Hiorth, 2011; Nerموen et al., 2015; Wang et al., 2016; Andersen et al., 2017). One major advantage of these experiments is that they have been executed at reservoir conditions in terms of temperature and pressure (Wang et al., 2016; Andersen et al., 2017).

Madland and Zimmermann (2013) concluded that when flooding chalk with a MgCl_2 -brine, carbonate minerals high in Mg precipitated as other minerals dissolved. Wang et al. (2016) measured that the brine was depleted in Mg^{2+} and enriched in Ca^{2+} ions after propagating through the core. FEG-SEM micrographs displayed that significant mineralogical compositional changes occurred during flooding. A notable increase in Mg-rich carbonates or magnesite that was formed on top of pre-existing calcite grains was observed (Wang et al., 2016).

Andersen et al. (2017) executed compaction tests on chalks while injecting a 0.219 mol/L MgCl_2 -brine at reservoir conditions ($T = 130^\circ\text{C}$; 1 PV/d), that lasted 2-3 months. They applied the flooding test to five different chalk samples (A, K, L, MT and SK – studied in this thesis, and presented in Chapter 3.1), and observed that the mineralogical and chemical composition of the samples changed after flooding and depending on the chalk type and the distance from injection. They also observed that K was the strongest chalk, followed by MT, and the rest (A, L and SK) behaved similarly. For more details on the flooding experiments, the reader is referred to Andersen et al. (2017)

The results from both studies (Wang et al., 2016; Andersen et al., 2017) concluded that inlet position (closest to injection) display higher wt% (weight percent) of MgO than outlet position

(farthest from injection) (Figure 25). As the calcareous nannofossils displayed alteration after flooding, it is postulated that if a chalk sample's calcareous nannofossil assemblage is dominated by species that are more robust against dissolution, such as *Watznaueria barnesiae* and *Micula staurophora* (Thierstein, 1981; Roth, 1983; Moshkovitz and Eshet, 1989; Eshet et al., 1992; Eshet and Almogi-Labin, 1996; Faris and Abu Shama, 2006; Mandur and El Ashwah, 2015), the chalk sample should display lower MgO wt% after flooding. Samples that have assemblages consisting of calcareous nannofossils with more delicate morphologies that are less resistant against dissolution should display higher MgO wt% after flooding. The calcareous nannofossils dissolve during flooding and precipitate as MgO elsewhere in the core. In addition, since it has been observed that the dissolution is strongest at inlet position, the calcareous nannofossil abundance should be lowest at inlet position (Minde, M. W., personal communication, 2018).

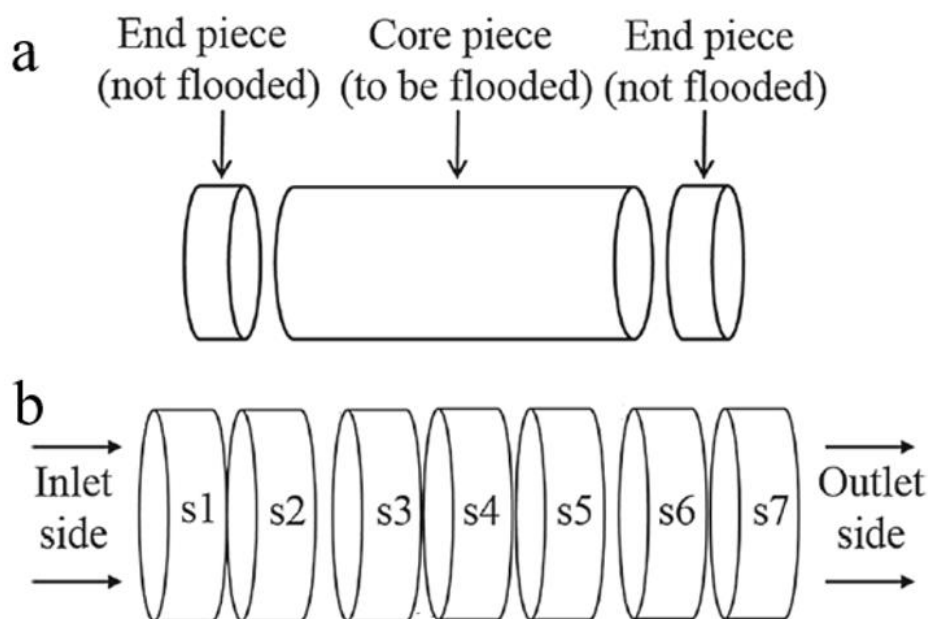


Figure 25: Five cylindrical onshore chalk cores were divided as displayed in this figure. a: First the core was cut in three pieces, where only the central core was used for flooding. b: The central core was divided into seven slices after flooding, with slice number 1 being closest to inlet and slice number 7 being closest to outlet. Modified after Andersen et al. (2017).

3. Sample Preparation and Methodology

3.1. Sample Preparation and Sample ID

A total of eight onshore outcrop chalk cores drilled out of chalk blocks were first divided into 40 samples by applying the following procedure: Each core was cut into six slices; five slices for various analyses ranging from 1.2-1.3 cm in thickness, depending on the total core length, and the sixth slice was thinner, ranging from 0.25-0.4 cm, and was to be used for possible geochemistry analyses (Figure 26). The five slices were labelled with letters according to sample-names followed by a number, from 1-5. Since the origin of the samples is unknown, the stratigraphic position is unknown, hence the numbers are not reflecting relative depth. Each of the five sample slices were then cut in half, in horizontal direction, giving $\frac{1}{2}$ of the total slice. Finally, one of each of the $\frac{1}{2}$ samples were cut in half again, giving pieces representing $\frac{1}{4}$ of the total slice (Figure 27), approximately 5.4 cm³. The cutting was performed using a *Struers Accutom-50* with a *Struers Diamond Cut-off Wheel MOD15* at the University of Stavanger.

Only sample 1 and 5 of each core were used for biostratigraphic and paleontological investigations, to capture the largest variation in the core. The Danish samples were named “A” after Aalborg and “SK” after Stevns Klint. The Belgium samples were named “MS” after Mons Spiennes, “MT” after Mons Trivières, “MON” after Mons Limit Obourg Nouvelles, “L” after Liège and “MOV” after Mons Obourg Saint Vaast. The North American sample was named “K” after Kansas (but the geographical position is in fact Niobrara, Nebraska).

The offshore reservoir chalk samples consisted of a sequence of several cores of variable quality from the Tor field (a total of 34 samples) from the Norwegian North Sea. Some of the cores were broken into several pieces, while others were more intact. The cores were organized after depth in feet, see Appendix 1, and named in this thesis as TOR1-TOR34 (from oldest to youngest). As only the first 15 samples (TOR1-TOR15) proved to be of Cretaceous age, the rest of them (TOR16-TOR34) were not investigated further.

Five onshore samples were available with flooded versions and were named after onshore sample ID (for example A), followed by “_inlet” to indicate inlet position. “Mon” corresponds to onshore unflooded “MT”. The overview of the original core IDs and the new sample IDs that are used in this thesis are presented in Table 1 below. As SK_inlet proved to have a different age than the unflooded SK, it was not counted (see Chapter 4.1.3 for biostratigraphic analyses and Chapter 5.3 for discussion regarding this issue).

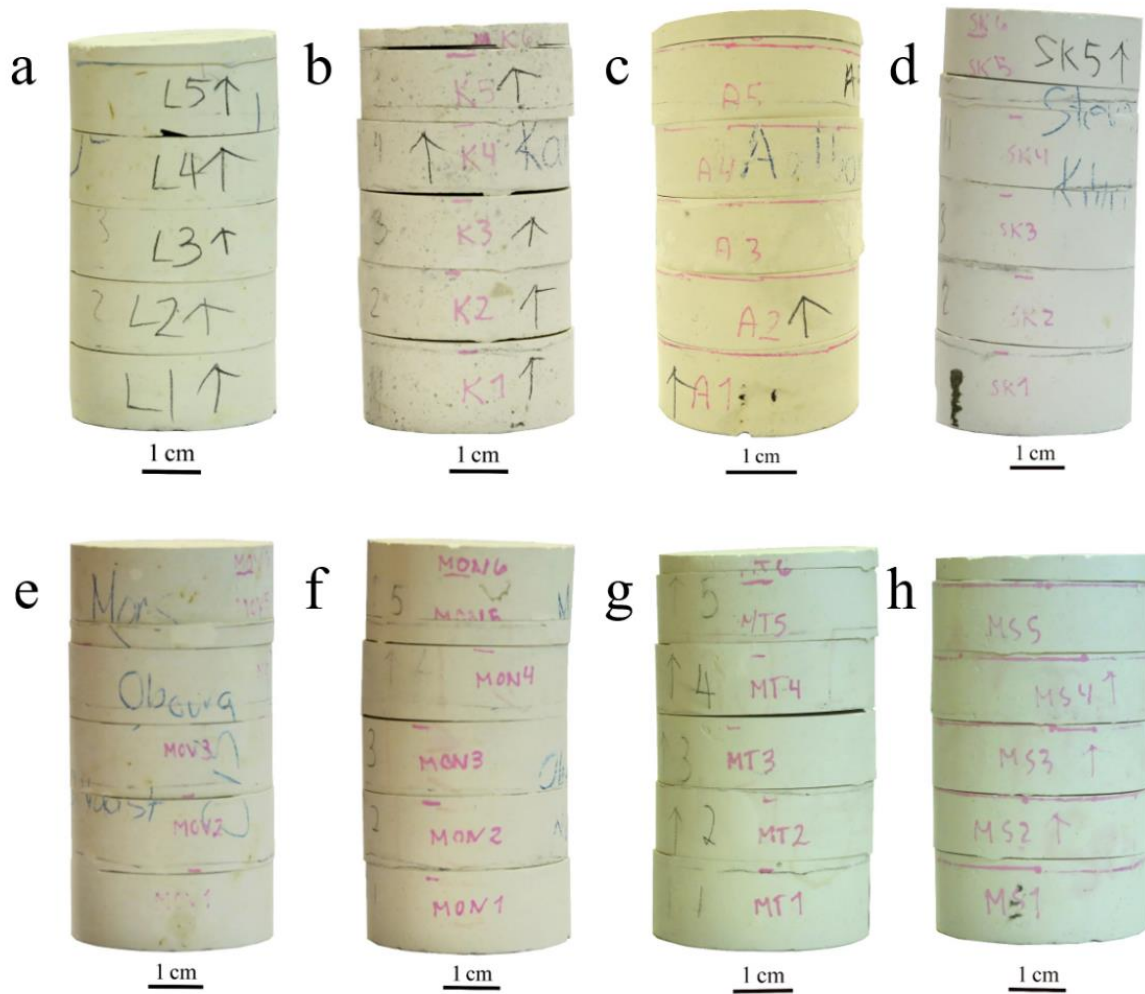


Figure 26: Eight cores cut in five slices and a sixth, thinner slice. a: L; b: K; c: A; d: SK; e: MOV; f: MON; g: MT and h: MS. For sample IDs, see Table 1 on the next page.

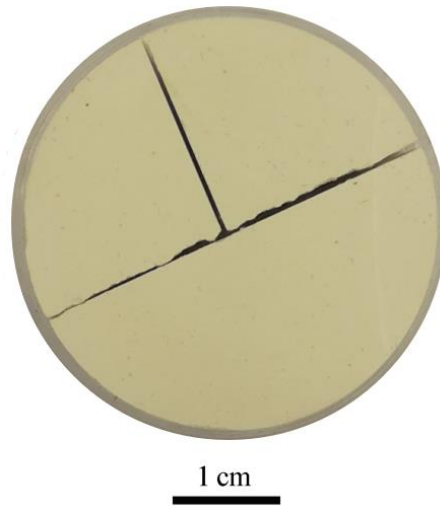


Figure 27: Each slice was cut in half, and then one half was cut in half again.

Table 1: Overview of the original core IDs and the sample IDs used in this thesis.

Samples	Original Core ID	Sample ID in this thesis
Offshore	Sample depth (ft), see Appendix 1	TOR1-TOR15 (oldest to youngest)
Onshore	Aalborg	A1 and A5
	Stevns Klint	SK1 and SK5
	Mons Spiennes	MS1 and MS5
	Mons Trivières	MT1 and MT5
	Mons Limit Obourg Nouvelles	MON1 and MON5
	Liège	L1 and L5
	Mons Obourg Saint Vaast	MOV1 and MOV5
	Kansas (Niobrara)	K1 and K5
Flooded	Aa5-1 (Aalborg)	A_inlet
	SK6-1 (Stevns Klint)	SK_inlet
	Mon10-1 (Mons Trivières)	MT_inlet
	L1-1 (Liège)	L_inlet
	KA8-1 (Kansas)	K_inlet

3.2. Optical Light Microscopy (OLM)

For the examination of smear slides at the University of Stavanger, an *Olympus BH-2* polarization microscope was used with an oil immersion objective with magnification x100. The eyepiece oculars were x10 and combined with an extra x1.25 between the oculars and objectives, it gave a total magnification of x1250. At the University of Milan, smear slides were examined using a *Leitz Laborlux 12 Pol S* polarization microscope, with oil immersion objective with magnification x100 and eyepiece oculars with magnification x12.5, giving a total magnification of x1250.

3.2.1. Simple Smear Slides of Dry and Wet Powder

Smear slides are cheap and quick to produce, and therefore a preferable tool for examining marine sediments. For calcareous nannofossils, simple smear slides can be made in minutes and no toxic chemicals are needed, which gives them a major advantage over other microfossil groups. This is one of the reasons why calcareous nannofossils are widely used for biostratigraphic correlation, especially on ships and offshore drilling platforms.

The preparation of simple smear slides was done at the University of Milan, Italy, for all the unflooded onshore and offshore samples to quickly assess the calcareous nannofossil preservation and to check if the samples could be used for biostratigraphy and counts. The slides were prepared after standard simple smear slide procedures, as described by Bown (1998). As the flooded onshore samples were not available until later in the thesis, they had to be prepared as simple smear slides using dry powder at the University of Stavanger.

Each smear slide was subsampled from each of the $\frac{1}{4}$ slice samples (approximately 5.5 cm³ / 5 grams raw sample to work with). A fresh surface of the sample was scratched off using a clean knife (Figure 28a). This was done to avoid any contamination from other samples during the cutting process. A piece of the sample put in a mortar and crushed off from the sample using a pestle (Figure 28b). For the next step, the methodology varies: For the dry powder method, the piece in the mortar was grinded with the pestle straight away (Figure 28c), while for the wet powder method, a few drops of distilled water was added and the pieces were dissolved as far as possible, before grinding (Figure 28d). By dissolving the chalk into water before grinding, one may avoid damaging the nannofossils to some extent. The grinded dry powder, or the grinded wet powder (soup consistency) was then put into a plastic box (Figure 28e) and labelled (Figure 28f). Before continuing making dry and wet powder of another sample, the equipment

was cleaned appropriately. The knife was put into HCl 18% (Figure 28g) for a few seconds to dissolve the remaining chalk, and then into distilled water and dried. The mortar and pestle were first washed under water (Figure 28h), then washed using HCl 18%, and then washed under water again and dried. This methodology was repeated for all samples, and the result was two plastic boxes for each sample: One containing dry powder and the other one containing the wet powder.

To prepare the simple smear slides, some dry powder was added to a backslide (Figure 28i) and a drop of distilled water was added. For the wet powder, a drop was added to a backslide, and could be smeared across directly using a clean toothpick (Figure 28j). For the dry powder, it needed to be dissolved in the water before it could be smeared. Depending on the pressure of the toothpick while smearing, different strips of material can be produced (Figure 28k) and it is a question of preference. The backslides were dried on a hot plate (Falc Jolly 2) with a temperature averaging at 90-100 degrees Celsius (Figure 28l). *Norland Optical Adhesive glue* was used to glue the coverslide to the backslide (Figure 28m). To avoid bubbles, the coverslide was pressed down carefully to press the bubbles to the borders. To dry the glue, the samples were placed under UV-light for five to ten minutes (Figure 28n). The excess glue was scratched off using a knife (Figure 28o), and the smear slide was cleaned using ethanol.

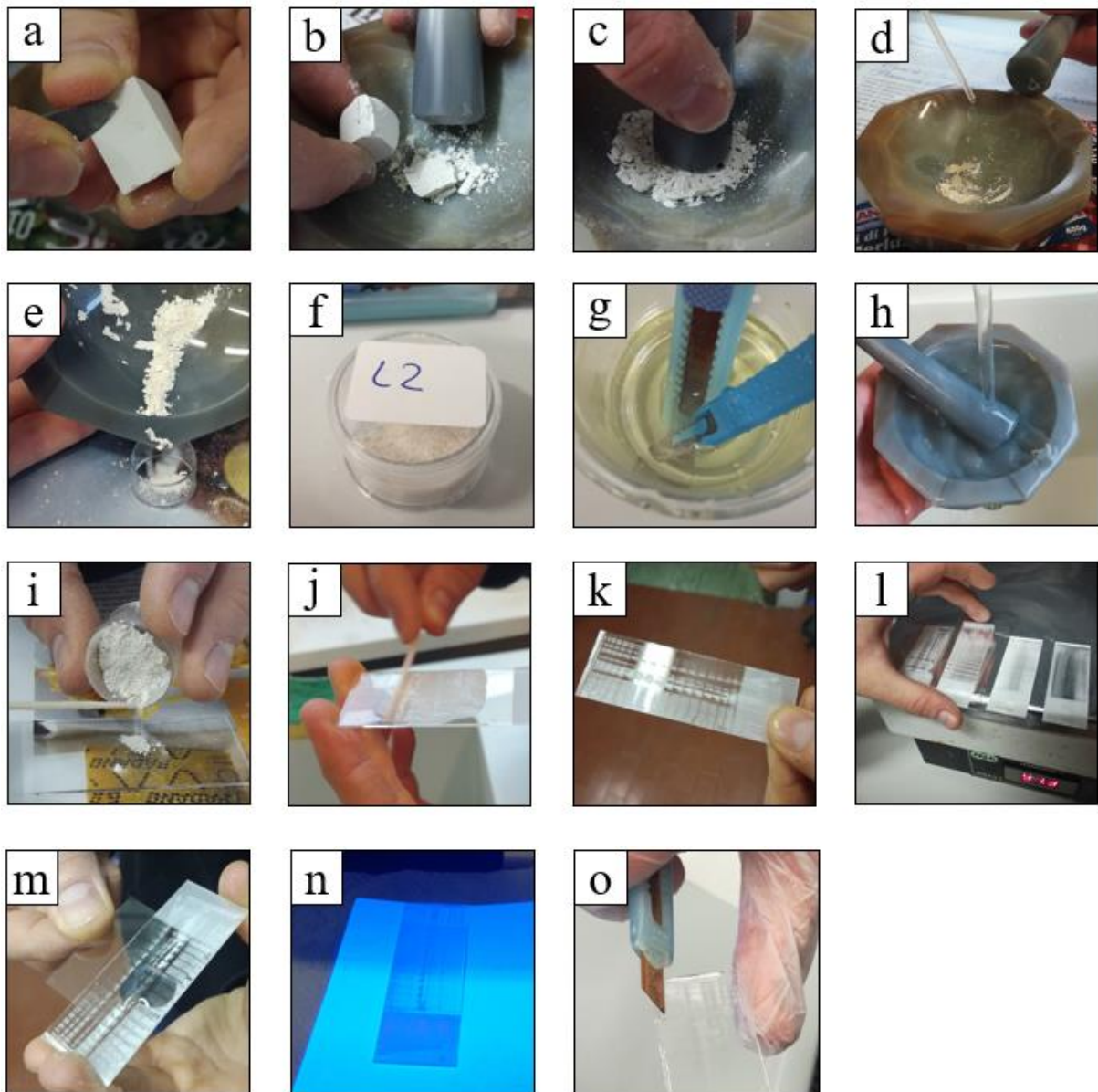


Figure 28: The different steps in simple smear slide production using dry and wet powder.

3.2.2. Simple Smear Slides using the Random Settling Technique

The random settling technique was developed to allow calculation of absolute abundances of nannofossils. Since the preparation of simple smear slides do not account for the quantity of sediment used on the cover slide, they cannot be used to calculate absolute abundances. The random settling technique was performed as described by Geisen et al. (1999).

The dry powder that was prepared for the simple smear slides was used for the random settling slides as well. For each random settling smear slide, an amount of sediment was weighted using a microbalance (*Gibertini Micro1000* with a readability of 10^{-6} g) (Figure 29a). First, a small

plastic cup was placed on the microbalance, and the lid was taken down to avoid disturbances and the weight was calibrated to zero. Then, a small amount of sediment was added to the plastic cup with a spatula. The ideal sediment weight for the onshore samples turned out to be around 25 mg, and for the offshore samples around 40 mg. The exact weights are listed in Appendix 2. The lid was put down again, and the weight of the sediment was written down. The cup was taken out of the weight using a pincher and was emptied into a sealed plastic test tube (Figure 29b). In case some of the sediment was left behind in the plastic cup, the plastic cup was weighted again, and the weight of the sediment that was left behind was written down. Then the resulting weight of only the sediment that was added to the test tube could be calculated, see Appendix 2. This methodology to weight the samples was carried out for all of them, resulting in a sealed test tube with the exact mg of sediments for each sample.

10 l of distilled water was buffered with approximately 1 ml ammonia and 3-4 drops of soap (Gocce di Triton) until a pH of 8.5 was obtained to prevent etching (Figure 29c). The ammoniac water was mixed well, and a small amount was tapped into each of the sealed plastic cylinders with sediment until the tubes were about half full. The tubes got shook well to mix the sediment into the ammoniac water, and ultrasonicated for about 10 seconds at standard power to make all sediment particles go into suspension (Figure 29d). Some more ammoniac water was added to each tube and shook well again. One tube was emptied out into a 500 ml volumetric flask and diluted with ammoniac water to 500 ml/cm³. The flask was inverted several times before the suspension was poured into the settling device (Figure 29e). Immediately after, two cover slides were put on the petals inside of the device (Figure 29f), and the lid was placed on top. The suspension was left to settle for 24 hours (Figure 29g). The volumetric flask was cleaned with ethanol between each use. Each of the device boxes were labelled with a number, and which sample that went into which device box was noted to keep track.

According to Stokes' Law and discussed by Walsby and Reynolds (1981) and Young (1994), a 2 µm diameter calcite sphere will sink at approximately 0.2 mm per minute, i. e. 300 mm per day (Geisen et al., 1999). Giving the suspended sediments 24 hours to settle should ensure complete sedimentation of the particles through the water column and a random settling onto the cover slides.

After letting the suspension settle for 24 hours, the water was carefully drained by using a drain valve, letting out approximately one drop per second to avoid evaporation and turbulence in the water (Figure 29h). When the water dropped below the cover slides (Figure 29i), they could be

taken out and dried on a hot plate (60-70 degrees Celsius). Afterwards they were mounted using the same methodology as for the dry and wet powder smear slides. The device boxes were cleaned after use.

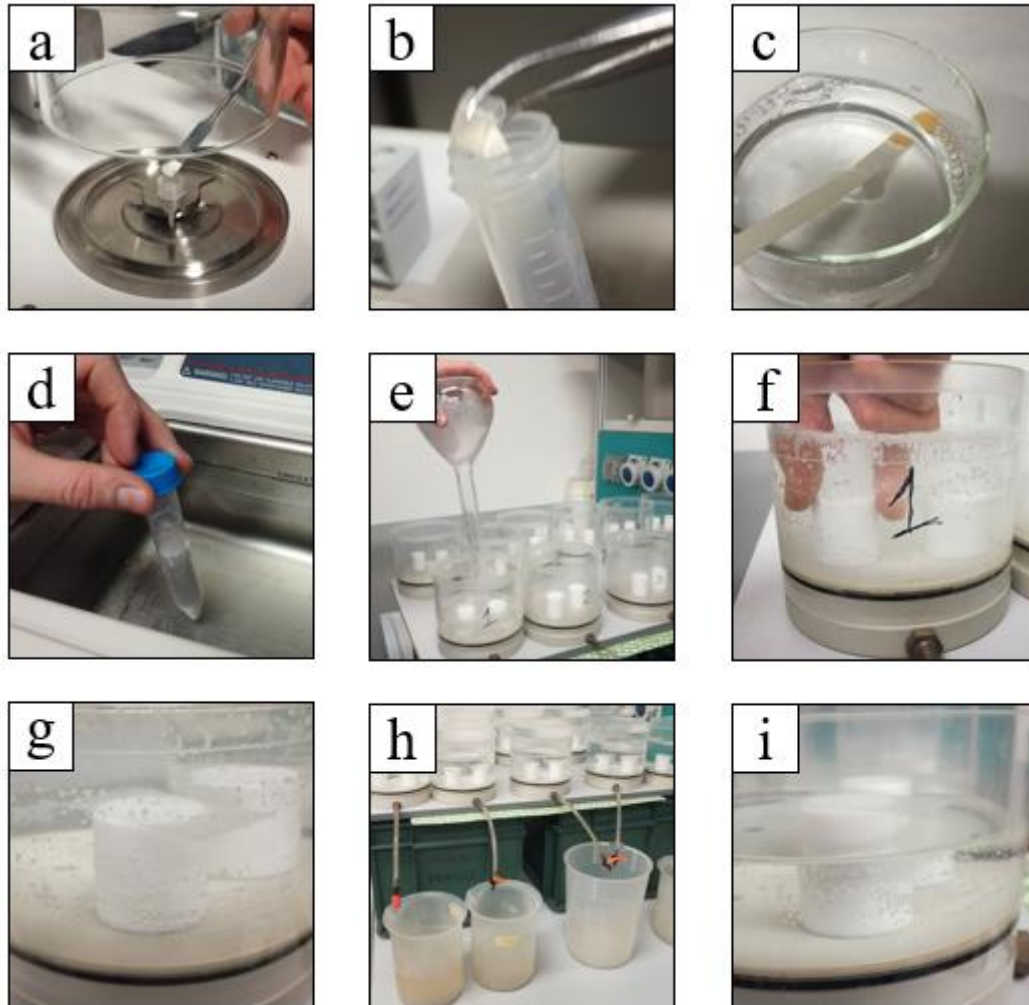


Figure 29: Photos showing the methodology of preparing random settling smear slides.

3.2.3. Calcareous Nannofossil Preservation

Calcareous nannofossils are subject to dissolution and diagenetic alteration, such as overgrowth. Some taxa are more susceptible than others. Generally, the taxa with the more delicate structures such as central areas with nets and bars are dissolved or overgrown first.

The species *Watznaueria barnesiae* has been subject to studies about its value as a quantitative indicator of preservation, and it has been proposed that this species is among one of the most resistant to diagenetic alteration and less affected by dissolution (Hill, 1975; Thierstein, 1980; Roth and Bowdler, 1981; Roth and Krumbach, 1986). The genus *Watznaueria* ranges from the

Hettangian to the Maastrichtian stage and is in terms of abundance and paleoecological tolerance considered to be the most successful Mesozoic coccolithophore (Svobodova and Košťák, 2016). An assemblage containing more than 40 % of *Watznaueria barnesiae* was described to be heavily altered by diagenesis by Roth and Krumbach (1986).

It is important to characterize the preservation of calcareous nannofossils because it can influence the abundance of nannofossil species significantly. To be able to compare samples, the preservation level should be specified. The categorization of nannofossil preservation in this thesis follows that of Lees (2002) and Tremolada (2002) and has been summarized in Table 2:

Table 2: Nannofossil preservation levels used in OLM, based on Lees (2002) and Tremolada (2002).

Preservation	Very good	Good	Moderate	Poor	Very poor
Abbreviation	VG	G	M	P	VP
Evidences of dissolution and/or overgrowth?	No	Little or none	Some	Extensive	Severe
Alteration of primary morphological characteristics?	No	Slightly	Some	Extensive	Largely destroyed
Specimens identifiable to the species level?	All	Most	Most	Difficult	Unidentifiable

The different calcareous nannofossil preservation levels are illustrated in Figure 30 by photographs taken in the light microscope of three different genera, one in each column. The very good preservation level was rarely present in the samples studied in this thesis, and therefore it was not possible to find *Eiffellithus* and *Reinhardtites* of very good preservation, hence the blank spots. Figure 30a displays a *Watznaueria fossacincta* (sample MT1) of very good preservation. There is no evidence of dissolution or overgrowth, the margin is still smooth and without any abrasion and the specimen can be recognized down to species level without any issues.

Figure 30b-d illustrates specimens with good preservation. *Watznaueria manivittiae* (sample SK1) in Figure 30b has experienced some dissolution along the margin and the central area is slightly altered. *Eiffellithus eximius* (MOV1) in Figure 30c also exhibits a little dissolution in the margin, and the central area has been slightly overgrown; the bifurcated tips of the central cross are still clearly visible, but there is evidence of alteration. *Reinhardtites levis* (sample SK1) in Figure 30d might have experienced a little dissolution along the margin, but most evident is the central diamond-shaped bridge, which has been slightly dissolved – it does not

have a clean diamond-shape anymore. Most specimen at this preservation level can still be identified down to species level without problems.

The moderate preservation level is illustrated in Figure 30e-g. At this level, the identification of most specimens down to species level should be possible. However, for a very few specimens, if crucial morphological details have been altered, it might be challenging. *Watznaueria manivittiae* (sample MS1) in Figure 30e displays clear evidences of dissolution and overgrowth along the margin, but the central area and the size of the specimen still allows identification down to species level. *Eiffellithus eximius* (sample L5) in Figure 30f has the margin nicely intact, but the central area has experienced moderate alteration. The crucial bifurcated tips of the central cross are only visible in one of four tips, barely allowing species identification. *Reinhardtites levis* (sample MS1) in Figure 30g shows dissolution along the margin and overgrowth in the central area.

Figure 30h-j illustrates the poor preservation level. All specimens show strong alteration of the margin and the central area. Identification down to species level is getting difficult.

The very poor preservation level is demonstrated in Figure 30k-m. The specimens show severe alteration, and crucial morphological characteristics for species and/or genera identification are lost. Fragmentation of specimens might occur; the specimen in Figure 30k has been broken in half, and the central area of the specimen in Figure 30l has been lost. At this level, assemblage characterization will be very uncertain.

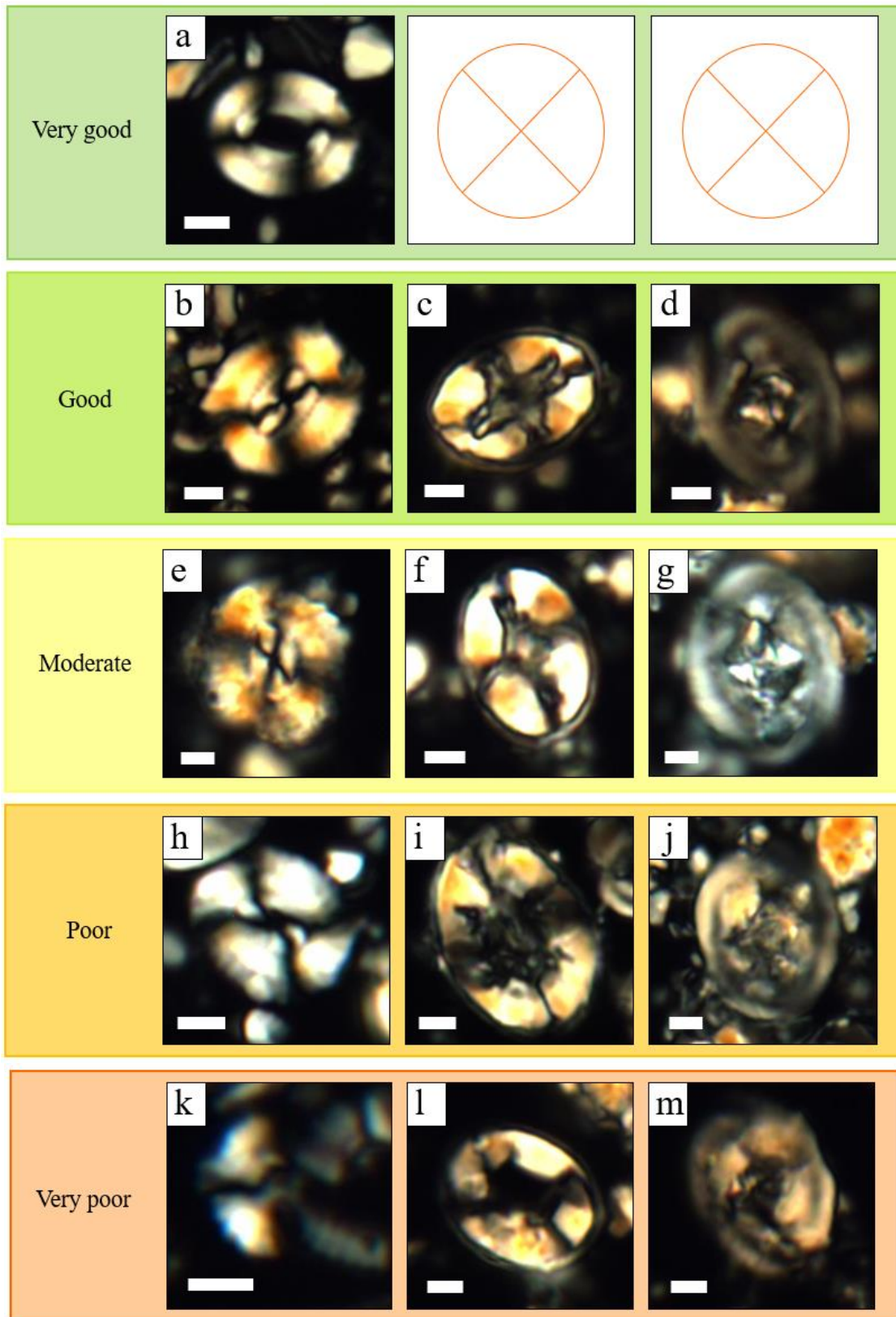


Figure 30: Photos illustrating the different degrees of preservation using three different genera: Left column: *Watznaueria*; middle column: *Eiffellithus* and right column: *Reinhardtites*. White scale bar = 2 μ m.

3.2.4. Calcareous Nannofossil Abundance and Diversity

Nannofossil abundances can be coded after Bown (1998) as follows:

A = abundant (more than 11 specimens per field of view (FOV))

C = common (1-10 specimens per FOVs)

F = few to frequent (1 specimen per 2-20 FOVs)

R = rare (1 specimen per more than 20 FOVs)

The random settling technique was developed to convert point counts of nannofossils into absolute abundances per gram of sample, assuming the number of counted particles “per unit area of the cover slide is proportional to the volume of suspension originally present above the cover slide” (Geisen et al., 1999). However, as discussed by Geisen et al. (1999), the equation to calculate particles per area yields incorrect results. By spiking the samples with a known number of standardized microbeads and counting them, the nannofossils per gram equation can be calculated again based on the ratio between nannofossils and microbeads, to check the results and its accuracy. This was not done in this thesis. However, Geisen et al. (1999) demonstrated by using the microbeads that there is an enrichment of approximately 2.5 times for the settling device. The anomalies were interpreted to be due to convection currents within the device, disturbing the settling, and because the cover slides were elevated. Nevertheless, their conclusion was that if the cover slide is placed close to the bottom of the settling device, the particles per area equation remains valid as method. There will always be some uncertainties due to the possibility of dissolution of nannofossils, altering of the distribution and nannofossils settling unevenly due to their spatial shapes.

The equation for the total number of nannofossils is, after Williams and Bralower (1995):

$$X = (N \times V) / (M \times F \times A \times H) \quad (1)$$

Where

X = particles per gram of sediment [n/g]

N = number of particles counted

V = volume of water used for dilution [ml]

M = grams of sediment added [g]

F = number of fields of view observed

- A = surface area of one FOV [cm²]
H = height of water column above slide [cm]

Species diversity is given as the total number of species encountered in a sample, and genera diversity is given as the total number of genera encountered in a sample. Calcareous nannofossil species diversity was at a maximum during the Upper Cretaceous, with up to 150 species recovered from the same assemblage (Perch-Nielsen, 1985). The species diversity was around 60-70 at the Jurassic/Cretaceous boundary, as well as across the Paleocene/Eocene boundary (Perch-Nielsen, 1985). The lowest species diversity (except for the calcareous nannofossil evolutionary beginning in the Triassic) was at the Cretaceous/Mesozoic boundary, when more than 90 % of all nannofossil species got extinct (Melinte et al., 2003). Based on this information, this thesis considers species diversity to be low when it is below 30, moderate when it is 31-100, and high when it is more than 101 species.

3.2.5. Identification of Taxa

The identification of nannofossil species was based on the criteria for taxonomy described in Appendix 3 and illustrated in Appendix 4. Since identification is based entirely on phenetic data, taxonomic pitfalls are obvious, so subjective judgement had to be present to some extent. Nannofossil morphologies depend on several factors, such as life cycle stages, ecological and preservational factors, and inconsistencies remain embedded in the classifications - so careful consideration was taken during the examinations, and comments regarding the classification are provided in the mentioned appendices.

3.2.6. Range Chart and Biostratigraphy

The only information given about the onshore samples prior to the analyses was that the eight cores are onshore chalks from open-pit quarries in various countries (Denmark, Belgium and USA). The offshore chalk was known to be a sequence (10128,7-10405,5 ft) from well 2/4-8 in the Tor field in the North Sea, see Appendix 1 for details. There is a biostratigraphic report available for this sequence by Church et al. (1978) and various literature for the onshore samples, but they were not considered before an unbiased assessment of the biostratigraphy of the offshore sequence and the onshore samples had been obtained through this thesis' study. The comparison between this thesis' analyses and the previous literature is discussed in Chapter 5.3.

A range chart was made for each sample by doing two transverses of the smear slide and noting which species were present. A range chart is used for biostratigraphic and paleoecological analyses, as some marker species might be too rare to be detected during the point count. A UC biozonation scheme based on Burnett (1998), modified by Erba, Miniati, Bottini, Russo in prep. (unpublished data) was used to assign biozones to the samples (Figure 31).

Calcareous nannofossil biozonations

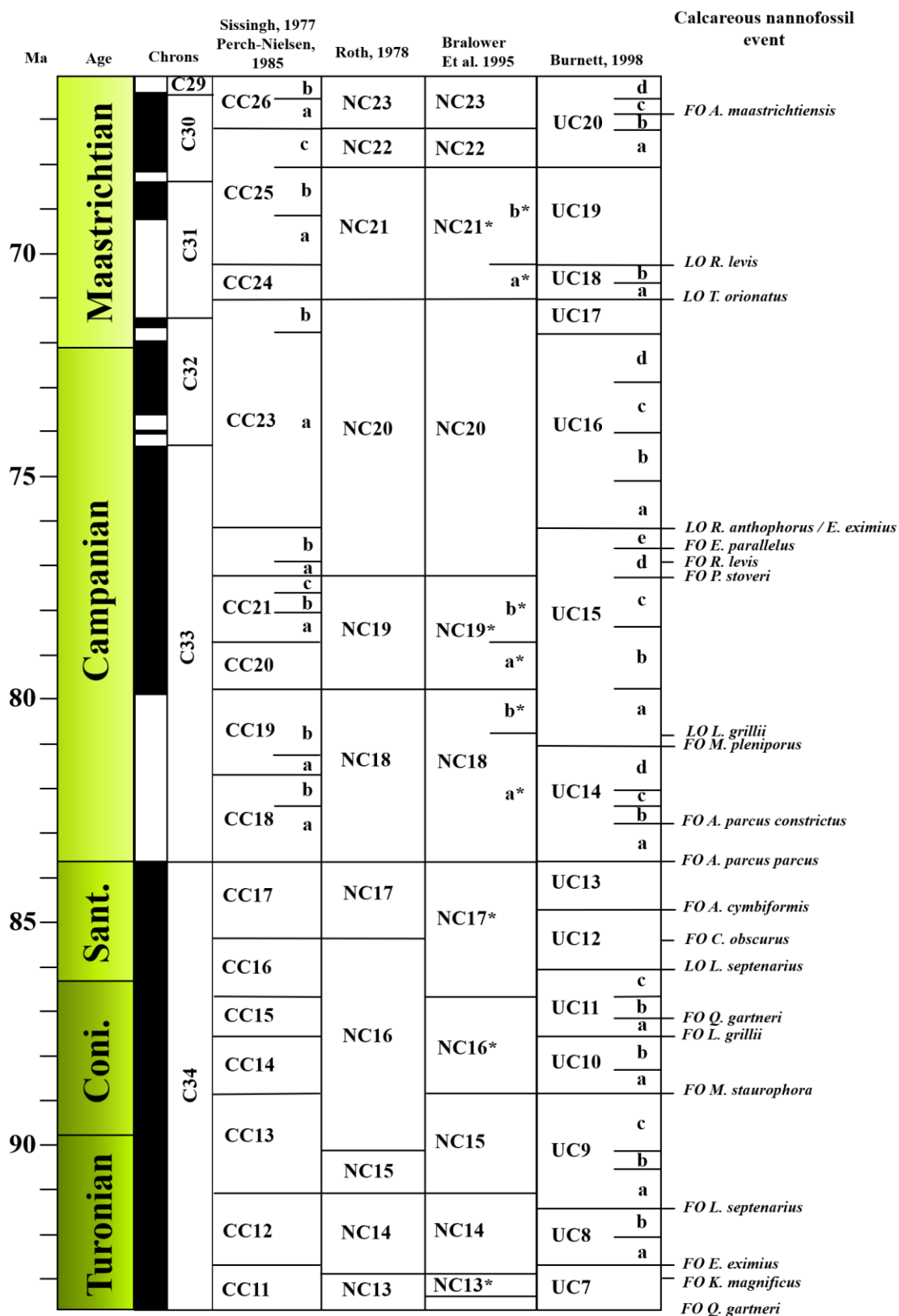


Figure 31: UC biozonation scheme after Burnett (1998), modified by Erba, Miniati, Bottini, Russo in prep. (unpublished data).

3.2.7. Point Counting

Point counting is done to obtain quantitative data to describe assemblages of nannofossils and can be used to calculate absolute abundances of individual taxa. However, one must be careful when converting a point count into absolute abundances of nannofossils. The preparation of the sample must be performed with a minimum alteration of the sample. The best is to count nannofossils using a thin section or in electron microscope, because the nannofossils will still be *in situ*. However, there is still a risk that some grains might be lost during preparation, especially for thin sections. In addition, the absolute abundances would be presented as nannofossils per area, as the quantity of sediment on the thin section or in the electron microscope view is not known.

It is more time consuming to prepare smear slides by using the random settling technique than the simple smear slide technique. However, the settling method is necessary to gain knowledge about the distribution of nannofossils in time and space, especially for comparison between different sample sets, which can be used for paleoecological and palaeobiogeographically interpretations (Geisen et al., 1999).

In this thesis, the random settling smear slides were counted for nannofossils. The counts lasted until 300 specimens were reached, to ensure statistically satisfying results. If a specimen could only be identified down to genus level, it was counted as “*Genus sp.*”. If the specimen was broken, but still identifiable down to species and/or genera level, it was counted if it was more than 50% left of the nannofossil, and not counted if it was less than 50% - to ensure that no specimens were counted twice.

FOVs for counts were chosen randomly but distributed throughout the smear slide. If a FOV was considerably different than the others (much sparser in nannofossils or strongly altered due to inconsistencies during preparation), it was skipped. The number of FOVs to reach a count of 300 were counted to calculate abundance (nannofossils/FOVs) to be able to compare nannofossil abundances between samples. In each FOV, estimations of calcite grains were conducted to correct the abundances for differences in concentration during settling.

For the offshore TOR samples, transverse-distances were measured instead of FOV, because the samples were sparse in nannofossils. The starting point was noted, and if the count lasted until 300, the end point was noted, and the total transverse distance could be measured. If two transverses were covered, and the count still did not reach 300, the count would end anyway.

FOV were calculated from the transverse-distances, by dividing the transverse-distance by the diameter of one FOV ($0.160 \text{ mm} = \text{field number} / \text{total objective magnification} = 20 / 125$).

Estimates of calcareous nannofossil species in the total assemblage was coded as follows:

D = dominant (more than 51 % of the total assemblage)

A = abundant (11-50 % of the total assemblage)

C = common (2-10 % of the total assemblage)

F = few (0.1-1 % of the total assemblage)

R = rare (< 0.1 % of the total assemblage)

As the flooded versions of the onshore samples were available too late to be prepared as random settling smear slides, they had to be counted in simple smear slides.

3.2.8. Paleoecology

A study by Andruleit (1995) of recent nannoflora suggest that it is better to use ratios of several common species than one single species alone for paleoecological analysis. Therefore, the paleoecological analyses were done based on the quantitative results of calcareous nannofossils and the different paleoecological factors as described in Chapter 2.3.4. An overview of species used as paleoecological indices (measures) in this thesis are listed in the table below:

Table 3: Species used as paleoecological indices.

High nutrient indices	<i>Biscutum constans</i>
	<i>Zeugrhabdotus sp.</i>
Low nutrients indices	<i>Eiffellithus sp.</i>
	<i>Lithraphidites sp.</i>
	<i>Prediscosphaera sp.</i> (excluding <i>Prediscosphaera stoveri</i>)
	<i>Watznaueria barnesiae</i>
Cold water indices	<i>Arkhangelskiella cymbiformis</i>
	<i>Lithraphidites carniolensis</i>
	<i>Lucianorhabdus cayeuxii</i>
	<i>Microrhabdulus decoratus</i>
	<i>Prediscosphaera spinosa</i>
	<i>Reinhardtites levis</i>
	<i>Staurolithites stradneri</i>
Warm water indices	<i>Braarudosphaera bigelowii</i>
	<i>Watznaueria barnesiae</i>
Diagenetic alteration indices	<i>Micula staurophora</i>
	<i>Watznaueria barnesiae</i>

3.2.9. Calcareous Nannofossil versus Micarb Ratios

Micarbs are calcite crystals smaller than 1 μm . Nannofossil versus micarb ratios (NvsM-ratio) were estimated during the count, in the same FOVs as the counts. The percentages were estimated visually by using the estimation chart by Baccelle and Bosellini (1965) in Appendix 5.

Figure 32 and Figure 33 are showing two examples of estimates, giving nannofossil percentages of 5 and 70 % (only considering versus micarbs and no other components), respectively. Note that fields of views are circular in the microscope, while these “FOVs” photographs are rectangular, due to the camera. The final estimate was calculated as an average of all the estimates per sample.

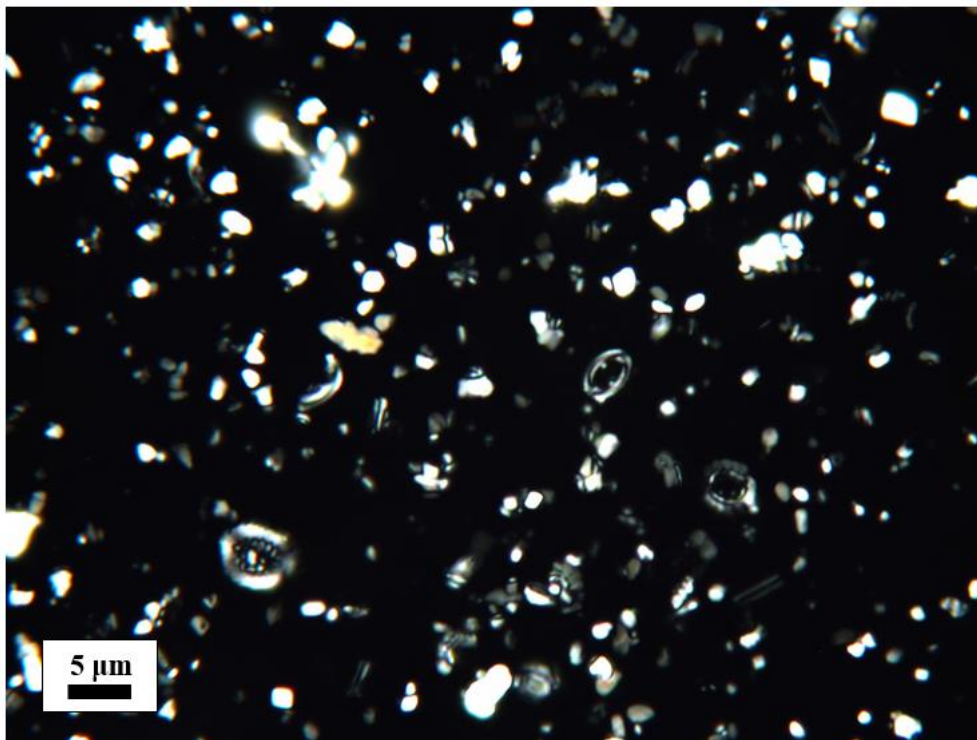


Figure 32: One “FOV” from sample A5, estimated to have a NvsM-ratio of 5:95.

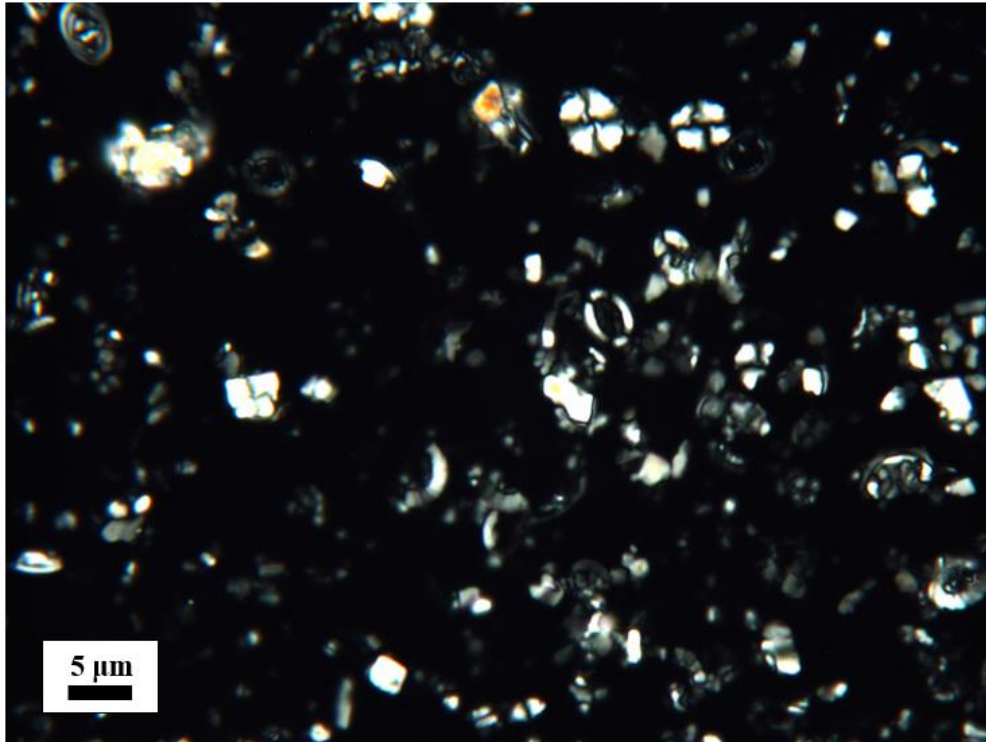


Figure 33: One “FOV” from sample K1, estimated to have a NvsM-ratio of 70:30.

3.3. Field Emission Gun Scanning Electron Microscopy (FEG-SEM)

A Zeiss Supra 35VP FE-SEM at the University of Stavanger was used to take micrographs for this thesis. Micrographs were taken with a 15-kV acceleration voltage, aperture of 30 μm and a working distance between 10-13 mm.

3.3.1. FEG-SEM Sample Preparation

A small piece of each of a total of 16 onshore unflooded samples and 5 onshore flooded samples was knocked off with a hammer and chisel, to ensure a fresh surface (Figure 34a). Each piece was mounted on a sample holder with Loctite Power Glue using clean tweezers (Figure 34b). The mounted samples were placed under a ventilator to dry over-night (Figure 34c).

The samples were sputter-coated with palladium to avoid overcharging, ensure a stable flux of electrons and to increase the emission of secondary electrons. The machine used was an Emitech K550X, with TK8885 Palladium 60 mm Dia x 0.1 mm x1. The samples rotated on the stage during coating to ensure even coating (Figure 34d). The deposition was set to 25 mA and coating lasted for 2.5 minutes (Figure 34e). After coating, the samples were ready to be mounted on to a FEG-SEM holder and put into the sample chamber (Figure 34f).

Since offshore samples from the Tor field originally have contained oil, they could not be prepared for the FEG-SEM without time-consuming cleaning procedures, which was decided to not be included in this thesis. Therefore, the offshore samples were not studied using the FEG-SEM.

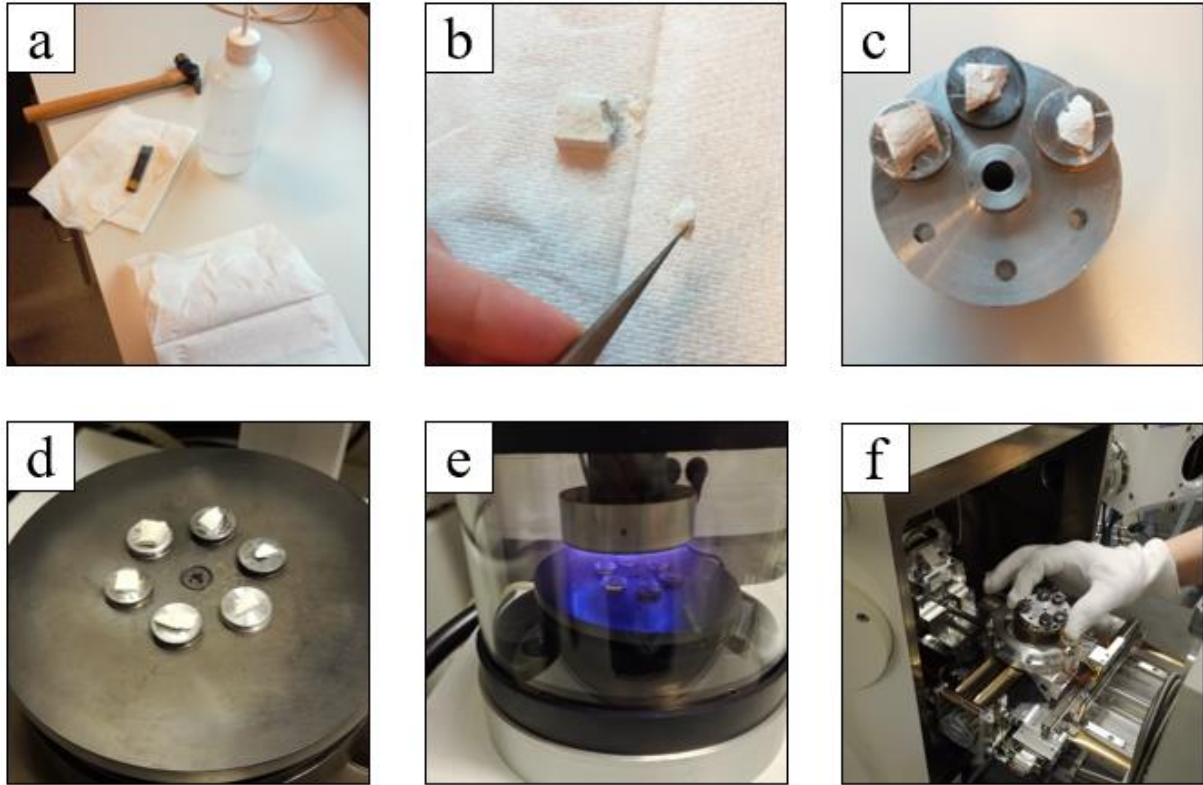


Figure 34: Photographs displaying the different steps of preparing chalk samples for the FEG-SEM: a: Hammer and chisel cleaned with ethanol between each sample were used to cut off a small piece of each sample; b: A small piece of each sample was picked with tweezers and glued on a FEG-SEM sample mount with the fresh surface upwards; c: The glued samples were put under ventilation to dry overnight; d: The samples were put on a rotating stage to ensure even coating of palladium; e: Coating of palladium lasted for 2.5 minutes and f: The samples were ready to be put into the sample chamber in the FEG-SEM.

3.3.2. Examination and Micrography

A joystick was used to move the samples up and down, and various rotating knobs were used to adjust the stigmator alignment, aperture alignment, magnification and focus (Figure 35). The samples were examined with different magnifications: x5000 (Figure 36) to get an overview and 10-50 specimens in one FOV, x10.000 (Figure 37) to get 10-20 specimens per FOV and

higher magnifications between $\times 15,000$ - $30,000$ (Figure 38 and Figure 39) for taxonomy of a single specimen, depending on its size.

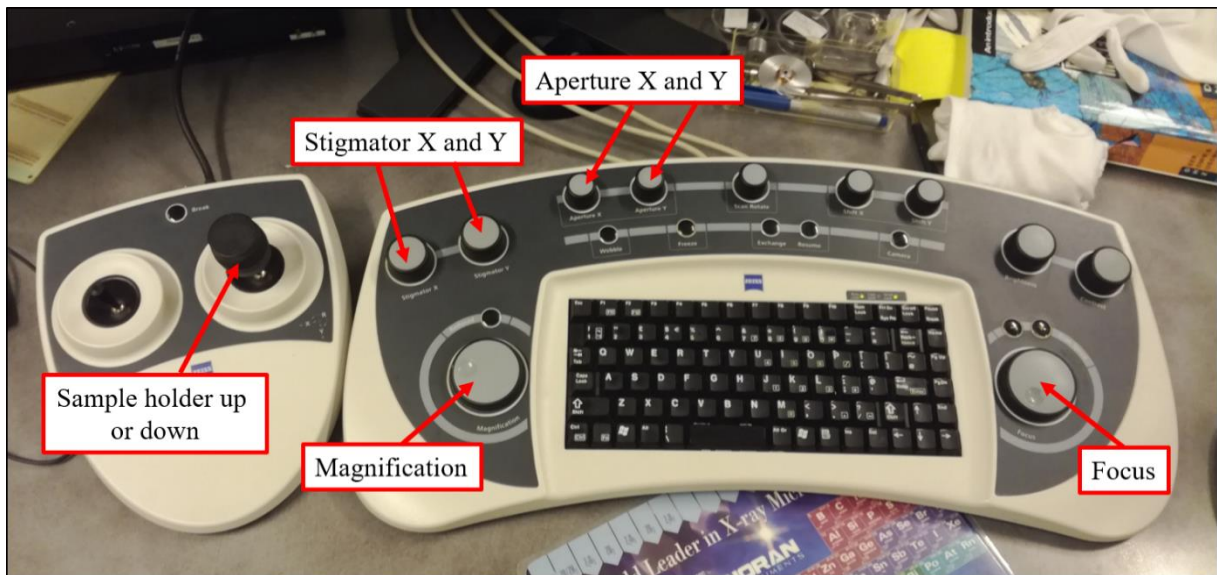


Figure 35: Joystick to move samples up or down, and various rotating knobs to adjust the stigmator alignment, aperture alignment, magnification and focus.

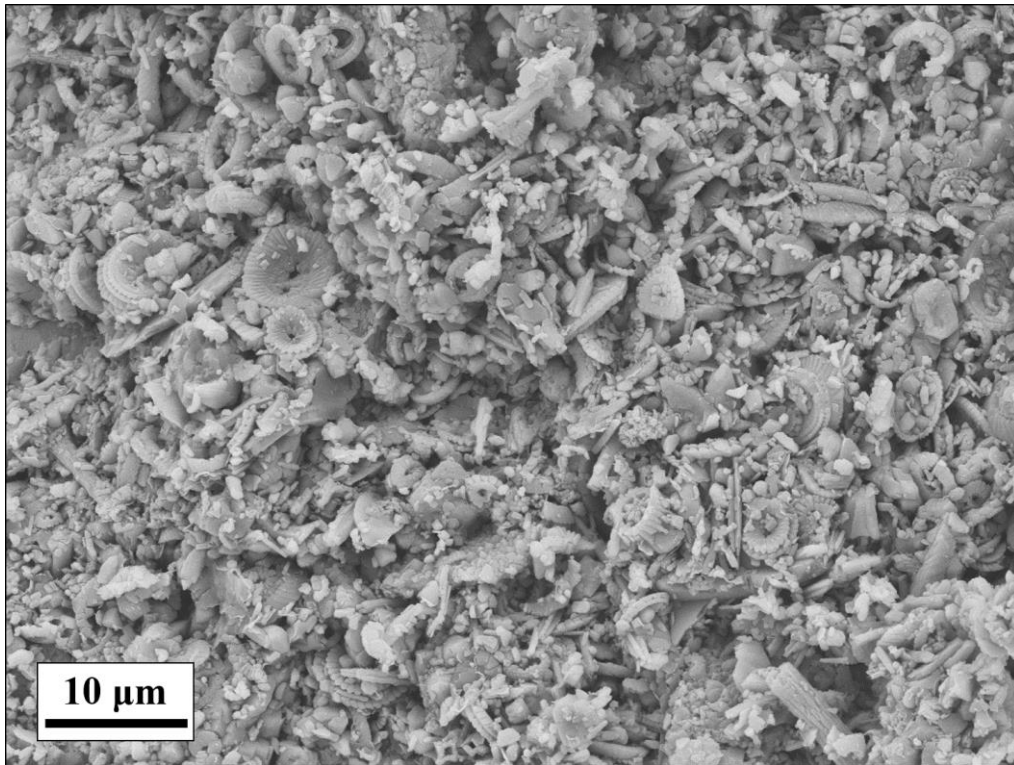


Figure 36: FEG-SEM micrograph with magnification x5000, displaying an overview of species in sample MOV5.

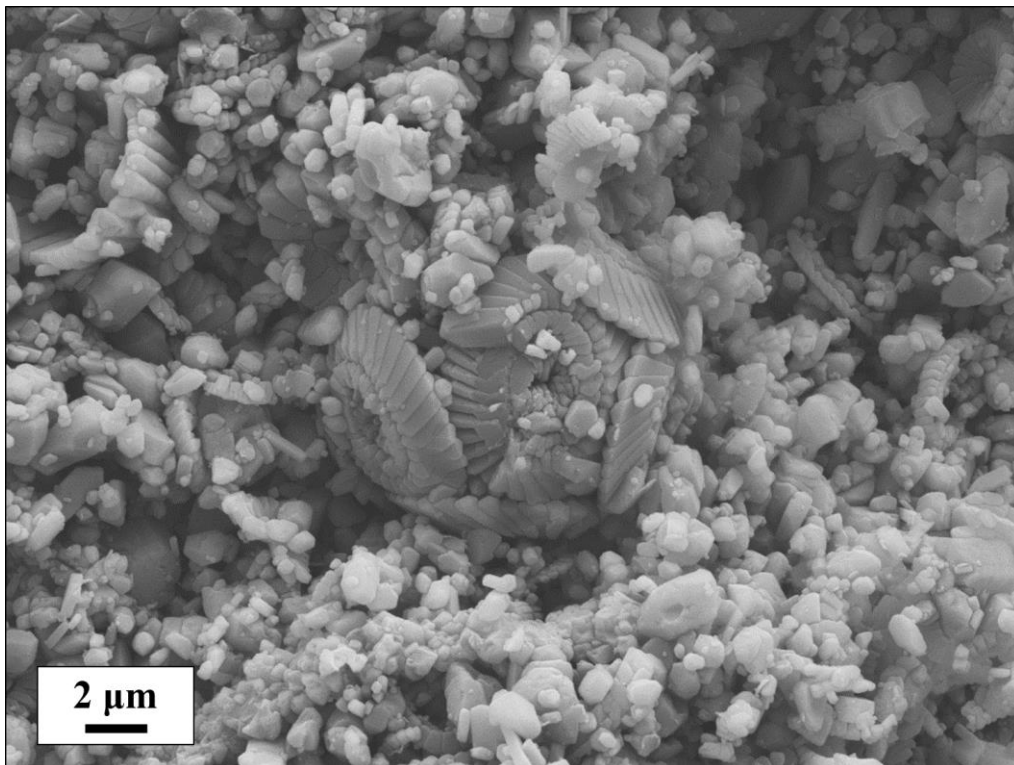


Figure 37: FEG-SEM micrograph with magnification x10.000, displaying a coccolithophore in sample MT1.

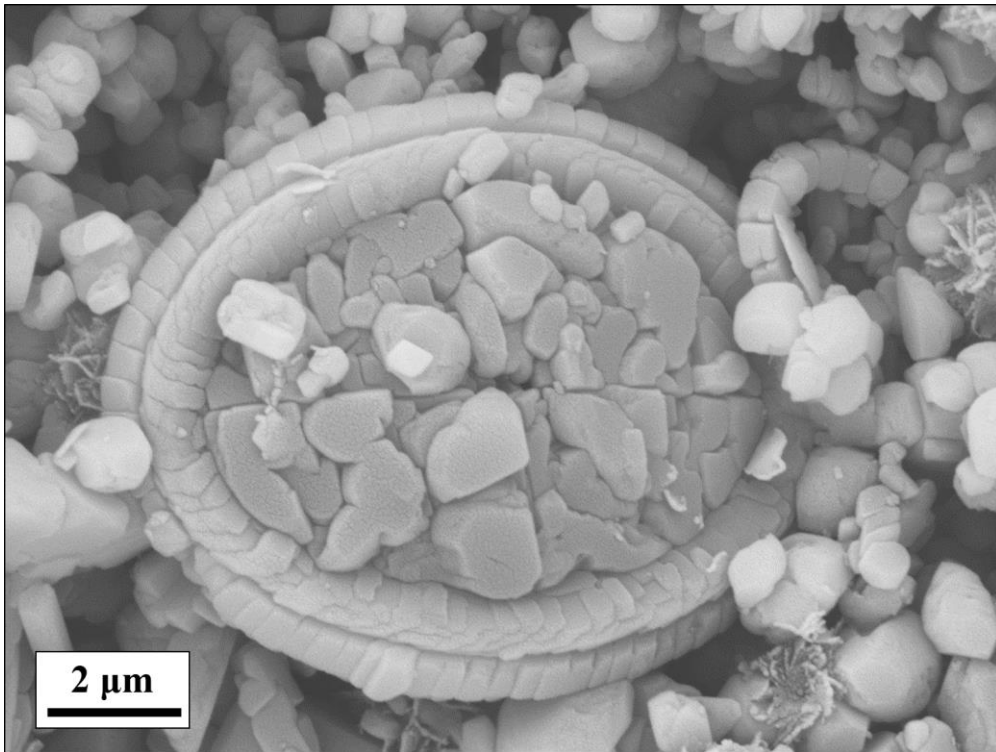


Figure 38: FEG-SEM micrograph with magnification x25.000, displaying an *Arkhangelskiella cymbiformis* in sample A5.

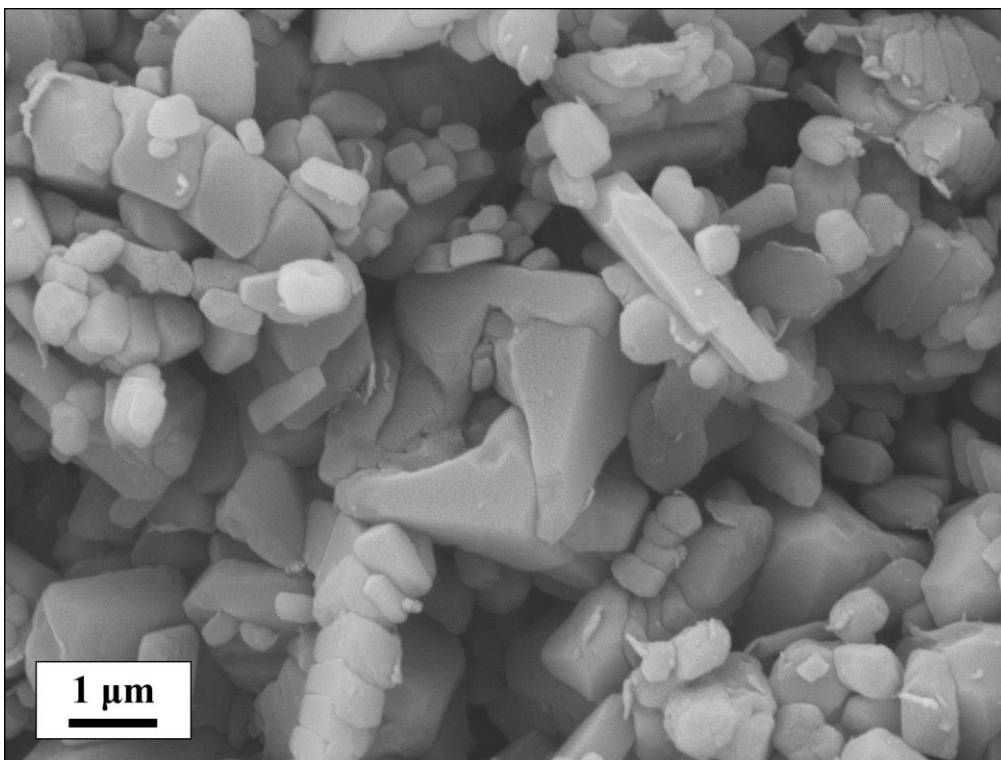


Figure 39: FEG-SEM micrograph with magnification x30.000, displaying a *Micula sp.* in sample MS1.

3.3.3. Calcareous Nannofossil Preservation

The categorization of nannofossil preservation in FEG-SEM follows the same as for the optical light microscope in Chapter 3.2.3, that of Lees (2002) and Tremolada (2002):

Table 4: Nannofossil preservation levels used in FEG-SEM, based on Lees (2002) and Tremolada (2002).

Preservation	Very good	Good	Moderate	Poor	Very poor
Abbreviation	VG	G	M	P	VP
Evidences of dissolution and/or overgrowth?	No	Little or none	Some	Extensive	Severe
Alteration of primary morphological characteristics?	No	Slightly	Some	Extensive	Largely destroyed
Specimens identifiable to the species level?	All	Most	Most	Difficult	Unidentifiable

Different levels of preservation are illustrated in Figure 40 by micrographs taken in the FEG-SEM of different genera. *Tranolithus* is displayed in the column to the left, *Prediscosphaera* in the middle column and various genera in the column to the right.

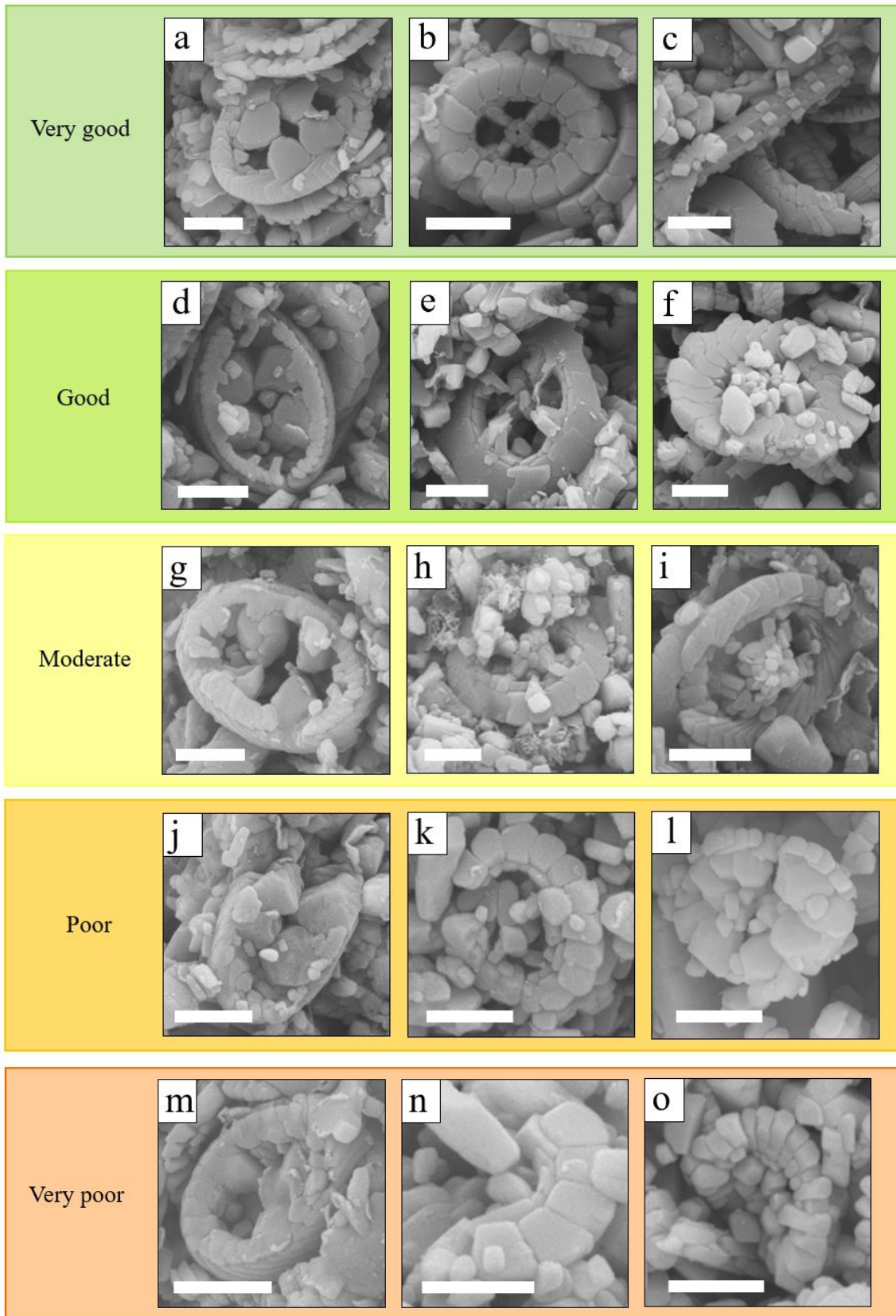


Figure 40: FEG-SEM micrographs illustrating the different degrees of preservation using several different genera: Left column: *Tranolithus*; middle column: *Prediscosphaera* and right column: Various genera. White scale bar = 2 μm .

3.3.4. Calcareous Nannofossil versus Micarb Ratios

Calcareous nannofossil versus micarb ratios (NvsM-ratio) estimates were estimated visually from 50 FEG-SEM micrographs per sample taken at magnification x5000, to give a rough estimate to compare to the estimate from the smear slides. The final estimate was the average estimate of all the estimates. The estimation was also performed on the flooded samples at inlet position. Two examples of estimates are given in Figure 41 and Figure 42.

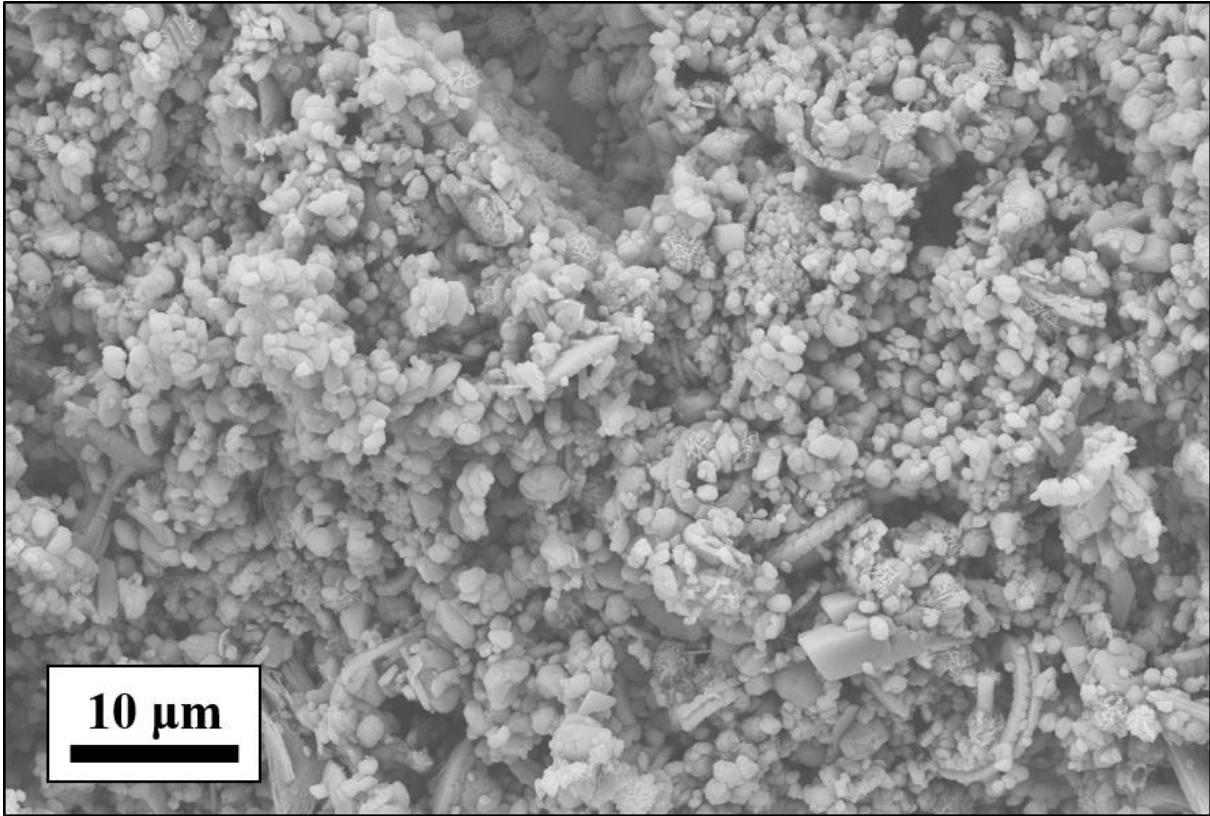


Figure 41: Sample A5, estimated to have a NvsM-ratio of 10:90.

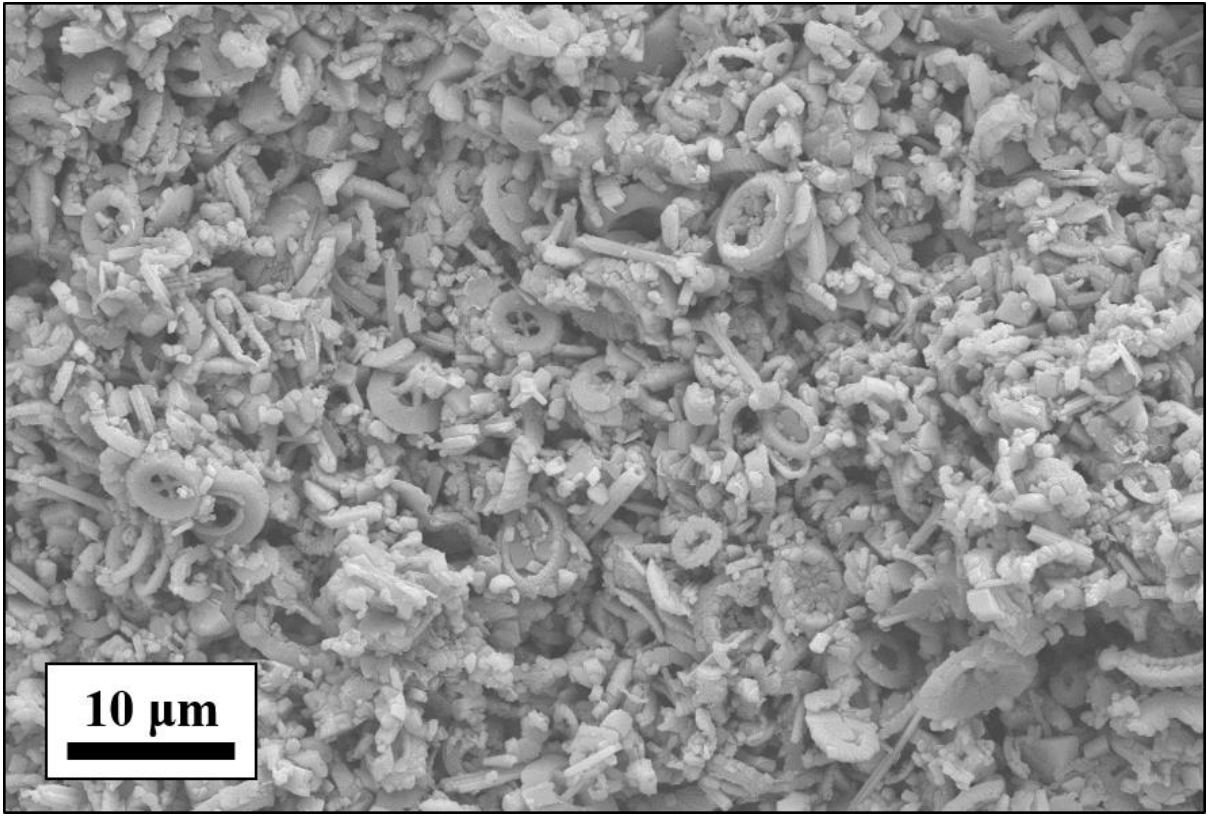


Figure 42: Sample K1, estimated to have a NvsM-ratio of 70:30.

4. Results

Please see Table 1 in Chapter 3.1 for the overview of original core IDs. Only the given sample IDs for this thesis will be used in the following chapters.

4.1. Optical Light Microscopy (OLM)

4.1.1. Calcareous Nannofossil Preservation

Calcareous nannofossil preservation has been coded into the point counting chart in Appendix 6, and visualized in Figure 43. All samples from the offshore-sequence are of poor preservation. The same preservation level was observed in onshore samples MON, MS and A. Onshore samples MOV, SK and L were of poor to moderate preservation. Sample K was of poor to moderate preservation, but slightly poorer than MOV, SK and L. Sample MT had the best preservation level, being moderate. The flooded samples at inlet position displayed very poor (A_inlet and K_inlet) and poor (MT_inlet and L_inlet) preservation.

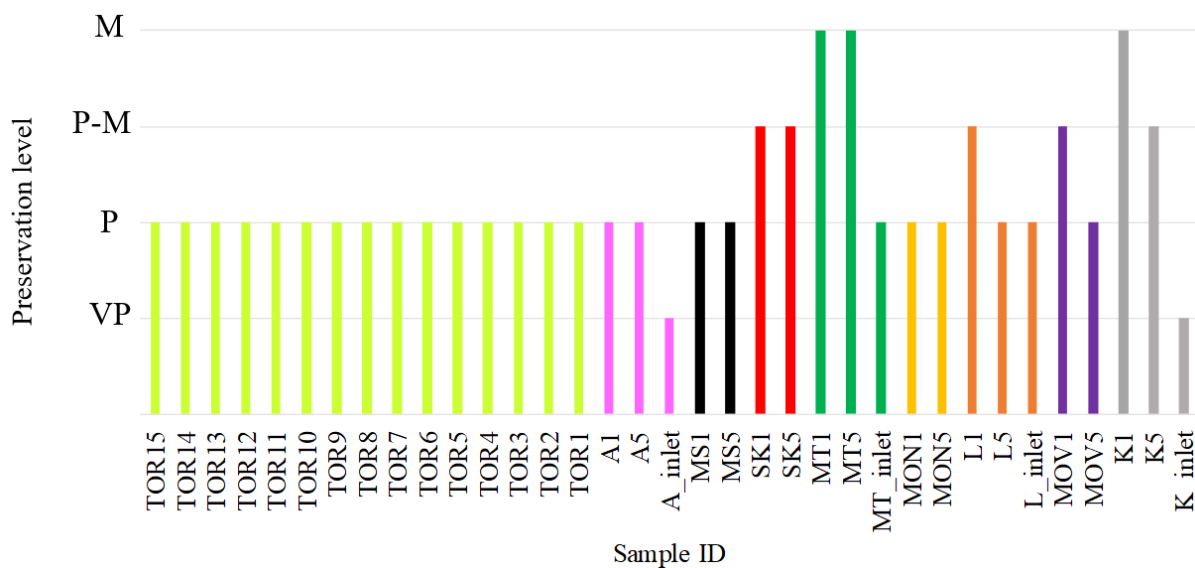


Figure 43: Preservation levels of the various samples, from youngest to oldest (left to right). VP: very poor; P: poor; P-M: poor to moderate and M: moderate.

4.1.2. Calcareous Nannofossil Abundance and Diversity

Abundances as nannofossils per field of view (FOV) [n/FOV], with corresponding abundance codes from Bown (1998) are listed in the point counting chart in Appendix 6. Total abundances calculated as nannofossils per gram of sample ([n/g]) from equation (1) described in Chapter 3.2.4 by Williams and Bralower (1995) are presented in Appendix 2. Abundances as n/FOV and [n/g] are visualized in Figure 44.

Samples A, SK, MON and L have differences in [n/g] from one end of the core to the other of < 1100 thousand (k). The smallest difference is for core SK, with only a difference of 40k decrease from SK1 to SK5 (decrease of 0.9%). Samples K, MOV, MT and MS have differences > 1100k. Sample K has the largest difference within the core as calculated abundance, with an increase of 4784k from K1 to K5, while sample MT has the largest difference in percentage, with an increase of 68.6% of total calculated abundance from MT1 to MT5.

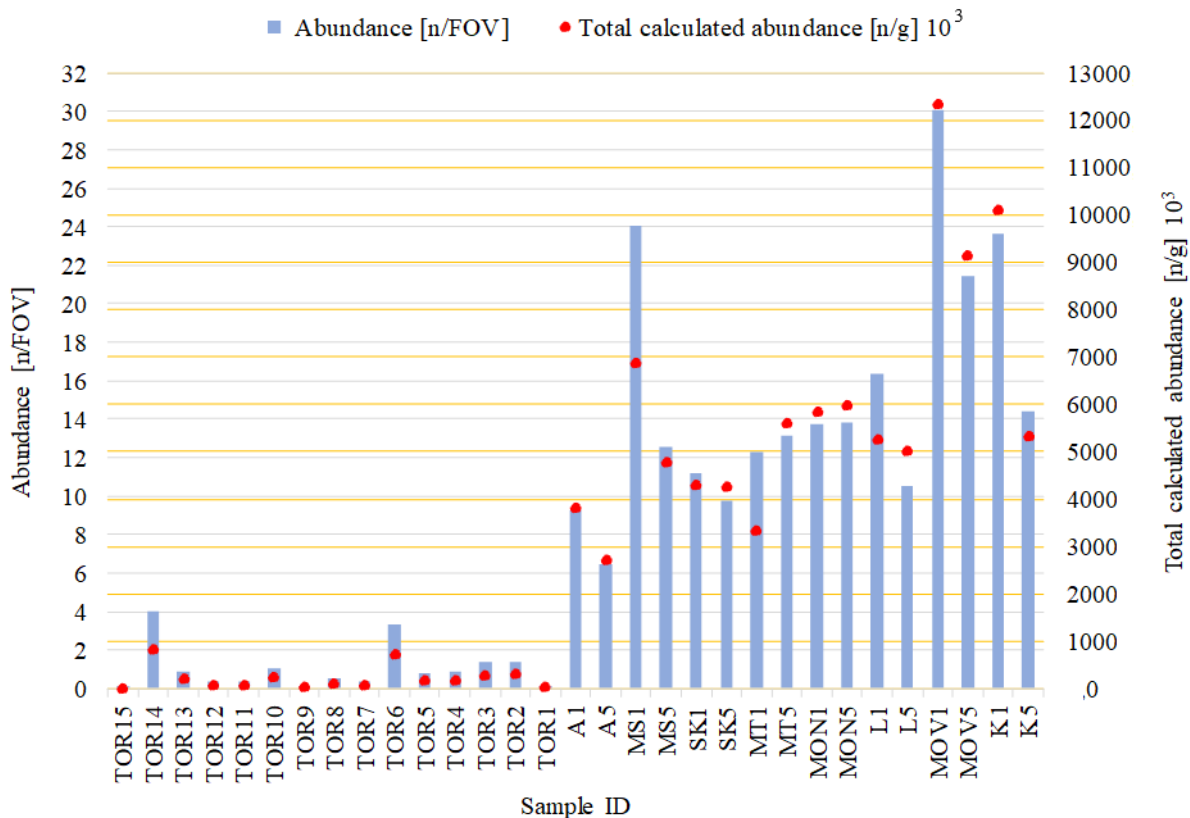


Figure 44: Abundance results from all samples, as abundance in nannofossils per FOV [n/FOV] and total calculated abundance of nannofossils per gram of sample [n/g] 10³.

As the flooded samples were not prepared using the random settling technique, abundances could not be calculated as nannofossils per gram of sample, and their abundance codes (in

Appendix 6) are based on transverses of simple smear slides. A_inlet and K_inlet are coded as few (0.70 and 0.28 n/FOV, respectively), and MT_inlet and L_inlet are coded as common (4.83 and 2.14 n/FOV, respectively). The flooded samples display a clear decrease in abundances from their unflooded equivalents.

Diversity of species and genera can be a measurement of stability of the paleoecological ocean conditions. Table 5 summarizes the species and genera diversities in the studied samples. The results are presented in Figure 45 and Figure 46.

Table 5: Species and genera diversity in the studied samples, listed from youngest to oldest (left to right, top to bottom).

Samples:	TOR	A1	A5	A_inlet	MS1	MS5	SK1	SK5	MT1	MT5	MT_inlet
# species	-	31	32	14	40	39	37	39	34	40	25
# genera	-	21	22	12	25	26	26	25	24	26	20
Av. # spe.	13	32		-	40		38		37		-
Av. # gen.	11	22		-	26		26		25		-

Samples:	MON1	MON5	L1	L5	L_inlet	MOV1	MOV5	K1	K5	K_inlet
# species	37	35	37	41	24	39	41	40	37	6
# genera	26	25	24	29	20	28	27	26	24	6
Av. # spe.	36		39		-	40		39		-
Av. # gen.	26		27		-	28		25		-

The offshore TOR samples have a low species diversity (average of 13 species and 11 genera) and less diversity than the onshore samples (Table 5 and Figure 45). However, there is a difference within the sequence (Figure 46), with peaks of species and genera diversity in TOR2 and TOR10, and extremely low species diversity in TOR1 (12 species and 8 genera) and TOR15 (7 species and 7 genera).

The onshore samples generally display similar species and genera diversity (Table 5). A has the lowest diversity with an average of 31 species and 22 genera, while sample MOV has the highest diversity with 40 species and 28 genera. The flooded samples at inlet position display lower numbers of average species and genera than their unflooded equivalents. K_inlet has the largest decrease in species and genera from the average diversity values of K1 and K5, with

84% decrease in species diversity and 76% decrease in genera diversity (Figure 45). A_inlet displays 56% decrease in species diversity and 44% decrease in genera diversity, from the average diversity values of A1 and A5. MT_inlet has the smallest diversity decrease of all the flooded samples; 32% decrease in species diversity and 20% decrease in genera diversity, compared to the average diversity values of MT1 and MT5. L_inlet shows 38% decrease in species diversity and 25% decrease in genera diversity compared to the average diversity values of L1 and L5.

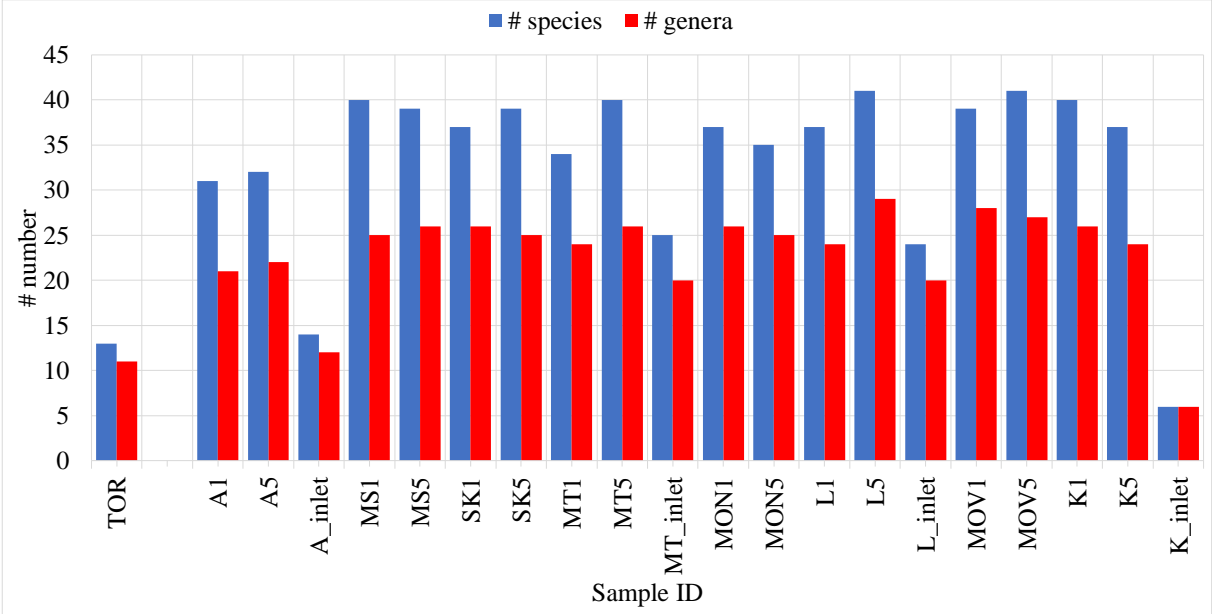


Figure 45: Species and genera diversity in the offshore samples are presented as an average, and the onshore samples are presented from both ends of the core (1 and 5), as well as their flooded inlet position equivalents. Listed from youngest to oldest (left to right).

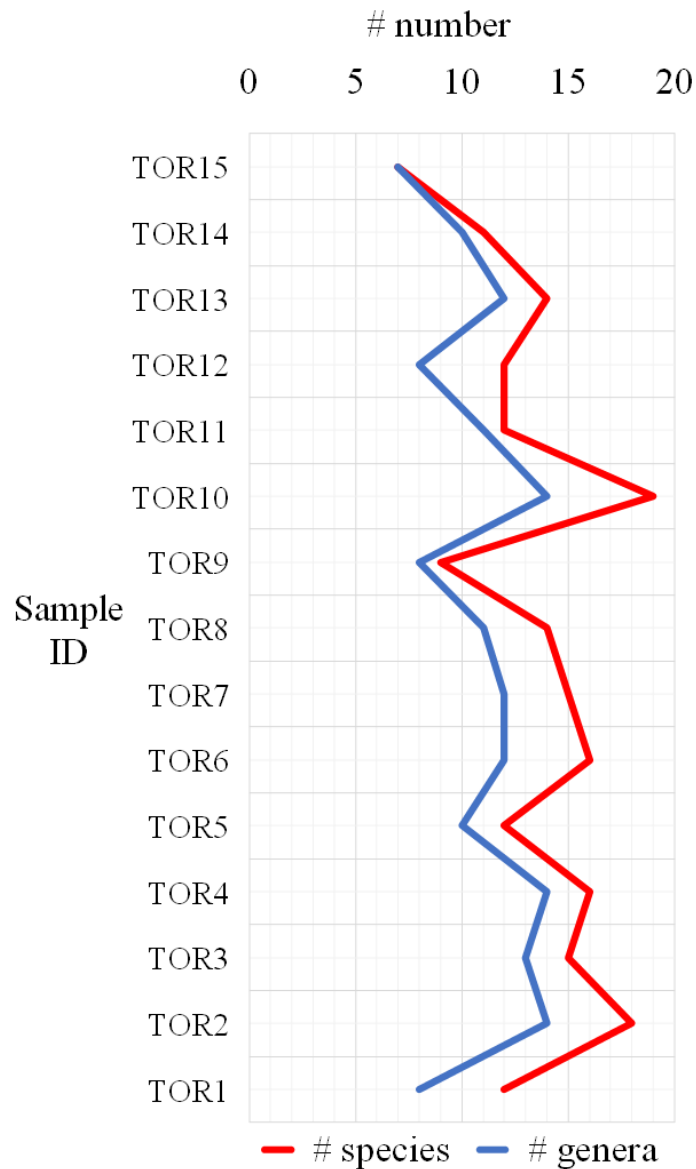


Figure 46: Species and genera diversity in the offshore TOR sequence, from oldest to youngest (bottom to top).

4.1.3. Range Chart and Biostratigraphy

A total of 59 calcareous nannofossil species belonging to 33 genera were identified in total for all the offshore and onshore samples. Figure 47 and Figure 48 display the range charts for the offshore and onshore samples, respectively. The range charts contain much information: The left column is the biozonation scheme based on Burnett (1998) and modified by Erba, Miniati, Bottini, Russo in prep. (unpublished data), the uppermost row consists of the encountered species and genera, listed from oldest first occurrence to youngest first occurrence (left to right), with their age range in million years and biozones (if applicable) in the table just below. The

right column lists the samples from oldest to youngest (bottom to top). The middle part of the schemes contains information about the age ranges of the species (red lines corresponding to species above), which species are present in which samples (circles correspond to species above and sample to the right) and which species that might have been encountered, but poor preservation made it impossible to confirm them (question marks correspond to species above and sample to the right).

Figure 49 and Figure 50 display the biostratigraphic charts for the offshore and onshore samples, respectively. The biostratigraphic charts are identical to the range charts, except all species of no biostratigraphic value have been removed. The biostratigraphic charts also contain a column for determined biozonation for each sample, in addition to a column describing which species have been used for biozonation. A total of five different biozonation-ranges were encountered in the various onshore and offshore samples.

The oldest sample is K, which could not be delimited to a single biozone, but was determined to be between UC9a and UC12 (Late Turonian to Late Coniacian/Early Santonian) due to the occurrence of *Lithastrinus septenarius*, which makes it a local range biozone limited by *Lithastrinus septenarius*' range. Younger than K is sample MOV, which could not be delimited to a single biozone either but determined to be between UC13 (FO *Arkhangelskiella cymbiformis*) and UC15a (LO *Lithastrinus grillii*) (Middle Santonian to Early Campanian), making it a concurrent interval biozone. Samples L, MON, MT and SK were determined to be in biosubzone UC15d (Middle Campanian), delimited by FO of *Reinhardtites levis* and LO of *Aspidolithus parvus parvus*; a concurrent interval biozone. Sample MS belongs to biosubzone UC15e (Middle-Late Campanian) – also a concurrent interval biozone, delimited by the FO of *Eiffellithus parallelus* and the LOs of *Reinhardtites anthophorus* and *Eiffellithus eximius*. The youngest of the onshore samples might be A, which was determined to have a biozonation from UC15d (FO *Prediscosphaera stoveri*) to UC20a (LO *Ahmullerella octoradiata*) (Middle Campanian to Middle/Late Maastrichtian), making it a concurrent interval biozone. The offshore TOR samples are the youngest. They all contained *Arkhangelskiella maastrichtiensis*, which has its FO in biosubzone UC20c (Uppermost Maastrichtian) and LA at the Cretaceous/Cenozoic boundary, making it a local range biozone.

Figure 51 summarizes the biostratigraphic results visually. The presumed ages and the new determined ages from the biostratigraphic analyses of this thesis are summarized in Table 6.

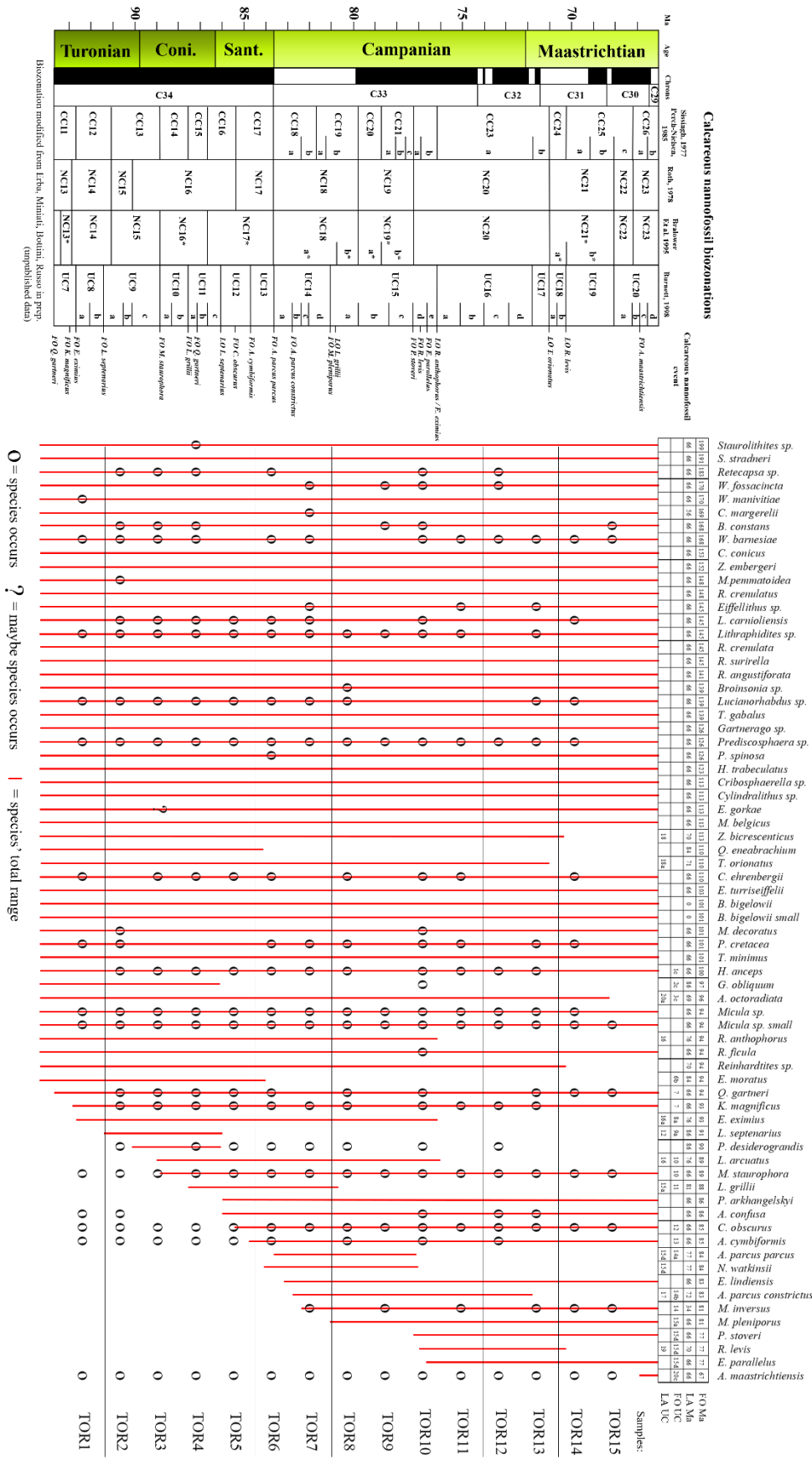


Figure 47: Range chart for offshore samples.

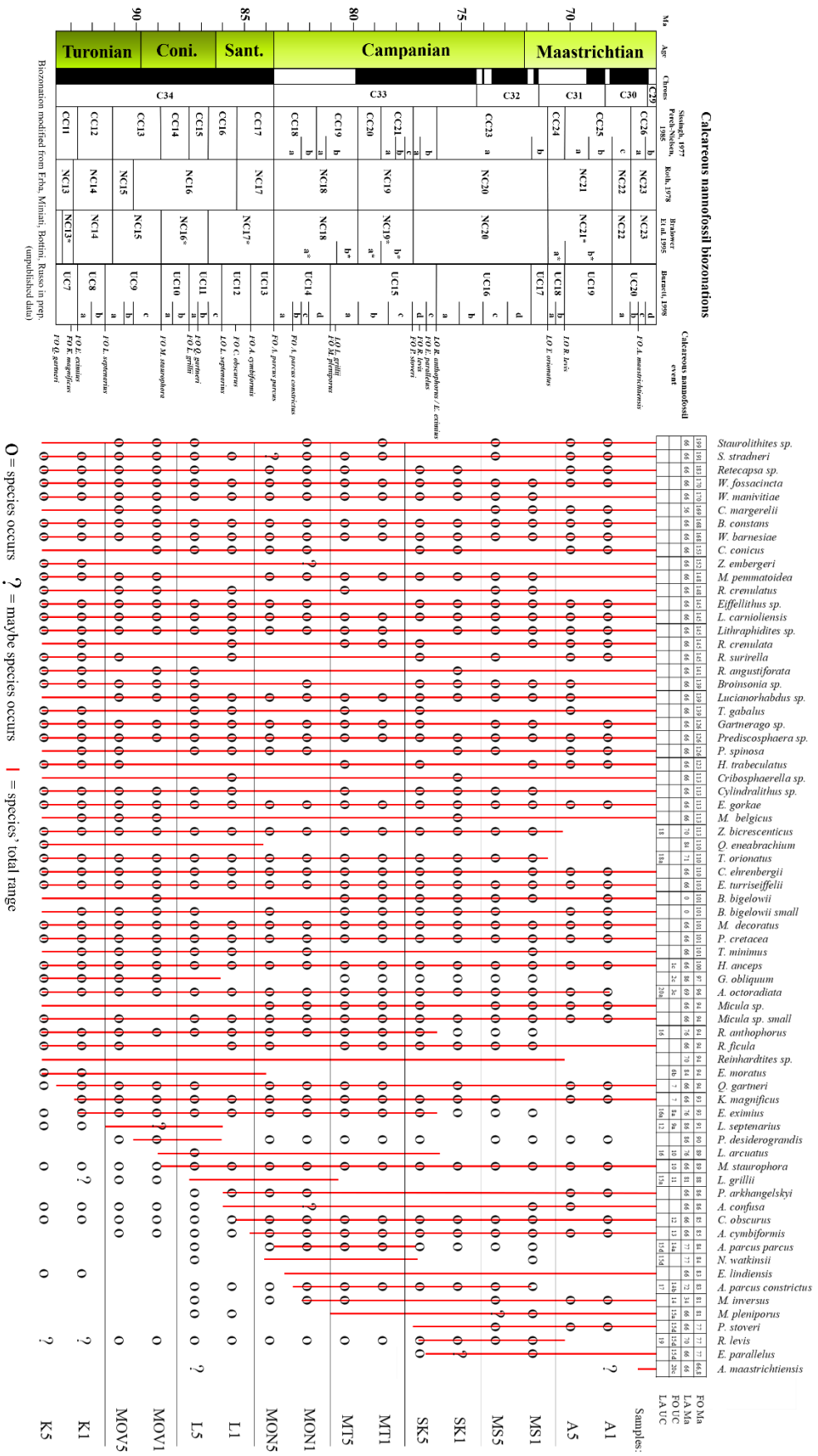


Figure 48: Range chart for onshore samples.

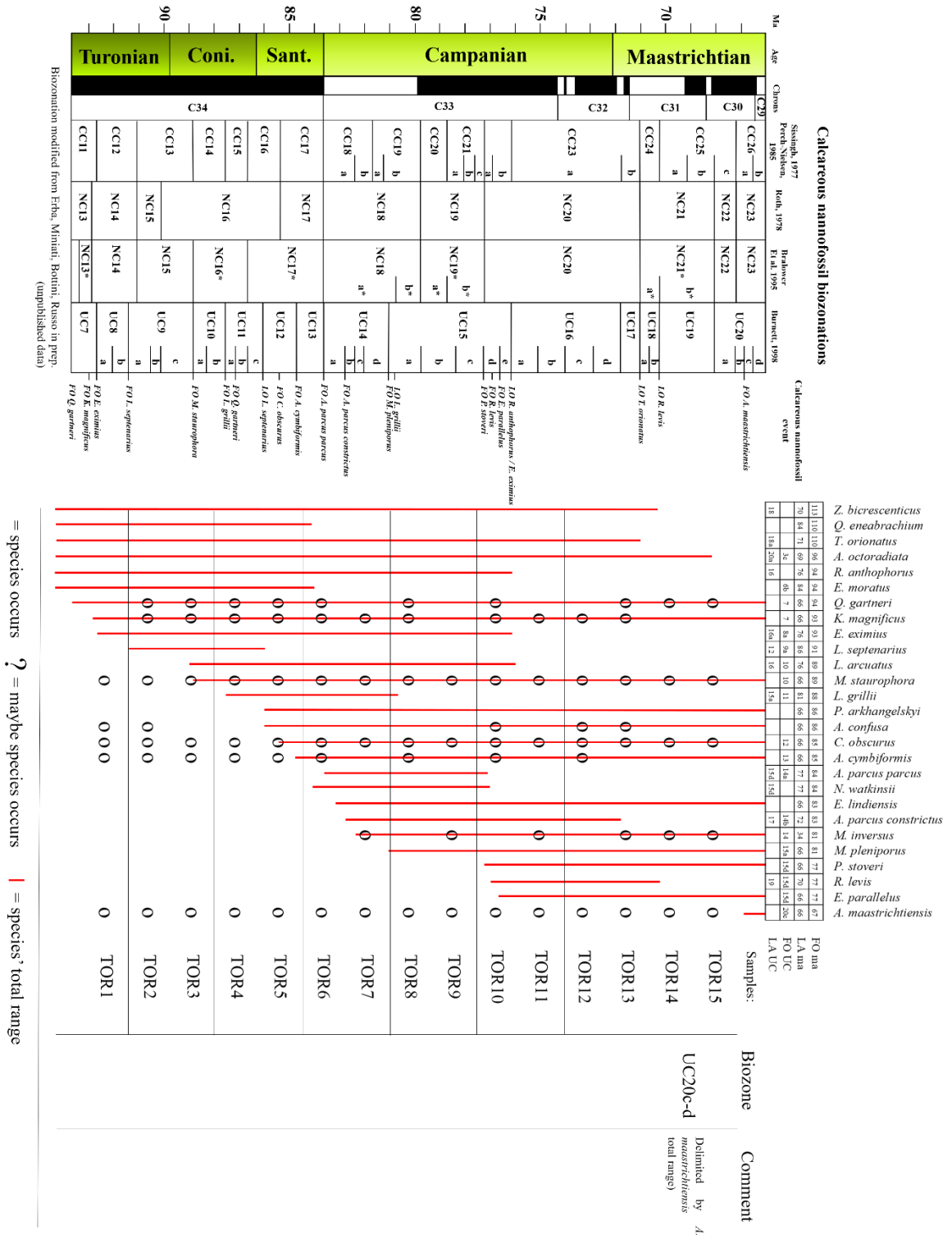


Figure 49: Biostratigraphic chart for the offshore samples.

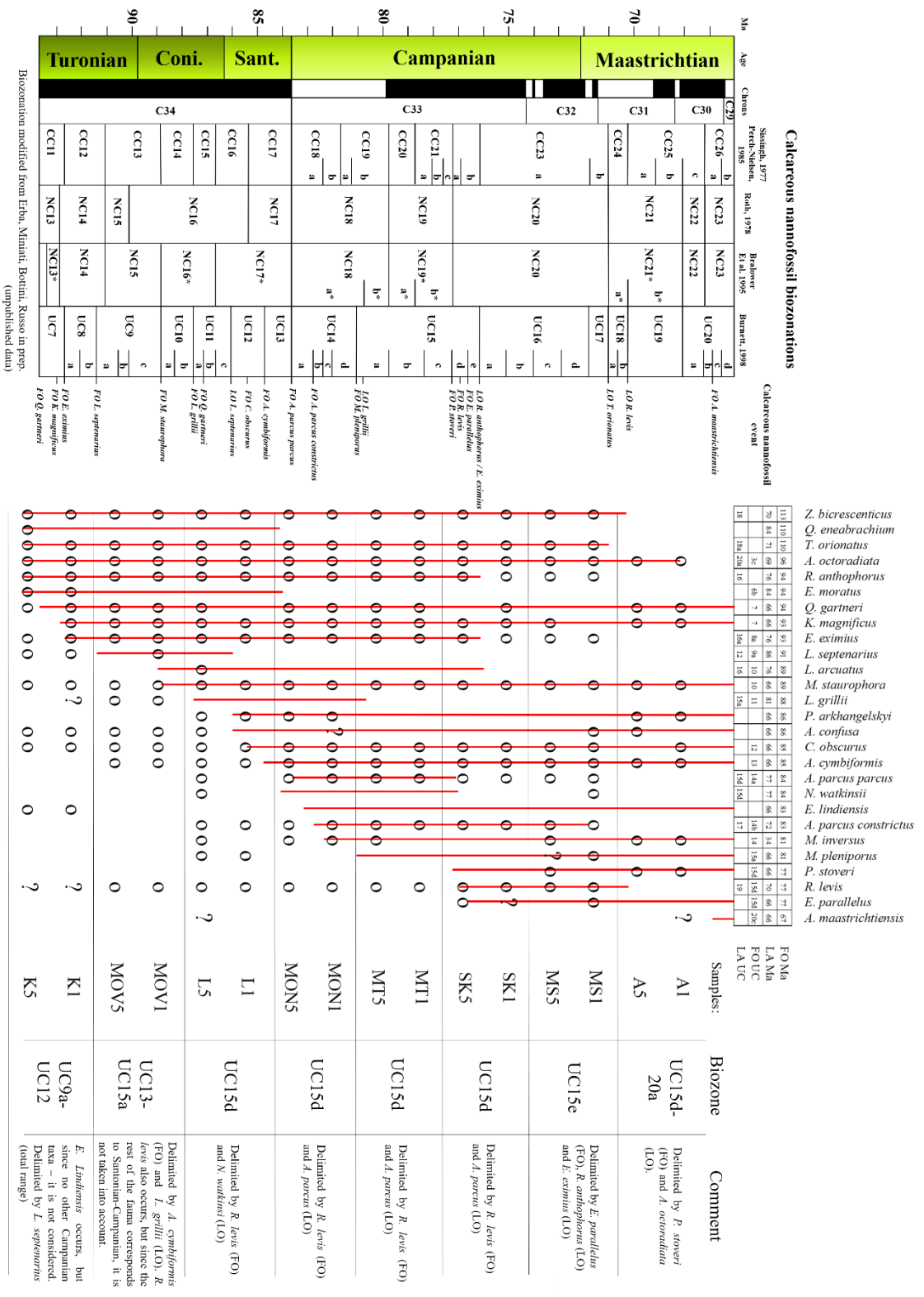
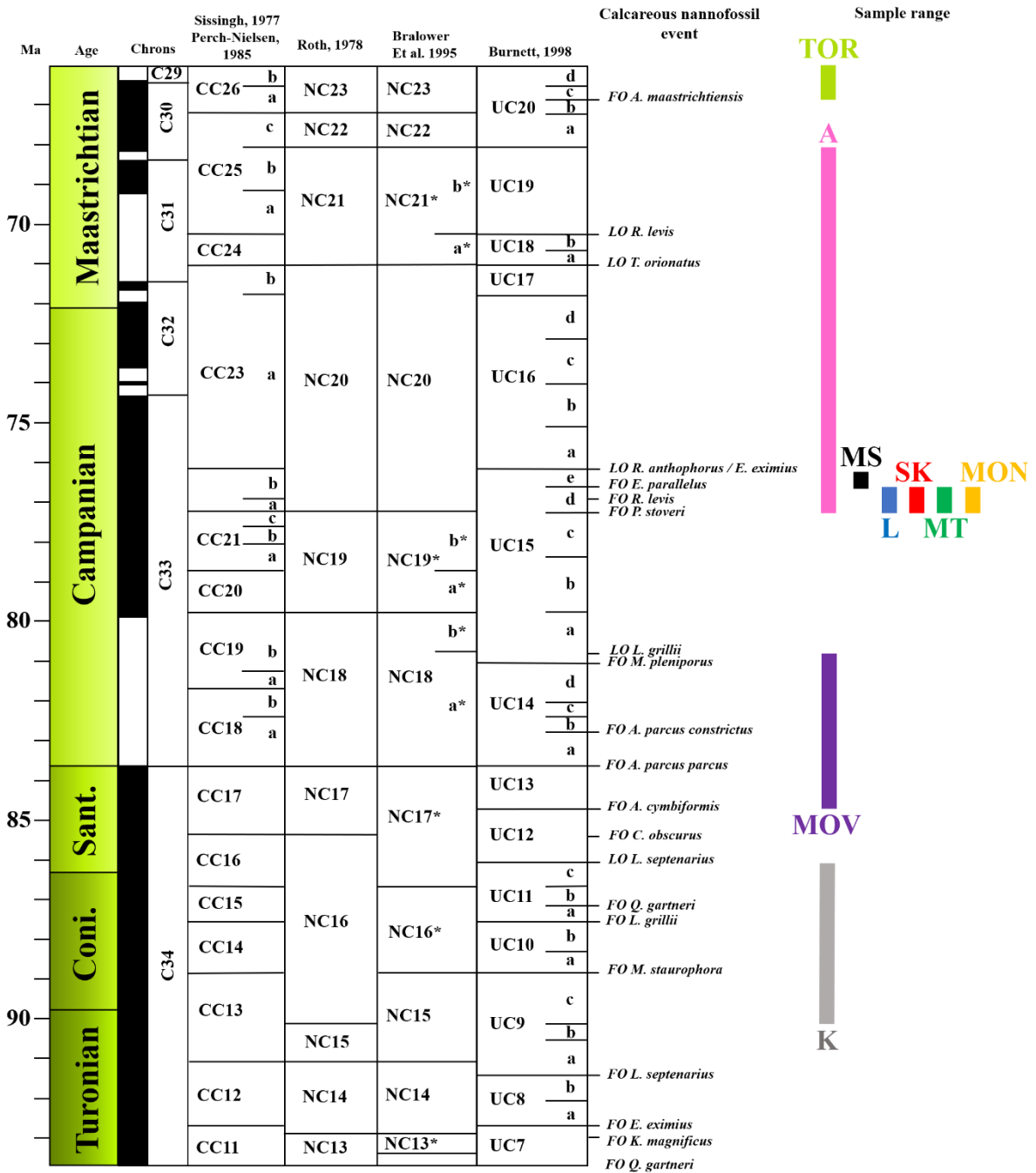


Figure 50: Biostratigraphic chart for the onshore samples.

Calcareous nannofossil biozonations



Biozonation modified from Erba, Miniati, Bottini, Russo in prep.
(unpublished data)

Figure 51: Conclusion of biostratigraphy for the offshore and onshore samples, represented by colored lines corresponding to the age span of the samples.

Table 6: Presumed ages for the samples (for references, see Chapter 5.3), and the results for new determined ages from this thesis' biostratigraphic analyses.

Sample	Presumed age	Determined age	Det. age UC
TOR15	K/T-boundary	K/T-boundary	UC20c-d
TOR14	Maastrichtian	Uppermost Maastrichtian	UC20c-d
TOR13			
TOR12			
TOR11			
TOR10			
TOR9			
TOR8			
TOR7			
TOR6			
TOR5			
TOR4			
TOR3			
TOR2			
TOR1			
A1	Uppermost Maastrichtian	Middle Campanian-Middle/Late Maastrichtian	UC15d-20a
A5			
MS1	Campanian	Middle Campanian	UC15e
MS5			
SK1	Uppermost Maastrichtian	Middle Campanian	UC15d
SK5			
MT1	Early Campanian - Early Late Campanian	Middle Campanian	UC15d
MT5			
MON1	Campanian	Middle Campanian	UC15d
MON5			
L1	Campanian	Middle Campanian	UC15d
L5			
MOV1	Campanian	Middle Santonian-Early Campanian	UC13-15a
MOV5			
K1	Early Coniacian	Late Turonian-Late Coniacian/Early Santonian	UC9a-12
K5			

All the flooded samples were biostratigraphically analysed to ensure they were of the same age as their unflooded equivalent. Only the flooded version of SK, core SK6 proved to have a different age than its unflooded equivalent (SK). It was therefore not comparable in terms of species and genera diversities and assemblages. The flooded SK6-core contained reniform coccoliths, resembling *Nephrolithus frequens* of Uppermost Maastrichtian age, as well as abundant *Arkhangelskiella maastrichtiensis*, also of Uppermost Maastrichtian age (Figure 52). SK6 is therefore likely to have an age of Uppermost Maastrichtian, while the unflooded SK core is of Middle Campanian age. Sample SK_inlet was not counted or analysed further.

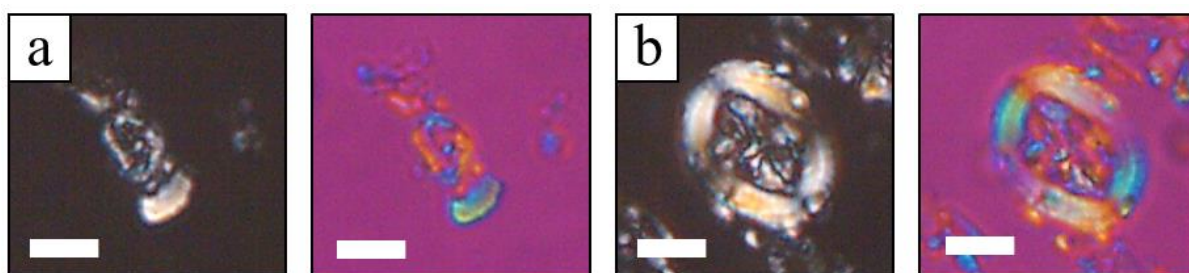


Figure 52: Coccoliths contained in the flooded SK6 core, at inlet position: sample SK_inlet. a: Reniform coccolith resembling *Nephrolithus frequens* and b: *Arkhangelskiella maastrichtiensis*. White scale bar = 5 μm .

4.1.4. Point Counting

The point count results are presented in Appendix 6. The samples have complex assemblage compositions - up to 41 species per sample (sample L5). Various genera and species constituting more than 3 % of the total assemblage are presented as percentages of the total assemblage for the offshore samples in Figure 53, since the total number of counts vary throughout the samples. Figure 54 displays the same as Figure 53, but for all samples, both offshore and onshore, also as counts. As all the onshore samples reached a count of ~ 300 , the assemblages can be compared as counts. Appendix 7 shows the calculations of species and genera in percentages of total count.

Estimates of calcareous nannofossil species in the total assemblage is coded as follows:

D = dominant (more than 51 % of the total assemblage)

A = abundant (11-50 % of the total assemblage)

C = common (2-10 % of the total assemblage)

F = few (0.1-1 % of the total assemblage)

R = rare (< 0.1 % of the total assemblage)

The offshore chalk assemblages are very different from the onshore chalk assemblages. Samples TOR1-9 generally contain a dominance of *Lithraphidites sp* and abundant presence of *Micula staurophora* and *Arkhangelskiella maastrichtiensis*, and common presence of *Prediscosphaera sp.*, *Kamptnerius magnificus* and *Calculites obscurus* (Figure 53). Samples TOR1 and TOR9 have significantly lower total calculated abundances of calcareous nannofossils per gram of sample ([n/g]) (22.9k and 28.4k, respectively), compared to TOR2-

TOR8 with [n/g] average 257.3k. Younger than TOR9, the assemblage composition changes. TOR10-TOR14 have an absolute dominance of *Micula sp.* (average at 66%), abundant presence of *Arkhangelskiella maastrichtiensis* and common presence of *Watznaueria barnesiae* and *Prediscosphaera sp* (Figure 53). Interestingly, TOR10 is the last offshore sample with a common presence of *Lithraphidites sp.* From TOR11 and on, the assemblages have 0% *Lithraphidites sp.* TOR15 is considerably different than the other offshore samples - first because, together with TOR9, it has a very low [n/g] (8.7k), but also since it contains an assemblage consisting of 21% *Biscutum constans* (versus 1% in TOR10) and 14% *Watznaueria barnesiae* (versus 4.4% in TOR11). However, the very low [n/g] must be considered when interpreting TOR15, as few counts constitute the assemblage composition.

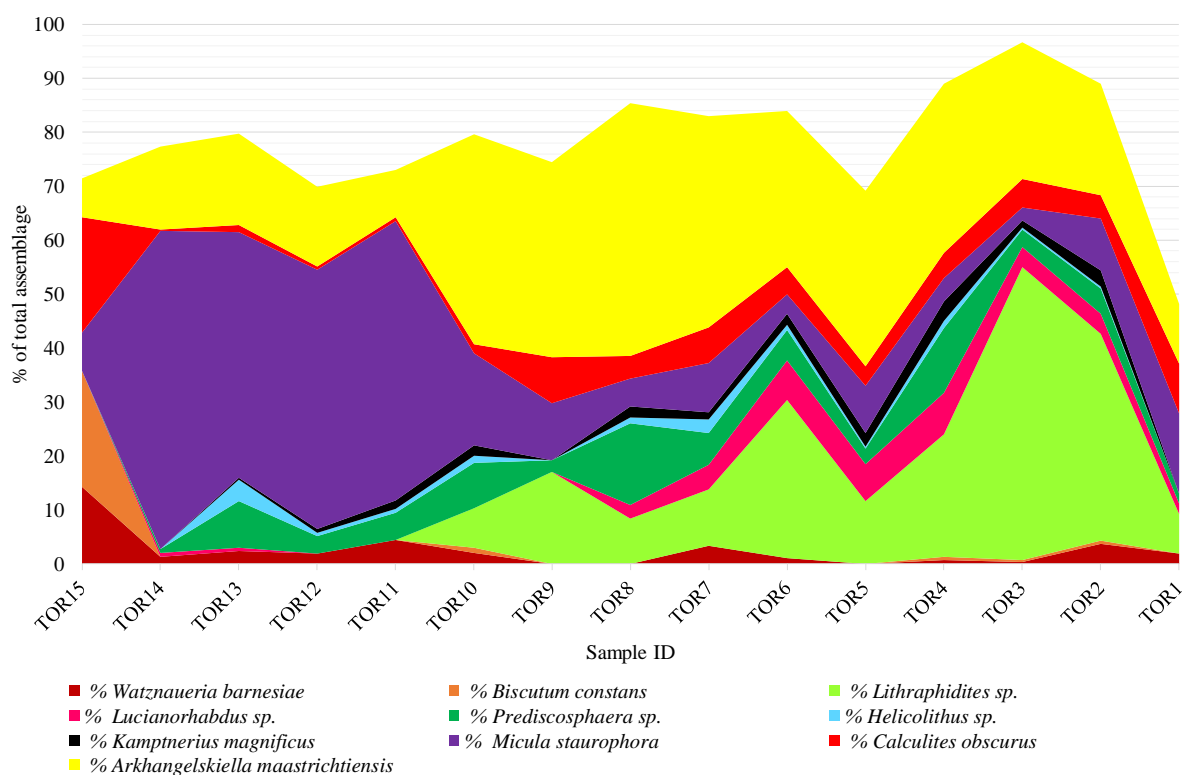


Figure 53: Assemblage composition in the offshore samples listed from youngest to oldest (left to right), represented by genera and species as percentages of total assemblage that are constituting more than 3 % of the total assemblage.

The onshore samples can be roughly divided into three main assemblages. The percentages that will be presented are the average for each core (average of sample 1 and 5). The first typical assemblage, named (for this thesis only) the *Tranolithus orionatus*-assemblage is found in samples K and MOV, which display similar assemblages, with an abundant presence of *Watznaueria barnesiae* (37% for K and 23% for MOV), *Prediscosphaera sp.* (14% for K and

23% for MOV), a common presence of *Eiffellithus sp.* (13% for K and 3.7% for MOV) and unlike the other samples, *Tranolithus orionatus* (11% for K and 7.2% for MOV). However, there are a few differences between them; Sample MOV has a common presence of *Biscutum constans* (5.5%), *Lithraphidites sp.* (6.8%) and *Ahmuellerella octoradiata* (4.2%), while K has few (< 1%). On the other hand, K has a common presence of *Helicolithus sp.* (8%), while for MOV this genus is few (< 1%).

The second typical assemblage, named (for this thesis only) the *Calculites obscurus*-assemblage constitutes samples L, MON, MT, SK and MS, which have a common to abundant presence of *Calculites obscurus*, unlike the other onshore samples. They all have an abundant presence of *Watznaueria barnesiae* (highest for SK with 40% and lowest for MON and MS with 22%), and common presence of *Reinhardtites levis*. *Biscutum constans* is abundant in sample MT (11%) and common in the remaining four samples. *Prediscosphaera sp.* is abundant in all samples but SK (5.8%). Samples L, MON and MS have abundant presence of *Micula staurophora*.

Sample A holds the third typical assemblage, which is particularly different from all the other onshore samples. This assemblage is named (for this thesis only) the few-*Watznaueria barnesiae*-assemblage. It is remarkable how few *Watznaueria barnesiae* it is in this sample (0.8%), as *Watznaueria barnesiae* usually dominate in Mesozoic assemblages. *Prediscosphaera sp.* is much more abundant in sample A than the remaining onshore samples (39% in A versus at the most 23% in MOV). *Micula staurophora* is also common (13%). Sample A is also differing from the other samples' assemblages (except MOV) by having a common presence of *Ahmuellerella octoradiata* (4.1%).

It is also noteworthy that the onshore cores display various variation from one end to the other end of the core. Samples K, MOV and A display less variety from sample 1 to 5 (for example decrease of only 0.6% of *Eiffellithus sp.* from A1 to A5) than the *Calculites obscurus*-assemblage samples that show significant variation (for example 9.6% decrease in *Watznaueria barnesiae* from L1 to L5).

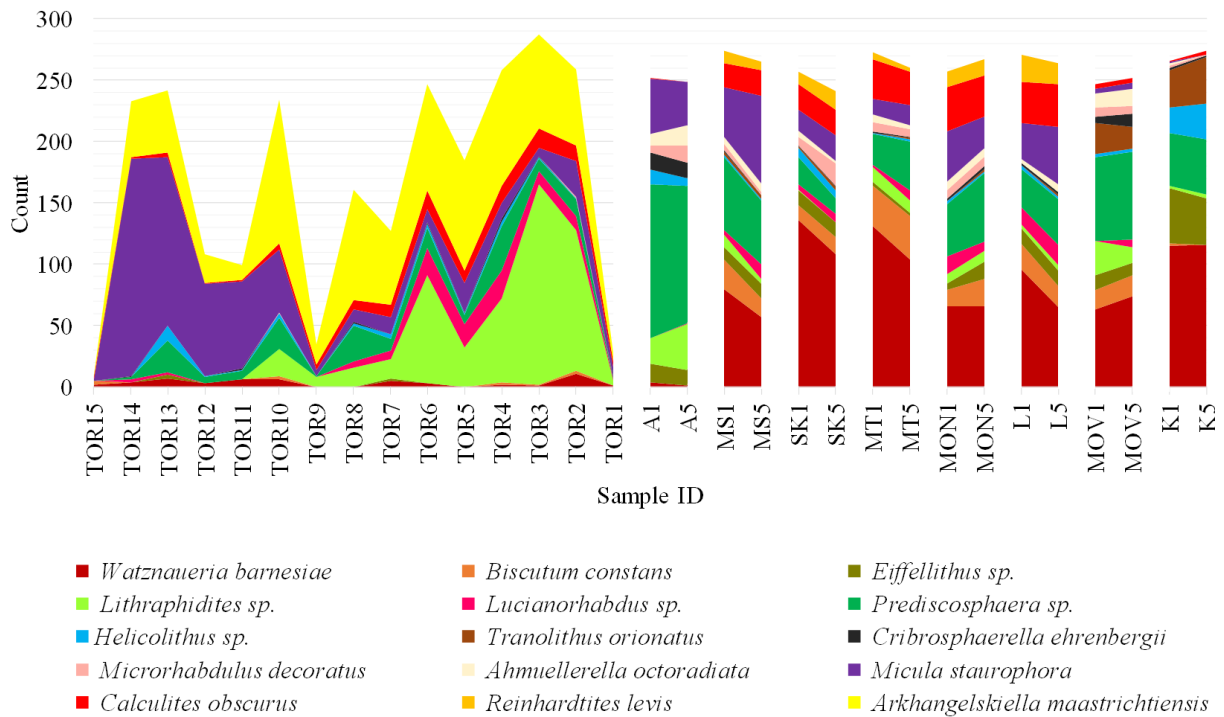


Figure 54: Assemblage composition in the various samples listed from youngest to oldest (left to right), represented by genera and species counts constituting more than 3 % of the total assemblage.

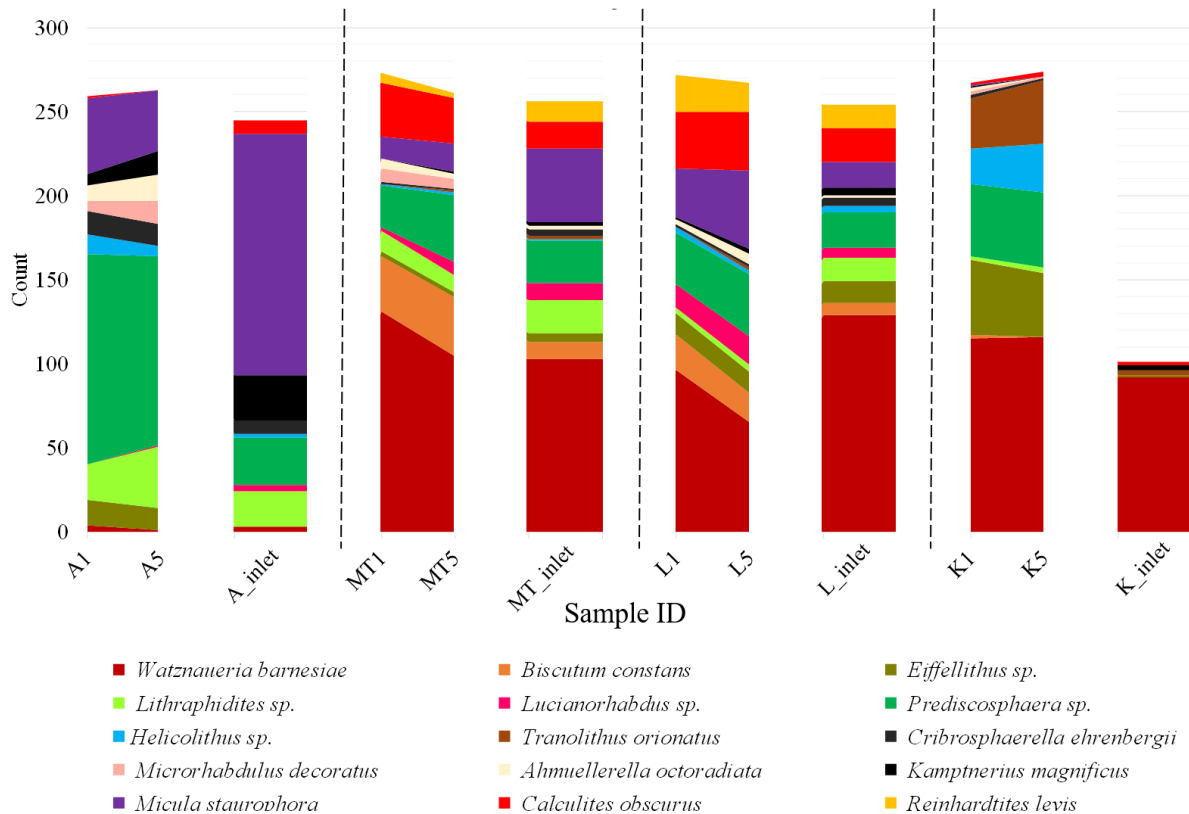


Figure 55: Comparison of assemblage compositions from unflooded to flooded samples at inlet position, as counts per sample.

The change of assemblage compositions from unflooded to flooded are displayed in Figure 55 as counts per sample. Sample A displays a 30% decrease of *Prediscosphaera sp.* and a 48% increase of *Micula staurophora* from the average unflooded to flooded sample at inlet position. Samples MT and L display opposite assemblage compositional changes from unflooded to flooded at inlet position: while MT has a 4.3% decrease in *Watznaueria barnesiae* and a 10% increase of *Micula staurophora*, L displays a 26% increase of *Watznaueria barnesiae* and a 7.4% decrease of *Micula staurophora*. *Biscutum constans* decreases with 7.8% in MT and 3.8% in L, from the average unflooded to flooded sample at inlet position.

Sample K shows a decrease of all assemblage components after flooding. However, since the calcareous nannofossil abundance was few, the assemblage constituents' percentages changes drastically from unflooded to flooded, with an increase of 52% of *Watznaueria barnesiae* in the total assemblage composition (Figure 56). There is also a slight increase of *Kamptnerius magnificus*, of 2.75%.

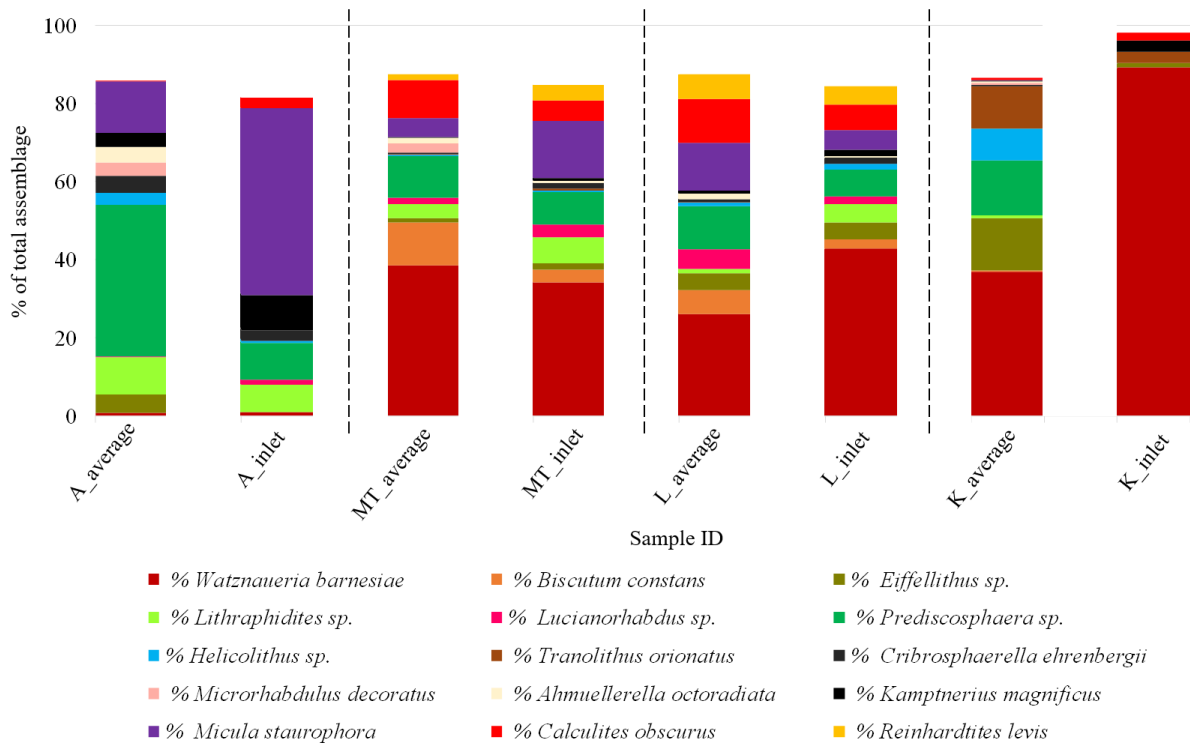


Figure 56: Change of assemblage compositions from unflooded to flooded samples at inlet position, as species or genus percentages of the total assemblage.

4.1.5. Paleoecology

Figure 57 summarizes the various paleoecological indices as percentages of total assemblage in each sample. The offshore sequence displays a change in paleoecological indices around sample TOR9. Samples TOR1-TOR9 have fewer diagenetic alteration indices and more cold-water indices than the upper and younger part of the sequence. It must be noted that although TOR15 has few counts of high nutrient indices, *Biscutum constans* (high nutrient index) constitutes 21% of the assemblage composition, which is high compared to the other samples (next highest is 7.7% for MS1).

Sample A shows similarities to the offshore samples, as both have low nutrient indices together with few cold-water indices. Samples MS, SK, MT, MON, L and MOV display similar abundance of paleoecological indices, with a dominance of warm water and low nutrient indices, as well as an average of 9.6% cold water indices and 7.8% high nutrient indices. Sample K also has a dominance of warm water and low nutrient indices, but cold water and high nutrient indices constitute less of the total assemblage, only 1.4% and 2.9% respectively. All samples contain diagenetic alteration indices.

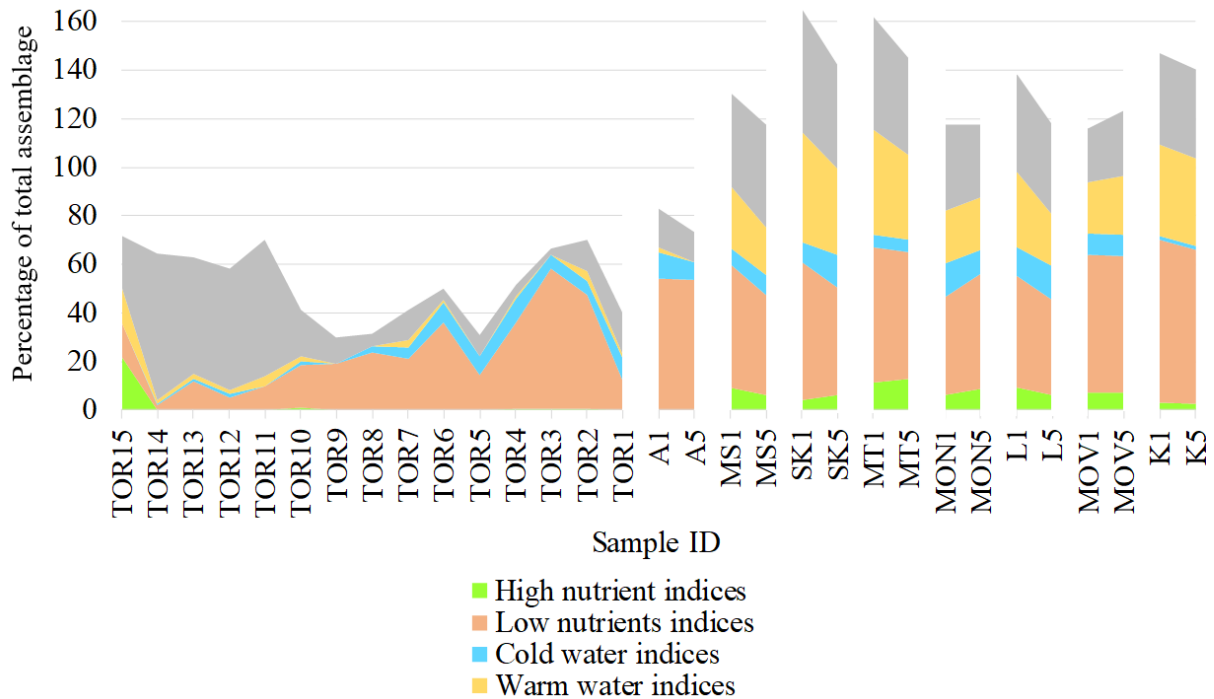


Figure 57: Various paleoecological indices in the offshore and onshore samples in percentage of total assemblage, from youngest to oldest (left to right). The combined percentages go above 100% for some samples due to that certain species are used as several paleoecological indices.

4.1.6. Calcareous Nannofossil versus Micarb Ratios

Since the offshore samples generally had very low calcareous nannofossil versus micarb ratios (NvsM-ratio), from approximately 1:99 – to 10:90, the estimations were not done for the offshore samples. As the flooded samples at inlet positions were prepared as simple smear slides, the estimations would not be comparable to the unflooded samples as random settling smear slides, and therefore the estimation was not performed on the flooded samples either.

Figure 58 displays the average estimated NvsM-ratios for the onshore samples. Samples A and MON show a decrease of nannofossil percentages from sample 1 to 5 of more than 50%. The rest of the samples have an average difference of 9.6%. MS has less variation with an increase of 2.7% from MS1 to MS5, while sample A has the greatest variation with a decrease of almost 82% from A5 to A1.

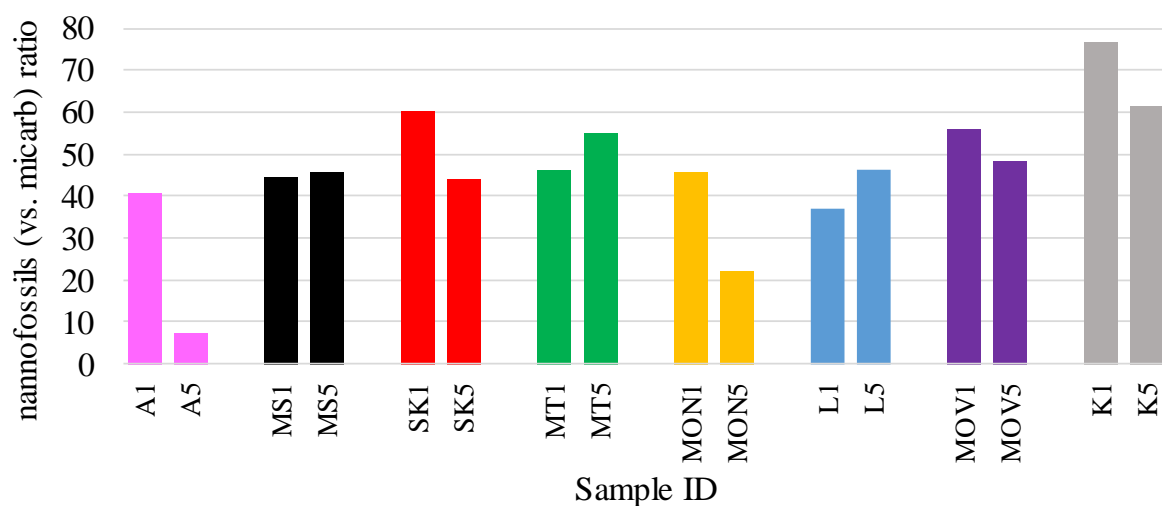


Figure 58: Nanofossil versus micarb ratios for the various samples estimated in the OLM, listed from youngest to oldest (left to right).

4.1.7. Special Observations

A few special observations have been done during this thesis work that will be presented. According to Burnett (1998), *Gartnerago obliquum* has an age span from the mid part of UC2c subzone (Cenomanian) to the Late Coniacian. This age span is also presented on Nannotax by Young et al. (2016). However, during this thesis' study, *Gartnerago obliquum* was encountered as well-preserved specimens in samples MT, SK and MS – samples that certainly are younger than Coniacian – and that through the biostratigraphic analyses are concluded to have an age of Middle to Late Campanian. In addition, *Eiffelithus lindiensis* was only encountered in sample K (age Late Turonian to Late Coniacian/Early Santonian), even though Lees (2007) determined an age range of Early Campanian to Late Maastrichtian for this species.

In all samples, onshore and offshore, small *Micula sp.* (diameter from corner to opposite corner < 3 μm) (Figure 59a-d) were observed. The younger offshore samples had the highest counts (up to 40 for TOR13), and the oldest onshore samples had the fewest (only 1 for K5) (Figure 60). All onshore sample also had small versions (< 8 μm) of *Braarudosphaera bigelowii* (Figure 59e-h), but they were rare.

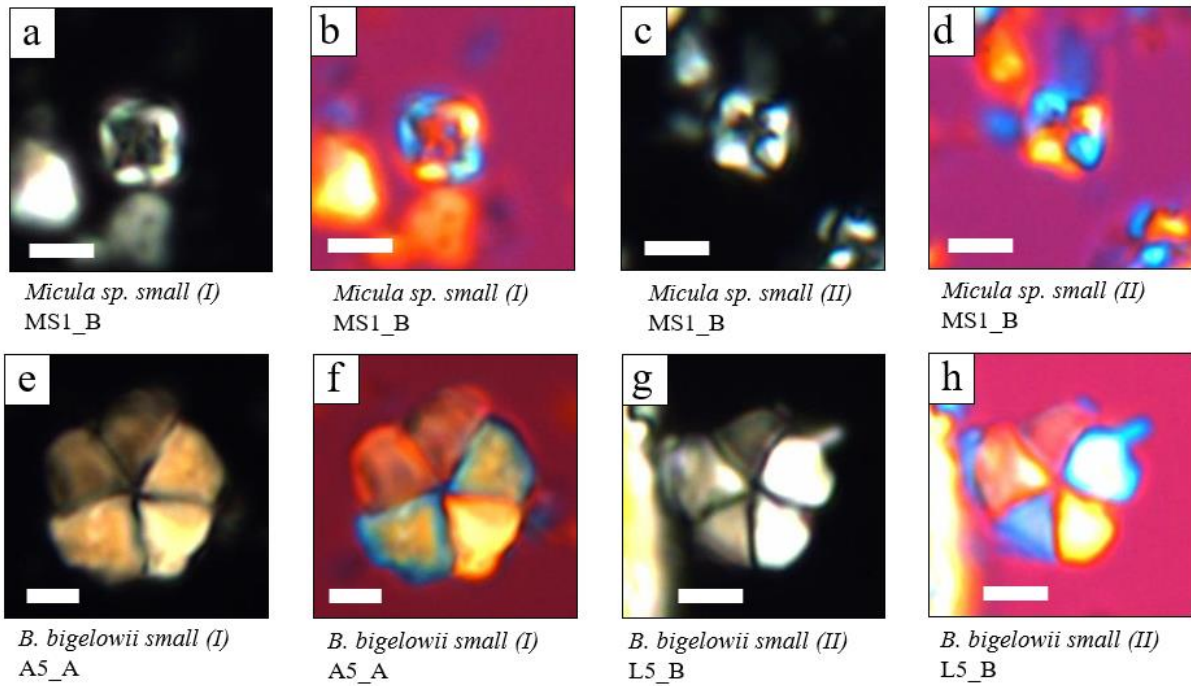


Figure 59: Small versions of calcareous nannofossil species. a-d: Small *Micula sp.*, e-h: small *Braarudosphaera bigelowii*. White scar bar = 2 μ m.

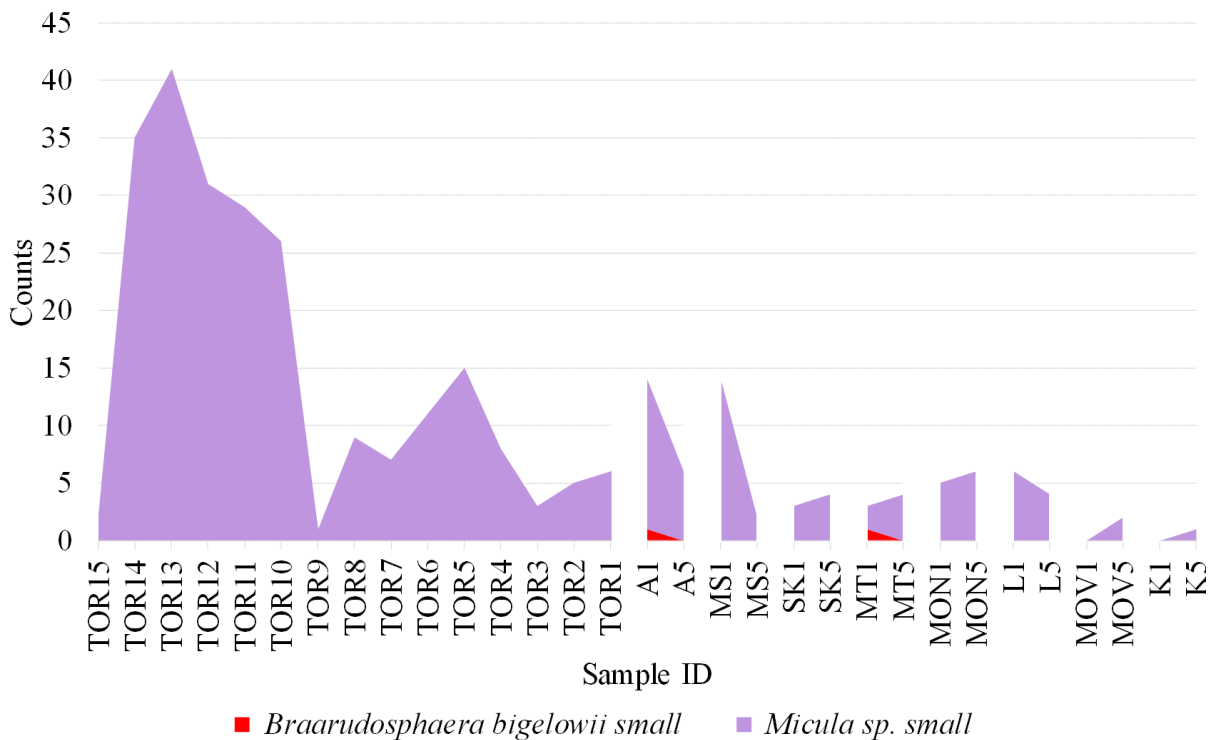


Figure 60: Counts of dwarf-species in the various offshore and onshore samples, from youngest to oldest (left to right).

Several specimens that are thought to belong to the genus *Micula* were encountered, that could not be identified according to existing species, even though they displayed distinctive morphologies. Their photographs can be found in Appendix 4, Plate VIIIp-t and Plate IXa-i.

4.2. Scanning Emission Gun Scanning Electron Microscopy (FEG-SEM)

4.2.1. Calcareous Nannofossil Preservation

Calcareous nannofossil preservation levels determined using the optical light microscope (OLM) were mostly confirmed using the FEG-SEM, except for the offshore samples that could not be prepared as FEG-SEM samples during the thesis time due to oil-contamination. An exception was sample MT1 (Figure 61) which after being investigated in the FEG-SEM was determined to be of poor-moderate preservation (in contrast to moderate preservation level as determined with the OLM). Sample K proved to have the best preservation level of all the samples after being studied in the FEG-SEM, being moderate (Figure 63) (in contrast to poor-moderate using the OLM). Its flooded equivalent, sample K_inlet, shows a very poor preservation (Figure 64).

Figure 62 display sample MT_inlet, where the preservation level has decreased to poor after flooding at inlet position. Figure 65 displays sample A1 of poor preservation, and sample A_inlet in Figure 66 has been strongly dissolved during flooding causing the preservation level to decrease from poor to very poor.

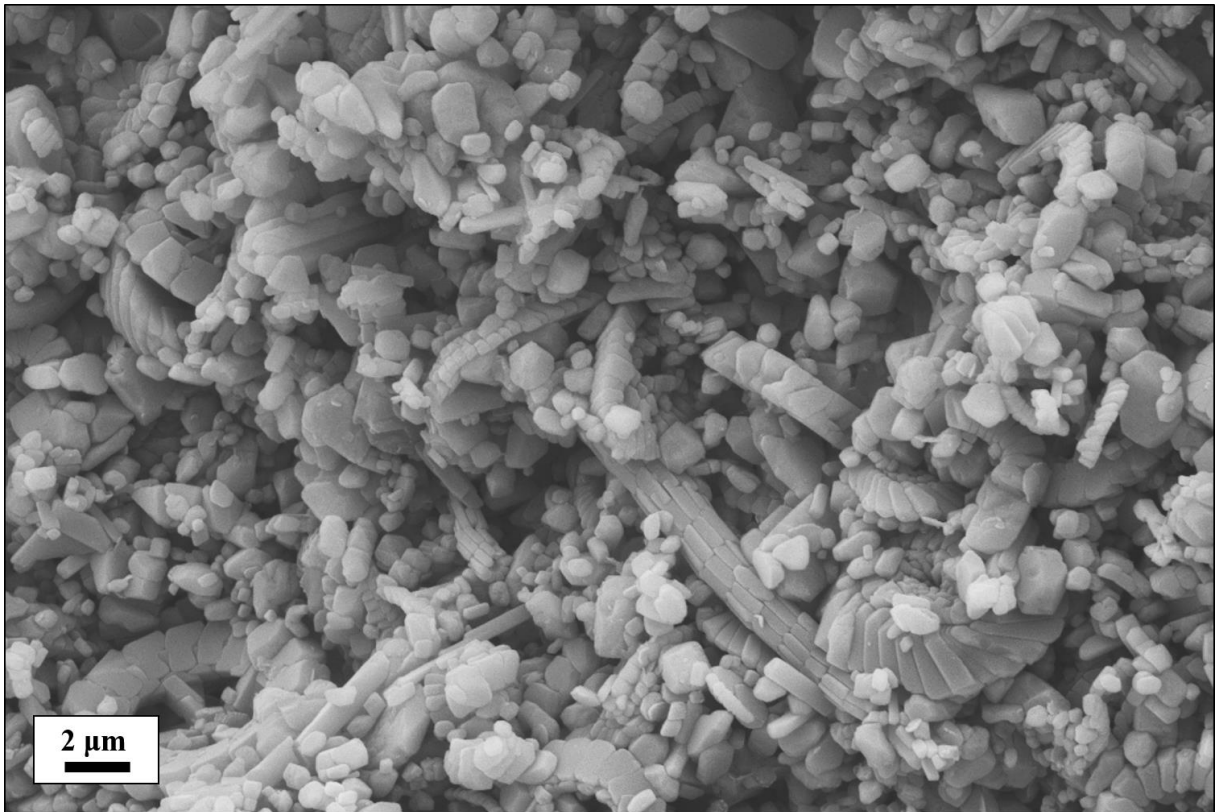


Figure 61: FEG-SEM micrograph of sample MT1, displaying poor-moderate preservation.

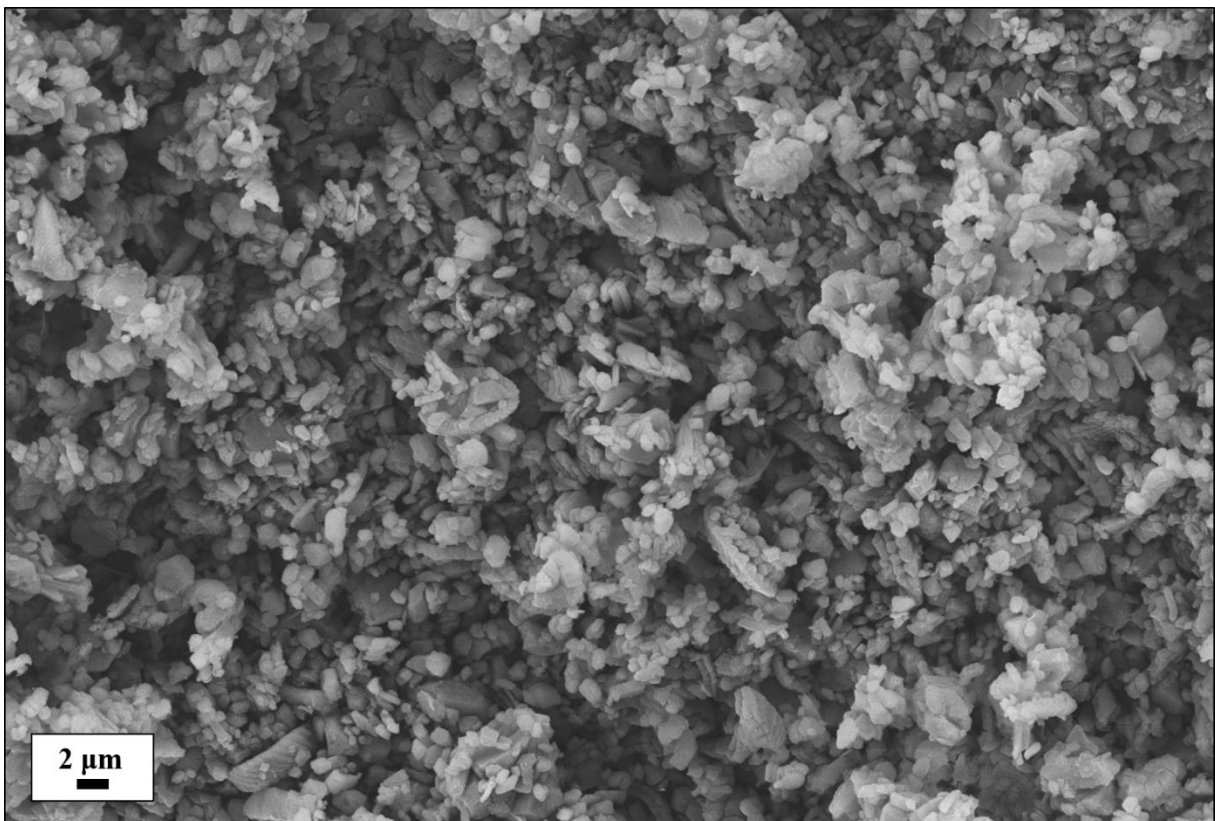


Figure 62: FEG-SEM micrograph of sample MT_inlet, displaying poor preservation.

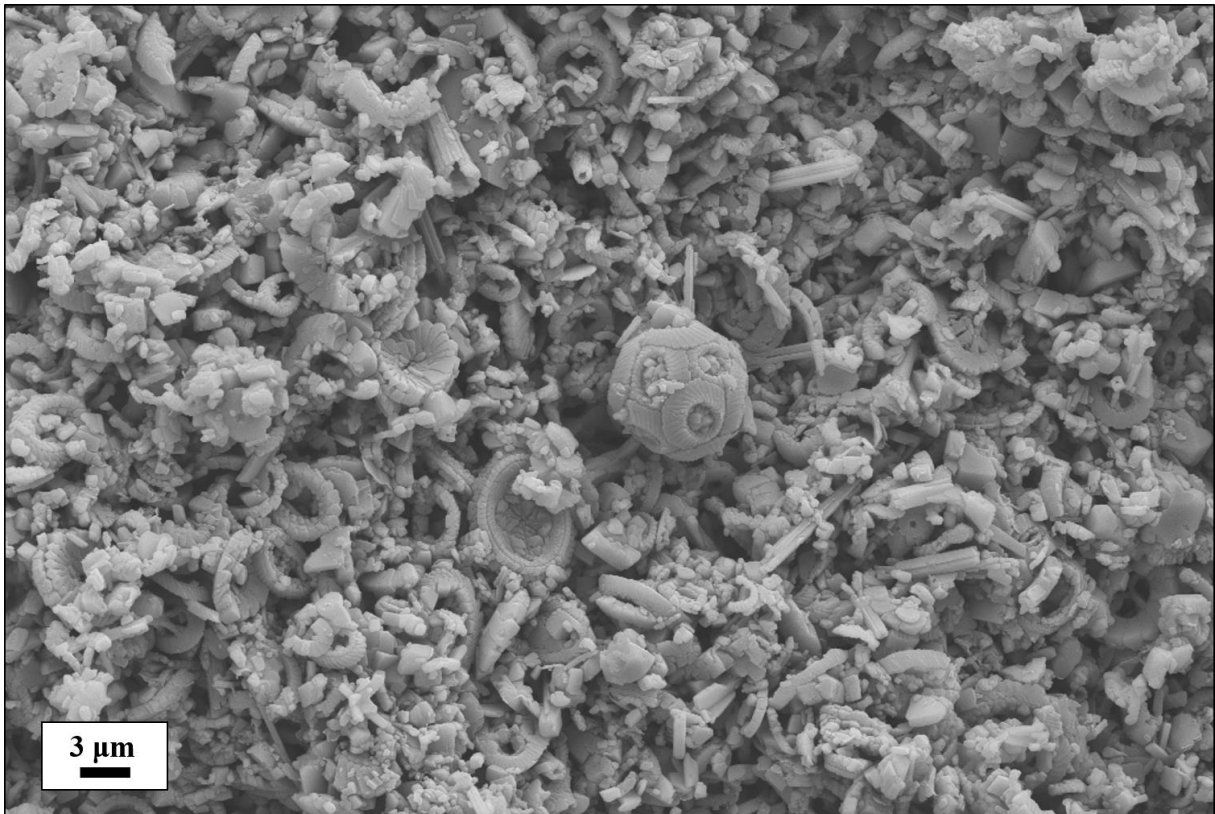


Figure 63: FEG-SEM micrographs of sample K1, displaying moderate preservation, as opposed to poor-moderate as determined using the OLM.

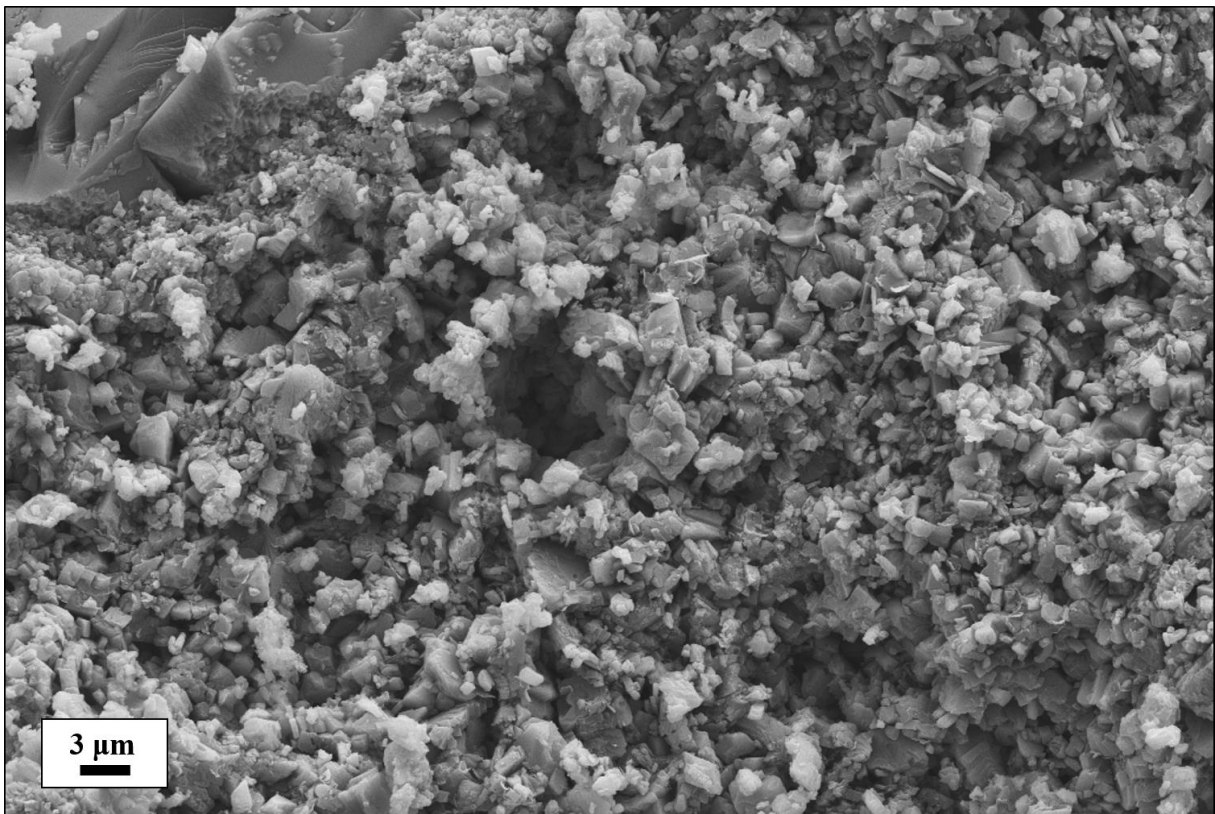


Figure 64: FEG-SEM micrographs of sample K_inlet, displaying very poor preservation.



Figure 65: FEG-SEM micrograph of sample A1, displaying poor preservation.

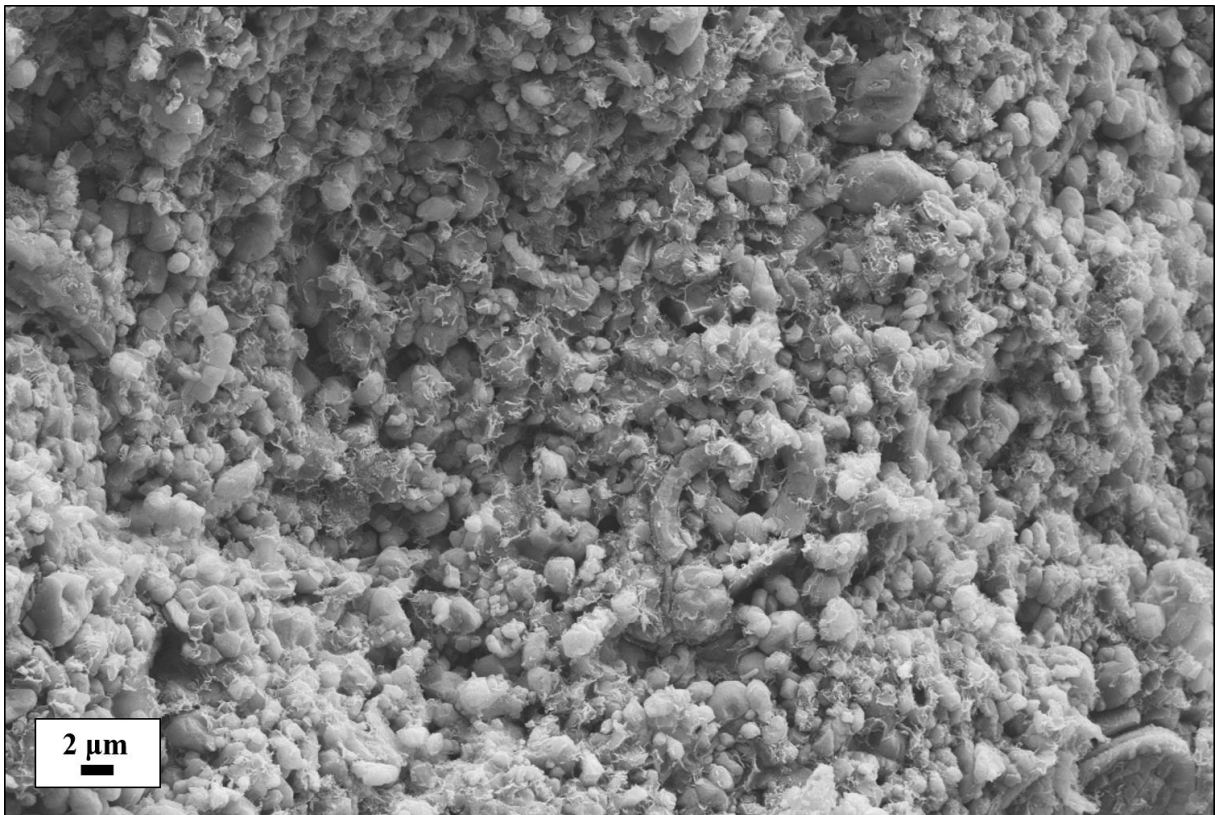


Figure 66: FEG-SEM micrograph of sample A_inlet, displaying very poor preservation.

4.2.2. Calcareous Nannofossil versus Micarb Ratios

The results of the average estimates of the calcareous nannofossil versus micarb ratios (NvsM-ratio) using FEG-SEM micrographs are displayed in Figure 67. Sample MS contains the least variation from one end of the core to the other, with an increase of only 2.8% from MS2 to MS5. The greatest variation is evident for sample MON, that has a decrease of nannofossils from MON1 to MON5 of 74.5%. A great decrease is also apparent in sample MOV, of 35.6%. Samples A, SK, MT and K have an average increase from sample 1 to 5 of 14.8%, and sample L has a decrease from sample 1 to 5 of 46.3%.

Estimations were also performed on the flooded equivalents of each core at inlet position. It is obvious that the flooded inlet samples experience a drastic decrease in % nannofossils (versus micarbs), compared to their average unflooded equivalents. Samples A and K have the more extreme decreases, of 94.5% and 93.9% respectively. Sample MT and L have decreases of 73.9% and 65.4% respectively.

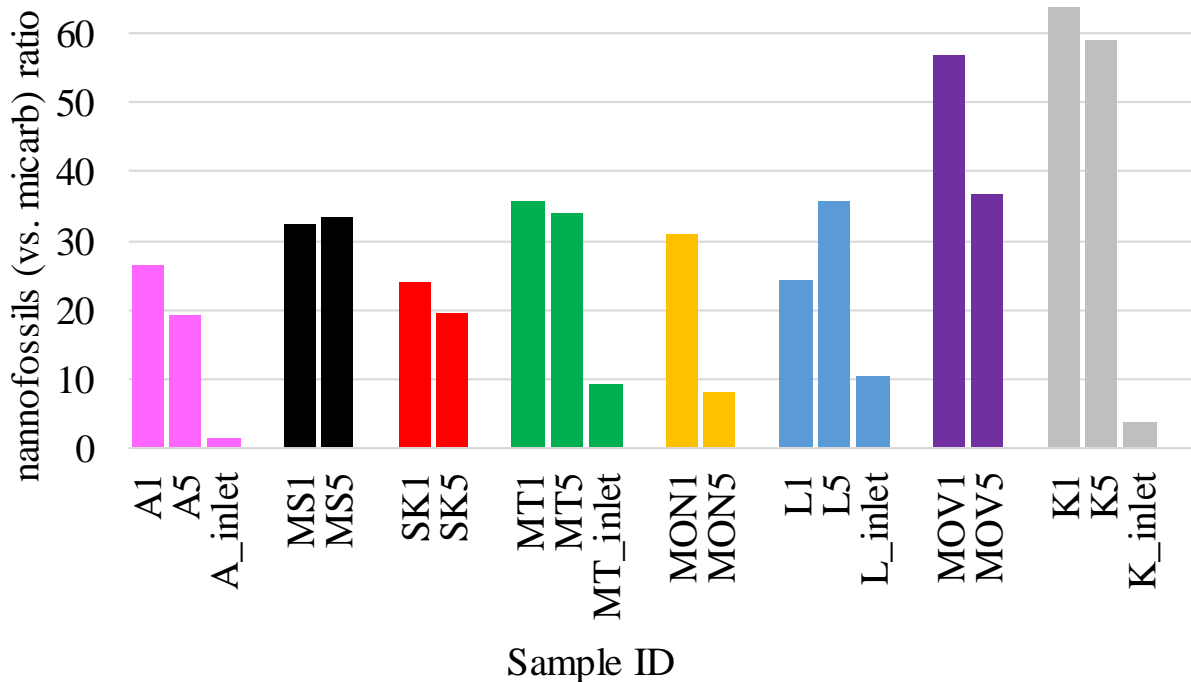


Figure 67: Nannofossil versus micarb ratios for the various samples estimated in the FEG-SEM, listed from youngest to oldest (left to right).

5. Discussion

5.1. Calcareous Nannofossil Preservation in OLM and FEG-SEM

Interestingly, there is no correlation between age and preservation level in neither the offshore or onshore samples. The offshore samples are the youngest but show the poorest preservation level. This might be linked to the depth of burial and level of diagenesis, as it has been demonstrated by Jørgensen (1986) that the diagenetic impact on chalk cores from the Late Cretaceous in the North Sea generally is related to pressure-dissolution processes and reprecipitation, which likely leads to poorer preservation of calcareous nannofossils.

The light microscope is a quick way to assess the preservation level of chalk samples. However, as presented in Chapter 4.2.1, the FEG-SEM might be more reliable as it allows highly detailed micrographs of the calcareous nannofossils. The preservation levels of the various samples were therefore adjusted according to the FEG-SEM results and are presented in Table 7. When preparing random settling smear slides, there is a small risk that the samples might get altered during the settling. This would be valid if the preservation levels were poorer in OLM than in the FEG-SEM. However, this is not the case, as sample MT was determined to be of poorer preservation in FEG-SEM than in OLM. Perhaps the correct preservation level might be somewhere in the middle of the determined levels obtained with OLM and FEG-SEM, but closer to FEG-SEM due to its superior detail-level. The two methodologies can with advantage be complimentary. The determination of preservation levels, combining results from both OLM and FEG-SEM are displayed in the right column in Table 7.

Table 7: Comparison of preservation levels determined from the OLM and FEG-SEM, and final determination by combining them. The preservation levels are assigned a colour range depending on the level: from dark grey (very poor) to white (moderate).

Sample	Preservation level from		
	OLM	FEG-SEM	Combined
TOR	P	-	P
A	P	P	P
A_inlet	VP	VP	VP
MS	P	P	P
SK	P-M	P-M	P-M
MT	M	P	M
MT_inlet	P	P	P
MON	P	P	P
L	P-M	P-M	P-M
L_inlet	P	P	P
MOV	P-M	P-M	P-M
K	P-M	M	M
K_inlet	VP	VP	VP

The IOR flooding experiments with a brine of $MgCl_2$ decreased the preservation level in all the flooded samples. The preservation level generally decreased one to two levels during flooding. However, it is interesting that the two samples with the best unflooded preservation levels combining the results from OLM and FEG-SEM (moderate preservation level), MT and K, displays different impact by flooding. MT decreases from moderate preservation to poor preservation during flooding, while K decreases from moderate to very poor. This is likely explained by the duration of the flooding experiments, as sample K was flooded for 15 days longer than MT. Sample A also displays very poor preservation after flooding, but the flooding lasted only three days longer than for MT. This might be linked to the original preservation level of the sample, as sample A had poorer original preservation than MT, as the preservation has a trend of decreasing one level after flooding for ~ 60 days.

Table 8: Comparison of preservation level and duration of flooding (d = day). Duration data from Andersen et al. (2017). The preservation levels are assigned a colour depending on the level: from dark grey (very poor) to white (moderate).

Sample	Preservation level	T (d)
A	P	-
A_inlet	VP	63
MT	M	-
MT_inlet	P	60
L	P-M	-
L_inlet	P	65
K	M	-
K_inlet	VP	75

5.2. Calcareous Nannofossil Abundance and Species Diversity

Calcareous nannofossil abundances might be linked to paleoecological factors and diagenetic history, and abundance changes from one end of a core to the other can indicate different paleoecological settings. This might clarify if the onshore samples have been sampled horizontally or vertically through the stratigraphy. If sampled horizontally within the same stratigraphy, the core should display similar abundances as the depositional setting would be the same, as the core length is only 8-10 cm. The depositional rate of Maastrichtian chalk in the North Sea has been estimated to be between 10 cm per thousand years (cm/ka) in the central North Sea basin and 2 cm/ka at the margins (Zijlstra, 1995). The depositional setting of the onshore chalk is likely more comparable to the margin settings, giving less than 2 cm/ka. If sampled vertically, there might be large abundance differences as each end of the core could represent paleoecological settings of several thousands of years in difference (8-10 cm of chalk might represent more than ten thousand depositional years). This is the case for the 84.4 metres long TOR sequence, that displays various abundances throughout time, which might be linked to different paleoecological or depositional factors.

The three onshore samples with the largest total calculated abundance changes from one end to the other in percentages (> 30%) are MS, MT and K. This might indicate that these cores have been sampled vertically. Samples A and MOV have changes between 25-30%, which might indicate less vertical sampling through stratigraphy, perhaps more diagonal as it captures less abundance change. Samples SK, MON and L have total calculated abundance changes less than

5%, which is remarkably less than the other samples. This could support a closer to horizontal sampling through stratigraphy.

The calculated total abundances of calcareous nannofossils cannot be used to indicate sampling-direction through stratigraphy alone. It is important to combine the results with changes in number of species, genera, assemblage constituents and paleoecological index nannofossils. The results will be compared in the following chapters.

Samples K and A have the lowest average number of species (28 and 32, respectively) and genera (25 and 22, respectively), which might indicate that these samples were deposited in more unstable and stressed paleoecological conditions, such as cold waters with high nutrient-levels, than the other onshore samples. Change of species and genera diversity from one end to the other of each core might also indicate sampling-direction, as larger differences might indicate vertical sampling and smaller differences might indicate horizontal sampling. Sample MT displays the largest species diversity change, with an increase of 6 species (16% diversity increase) from MT1 to MT5 – which might indicate more vertical sampling, supporting the evidence from abundance change. Sample K has a species diversity decrease of 11%, also supporting the abundance change trend. Sample L shows a species diversity increase of 10%, which is odd compared to its 4.6% abundance increase, in conflict with its presumably horizontal sampling through stratigraphy. Samples A, MS, SK, MON and MOV have species diversity changes of less than 2 species. Sample MS therefore also has incompatible evidence for sampling-direction.

The species/genera (S/G) ratio has increased with time (Flessa and Jablonski, 1985; Alroy, 2008), with genera becoming more species-rich over time (Lloyd et al., 2012). The S/G ratios of the samples are in accordance with the results from the biostratigraphic analyses, with MOV and K having the lowest S/G ratios (1.0 and 1.1, respectively), followed by L and MON (1.4) and at last MT, SK, MS and A - all with S/G of 1.5.

The offshore TOR samples have an average species diversity of 13 and genera diversity of 11, which is much lower than the onshore samples, and might indicate even more unstable and stressed paleoecological conditions. It could also be due to its poor preservation. Preservation or unstable paleoecological conditions might also explain the average S/G ratio of 1.2, which is lower than the Middle Campanian samples, even though TOR is of Uppermost Maastrichtian age. The species and genera diversity variations within the sequence might display times when

the paleoecological conditions were more stable (TOR2 and TOR10), and times when conditions were extremely unstable (TOR1 and TOR15).

5.3. Biostratigraphic Analyses

The TOR samples had a presumed age of Maastrichtian. Through the biostratigraphic analyses, it was possible to narrow down the age-range to Uppermost Maastrichtian (biozone UC20c-d). The same TOR-sequence had been biostratigraphically analysed by Perch-Nielsen in the well-report by Church et al. (1978). Perch-Nielsen stated that due to the presence of *Arkhangelskiella cymbiformis*, the sequence cannot be older than the middle Maastrichtian. Further on, the report claims that the absence of *Nephrolithus frequens*, which is a marker species of the Uppermost Maastrichtian does not necessarily mean that there is a hiatus before the Cretaceous/Cenozoic (K/T) boundary, but that the species was likely lost due to poor preservation.

The species that is known today as *Arkhangelskiella maastrichtiensis* (Burnett, 1997) (also named *Arkhangelskiella maastrichtiana* in some literature) was first described as *Arkhangelskiella cymbiformis* var. by Varol (1989), after Perch-Nielsen had completed her report from the well. The description she used to identify *Arkhangelskiella cymbiformis* in 1978 is not included in the report, but as the three different species within the *Arkhangelskiella cymbiformis* group were not distinguished before Burnett did it in 1997, the species that Perch-Nielsen identified is likely based on the *Arkhangelskiella cymbiformis* description by Vekshina (1959). *Arkhangelskiella maastrichtiensis* (Burnett, 1997) has a range of Campanian to Maastrichtian according to (Young et al., 2016). In her species description, Burnett (1997) remarks that the species becomes common in the Upper Maastrichtian in higher latitudes (such as the North Sea) and can be used as a marker species as its first occurrence marks the beginning of UC20c (Burnett, 1998).

Sample TOR15 is very different than the other TOR samples, as it has a very rare nannofossil abundance. In her report, Perch-Nielsen marked this sample to be the last of Cretaceous age, thus representing the K/T boundary. Samples TOR16-TOR20 were briefly analyzed for calcareous nannofossils, but no Cenozoic taxa could be determined with confidence. A few *Markalius inversus* (which survived the K/T boundary), *Prediscosphaera* sp. and *Micula* sp. were encountered, but they are likely reworked Cretaceous taxa, as this is a common phenomenon described by Pospichal and Wise (1990). According to Burnett (1998), the K/T boundary often consists of clay which is carbonate-poor and barren. As sample TOR15

experienced such a drastic decrease in both species diversity and calcareous abundance, it fits the description of the K/T boundary. Another supporting evidence will be presented in Chapter 5.5.

The onshore samples will now be discussed from youngest to oldest, and the determined ages will be compared to the presumed ages (if previous literature exists). First, it is important to highlight that it is challenging to give a single biozone for a chalk core of 8-10 cm, as biozonation analyses usually are performed on longer sequences, where first and last occurrences can be determined within the sequence, and the evolution of assemblages can be described throughout the sequence. A chalk core of 8-10 cm gives at best a peak into a narrow age window, and if lucky – the first or last occurrences of marker species can determine the exact biozonation.

The A sample has been sampled from the Rørdal Member (Rørdal quarry, east of Aalborg) of the Tor Formation, which according to Surlyk et al. (2010) is of Uppermost Maastrichtian age, based on the *semiglobularis-humboldtii* brachiopod zone (Surlyk, 1970, 1984) and the UC20b-c (high latitude) nannofossil zone (Sheldon, 2008; Thibault, 2010). This thesis' biostratigraphic analysis concluded with a biozonation range of UC15d-UC20a. As no marker species delimiting single biozones were encountered, the age could not be determined further. Based on this thesis' work, the most correct age for core A is therefore the range Middle-Campanian to Middle/Late Maastrichtian until a carefully sampled section can be studied to determine first and last occurrences through a sequence.

Sample MS had a presumed age of Campanian (Zimmermann, U., personal communication, 2018). Biostratigraphic analyses in this thesis could limit the sample to biozone UC15e, of Middle Campanian age.

Samples SK was the only sample that had its presumed age drastically changed, from Uppermost Maastrichtian to Middle Campanian. It is also the only sample that had a flooded equivalent core which was of a different age (Uppermost Maastrichtian). According to Surlyk et al. (2006), the Stevns Klint cliff displays the stratigraphic evolution from the uppermost Maastrichtian to Danian. It was presumed that sample SK was collected from the Sigerslev Member of Tor Formation in the Sigerslev quarry and therefore belongs to the upper Maastrichtian *Nephrolites frequens* nannofossil zone and *Pseudotextularia elegans* foraminifer zone based on Surlyk et al. (2006) (Zimmermann, U., personal communication, 2018). However, the unflooded sample SK is certainly of Middle Campanian age, as it contains

Aspidolithus parvus parvus and *Reinhardtites levis*, and no *Nephrolites frequens*. The flooded SK6 core on the other hand contained *Nephrolites frequens* and *Arkhangelskiella maastrichtiensis* and can be assigned to the Uppermost Maastrichtian. As the SK samples come from an onshore open pit quarry, it is possible that the unflooded SK core of Middle Campanian age and the flooded SK6 core of Uppermost Maastrichtian age have been sampled from different stratigraphic sections within the same quarry (Korsnes, R. I., personal communication, 2018), as seen in Figure 68. This is important to keep in mind when performing increased oil recovery experiments and research, as the assemblages change with the stratigraphy, which might affect the experiments. If used as time-equivalent analogues to reservoir chalks, it would be incorrect to use the unflooded sample SK as an analogue to Maastrichtian reservoir chalks.



Figure 68: Stevns Klint onshore chalk quarry with different lithostratigraphic sections, photographed by Pedersen (2013).

Sample MT was sampled from the quarry Lixhe (Belgium) and belongs to the Trivières chalk, from the belemnite zone *Goniatites Quadrata*, and was therefore presumed to have an age of Early Campanian to Early Late Campanian (Richard et al., 2005). This thesis' biostratigraphic analyses determined a biozone of UC15d for sample MT, corresponding to Middle Campanian, hence the presumed age range could be narrowed down significantly by using calcareous nannofossil biozonations.

Sample MON had a presumed age of Campanian (Zimmermann, U., personal communication, 2018). Biostratigraphic analyses in this thesis could limit the sample to biozone UC15e, of Middle Campanian age.

Sample L was sampled from the Zevenwegen Member (Robaszynski et al., 2001), deposited during the presumed age Campanian belemnite zone *Belemnitella mucronata* (Slimani, 2001). This thesis' biostratigraphic analyses determined a biozonation of UC15d, limiting the age to Middle Campanian by using calcareous nannofossils.

Sample MOV had a presumed age of Campanian (Zimmermann, U., personal communication, 2018). This thesis' biostratigraphic analyses could not conclude on a Campanian age alone but determined an age range of Middle Santonian-Early Campanian using calcareous nannofossils.

Sample K was sampled from the Niobrara Formation which was deposited during the Early Coniacian (Frey, 1972; Da Gama et al., 2014). This thesis' biostratigraphic analyses could not determine an exact biozone but could conclude on an age range from Late Turonian-Late Coniacian/Early Santonian by using calcareous nannofossils.

5.4. Point Count: Calcareous Nannofossil Assemblages and Implications

The point count of the offshore TOR samples revealed an assemblage change around sample TOR9. The older section (TOR2-TOR8) contains a dominance of *Lithraphidites sp.*, while the younger section (TOR10-TOR14) contains a dominance of *Micula staurophora*. As *Micula staurophora* is a dissolution-resistant species, a dominance might indicate poorer nannofossil preservation and greater diagenetic alteration (Thierstein, 1981; Roth, 1983; Moshkovitz and Eshet, 1989; Eshet et al., 1992; Eshet and Almogi-Labin, 1996; Faris and Abu Shama, 2006; Mandur and El Ashwah, 2015). This can indicate that the assemblage in TOR10-TOR14 might not represent the true original nannoflora, and that section TOR2-TOR8 might be a better representation. A dominance of *Watznaueria barnesiae* has also been interpreted to indicate poorer preservation and diagenetic alteration (Thierstein, 1981; Roth, 1983; Moshkovitz and Eshet, 1989; Eshet et al., 1992; Eshet and Almogi-Labin, 1996; Faris and Abu Shama, 2006; Mandur and El Ashwah, 2015). However, as the assemblage composition generally is very low throughout the section, it might point towards that there were paleoecological changes after TOR9 which favored a dominance of *Micula staurophora*, and not a change of preservation (as the whole TOR section was determined to have the same preservation level) nor diagenetic alteration.

It is interesting to note that *Lithraphidites sp.*, that was dominant or abundant in TOR2-TOR8 declines from being 53% of the total assemblage in TOR3, to be 0% in TOR11. *Lucianorhabdus sp.* follows the same trend, being present in TOR1-TOR8 and reaching 0% in TOR9. As TOR15

represent the K/T boundary, one might speculate if the assemblage composition in Figure 53 in fact displays the time when certain genera got extinct locally, approaching the K/T extinction event.

The onshore sample were roughly divided into three main assemblages, as described in Chapter 4.1.4. The *Tranolithus orionatus*-assemblage, found in samples K and MOV might be age related, as *Tranolithus orionatus* has been reported in the Neptune occurrence data from DSDP and ODP proceedings (Young et al., 2016) to have higher occurrences during the Cenomanian to Coniacian, than from the middle Campanian until its last occurrence at top of the UC17. As the MOV sample has been sampled close to samples MS, MT and MON (as they are all related to the Mons basin, Belgium) – it might indicate a local range of *Tranolithus orionatus*, as it constitutes 7% of the total assemblage in MOV, but 0% in MS, MT and MON. The youngest age that MOV can possible have was determined to be Early Campanian (UC15a, due to last occurrence of *Lithastrinus grillii*). MT and MON were determined to have an age of Middle Campanian (UC15d). Hence, *Tranolithus orionatus* might have a local last occurrence between Early to Middle Campanian in the Mons basin, southeast of Belgium.

The *Calculites obscurus*-assemblage, found in samples L, MON, MT, SK and MS (sharing an age of Middle Campanian) all have a common to abundant presence of *Calculites obscurus*, unlike the rest of the onshore samples. This might also be age related, as this species have been reported in Neptune occurrence data from DSDP and ODP proceedings (Young et al., 2016) to be more common during the Campanian-Maastrichtian, even though the first occurrence is a marker within the UC12 during Santonian (Burnett, 1998). Interestingly, sample SK from Denmark is grouped within the same assemblage as the Belgium samples – while sample A (also Danish) has a 0% occurrence of *Calculites obscurus*. As *Calculites obscurus* is rather dissolution-neutral (see Table 9 below), it is likely to assume that it should be present within the assemblages if it was a constituent of the original nannoflora. This might indicate that either sample A had a local nannoflora where *Calculites obscurus* was absent, or that the age of sample A could be limited further – meaning that it might be unlikely that sample A is sharing an age with the *Calculites obscurus*-assemblage samples. The age range of sample A could be younger than that determined using calcareous nannofossil biostratigraphy. Considering that the TOR samples had common occurrences of *Calculites obscurus* and are of Uppermost Maastrichtian age – it might be reasonable to assume that sample A might have an age younger than the *Calculites obscurus*-assemblage samples, but older than the TOR samples. However, it is important to highlight that it might not be age-related at all, but that it could instead be a local variation within the paleoecological environment of sample A, disfavours *Calculites obscurus*.

Sample A was determined to have an assemblage distinctively different than the other samples, which was named the few-*Watznaueria barnesiae*-assemblage. As *Watznaueria barnesiae* is one of the most common Mesozoic species and considered to be one of the most dissolution-resistant – it is reasonable to assume that this species was not common in the original nannoflora of this sample. The extremely low assemblage constituent of *Watznaueria barnesiae* in sample A (0.8%) is remarkable and might indicate that sample A had a particular paleoecological environment. This could strengthen the theory that the low abundance of *Calculites obscurus* in sample A might not be age-related, but due to a different paleoecological environment.

The variation in assemblage from one end of the core to the other might also indicate sampling direction through stratigraphy, as discussed for changes in nannofossil abundances and species diversity in Chapter 5.2. Following the same logic, larger variation from one end to the other might indicate diagonal to vertical sampling through stratigraphy, while less variation might indicate horizontal sampling. The samples with the least variation within the core are A, MOV and K (Figure 54), indicating that these samples might have been sampled horizontally through stratigraphy. However, this conflicts with previous results in Chapter 5.2. Sample A and MOV displayed abundance changes between 25-30%, which might indicate diagonal sampling direction. Sample K had an abundance change of 47.4% - which points towards vertical sampling. Combining it with the number of species and genera changes, which also indicated variation within the core, it might be unlikely that the stable assemblage within core K indicates horizontal sampling. Overall, the assemblage-change patterns do not match well with the abundance and number of species and genera changes. It is uncertain which factor should be weighted as the most important to determine sampling direction.

The change of assemblage compositions from unflooded core to their flooded equivalents is interesting, as the results might indicate which species and genera are the least and most dissolution-resistant. The general results from all flooded cores compliments what has been concluded in previous studies (Thierstein, 1981; Roth, 1983; Moshkovitz and Eshet, 1989; Eshet et al., 1992; Eshet and Almogi-Labin, 1996; Faris and Abu Shama, 2006; Mandur and El Ashwah, 2015): That *Watznaueria barnesiae* and *Micula staurophora* are the most dissolution-resistant, also when flooding with a MgCl₂-brine, and experiences an average increase of 16% and 9.2% of the total assemblages respectively (average of all flooded samples). The results also display species that generally decrease in percentage of the total assemblage: *Prediscosphaera sp.*, *Eiffellithus sp.* and *Biscutum constans*, with average decrease of 13%, 4%

and 3% respectively (average of all flooded samples). This makes it possible to rank species from dissolution-resistant to least dissolution-susceptible, see Table 9 below.

These results could be interesting to consider prior to flooding experiments, as it might be able to predict how severely the assemblage of a sample will be dissolved during flooding. A sample consisting of low abundance of dissolution-resistant species, such as *Watznaueria barnesiae* and *Micula staurophora*, and higher abundances of species susceptible to dissolution, such as *Prediscosphaera sp.*, might be more affected when it comes to dissolution than a sample with higher abundance of the dissolution-resistant species. This might have been the case for samples A and K. Sample A had the highest average abundance of *Prediscosphaera sp.* (39%) and the lowest abundance of *Watznaueria barnesiae* (0.8%) of all the onshore samples – and sample A displayed a very poor preservation after flooding. Sample K had an abundant average presence of *Watznaueria barnesiae* (37%), but rare presence of *Micula staurophora* (0.2%) and abundant presence of *Prediscosphaera sp.* (14%). However, as samples MT and L had average presence of *Watznaueria barnesiae* (32%) like sample K, but higher abundance of *Micula staurophora* (8.6%) and less abundance of *Prediscosphaera sp.* (11%) – the overall assemblage might be similar in terms of dissolution-resistant and dissolution-susceptible species or genera. The reason why sample K was left with very poor preservation after flooding is more likely linked to the longer duration of the flooding experiment, as discussed in Chapter 5.1. As sample A already had a poor preservation level to begin with, it might be more proofs to say that the flooding duration impacts the degree of dissolution stronger than the assemblage composition does. However, the assemblage composition will have an impact, but to a lesser degree, which may be neglected in certain IOR flooding experiments. However, there is yet no scientific proof. If two samples with very different assemblage compositions are to be compared, where one has only dissolution-resistant species and the other has only dissolution-susceptible species – it might be beneficial to consider the impact of assemblage composition on the degree of dissolution.

Table 9: Rank of species or genera from dissolution-resistant (negative decrease, top) to dissolution-susceptible (positive decrease, bottom), based on average data from four unflooded samples with their flooded equivalents.

Species or genera	% decrease
% <i>Watznaueria barnesiae</i>	-16,2
% <i>Micula staurophora</i>	-9,2
% <i>Kamptnerius magnificus</i>	-2,4
% <i>Lithraphidites sp.</i>	-0,8
% <i>Reinhardtites levis</i>	-0,2
% <i>Lucianorhabdus sp.</i>	0,1
% <i>Cribrosphaerella ehrenbergii</i>	0,1
% <i>Calculites obscurus</i>	1,3
% <i>Microrhabdulus decoratus</i>	1,5
% <i>Ahmuellerella octoradiata</i>	1,6
% <i>Tranolithus orionatus</i>	1,9
% <i>Helicolithus sp.</i>	2,5
% <i>Biscutum constans</i>	3,0
% <i>Eiffellithus sp.</i>	4,0
% <i>Prediscosphaera sp.</i>	12,6

5.5. Paleocology

The offshore TOR samples displayed a change in paleoecological indices around sample TOR9 (Figure 57). Overall, there are higher percentages of low nutrients (corresponding to warmer surface waters) in the TOR sequence. However, the older section (TOR1-TOR8) might be interpreted to have had a paleoecological setting with slightly colder waters than the younger section (TOR10-TOR14) due to the presence of cold water indices. As the low nutrient indices (corresponding to warm water) becomes a smaller constituent of the total assemblage after TOR9 – it might also indicate that the water become colder, although this is uncertain. There are no clear indices to make a confident statement about a change in the paleoecology until TOR14. Alteration indices are increasing from sample TOR9, which corresponds to an increase in *Micula sp.*, which could be related to higher degree of alteration or a change in paleoecology that favours *Micula sp.*. As already discussed in Chapter 5.4, the preservation level does not change drastically throughout the sequence, therefore a change in paleoecology might be more likely.

Sample TOR15 is interesting as the paleoecological indices change strikingly from TOR14. *Biscutum constans* has not been common within the TOR sequence, but in TOR15 it constitutes 21% of the assemblage composition. As it is a high nutrient index nannofossil, it might indicate that there was a drastic increase of nutrient-levels in the surface waters at the time. According to Keller (2008), surface waters can experience a eutrophication (a large influx of nutrients) from mantle plume volcanism and increased weathering. The Deccan Traps (located in India and one of the largest volcanic events in Earth's history) had its bulk of the volcanic eruptions at the K/T boundary (Keller, 2008). A study on benthic foraminifers by Coccioni and Galeotti (1994) suggested that an abnormally large influx of nutrients reached the ocean at the time of the K/T extinction event. The sudden increase of the nutrient-rich index fossil *Biscutum constans* at the K/T boundary might support this. However, as sample TOR15 had rare occurrences of calcareous nannofossils – this last suggestion is only a hypothesis for now.

It is also interesting that the presence of dwarf-species, as presented in Chapter 4.1.7, is higher in the TOR offshore samples than the onshore samples, and especially in the interval TOR10-TOR14. Erba et al. (1995) studied Campanian calcareous nannofossils from Wodejebato Guyot and found dwarf nannofossils in lagoonal assemblages. The small sized nannofossils seemed to be a peculiarity of unusual environmental settings. The higher abundances of dwarf *Micula sp.*

small in the TOR10-TOR14 interval might indicate abnormal paleoecological conditions with a response in *Micula sp.* that adjusted by becoming smaller.

Based on the paleoecological results presented in Chapter 4.1.5, the offshore samples and sample A are interpreted and assigned to a paleoecological setting of cold water and low nutrient levels. The rest of the onshore samples are interpreted and assigned to warm waters with low nutrient levels. However, sample K contains even less cold water and high nutrient indices and might therefore have had a paleoecological setting with even warmer waters and lower nutrient levels than the rest.

Species diversity might be an indicator of how stable the paleoecological conditions were, as warm water and low nutrient levels likely generates higher species diversity, and cold water and high nutrient levels generated lower species diversity. When comparing the species diversity-results with paleoecological results they match well, except for one contradiction: Sample K has a lower species diversity than the rest of the onshore samples, but the paleoecological interpretation revealed that this sample might have had the warmest waters with the lowest nutrient levels. It remains unclear what caused this contradiction.

The paleoecological changes from one end of the core to the other display the same results as the assemblage changes. As the paleoecological index changes are a direct result of the assemblage composition changes, they should not be complimentary in terms of additional evidences for interpreting sampling direction through stratigraphy.

5.6. Nannofossil versus Micarb Ratios

The comparison between nannofossil versus micarb ratios (NvsM-ratio) estimates in FEG-SEM and OLM is displayed in Figure 69. The estimation of NvsM-ratios using FEG-SEM micrographs overall shows the same trends of decrease or increase from sample 1 to 5 in cores A, SK, MON, L, MOV and K as the estimations using the OLM. The opposite trend was determined in sample MT, which displayed an increase in nannofossils in the OLM, but a slight decrease in FEG-SEM (Figure 69).

An interesting observation is that there is a trend of the OLM estimation to be greater than the FEG-SEM estimation. In 10 of 16 average estimates are OLM nannofossil percentages (versus micarbs) 10-15% higher than the corresponding FEG-SEM estimations. The average difference in nannofossil percentage (versus micarbs) estimates from one end to the other of each core is

9.3% using the FEG-SEM and 14.3% using the OLM. This is interesting as it seems to be lower quantities of micarbs in smear slides, than in the chalk samples prepared for the FEG-SEM.

One explanation might be that the random settling technique to produce smear slides alter the samples, by dissolving some of the smaller particles which are micarbs. If this is correct, the results might indicate that generally 10-15% of the micarbs are dissolved during the 24 hours settling, giving 10-15% higher quantities of nannofossils in smear slides. The other explanation is that there is a tendency of overestimation in the OLM, or underestimating in the FEG-SEM. The most correct estimation might therefore be something in the middle. However, since the estimation of each end of the core generally has a 5% higher difference when estimating with OLM than FEG-SEM – it might point towards that the FEG-SEM generally gives more stable estimates. This is reasonable as the FEG-SEM provides much more detailed insight into the chalk samples. In addition, the FEG-SEM sample preparation is gentler, while the settling smear slides are prepared through crushing and grinding as well as settling through a water column.

The only sample that displayed the same strong trend using both methodologies from one end to the other was MON, with a notable decrease of micarbs from MON1 to MON5. This is peculiar, as the two samples display the same preservation level. It is not clear what can cause such a difference, but it might be linked to sampling direction.

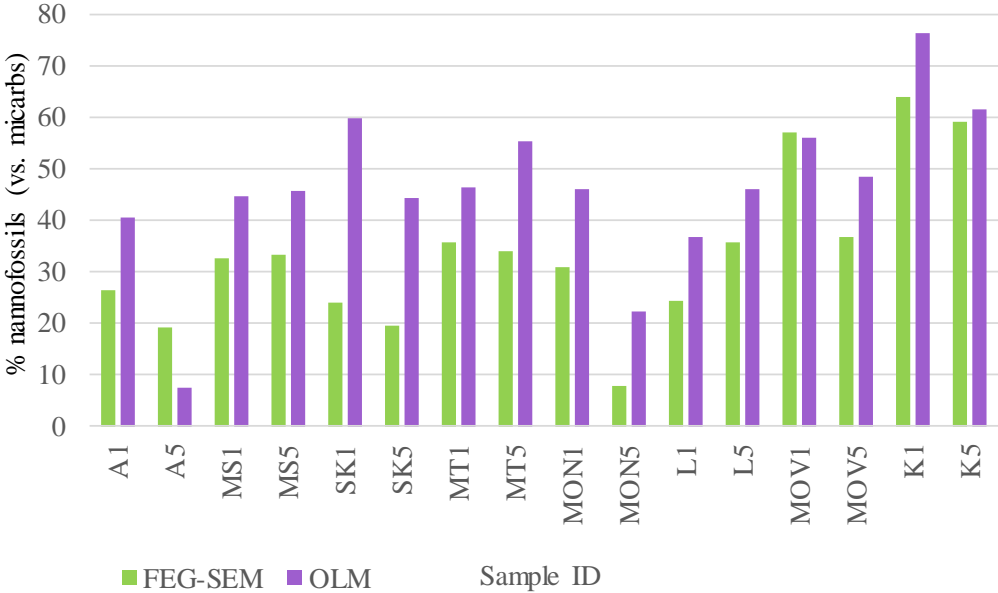


Figure 69: Comparison of estimation of % nannofossils versus micarbs in the onshore samples.

5.7. Special Observations

Regarding *Gartnerago obliquum* appearing in younger sediments (samples MT, SK and MS) than its last occurrence from Young et al. (2016), it is important to consider the following: According to Young et al. (2016), the two most common reasons for why a species is found in sediments outside of its age range is typically due to reworking or misidentification. The *Gartnerago obliquum* specimens were of good preservation and the species' identification was certain. This leaves reworking as a plausible cause, which might be backed up by the paleoecological results where the same samples, MT, SK and MS contain the highest average percentages (of the onshore samples) of diagenetic alteration indices: 40.4%, 46.7% and 43.3% respectively.

The explanation of reworking to why species occur in samples outside of the species' age range is not plausible for the appearance of *Eiffellithus lindiensis* in sample K, as this species was found in samples older than its age range. This leaves misinterpretation as an explanation, or that the species' age range could be reconsidered. As *Eiffellithus lindiensis* is a relatively new species, first described by Lees (2007) from its type locality in Tanzania – the paleogeographical extent of this species might not be certain yet. As sample K is from northern USA, perhaps this species appeared earlier in this locality than in Tanzania. The species identified as *Eiffellithus lindiensis* undoubtedly has an axial cross without bifurcated tips and is smaller than *Eiffellithus eximius*. Hence, it fits better the description of Lees (2007) as *Eiffellithus lindiensis*. This is an observation that requires further studies.

5.8. IOR Flooding Experiment

It was postulated that samples with dissolution-susceptible calcareous nannofossil assemblages would display higher MgO wt% after flooding. If that was correct, sample A should display the highest MgO wt% after flooding, but this is not the case. Sample A displays the lowest MgO wt% (0.4%) after flooding, and sample K displays the highest (6.5 wt%) (Table 10).

There might be correlation between MgO wt% after flooding and the original estimated nannofossil versus micarb (NvsM) ratios. Sample K had the highest content of nannofossils versus micarbs (average 65.2% nannofossils and 34.8% micarbs) – and displays the highest MgO wt% after flooding. However, as previously discussed: it must be considered that sample K was flooded for about 2 weeks longer, and this is likely to impact the MgO wt%. Figure 70 shows % nannofossil (versus micarbs) in the unflooded core plotted against MgO wt% after

flooding, with a blue line corresponding to the trendline of samples L, MT and A, which were flooded for 60-65 days. The trend line fits well. Figure 71 displays the same plot as Figure 70, but with a trendline that includes sample K. This trendline does not fit the samples as well as the previous, indicating sample K deviates from the other three samples – possibly due to a longer flooding duration. The same trend is evident when plotting average total calculated nannofossil abundance (from the unflooded random settling smear slides) against MgO wt% after flooding, with a trendline excluding sample K (Figure 72) and a trendline including all samples (Figure 73).

It seems to be that the higher nannofossil content and the lower content of micarb in an unflooded core generates higher MgO wt% after flooding. This could indicate that dissolution during flooding takes place preferentially in calcareous nannofossils instead of micarbs.

Table 10: Flooded samples at inlet position different data: MgO wt% after flooding, data from Andersen et al. (2017); average NvsM-ratios in % nannofossils in the unflooded sample equivalent (Unfl. NvsM); average NvsM-ratios in % nannofossils in the flooded samples (F. NvsM); the difference between Unfl. NvsM and F. NvsM, giving the % nannofossils which were lost during flooding; average total calculated nannofossil abundance of the original unflooded core (O. Tot. C. N. A.); and duration of the flooding in days (T(d)).

Sample ID	MgO (wt%)	Unfl. NvsM	F. NvsM	Unfl.-F. NvsM	O. T. C. N. A.	T (d)
K_inlet	6,5	65,2	3,76	61,44	7703,0	75
L_inlet	1,7	42,9	10,4	32,5	5121,1	65
MT_inlet	1,31	35,6	9,12	26,48	4472,5	60
A_inlet	0,4	23,3	1,24	22,06	3249,1	63

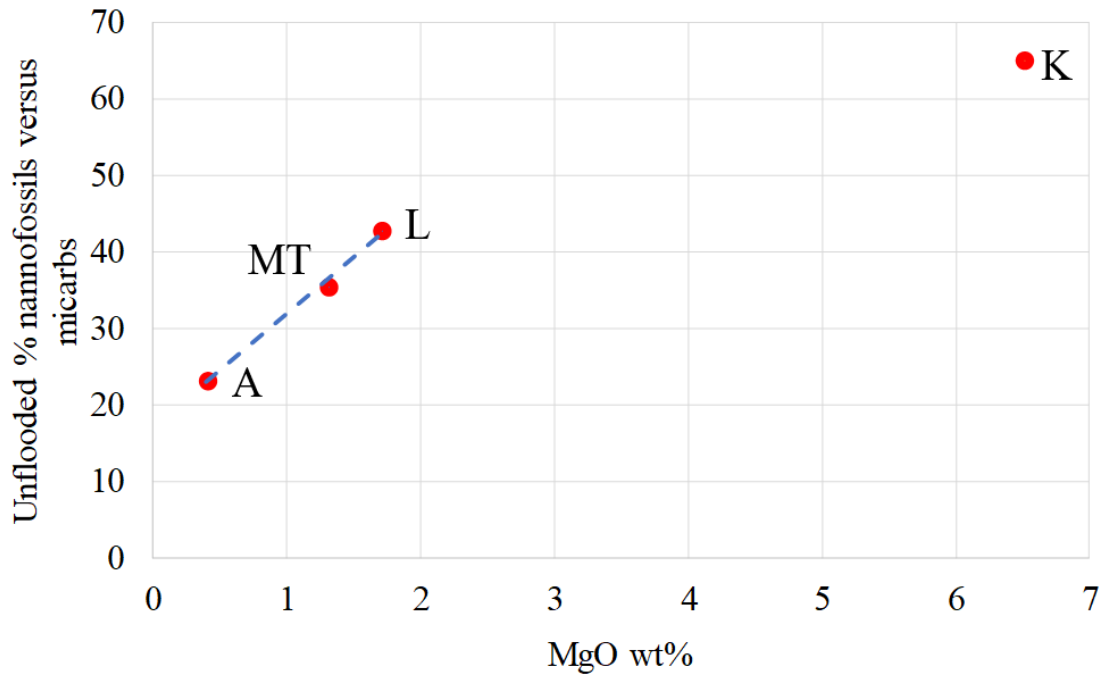


Figure 70: MgO wt% after flooding plotted against % nannofossils versus micarbs in the unflooded equivalent core. Blue line shows linear trend for samples L, MT and A which were flooded for 60-65 days.

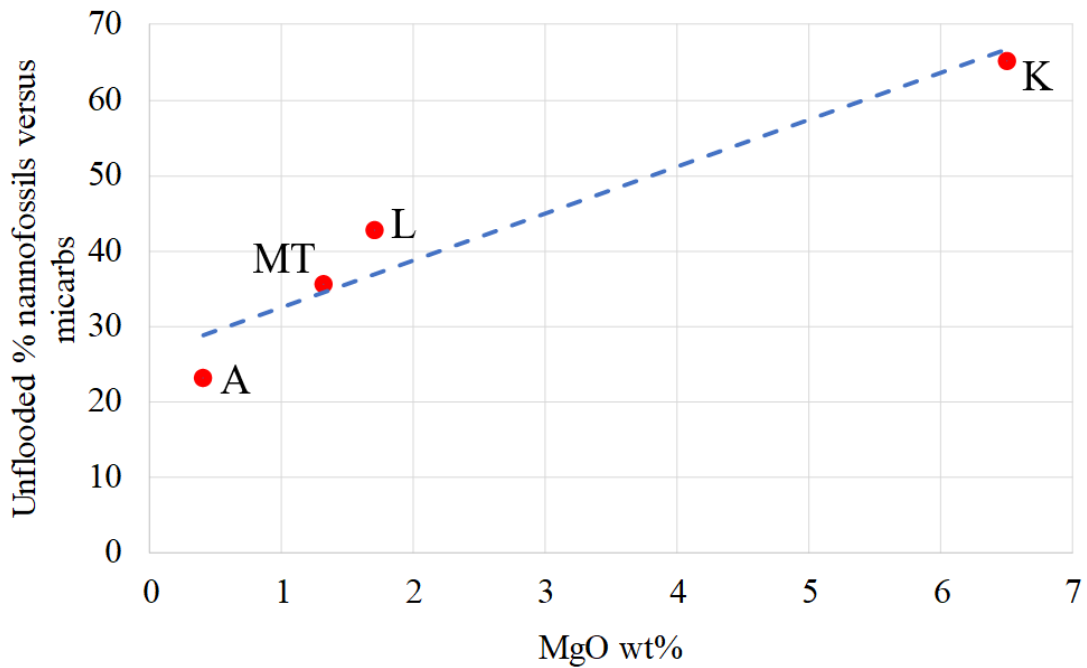


Figure 71: MgO wt% after flooding plotted against % nannofossils versus micarbs in the unflooded equivalent core. Blue line shows linear trend for all samples.

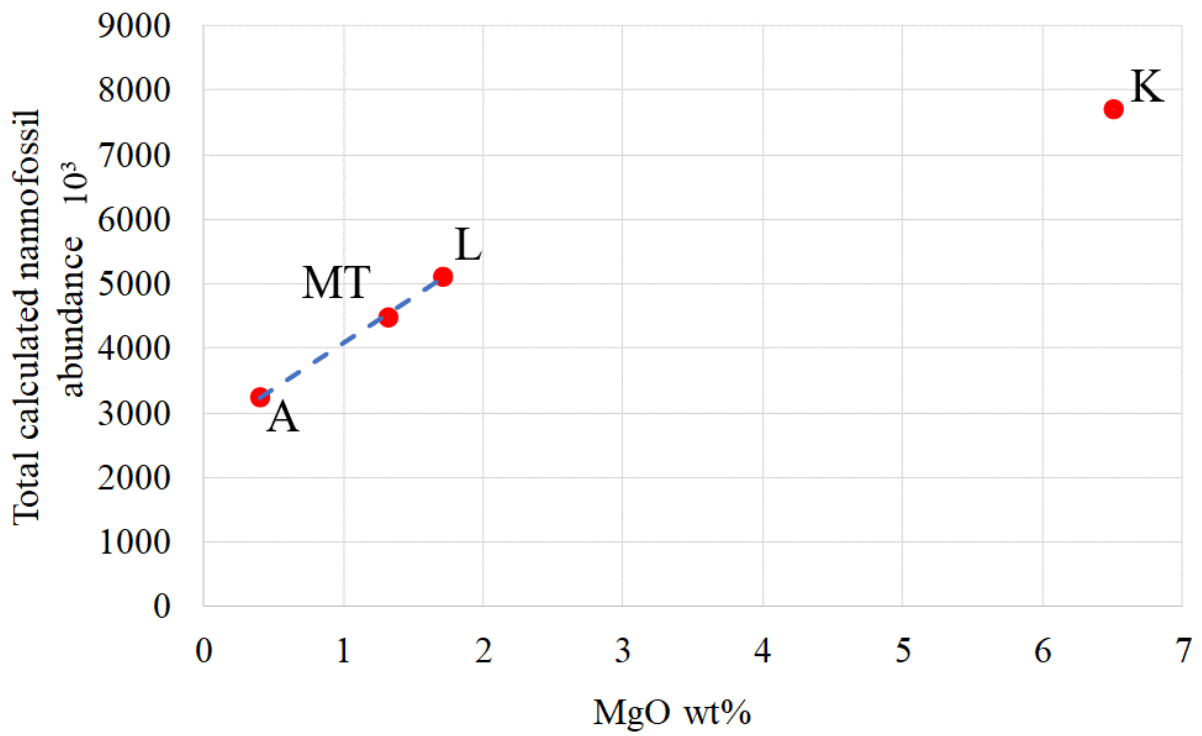


Figure 72: MgO wt% after flooding plotted against average total calculated nannofossil abundance in the unflooded equivalent core. Blue line shows linear trend for samples L, MT and A which were flooded for 60-65 days.

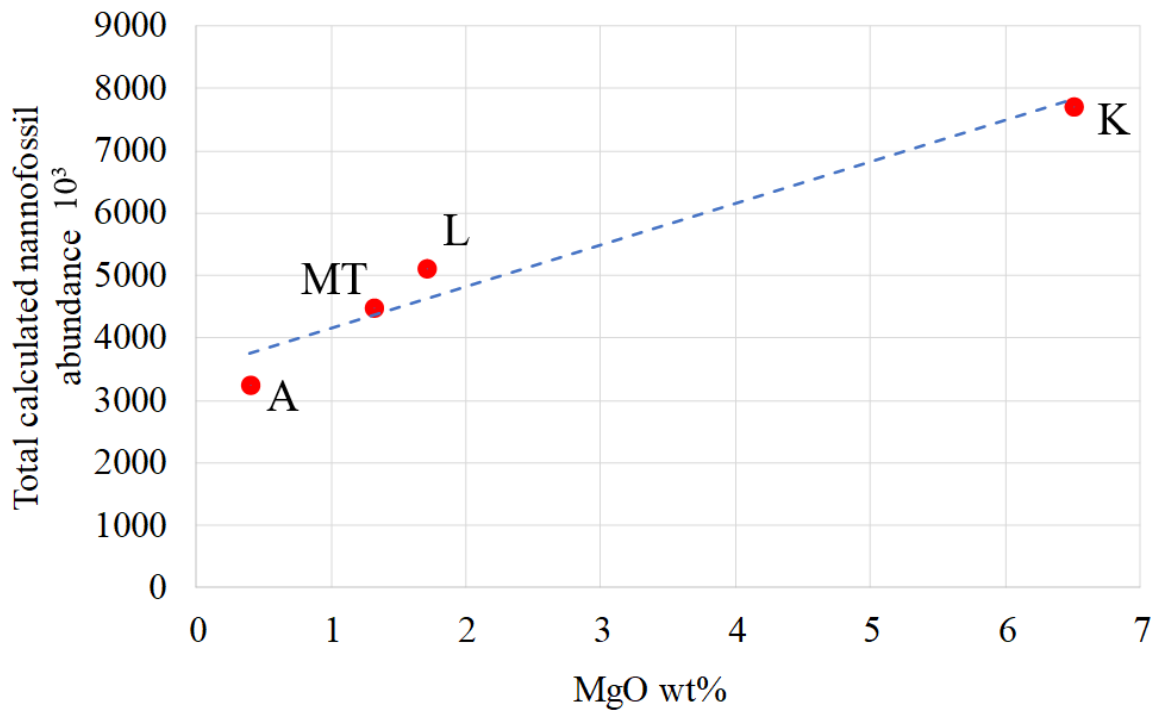


Figure 73: MgO wt% after flooding plotted against average total calculated nannofossil abundance in the unflooded equivalent core. Blue line shows linear trend for all samples.

6. Conclusion

Chalk is a highly fossiliferous rock, with calcareous nannofossils being the main constituent. It is evident that reservoir properties such as porosity and density will heavily depend on the type, the amount and the form of the paleontological components, and thus affect fluid-flow. Eight onshore samples, with five flooded versions and an offshore sequence from the Tor field in the North Sea have been studied, all of Cretaceous age. This thesis has performed various methodologies to describe the paleontological material in all samples. Through biostratigraphic analyses, it became evident that the presumed ages needed adjustments. New unbiased ages were determined for all the samples and compared with presumed ages from available literature. Sample SK proved not to be of Uppermost Maastrichtian age as presumed, but of Middle Campanian age. Its flooded “equivalent” core however, was of Uppermost Maastrichtian. This demonstrates that one cannot depend on general age data from quarries, as the sampling might not be accurate. For IOR-research, this might be a pitfall when using onshore chinks as analogues to real reservoir chinks.

There was no correlation between age and calcareous nannofossil preservation level. The offshore reservoir chalk was of poorest preservation. The determination of preservation level yielded more accurate results from the FEG-SEM than the OLM. The preservation levels typically decreased one to two levels after flooding with MgCl₂. By combining the results from calcareous nannofossil abundance, species diversity and assemblages – sampling direction through stratigraphy could be suggested. However, the results must be interpreted with care, as they sometimes are contradictory. Assemblage analyses generated three assemblage-types for the onshore chinks. The offshore assemblage-evolution towards the K/T boundary might indicate at what time different genera got extinct locally. In addition, evidence of the K/T extinction event might be observable in the offshore section. Paleoecological indices point towards generally warmer waters with lower nutrient levels for all samples, except sample A which displays cold-water indices. Estimates of nannofossil versus micarb ratios from random settling smear slides trended to be 10-15% higher than estimates from the FEG-SEM. This result might indicate that micarbs get dissolved during the random settling technique.

Analyses of the flooded samples at inlet position uncovered that certain species were dissolution-resistant and others dissolution-susceptible. However, the assemblage content of

these species did not affect MgO wt% after flooding. What did affect MgO wt% were total calculated nannofossil abundance and nannofossil content (versus micarbs). Higher nannofossil abundance and lower micarb content in the original unflooded core yielded higher MgO wt% after flooding. More data is needed to verify this correlation.

During this thesis, valuable knowledge about chalk and its paleontological components has been gained. Various aspects of calcareous nannofossils have been studied and discussed to clarify how various chalk samples might react differently to, and control IOR flooding experiments. The methodologies described in this thesis proved to be of importance for the chalk characterization and might even to some extent be used to predict how chalk samples will react to flooding with MgCl₂. The applied calcareous nannofossil methodologies should not be neglected but be included in future EOR research.

7. Recommendations for Future Work

This thesis' work should be continued in the future. More samples should be studied using the same methodologies to gain additional data to obtain more certain results. If nannofossil versus micarb ratios proves to be useful to assess a quick nannofacies analysis – the methodology should be digitalized by developing an image analysis program which can quickly scan FEG-SEM micrographs and recognize nannofossils and micarbs from other grains to provide precise and unbiased estimates.

It has been observed that magnesium overgrowth takes place in favoured areas within chalk during flooding. It would therefore be of interest to investigate if certain genera or species are favoured for magnesium overgrowth and mineral replacement during flooding IOR-experiments due to their morphologies.

At last, stable isotope measurements with microprobes on single calcareous nannofossils would allow to determine if crystals are new-grown or original. This would without doubt be valuable insight for future EOR research, as well as for calcareous nannofossil paleoecology and paleoceanography.

8. References

- Alroy, J. (2008). Dynamics of origination and extinction in the marine fossil record. *Proceedings of the Academy of Natural Sciences*, 105, 11536-11543.
- Andersen, P., Wang, W., Madland, M., Zimmermann, U., Korsnes, R., Berolino, S., Minde, M., Schulz, B., Gilbricht, S. (2017). Comparative study of five outcrop chalks flooded at reservoir conditions: Chemo-mechanical behaviour and profiles of compositional alteration. *Transport in Porous Media*, 121(1), 135-181.
- Andruleit, H. (1995). Coccolithophoriden im Europäischen Nordmeer: Sedimentation und Akkumulation, sowie ihre Entwicklung während der letzten 15000 Jahre. *Berichte aus dem Sonderforschungsbereich 313*(59), 1-111.
- Arkhangelsky, A. D. (1912). Upper Cretaceous deposits of east European Russia. *Materialien zur Geologie Russlands*, 25, 1-631.
- Armstrong, H. A., Brasier, M. D. (2005). *Microfossils* (2nd ed. ed.). Malden, Mass: Blackwell Publ.
- Aubry, M.-P. (2013). *Cenozoic Coccolithophores: Braarudosphaerales*. *Atlas of Micropaleontology Series*. New York: Micropaleontology Press.
- Baccelle, L., Bosellini, A. (1965). Diagrammi per la stima visiva della composizione percentuale nelle rocce sedimentarie. *Università di Ferrara, Annali, Sezione IX, Scienze geologiche e paleontologiche*, 1, 59-62.
- Beerling, D. J., Lomas, M. R., Gröcke, D. R. (2002). On the nature of methane gas-hydrate dissociation during the Toarcian and Aptian oceanic anoxic events. *Am. J. Sci.*, 302, 28-49.
- Bignot, G. (1985). *Elements of micropalaeontology : microfossils - their geological and palaeobiological applications*. London: Graham Trotman.
- Black, M. (1968). Taxonomic problems in the study of coccoliths. *Palaeontology*, 11, 793-813.
- Black, M. (1971). Coccoliths of the Speeton Clay and Sutterby Marl. *Proceedings of the Yorkshire Geological Society*, 38, 381-424.
- Black, M., Barnes, B. (1959). The structure of Coccoliths from the English Chalk. *Geological Magazine*, 96, 321-328.
- Blair, S. A., Watkins, D. K. (2009). High-resolution calcareous nannofossil biostratigraphy for the Coniacian/Santonian Stage boundary, Western Interior Basin. *Cretaceous Research*, 30(2), 367-384.
- Bown, P. R. (1987). Taxonomy, evolution, and biostratigraphy of Late Triassic-Early Jurassic calcareous nannofossils. *Special Papers in Palaeontology*, 38, 118.
- Bown, P. R. (1998). *Calcareous Nannofossil Biostratigraphy*. London: Kluwer Academic Publishers.
- Bown, P. R., Burnett, J. A., Gallagher, L. T. (1991). Critical events in the evolutionary history of calcareous nannoplankton. *Historical Biology*, 5, 279-290.
- Bown, P. R., Burnett, J. A., Gallagher, L. T. (1992). Calcareous nannoplankton evolution. *Memorie di Scienze Geologiche*, XLIII, 1-17.
- Bown, P. R., Cooper, M. K. E. (1989). New calcareous nannofossils from the Jurassic. *Journal of Micropalaeontology*, 8, 91-96.
- Bown, P. R., Rutledge, D. C., Crux, J. A., Gallagher, L. T. (1998). Early Cretaceous. In P. R. Bown (Ed.), *Calcareous nannofossil biostratigraphy* (pp. 86-131): Chapman and Hall.
- Bown, P. R., Young, J. R. (1997). Mesozoic calcareous nannoplankton classification. *Journal of Nannoplankton Research*, 19(1), 21-36.
- Bralower, T. J. (1988). Calcareous nannofossil biostratigraphy assemblages of the Cenomanian–Turonian boundary interval: Implications for the origin and timing of oceanic anoxia. *Paleoceanography*, 3, 275-316.

- Bralower, T. J., Arthur, M. A., Leckie, R. M., Sliter, W. V., Allard, D. J., Schlanger, S. O. (1994). Timing and paleoceanography of oceanic dysoxia/anoxia in the Late Barremian to Early Aptian. *Palaios*, 9(335-369).
- Bralower, T. J., Bown, P. R., Siesser, W. (1991). Significance of Upper Triassic nanofossils from the Southern Hemisphere (ODP Leg 122, Wombat Plateau, NW Australia). *Marine Micropaleontology*, 17, 119-154.
- Bralower, T. J., CoBabe, R., Clement, B., Sliter, W. V., Osburne, C., Longoria, J. (1999). The record of global change in mid-Cretaceous, Barremian-Albian sections from the Sierra Madre, northeastern Mexico. *J. Foraminiferal Res.*, 29, 418-437.
- Bralower, T. J., Leckie, R. M., Sliter, W. V., Thierstein, H. R. (1995). An integrated Cretaceous microfossil biostratigraphy. In W. A. Berggren, D. V. Kent, M. Aubry (Eds.), *Geochronology, Time Scales and Global Stratigraphic Correlation* (Vol. 54, pp. 65-79): Society of Economic Paleontologists and Mineralogists, Special Publication.
- Bralower, T. J., Monechi, S., Thierstein, H. R. (1989). Calcareous nanofossil zonation of the Jurassic-Cretaceous boundary interval and correlation with the geomagnetic polarity timescale. *Marine Micropaleontology*, 14, 153-235.
- Bralower, T. J., Sliter, W. V., Arthur, M. A., Leckie, R. M., Allard, D. J., Schlanger, S. O. (1993). Dysoxic/anoxic episodes in the Aptian-Albian (Early Cretaceous). In M. Pringle and et. al. (Eds.), *The Mesozoic Pacific: Geology, Tectonics and Volcanism* (Vol. 77, pp. 5-37): AGU Geophys. Monogr.
- Bramlette, M. N., Martini, E. (1964). The great change in calcareous nannoplankton fossils between the Maestrichtian and Danian. *Micropaleontology*, 10(2), 291-322.
- Brand, L. E. (1994). Physiological ecology of marine coccolithophores. In A. Winter, W. G. Siesser (Eds.), *Coccolithophores* (pp. 39-50). Cambridge: Cambridge University Press.
- Bukry, D. (1969). Upper Cretaceous coccoliths from Texas and Europe. *The University of Kansas Paleontological Contributions, Article 51 (Protista 2)*, 1-79.
- Bukry, D. (1973). Phytoplankton stratigraphy, Deep Sea Drilling Project Leg 20, Western Pacific Ocean. *Initial Reports of the Deep Sea Drilling Project*, 20, 307-317.
- Bukry, D. (1974). Coccoliths as paleosalinity indicators - evidence from Black Sea. In E. T. Degens, D. A. Ross (Eds.), *The Black Sea - Geology, Chemistry, and Biology* (Vol. 20): American Association of Petroleum Geologists Memoir
- Burnett, J. A. (1997). New species and new combinations of Cretaceous nanofossils and a note on the origin of *Petrarhabdus* (Deflandre) Wise and Wind. *Journal of Nannoplankton Research*, 19(2), 133-146.
- Burnett, J. A. (1998). Upper Cretaceous. In P. R. Bown (Ed.), *Calcareous Nannofossil Biostratigraphy* (pp. 132-199). London: Chapman and Hall.
- Caratini, C. (1963). *Contribution à l'étude des coccolithes du Cénomanién supérieur et du Turonien de la région de Rouen*. Université d'Alger, Faculté des Sciences, Publication du Laboratoire de Géologie Appliquée.
- Cavalier-Smith, T. (1981). Eukaryote kingdoms: seven or nine? *BioSystems*, 10, 93-114.
- Cavalier-Smith, T. (1986). The Kingdom Chromista: Origins and systematics. *Progress in Phycological Research*, 4, 309-344.
- Chatton, É. (1925). *Pansporella perplexa*, amœbiens à spores protégées parasite de daphnies. Réflexions sur la biologie et la phylogénie des protozoaires. *Ann Sci Nat Zool (Sér. 10)*, 8, 5-84.
- Church, J. W., Lomas, C. G., Nicholson, C. A. (1978). *Report No. 2395: Phillips 2/4-8X Norwegian North Sea Well: Biostratigraphy of core samples from the interval 9795'-10635'*. Retrieved from Wales, U. K.:
- Clarke, L. J., Jenkyns, H. C. (1999). New oxygen isotope evidence for long-term Cretaceous climatic change in the Southern Hemisphere. *Geology*, 27, 699-702.

- Coccioni, R., Galeotti, S. (1994). K-T boundary extinction: Geologically instantaneous or gradual event? Evidence from deep-sea benthic foraminifer. *Geology*, 22(9), 779-782.
- Corbett, M., Watkins, K. (2013). Calcareous nannofossil paleoecology of the mid-Cretaceous Western Interior Seaway and evidence of oligotrophic surface waters during OAE2. *Palaeogeography, Palaeoclimatology, Palaeoecology*, 392, 510-523.
- d'Orbigny, A. (1842-1951). *Paléontologie Française; Terrains jurassiques, I. Céphalopodes*. Paris.
- Da Gama, R. O. B. P., Lutz, B., Desjardins, P., Thompson, M., Prince, I., Espejo, I. (2014). Integrated paleoenvironmental analysis of the Niobrara Formation: Cretaceous Western Interior Seaway, northern Colorado. *Palaeogeography, Palaeoclimatology, Palaeoecology*, 413, 66-80. doi:<https://doi.org/10.1016/j.palaeo.2014.05.005>
- Deflandre, G. (1947). *Braarudosphaera* nov. gen., type d'une famille nouvelle de Coccolithophorides actuels a elements composites. *Comptes Rendus Hebdomadaires des Séances de l'Académie des Sciences*, 225, 439-441.
- Deflandre, G. (1959). Sur les nannofossiles calcaires et leur systématique. *Revue de Micropaleontologie*, 2, 127-152.
- Deflandre, G. (1963). Sur les Microrhabdulidés, famille nouvelle de nannofossiles calcaires. *Comptes Rendus (Hebdomadaires des Séances) de l'Académie des Sciences Paris*, 256, 3484-3487.
- Deflandre, G., Fert, C. (1954). Observations sur les coccolithophoridés actuels et fossiles en microscopie ordinaire et électronique. *Annales de Paléontologie*, 40, 115-176.
- Deres, F., Achéritéguy, J. (1980). Biostratigraphie des Nannoconids *Bulletin des Centres de Recherches Exploration-Production Elf-Aultaine* (Vol. 4, pp. 1-53). Pau, France.
- Dunham, R. J. (1962). Classification of carbonate rocks according to depositional texture. In W. E. Ham (Ed.), *Classification of carbonate rocks* (pp. 108-121): American Association of Petroleum Geologists Memoir.
- Erba, E. (1987). Mid-Cretaceous cyclic pelagic facies from the Umbrian-Marchean Basin: what do calcareous nannofossils suggest? *International Nannoplankton Association Newsletters*, 9, 52-53.
- Erba, E. (1992). Middle Cretaceous Calcareous Nannofossils from the Western Pacific (Leg 129): Evidence for Paleoequatorial Crossings. In R. L. Larson, Y. Lancelot, A. Fisher, L. Abrams, R. Behl, W. H. Busch, G. Cameron, P. R. Castillo, J. M. Covington, G. Dürr, E. Erba, P. A. Floyd, C. France-Lanord, E. H. Hauser, S. M. Karl, A. Karpoff, A. Matsuoka, A. Molinie, J. G. Ogg, A. R. M. Salimullah, M. Steiner, B. P. Wallick, W. Wightman (Eds.), *Proceedings of the Ocean Drilling Program, Scientific Results* (Vol. 129, pp. 189-201).
- Erba, E. (1994). Nannofossils and superplumes: The Early Aptian "nannoconid crisis". *Paleoceanography*, 9(3), 483-501.
- Erba, E. (2004). Calcareous nannofossils and Mesozoic oceanic anoxic events. *Marine Micropaleontology*, 52, 85-106.
- Erba, E., Castradori, D., Guasti, G., Ripepe, M. (1992). Calcareous nannofossils and Milankovitch cycles: the example of the Albian Gault Clay Formation (southern England). *Palaeogeography, Palaeoclimatology, Palaeoecology*, 93, 47-69.
- Erba, E., Da-Yong, J., Tintori, A., Motani, R. (2013). *The oldest calcareous nannofossil: Middle Triassic coccoliths from China*. Paper presented at the INA14 abstracts, Reston, Virginia.
- Erba, E., Tremolada, F. (2004). Nannofossil carbonate fluxes during the Early Cretaceous: phytoplankton response to nutrification episodes, atmospheric CO₂, and anoxia. *Paleoceanography*, 19. doi:[10.1029/2993PA000884](https://doi.org/10.1029/2993PA000884)

- Erba, E., Watkins, D. K., Mutterlose, J. (1995). Campanian dwarf calcareous nannofossils from Wodejebato Guyot. In J. A. Haggerty, I. P. Silva, F. Rack, M. K. McNutt (Eds.), *Proceedings of the Ocean Drilling Program, Scientific Results: Ocean Drilling Program*.
- Eshet, Y., Almogi-Labin, A. (1996). Calcareous nannofossils as paleoproductivity indicators in Upper Cretaceous organic-rich sequences in Israel. *Marine Micropaleontology*, 29, 37-61.
- Eshet, Y., Moshkovitz, S., Habib, D., Benjamini, C., Magaritz, M. (1992). Calcareous nannofossil and dinoflagellate Late stratigraphy across the Cretaceous/Tertiary boundary at Hor Hahar Israel. *Mar. Micropale.*, 18, 199-228.
- Fabricius, I. L. (2003). How burial diagenesis of chalk sediments controls sonic velocity and porosity. *AAPG Bulletin*, 87(11), 1755-1778. doi:10.1306/06230301113
- Fabricius, I. L., Borre, M. K. (2007). Stylolites, porosity, depositional texture, and silicates in chalk facies sediments. Ontong Java Plateau-Gorm and Tyra fields, North Sea. *Sedimentology*, 54, 183-205.
- Faris, M., Abu Shama, A. M. (2006). Calcareous nannofossils of the Campanian Maastrichtian Surd Formation in Abu Zenima area, west central Sinai, Egypt. *Egypt J. Paleontol.*, 6, 251-274.
- Feazel, C. T., Farrell, H. E. (1998). Chalk from the Ekofisk area, North Sea: nannofossils + micropores = giant fields. In A. J. Lomando, P. M. Harris (Eds.), *Giant Oil and Gas Fields* (Vol. 1, pp. 155-178): Soc. Econ. Paleont. Mineralogists.
- Flessa, K. W., Jablonski, D. (1985). Declining Phanerozoic background extinction rates: effects of taxonomic structure? *Nature*, 313, 216-218.
- Flügel, E. (2004). *Microfacies of Carbonate Rocks: Analysis, Interpretation and Application*: Springer-Verlag Berlin Heidelberg.
- Folk, R. L. (1959). Practical petrographic classification of limestones. *American Association of Petroleum Geologists Bulletin*, 43, 1-38.
- Folk, R. L. (1962). Spectral subdivision of limestone types. In W. E. Ham (Ed.), *Classification of carbonate Rocks-A Symposium* (pp. 62-84): American Association of Petroleum Geologists Memoir 1.
- Forchheimer, S. (1972). Scanning electron microscope studies of Cretaceous coccoliths from the Köpingsberg Borehole No. 1, SE Sweden. *Sveriges Geologiska Undersökning; Series C*, #668, 65, 1-141.
- Frey, R. W. (1972). *Article 3 (Cretaceous 3): Paleoecology and depositional environment of Fort Hays limestone member, Niobrara chalk (Upper Cretaceous, West-Central Kansas)*. The University of Kansas Paleontological Institute: The University of Kansas Publications.
- Gale, A. S., Kennedy, W. J., Burnett, J. A., Caron, M., Kidd, B. E. (1996). The Late Albian to Early Cenomanian succession at Mont Risou, near Rosans (Drôme, SE France): an integrated study (ammonites, inoceramids, planktonic foraminifera, nannofossils, oxygen and carbon isotopes). *Cretaceous Research*, 17(515-606).
- Gardet, M. (1955). Contribution à l'étude des coccolithes des terrains néogènes de l'Algérie. *Publications du Service de la Carte Géologique de l'Algérie (Nouvelle Série)*, 5, 477-550.
- Gartner, S. (1968). Coccoliths and related calcareous nannofossils from Upper Cretaceous deposits of Texas and Arkansas. *The University of Kansas Paleontological Contributions, Article 48 (Protista 1)*, 1-56.
- Geisen, M., Billard, C., Broerse, A. T. C., Cros, L., Probert, I., Young, J. R. (2002). Life-cycles associations involving pairs of holococcolithophorid species: intraspecific variation or cryptic speciation? *European Journal of Phycology*, 37, 531-550.

- Geisen, M., Bollmann, J., Herrle, J. O., Mutterlose, J., Young, J. R. (1999). Calibration of the random settling technique for calculation of absolute abundances of calcareous nannoplankton. *Micropaleontology*, 45(4), 437-442.
- Górka, H. (1957). Les Coccolithophoridés du Maestrichtien supérieur de Pologne. *Acta Palaeontologica Polonica*, 2, 239-284.
- Gornitz, V. E. (2009). *Encyclopedia of Paleoclimatology and Ancient Environments*. Dordrecht: Springer.
- Gran, H. H., Braarud, T. (1935). A quantitative study of the phytoplankton in the Bay of Fundy and the Gulf of Maine (including observations on hydrography, chemistry and turbidity). *Journal of the Biological Board of Canada*, 1, 279-467.
- Grün, W., Allemann, F. (1975). The Lower Cretaceous of Caravaca (Spain): Berriasian Calcareous Nannoplankton of the Miravetes Section (Subbetic Zone, Prov. of Murcia). *Eclogae Geologicae Helvetiae*, 68, 147-211.
- Gümbel, C. E. (1870). Vorläufige Mittheilungen über Tiefseeschlamm *Neues Jahrbuch für Mineralogie, Geologie und Paläontologie* (pp. 753-767).
- Hardas, P., Mutterlose, J. (2007). Calcareous nannofossil assemblages of Oceanic Anoxic Event 2 in the equatorial Atlantic: Evidence of an eutrophication event. *Mar. Micropale.*, 66, 52-69.
- Hattner, J. G., Wind, F. H., Wise, S. W. (1980). The Santonian-Campanian boundary: comparison of nearshore-offshore calcareous nannofossil assemblages. *Cahiers de Micropaleontologie*, 3, 9-26.
- Hay, W. W., Towe, K. M. (1963). *Microrhabdulus belgicus*, a new species of nannofossil. *Micropaleontology*, 9, 95-96
- Hellmann, R., Renders, P. J. N., Gratier, J. P., Guiguet, R. (2002). Experimental pressure solution compaction of chalk in aqueous solutions. Part 1. Deformation behavior and chemistry. In R. Hellmann, S. A. Wood (Eds.), *Water Rock Interactions, Ore Deposits, and Environmental Geochemistry: A tribute to David A. Crerar* (Vol. 7, pp. 129-152): The Geochemical Society, Special Publications.
- Hermansen, H., Landa, G. H., Sylte, J. E., Thomas, L. K. (2000). Experiences after 10 years of waterflooding the Ekofisk Field, Norway. *Journal of Petroleum Science and Engineering*, 26, 11-18.
- Hermansen, H., Thomas, L. K., Sylte, J. E., Aasboe, B. T. (1997). *Twenty five years of Ekofisk reservoir management*. Paper presented at the SPE Annual Technical Conference and Exhibition, San Antonio, Texas.
- Herrle, J. O. (2003). Reconstructing nutricline dynamics of mid-Cretaceous oceans: evidence from calcareous nannofossils from the Niveau Paquier black shale (SE France). *Marine Micropaleontology*, 47(3), 307-321. doi:10.1016/S0377-8398(02)00133-0
- Herrle, J. O., Mutterlose, J. (2003). Calcareous nannofossils from the Aptian–Lower Albian southeast France: paleoecological and biostratigraphic implication. *Cretaceous Research*, 24, 1-22.
- Herrle, J. O., Pross, J., Friedrich, O., Kössler, P., Hemleben, C. (2003). Forcing mechanisms for Mid-Cretaceous black shale formation: Evidence from the upper Aptian and lower Albian of the Vocontian Basin (SE France). *Palaeogeography, Palaeoclimatology, Palaeoecology*, 190, 399-426.
- Hesselbo, S. P., Gröcke, D. R., Jenkyns, H. C., Bjerrum, C. J., Farrimond, P., Morgans Bell, H. S., Green, O. R. (2000). Massive dissociation of gas hydrate during a Jurassic oceanic event. *Nature*, 406, 392-395.
- Hibberd, D. J. (1976). The ultrastructure and taxonomy of the Chrysophyceae and Prymnesiophyceae (Haptophyceae): a survey with some new observations on the

- ultrastructure of the Chrysophyceae. *Botanical Journal of the Linnaean Society*, 72, 55-80.
- Hill, M. E. (1975). Selective Dissolution of Mid-Cretaceous (Cenomanian) Calcareous Nannofossils. *Micropaleontology*, 21(2), 227-235. doi:10.2307/1485025
- Hjelen, J. (1989). *Scanning elektron-mikroskopi*. Trondheim, Norway: Metallurgisk institutt, NTH.
- Houdan, A., Billard, C., Marie, D., Not, F., Sáez, A. G., Young, J. R., Probert, I. (2003). Flow cytometric analysis of relative ploidy levels in holococcolithophore-heterococcolithophore (Haptophyta) life stages. *Systematics and Biodiversity*, 1(4), 453-465.
- James, N. P., Jones, B. (2016). *Origin of carbonate sedimentary rocks* Wiley Works,
- Jenkyns, H. C. (1999). Mesozoic anoxic events and paleoclimate. *Zbl. Geol. Paläont. Teil.*, 943-949.
- Jørgensen, N. O. (1986). Geochemistry, diagenesis and nannofacies of chalk in the North Sea Central Graben. *Sedimentary Geology*, 48(3), 267-294. doi:https://doi.org/10.1016/0037-0738(86)90033-3
- Keller, G. (2008). Cretaceous climate, volcanism, impacts and biotic effects. *Cretaceous Research*, 29, 754-771.
- Korsnes, R. I. (2007). *Chemical induced water weakening of chalk by fluid-rock interaction. A mechanistic study*. (PhD thesis), University of Stavanger.
- Korsnes, R. I., Madland, M. V., Austad, T., Haver, S., Røslund, G. (2008). The effects of temperature on the water weakening of chalk by seawater. *Journal of Petroleum Science and Engineering*, 60, 183-193.
- Korsnes, R. I., Strand, S., Hoff, Ø., Pedersen, T., Madland, M. V., Austad, T. (2006). Does the chemical interaction between seawater and chalk affect the mechanical properties of chalk? In A. V. Cotthem, R. Charlier, J. F. Thimus, J. P. Tshibangu (Eds.), *Eurock 2006: multiphysics coupling and long term behaviour in rock mechanics : proceedings of the International Symposium of the International Society for Rock Mechanics, EUROCK 2006, 9-12 May 2006, Liège, Belgium*. Liège, Belgium: Taylor and Francis Group.
- Lees, J. A. (2002). Calcareous nannofossil biogeography illustrates palaeoclimate change in the Late Cretaceous Indian Ocean. *Cretaceous Research*, 23(5), 537-634.
- Lees, J. A. (2003). Calcareous nannofossil biogeography illustrates palaeoclimate change in the Late Cretaceous Indian Ocean. *Cretaceous Research*, 23, 537-634.
- Lees, J. A. (2007). New and rarely reported calcareous nannofossils from the Late Cretaceous of coastal Tanzania: outcrop samples and Tanzania Drilling Project Sites 5, 9 and 15. *Journal of Nannoplankton Research*, 29(1), 39-65.
- Lees, J. A., Bown, P. R. (2016). New and intriguing calcareous nannofossils from the Turonian (Upper Cretaceous) of Tanzania. *Journal of Nannoplankton Research*, 36(1), 83-95.
- Lees, J. A., Bown, P. R., Mattioli, E. (2005). Problems with proxies? Cautionary tales of calcareous nannofossil paleoenvironmental indicators. *Micropaleontology*, 51(4), 333-343.
- Linnert, C., Mutterlose, J. (2013). Biometry of Cenomanian-Turonian placoliths: A proxy for changes of fertility and surface-water temperature? *Lethaia*, 46(1).
- Lloyd, G. R., Young, J. R., Smith, A. B. (2012). Taxonomic Structure of the Fossil Record is Shaped by Sampling Bias. *Systematic Biology*, 61(1).
- Madland, M. V. (2005). *Water weakening of chalk: A mechanistic study*. (PhD thesis), University of Stavanger.
- Madland, M. V., Hiorth, A. (2011). Chemical alterations induced by rock - fluid interactions when injecting brines in high porosity chalks. *Transport in Porous Media*, 87, 679-702.

- Madland, M. V., Midtgarden, K., Manafov, R., Korsnes, R. I., Kristiansen, T. G., Hiorth, A. (2008). *The effect of temperature and brine composition on the mechanical strength of Kansas chalk*. Paper presented at the International Symposium of the Society of Core Analysts, Abu Dhabi, United Arab Emirates.
- Madland, M. V., Zimmermann, U. (2013). *Neoformed dolomite in flooded chalk for EOR processes*. Paper presented at the 75th EAGE Conference & Exhibition incorporating SPE EUROPEC, London, UK.
- Mandur, M. M. (2016). Late Cretaceous Calcareous Nannofossil Biostratigraphy and Paleoecology in the Northwestern Desert, Egypt. *Arab. J. Geosci.*, 41, 2271-2284.
- Mandur, M. M., El Ashwah, A. (2015). Calcareous nannofossil biostratigraphy and paleoecology of the Maastrichtian in the western coast of the Gulf of Suez, Egypt. *Arab. J. Geosci.*, 8, 2537-2550.
- Manivit, H. (1965). Nannofossiles calcaires de L'Albo-Aptien. *Revue de Micropaleontologie*, 8, 189-201.
- Manivit, H., Perch-Nielsen, K., Prins, B., Verbeek, J. W. (1977). Mid Cretaceous calcareous nannofossil biostratigraphy. *Proceedings of the Koninklijke Nederlandse Akademie van Wetenschappen*, B80(3), 169-181.
- McIntyre, A., Bé, A. W. H. (1967). Modern Coccolithophoridae of the Atlantic Ocean-I. Placoliths and Cyrtoliths. *Deep Sea Research*, 14, 561-597.
- McIntyre, A., Bé, A. W. H., Roche, M. B. (1970). Modern Pacific coccolithophorida: a paleontological thermometer. *Transactions of the New York Academy of Science*, 32, 720-731.
- Melinte, M. C., Lamolda, M. A., Kaiho, K. (2003). Nannofloral extinction and survivorship across the K/T Boundary Event at Caravaca section, SE Spain. *Palaeogeography, Palaeoclimatology, Palaeoecology*, 223, 27-52.
- Minde, M. W., Zimmermann, U., Madland, M. V., Korsnes, R. I., Schulz, B., Audinot, J.-N. (2016). *Fluid-flow during EOR experiments in chalk: insights using SEM-MLA, EMPA and nanoSIMS applications*. Paper presented at the International Symposium of the Society of Core Analysts, Snow Mass, Colorado, USA.
- Moshkovitz, S. (1982). On the findings of a new calcareous nannofossil (*Conusphaera zlabachensis*) and other calcareous organisms in the Upper Triassic sediments of Austria. *Eclogae Geologicae Helvetiae*, 75, 611-619.
- Moshkovitz, S., Eshet, Y. (1989). Inter-relative aspects of nannofossil and palynomorph biostratigraphy and paleoecology at the K/T boundary, Hor Hahar section, southern Israel. *Abs INA Newsl.*, 11, 80-81.
- Murphy, B. D. (2001). *Fundamentals of light microscopy and electronical imaging*: Wiley-Liss.
- Mutterlose, J., Bornemann, A., Herrle, J. O. (2005). Mesozoic calcareous nannofossils - state of the art. *Paläontologische Zeitschrift*, 79(1), 113-133.
- Nagel, N. B. (2001). Compaction and subsidence issues within the petroleum industry: from Wilmington to Ekofisk and beyond. *Physics and Chemistry of the Earth*, 26(Part A), 2-14.
- Nermoen, A., Korsnes, R., Hiorth, A., Madland, M. V. (2015). Porosity and permeability development in compacting chalks during flooding of nonequilibrium brines: insights from long-term experiment. *Journal of Geophysical Research*, 120, 2935-2960.
- Newman, G. (1983). The effect of water chemistry on the laboratory compression and permeability characteristics of some north sea chalks. *Journal of petroleum Technology*, 35, 976-980.
- Noël, D. (1959). Étude de coccolithes du Jurassique et du Crétacé inférieur. *Publications du Service de la Carte Géologique de l'Algérie (Nouvelle Série) Bulletin*, 20, 155-196.

- Noël, D. (1965). *Sur les Coccolithes du Jurassique Européen et d'Afrique du Nord*. Paris.
- Noël, D. (1969). *Arkhangelskiella* (coccolithes Crétacés) et formes affines du Bassin de Paris. *Revue de Micropaleontologie*, 11, 191-204.
- Noël, D. (1970). *Coccolithes Crétacés: La Craie Campanienne du Bassin de Paris*. Paris.
- Noël, D. (1973). Nannofossiles calcaires de sédiments jurassiques finement laminés. *Bulletin du Muséum National d'Histoire Naturelle, 3e serie*, 75, 95-156.
- Noël, D. (1965). *Sur les Coccolithes du Jurassique Européen et d'Afrique du Nord*. Paris: Éditions du Centre National de la Recherche Scientifique.
- Okada, H., Honjo, S. (1973). The distribution of oceanic coccolithophorids in the Pacific. *Deep Sea Research*, 20, 619-641.
- Oppel, C. A. (1856-1858). *Die Juraformation Englands, Frankreichs und des Südwestlichen Deutschlands*. Stuttgart: Ebner and Seubert.
- Parke, M., Adams, I. (1960). The motile (*Crystallolithus hyalinus* Gaarder and Markali) and non-motile phases in the life history of *Coccolithus pelagicus* (Wallich) Schiller. *Journal of the Marine Biological Association*, 39, 263-274.
- Pedersen, B. (2013, February 2nd, 2013). Stevns Klint. Retrieved from <http://bennyp.dk/Stevns%20Klint/slides/Fakse%20Kalkbrud.html>
- Perch-Nielsen, K. (1968). Der Feinbau und die Klassifikation der Coccolithen aus dem Maastrichtien von Danemark. *Biologiske Skrifter. Kongelige Danske Videnskabernes Selskab*, 16, 1-96.
- Perch-Nielsen, K. (1973). Neue Coccolithen aus dem Maastrichtien von Danemark, Madagaskar und Agypten. *Geological Society of Denmark, Bulletin*, 22, 306-333.
- Perch-Nielsen, K. (1979). Calcareous nannofossils from the Cretaceous between the North Sea and the Mediterranean. In J. Wiedmann (Ed.), *Aspekte der Kreide Europas* (Vol. 6, pp. 223-272): Int. Union Geol. Sci. Ser. A.
- Perch-Nielsen, K. (1983). Recognition of Cretaceous stage boundaries by means of calcareous nannofossils. In T. Birkelund, R. Bromley, W. K. Christensen, E. Håkansson, F. Surlyk (Eds.), *Symposium on Cretaceous Stage Boundaries (abstract)* (pp. 152-156). Copenhagen.
- Perch-Nielsen, K. (1984). Validation of new combinations. *Newsletter of the International Nannoplankton Association*, 6(1), 42-46.
- Perch-Nielsen, K. (1985). Mesozoic calcareous nannofossils. In H. M. Bolli, J. B. Saunders, K. Perch-Nielsen (Eds.), *Plankton Stratigraphy* (pp. 329-426). Cambridge: Cambridge Univ. Press.
- Piveteau, J. (1952). *Traité de Paléontologie*. In P. P. Grassé (Ed.), *Traité de zoologie. Anatomie, systématique, biologie, 1, part 1, Phylogenie. Protozoaires: généralités. Flagellés*. (pp. 107-115). Paris: Masson and Cie.
- Pospichal, J. J. (1994). Calcareous nannofossils at the K-T boundary, El Kef: No evidence for stepwise, gradual, or sequential extinctions. *Geology*, 22(99-102).
- Pospichal, J. J., Wise, S. W. (1990). Maastrichtian calcareous nannofossil biostratigraphy of Maud Rise ODP leg 113 sites 689 and 690, Weddell Sea. *Proceedings of the Ocean Drilling Program. Scientific Results*, 113, 465-487.
- Ramberg, I. B. (2008). *The Making of a Land: Geology of Norway*: Geological Society Publishing House.
- Reinhardt, P. (1964). Einige Kalkflagellaten-Gattungen (Coccolithophoriden, Coccolithineen) aus dem Mesozoikum Deutschlands. *Monatsberichte der Deutschen Akademie der Wissenschaften zu Berlin*, 6, 749-759.
- Reinhardt, P. (1965). Neue Familien für fossile Kalkflagellaten (Coccolithophoriden, Coccolithineen). *Monatsberichte der Deutschen Akademie der Wissenschaften zu Berlin*, 192, 221-253.

- Reinhardt, P. (1966a). Fossile Vertreter coronoider und styloider Coccolithen (Family Coccolithaceae Poche 1913). *Monatsberichte der Deutschen Akademie der Wissenschaften zu Berlin*, 8, 513-524.
- Reinhardt, P. (1966b). Zur Taxonomie und Biostratigraphie des fossilen Nannoplanktons aus dem Malm, der Kreide und dem Alttertiär Mitteleuropas. *Freiberger Forschungshefte, C196*, 5-109.
- Reinhardt, P., Górka, H. (1967). Revision of some Upper Cretaceous Coccoliths from Poland and Germany. *Neues Jahrbuch für Geologie und Paläontologie Abhandlungen*, 129, 240-256.
- Richard, J., Suzun, J. P., Machhour, L. (2005). Environmental and diagenetic records from a new reference section for Boreal realm: The Campanian chalk of the Mons basin (Belgium). *Sedimentary Geology*, 178, 99-111.
- Risnes, R., Flaageng, O. (1999). Mechanical properties of chalk with emphasis on chalk-fluid interactions and micromechanical aspects. *Oil & Gas Science and Technology*, 54, 751-758.
- Risnes, R., Madland, M. V., Hole, M., Kwabiah, N. K. (2005). Water weakening of chalk - mechanical effects of water-glycol mixtures. *Journal of Petroleum Science and Engineering*, 48, 21-36.
- Robaszynski, F., Dhondt, A. V., Jagt, J. W. M. (2001). Cretaceous lithostratigraphic units (Belgium). *Geologica Belgica*, 4, 121-134.
- Romein, A. J. T. (1979). Lineages in Early Paleogene calcareous nannoplankton. *Utrecht Micropaleontological Bulletins*, 22, 231.
- Rood, A. P., Hay, W. W., Barnard, T. (1971). Electron Microscope Studies of Oxford Clay Coccoliths. *Eclogae Geologicae Helveticae*, 64(245-272).
- Rood, A. P., Hay, W. W., Barnard, T. (1973). Electron microscope studies of Lower and Middle Jurassic coccoliths. *Eclogae Geologicae Helveticae*, 66, 365-382.
- Roth, P. H. (1978). Cretaceous nannoplankton biostratigraphy and oceanography of the northwestern Atlantic Ocean. In W. E. Benson, R. E. Sheridan et. al. (Eds.), *Init. Repts. DSDP* (Vol. 44, pp. 731-759). Washington: U. S. Govt. Printing Office.
- Roth, P. H. (1983). Jurassic and Lower Cretaceous calcareous nanofossils in the western North Atlantic (Site 534): biostratigraphy, preservation, and some observations on biogeography and paleoceanography. *Initial Reports of the Deep Sea Drilling Project*, 76, 587-621.
- Roth, P. H., Bowdler, J. (1981). Middle Cretaceous Calcareous Nannoplankton Biography And Oceanography Of The Atlantic Ocean. In J. E. Warme, R. G. Douglas, E. L. Winterer (Eds.), *The Deep Sea Drilling Project: a Decade of Progress* (Vol. 32, pp. 517-546): Society of Economic Paleontologists and Mineralogists Special Publications.
- Roth, P. H., Krumbach, K. R. (1986). Middle Cretaceous calcareous nanofossil biogeography and preservation in the Atlantic and Indian oceans: Implications for paleoceanography. *Marine Micropaleontology*, 10(1), 235-266. doi:[https://doi.org/10.1016/0377-8398\(86\)90031-9](https://doi.org/10.1016/0377-8398(86)90031-9)
- Scotese, C. R. (2002). PALEOMAP website.
- Shafik, S., Stradner, H. (1971). Nanofossils from the Eastern Desert, Egypt. *Jahrbuch der Geologischen Bundesanstalt Sonderband*, 17, 69-104.
- Sheldon, E. (2008). Upper Campanian – Maastrichtian calcareous nanofossil biostratigraphy of the Stevns-1 borehole, Denmark. *Journal of Nannoplankton Research*, 30, 39-49.
- Silva, I. P., Erba, E., Salvini, G., Locatelli, C., Verga, D. (1999). Biotic changes in Cretaceous oceanic anoxic events of the Tethys. *The Journal of Foraminiferal Research*, 29(4), 352-370.

- Sissingh, W. (1978). Microfossil biostratigraphy and stage-stratotypes of the Cretaceous. *Geol. Mijnbouw*, 57, 433-440.
- Sissingh, W., Prins, B. (1977). Biostratigraphy of Cretaceous calcareous nannoplankton. *Geologie en Mijnbouw*, 56(1), 37-65.
- Slimani, H. (2001). Les kystes de dinoflagelles du Campanien au Danien dans la région de Maastricht (Belgique, Pays-Bas) et de Turnhout (Belgique): biozonation et corrélation avec d'autres régions en Europe occidentale. *Geol. Paleontol.*, 35, 161-201.
- Stover, L. E. (1966). Cretaceous coccoliths and associated nannofossils from France and the Netherlands. *Micropaleontology*, 12, 133-167.
- Stradner, H. (1962). Über neue und wenig bekannte Nannofossilien aus Kreide und Alttertiär. *Sonderabdruck aus den Verhandlungen der Geologischen Bundesanstalt*, 2, 363-377.
- Stradner, H. (1963). New contributions to Mesozoic stratigraphy by means of nannofossils. *Proceedings of the Sixth World Petroleum Congress, Section 1 Paper 4*, 167-183.
- Surlyk, F. (1970). Die Stratigraphie des Maastricht von Dänemark und Norddeutschland aufgrund von Brachiopoden. *Newsletters in Stratigraphy*, 1, 7-16.
- Surlyk, F. (1984). The Maastrichtian Stage in NW Europe, and its brachiopod zonation. *Bulletin of the Geological Society of Denmark*, 33, 217-223.
- Surlyk, F., Damholdt, T., Bjerager, M. (2006). The upper Campanian-Lower Maastrichtian chalks of the Mons Basin, Belgium: a preliminary study of belemnites and foraminifera in the Harmignies and Ciplu areas. *Bulletin of the Geological Society of Denmark*, 54, 1-48.
- Surlyk, F., Stemmerik, L., Ahlborn, M., Harlou, R., Lauridsen, B. W., Rasmussen, S. L., Schovsbo, N. H., Sheldon, E., Thibault, N. (2010). The cyclical Rørdal Member - a new lithostratigraphic unit of chronostratigraphic importance in the upper Maastrichtian of Denmark. *Bulletin of the Geological Society of Denmark*, 58, 89-98.
- Svobodova, A., Košťák, M. (2016). Calcareous nannofossils of the Jurassic/Cretaceous boundary strata in the Puerto Escaño section (southern Spain) - Biostratigraphy and palaeoecology. *Geologica Carpathica*, 67(3). doi:10.1515/geoca-2016-0015
- Thibault, N. (2010). Calcareous nannofossils from the Boreal upper Campanian – Maastrichtian Chalk of Denmark. *Journal of Nannoplankton Research*, 31, 39-56.
- Thibault, N., Gardin, S. (2007). Maastrichtian calcareous nannofossil biostratigraphy and paleoecology in the Equatorial Atlantic (Demerara Rise, ODP Leg 207 Hole 1258A). *Revue de Micropaleontologie*, 49, 199-214.
- Thierstein, H. R. (1971). Tentative Lower Cretaceous Calcareous Nannoplankton Zonation. *Eclogae Geologicae Helveticae*, 64, 459-488.
- Thierstein, H. R. (1973). Lower cretaceous calcareous nannoplankton biostratigraphy. *Abhandlungen der Geologischen Bundesanstalt*, 29, 3-52.
- Thierstein, H. R. (1980). Selective dissolution of late cretaceous and earliest tertiary calcareous nannofossils: Experimental evidence. *Cretaceous Research*, 1(2), 165-176. doi:https://doi.org/10.1016/0195-6671(80)90023-3
- Thierstein, H. R. (1981). Late Cretaceous nannoplankton and the change at the Cretaceous-Tertiary boundary. In J. E. Warme, R. G. Douglas, E. L. Winterer (Eds.), *The Deep Sea Drilling Project: A Decade of Progress* (Vol. 32, pp. 355-394). Tulsa: SEPM Special Publication.
- Tiraboschi, F., Erba, E., Jenkyns, H. C. (2009). Origin of rhythmic Albian black shales (Piobbico core, central Italy) Calcareous nannofossil quantitative and statistical analysis and paleoceanographic reconstructions. *Paleoceanography*, 24. doi:doi:10.1029/2008PA001670
- Tréjo, M. (1960). La familia Nannoconidae y su alcance estratigráfico América (Protozoa-incertae sedis). *Boll. Asoc. mexic. Geólogos Petrol*, 12(9), 259-314.

- Tremolada, F. (2002). Aptian to Campanian calcareous nannofossil biostratigraphy from the Bottaccione section, Gubbio, central Italy. *Rivista Italiana di Paleontologia e Stratigrafia*, 108(3), 441-456.
- Varol, O. (1989). Quantitative analysis of the *Arkhangelskiella cymbiformis* group and its biostratigraphical usefulness in the North Sea area. *Journal of Micropalaeontology*, 8, 131-134.
- Varol, O. (1992). Taxonomic revision of the Polycyclolithaceae and its contribution to Cretaceous biostratigraphy. *Newsletters on Stratigraphy*, 27, 93-127.
- Vekshina, V. N. (1959). Coccolithophoridae of the Maastrichtian deposits of the West Siberian lowlands. *Siberian Science Research Institute of Geology Geophysics Mineralogy and Raw Materials*, 2, 56-81.
- Verbeek, J. W. (1977). Calcareous nannoplankton biostratigraphy of Middle and Upper Cretaceous deposits in Tunisia, southern Spain and France. *Utrecht Micropaleontological Bulletins*, 16, 1-157.
- Walsby, A. E., Reynolds, C. S. (1981). Sinking and floating. In I. Morris (Ed.), *The Physiological Ecology of Phytoplankton* (pp. 371-412). Oxford, UK: Blackwell Scientific Publication.
- Wang, W., Madland, M., Zimmermann, U., Nermoen, A., Korsnes, R. I., Bertolino, S. R. A., Hildebrand-Habel, T. (2016). Evaluation of porosity change during chemo-mechanical compaction in flooding experiments on Liège outcrop chalk. In P. J. Armitage, A. R. Butcher, J. M. Churchill, A. E. Csoma, C. Hollis, R. H. Lander, J. E. Omma, R. H. Worden (Eds.), *Reservoir Quality of Clastic and Carbonate Rocks: Analysis, Modelling and Prediction* (Vol. 435). London: Geological Society Special Publications.
- Watkins, D. K. (1986). Calcareous nannofossil palaeoceanography of the Cretaceous Greenhorn Sea. *Bulletin of the Geological Society of America*, 97, 1239-1249.
- Watkins, D. K. (1989). Nannoplankton productivity fluctuations and rhythmically-bedded pelagic carbonates of the Greenhorn Limestone (Upper Cretaceous). *Palaeogeography, Palaeoclimatology, Palaeoecology*, 74, 75-86.
- Watkins, D. K., Cooper, M. J., Wilson, P. A. (2005). Calcareous nannoplankton response to the Late Albian oceanic anoxic event 1d in the western North Atlantic. *Paleoceanography*, 20, 1-14.
- Whittaker, R. H., Margulis, L. (1978). Protist classification and the kingdoms of organisms. *BioSystems*, 10, 3-18.
- Wiborg, R., Jewhurst, J. (1986). Ekofisk subsidence detailed and solutions accessed. *Oil and Gas Journal*, 2, 47-51.
- Wicander, R., Monroe, J. S. (2004). *Historical Geology Evolution of Earth and Life Through Time* (4th ed.). Belmont: Brooks/Cole.
- Williams, J. R., Bralower, T. J. (1995). Nannofossil assemblages, fine fraction stable isotopes, and the paleoceanography of the Valanginian-Barremian (Early Cretaceous) North Sea Basin. *Paleoceanography*, 10(4), 815-839.
- Winterman, D. (2012). White Cliffs of Dover: Why are they so important to the British? *BBC News Magazine*.
- Wise Jr, S. W. (1988). Mesozoic-Cenozoic history of calcareous nannofossils in the region of the Southern Ocean. *Palaeogeography, Palaeoclimatology, Palaeoecology*, 67, 157-179.
- Wise, S. W., Wind, F. H. (1977). Mesozoic and Cenozoic calcareous nannofossils recovered by DSDP Leg 36 drilling on the Falkland Plateau, south-west Atlantic sector of the Southern Ocean. *Initial Reports of the Deep Sea Drilling Project*, 36, 269-491.
- Young, J. R. (1994). Functions of coccoliths. In A. Winter, W. G. Siesser (Eds.), *Coccolithophores* (pp. 63-82). Cambridge: Cambridge University Press.

- Young, J. R. (1998). Neogene. In P. R. Bown (Ed.), *Calcareous Nannofossil Biostratigraphy* (pp. 225-265). London: Chapman and Hall.
- Young, J. R., Bown, P. R., Lees, J. A. (2016). Nannotax 3.
- Zijlstra, H. (1995). *The Sedimentology of Chalk*: Springer-Verlag Berlin Heidelberg.

9. Appendices

9.1. Appendix 1: Offshore Chalk Reservoir Samples

Sample ID	Sample depth (ft)	Sample depth (m)	Presumed age	Formation	Well	Field
TOR34	9796,5	2986,0	Danian	Ekofisk	2/4-8 AX	Tor
TOR33	9804,5	2988,4	Danian	Ekofisk	2/4-8 AX	Tor
TOR32	9823,1	2994,1	Danian	Ekofisk	2/4-8 AX	Tor
TOR31	9835,1	2997,7	Danian	Ekofisk	2/4-8 AX	Tor
TOR30	9852,5	3003,0	Danian	Ekofisk	2/4-8 AX	Tor
TOR29	9877	3010,5	Danian	Ekofisk	2/4-8 AX	Tor
TOR28	9913	3021,5	Danian	Ekofisk	2/4-8 AX	Tor
TOR27	9932,5	3027,4	Danian	Ekofisk	2/4-8 AX	Tor
TOR26	9942,3	3030,4	Danian	Ekofisk	2/4-8 AX	Tor
TOR25	9950	3032,8	Danian	Ekofisk	2/4-8 AX	Tor
TOR24	9971,5	3039,3	Danian	Ekofisk	2/4-8 AX	Tor
TOR23	9996,5	3046,9	Danian	Ekofisk	2/4-8 AX	Tor
TOR22	10022,5	3054,9	Danian	Ekofisk	2/4-8 AX	Tor
TOR21	10028,5	3056,7	Danian	Ekofisk	2/4-8 AX	Tor
TOR20	10046,8	3062,3	Danian	Ekofisk	2/4-8 AX	Tor
TOR19	10060,5	3066,4	Danian	Ekofisk	2/4-8 AX	Tor
TOR18	10076,8	3071,4	Danian	Ekofisk	2/4-8 AX	Tor
TOR17	10092,9	3076,3	Danian	Ekofisk	2/4-8 AX	Tor
TOR16	10112,9	3082,4	Danian	Ekofisk	2/4-8 AX	Tor
TOR15	10128,7	3087,2	Late Camp. - Maa	Tor	2/4-8 AX	Tor
TOR14	10130,2	3087,7	Late Camp. - Maa	Tor	2/4-8 AX	Tor
TOR13	10141	3091,0	Late Camp. - Maa	Tor	2/4-8 AX	Tor
TOR12	10150,5	3093,9	Late Camp. - Maa	Tor	2/4-8 AX	Tor
TOR11	10178,5	3102,4	Late Camp. - Maa	Tor	2/4-8 AX	Tor
TOR10	10199	3108,7	Late Camp. - Maa	Tor	2/4-8 AX	Tor
TOR9	10262	3127,9	Late Camp. - Maa	Tor	2/4-8 AX	Tor
TOR8	10273,1	3131,2	Late Camp. - Maa	Tor	2/4-8 AX	Tor
TOR7	10294,5	3137,8	Late Camp. - Maa	Tor	2/4-8 AX	Tor
TOR6	10314,5	3143,9	Late Camp. - Maa	Tor	2/4-8 AX	Tor
TOR5	10346,3	3153,6	Late Camp. - Maa	Tor	2/4-8 AX	Tor
TOR4	10358,7	3157,3	Late Camp. - Maa	Tor	2/4-8 AX	Tor
TOR3	10375	3162,3	Late Camp. - Maa	Tor	2/4-8 AX	Tor
TOR2	10396,5	3168,9	Late Camp. - Maa	Tor	2/4-8 AX	Tor
TOR1	10405,5	3171,6	Late Camp. - Maa	Tor	2/4-8 AX	Tor

Appendix 1: Offshore chalk reservoir samples with additional data.

9.2. Appendix 2: Sample Weight in Random Settling Smear Slides

Sample ID	Weight before [mg]	Weight after [mg]	Real weight [mg]	N	V [ml]	M [g]	F	A [cm ²]	H [cm]	X [n/g]
T15	40,345	0,517	39,828	14	500	0,03983	337,5	0,02	3	8679,3
T14	39,848	0,065	39,783	300	500	0,03978	75	0,02	3	837878,8
T13	39,163	0,070	39,093	301	500	0,03909	337,5	0,02	3	190113,3
T12	39,413	0,071	39,342	156	500	0,03934	412,5	0,02	3	80105,6
T11	40,180	0,071	40,109	137	500	0,04011	375	0,02	3	75904,3
T10	39,837	0,051	39,786	300	500	0,03979	275	0,02	3	228495,2
T9	41,656	0,027	41,629	47	500	0,04163	331,25	0,02	3	28403,0
T8	39,384	0,169	39,215	192	500	0,03922	350	0,02	3	116573,5
T7	40,360	0,110	40,250	153	500	0,04025	390,625	0,02	3	81093,2
T6	39,104	0,061	39,043	300	500	0,03904	90,625	0,02	3	706559,6
T5	40,171	0,050	40,121	276	500	0,04012	362,5	0,02	3	158142,3
T4	39,909	0,315	39,594	300	500	0,03959	356,25	0,02	3	177237,6
T3	42,900	0,088	42,812	300	500	0,04281	218,75	0,02	3	266947,9
T2	39,980	0,038	39,942	300	500	0,03994	212,5	0,02	3	294544,7
T1	43,156	0,055	43,101	54	500	0,04310	456,25	0,02	3	22883,5
A1	20,365	0,079	20,286	305	500	0,02029	33	0,02	3	3796717,0
A5	19,977	0,090	19,887	303	500	0,01989	47	0,02	3	2701433,3
MS1	29,218	0,011	29,207	313	500	0,02921	13	0,02	3	6869621,2
MS5	21,879	0,023	21,856	301	500	0,02186	24	0,02	3	4781931,2
SK1	21,857	0,134	21,723	302	500	0,02172	27	0,02	3	4290838,1
SK5	19,149	0,049	19,100	302	500	0,01910	31	0,02	3	4250408,2
MT1	30,827	0,002	30,825	308	500	0,03083	25	0,02	3	3330629,9
MT5	20,403	0,849	19,554	303	500	0,01955	23	0,02	3	5614330,0
MON1	19,740	0,113	19,627	302	500	0,01963	22	0,02	3	5828396,6
MON5	19,475	0,115	19,360	305	500	0,01936	22	0,02	3	5967474,3
L1	26,060	0,036	26,024	311	500	0,02602	19	0,02	3	5241450,5
L5	19,904	2,378	17,526	305	500	0,01753	29	0,02	3	5000780,4
MOV1	20,552	0,206	20,346	301	500	0,02035	10	0,02	3	12328385,6
MOV5	19,606	0,059	19,547	300	500	0,01955	14	0,02	3	9135490,3
K1	19,566	0,072	19,494	307	500	0,01949	13	0,02	3	10095150,9
K5	22,697	0,016	22,681	318	500	0,02268	22	0,02	3	5310812,8

Appendix 2: Sample weight in random settling slides with calculations for total nannofossil abundances. After Williams and Bralower (1995): X = particles per gram of sediment [n/g], N = number of particles counted, V = volume of water used for dilution [ml], M = grams of sediment added [g], F = number of fields of view observed, A = surface area of one FOV [cm²] and H = height of water column above slide [cm].

9.3. Appendix 3: Taxonomic Description

Appendix 3: Taxonomic descriptions: This appendix presents short taxonomic descriptions of every genus and species encountered in this thesis, followed with simplified sketches and photos from the light microscope and/or the FEG-SEM. The descriptions are based on various authors, which will be referenced accordingly.

All genera and species share the following taxonomic rank:

Domain: **EUKARYOTE** (Chatton, 1925) Whittaker and Margulis, 1978

Kingdom: **CHROMISTA** Cavalier-Smith, 1981

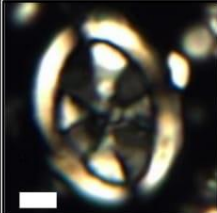
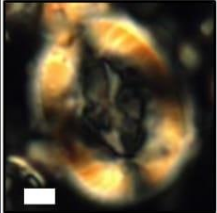
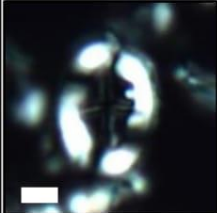
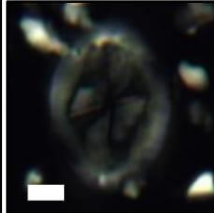
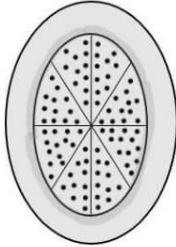
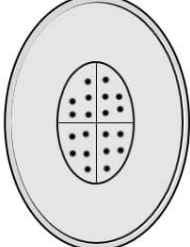
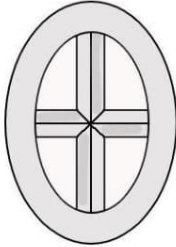
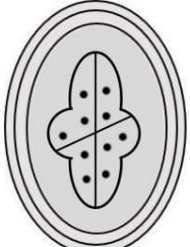
Phylum: **HAPTOPHYTA** Cavalier-Smith, 1986

Class: **PRYMNESIOPHYCEAE** Hibberd, 1976

Next, the organization follows the general grouping of heterococcoliths, holococcoliths and nannoliths. For each group, a four-level classification will be used: order-family-genus-species (and sub-species for a few). Each species is accompanied with its original description, as well as personal remarks if any.

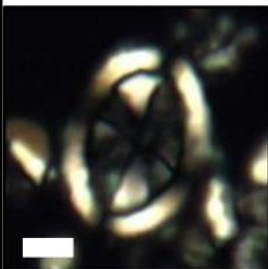
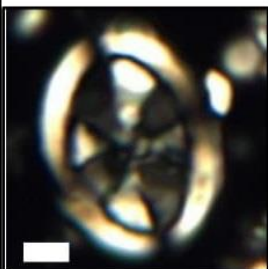
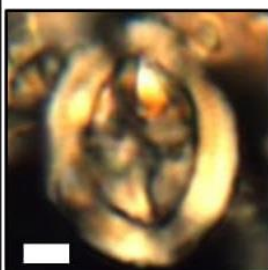
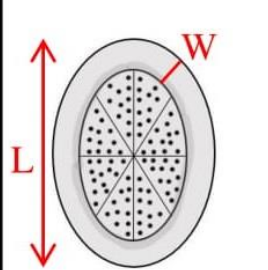
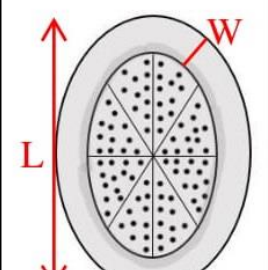
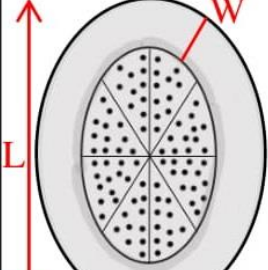
9.3.1. Heterococoliths

Order: Arkhangelskiales Bown and Hampton, 1997 *in* Bown and Young, 1997

Structural elements \ Genera	<i>Arkhangelskiella</i>	<i>Aspidolithus</i>	<i>Broinsonia</i>	<i>Gartnerago</i>
Central cross			✓	
Central plate	✓	✓		✓
Perforations	✓	✓		✓
Rim	Unicyclic, bright	Bicyclic, yellow-orange	Uni-bicyclic, bright	Tricyclic, bright medium cycle
Light microscope photograph Scale bar = 2 μm	 <i>A. cymbiformis</i> A5_A	 <i>A. p. parvus</i> MT1_B	 <i>Broinsonia sp.</i> MS1_B	 <i>G. obliquum</i> K1_B
Structural sketches based on personal observations				

Family: Arkhangelskiellaceae Bukry, 1969 emend Bown and Hampton, 1997 in Bown and Young, 1997

Genus: *Arkhangelskiella*

Species	<i>A. confusa</i>	<i>A. cymbiformis</i>	<i>A. maastrichtiensis</i>
Structural elements			
Rim width (W)	< 1.5 μm	< 1.5 μm	> 1.5 μm
Size, length (L)	< 8 μm	\geq 8 μm	> 10 μm
Light microscope photograph Scale bar = 2 μm			
	<i>A. confusa</i> MS1_B	<i>A. cymbiformis</i> A5_A	<i>A. maastrichtiensis</i> T4_A
Structural sketches based on personal observations			

Species: *A. confusa* Burnett, 1997, Plate Ia-b.

From Burnett (1997):

“Diagnosis: Small-to medium-sized *Arkhangelskiella* with a <1.5 μm thick rim. Remarks: This species first appears around the Coniacian. and is thus stratigraphically differentiated from the species of *Arkhangelskiella* described below which appear, respectively, in the Campanian and Maastrichtian. This form typically has a rim which is intermediate (1.0-1.5 μm) in width between the rim thicknesses of *A. cymbiformis sensu stricto* and *A. maastrichtiensis*, and also includes small (down to ~ 4 μm long) forms of the genus.”

Species: *A. cymbiformis* Vekshina, 1959, Plate Ic-d and Plate Xa.

From Vekshina (1959):

“Description: Discoliths elliptical in shape, often with pointed ends, concave, having a thickened edge, two-layered, of large and medium dimensions (8-12 μm on the long axis, and 6-7 μm on the short axis). The central plate is transected by four ribs, running along the axes of the ellipse. In the intervals between the ribs pores are situated. A small variation is observed in the dimensions of the coccoliths, and also in the width of the edge.

Dimensions in μm :

	Holotype	Original 1	Original 2
Long axis	10	9.15-4.5	12
Short axis	7.5	7	3.75
Thickness of edge	2.0	1	1.5

Remarks: Similar forms are *Arkhangelskiella cymbiformis f. rara* f. n. and *Arkhangelskiella specillata* cent. n. The century described has the shape of a flat discolith, while *Arkhangelskiella cymbiformis f. rara* f. n. has that of a shallow cup. *A. specillata* cent. n. differs from *Arkhangelskiella cymbiformis* only by a larger number of rows of pores. A. D. Arkhangel'skii (1910) gave a drawing of this form, but without a name or description.”

Species: *A. maastrichtiensis* Burnett, 1997, Plate Ie-f.

From Burnett (1997):

“Description: Large *Arkhangelskiella* with a $> 1.5\mu\text{m}$ thick rim Remarks: The large size ($>10\mu\text{m}$) and thick rim ($> 1.5 \mu\text{m}$) distinguish this from other *Arkhangelskiellas*. It becomes common in the Upper Maastrichtian in high latitudes, and can be used as a marker there.”

Genus: *Aspidolithus* Noël, 1969

From Noël (1969):

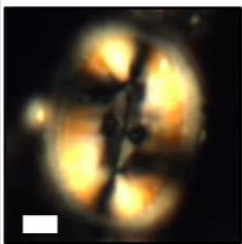
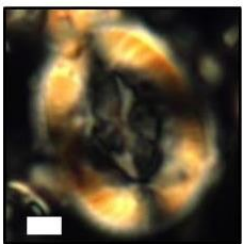
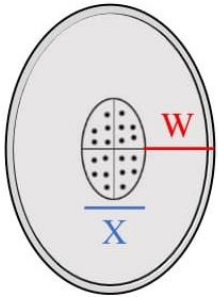
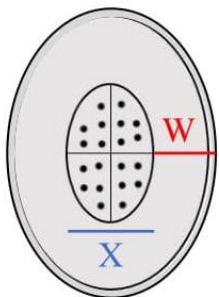
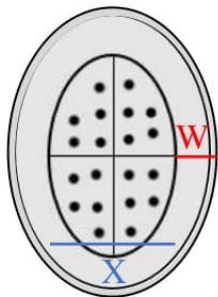
“Description: Diagnose: Coccolithes elliptiques composés d'une couronne marginale constituée de deux séries superposées d'éléments, formant entre elles un angle rentrant; série supérieure bordée intérieurement d'un cycle d'éléments plus ou moins développé, limitant une aire centrale nettement convexe, de dimensions variables et construite de cristaux di versement disposés;

série inférieure faite d'éléments en disposition radiaire. Remarks: Rapports et différences: Les coccolithes rangés dans ce nouveau genre diffèrent des *Arkhangelskiella* par la présence d'un cycle continu d'éléments bordant intérieurement la série supérieure de la couronne marginale. Note: In the subsequent publication (Noël D., 1970, Coccolithes crétacés. La craie campanienne du bassin de Paris. Centre Nat. Rech. Sei., Paris, p. 75), *Aspidolithus* is considered synonym of *Broinsonia* BUKRY, 1969.”

Personal remarks: *A. parvus* belongs to the *Broinsonia*-genus, together with *B. enormis* and *B. furtiva*, according to Young et al. (2016). However, in discussions with Elisabetta Erba and Cinzia Bottini, it became clear that this is problematic. *A. parvus* has a central plate, and not a cross – and therefore it cannot belong to *Broinsonia* but is put in the *Aspidolithus*-genus instead. In addition, it became unclear what distinguishes *B. enormis* and *B. furtiva* from the *A. parvus*-subspecies.

All *Aspidolithus* specimen in the samples in this thesis have a high birefringent rim. They can easily be distinguished from other genera of Arkhangelskiellaceae by their yellow-orange rim color and dark central areas.

Species: *A. parvus* (Stradner, 1963) Bukry, 1969

Species	<i>A. parvus constrictus</i>	<i>A. parvus parvus</i>	<i>A. parvus expansus</i>
Structural elements			
Rim width (W)	$W > X$	$W < 1-2 X$	$W < 0.5 X$
Central area width (X)	$X < W$	$X > 0.5-1 W$	$X > 2 W$
Light microscope photograph Scale bar = 2 μ m	 <i>A. p. constrictus</i> SK1_B	 <i>A. p. parvus</i> MT1_B	Not present in samples
Structural sketches based on personal observations			

From Stradner (1963):

“Description: Elliptical coccoliths with narrow central area and wide double marginal plates. A straight central cross divides the central area into sectors, which are perforated each by a few pores.”

Subspecies: *A. parvus constrictus* Hattner et al., 1980, Plate Ig-i and Plate Xb.

From Hattner et al. (1980):

“Description: A subspecies of *Broinsonia parca* with a very small central area whose width is approximately equal to or significantly less than the width of the shield margin. One to three rounded perforations per quadrant lie approximately parallel to the major axis and these

perforations are subdivided by fine processes which resemble a sieve plate with more or less rounded openings.

Remarks: This form is differentiated from *B. parca parca* by its smaller, more constricted central area and a smaller number of perforations aligned parallel to the major axis only. Its form differs from Stradner's (1963) holotype of *Arkhangelskiella parca* by the absence of more than one perforation per quadrant parallel to the minor axis and a central area whose width is approximately equal to or smaller than the shield margin. This form is probably synonymous with *Aspidolithus* sp. 3, 4, and 5 of Lauer (1975) which Verbeek (1976, 1977) suggests evolved during the early Campanian. Our data also suggest that *B. parca constricta* evolved from *B. parca parca* during the early Campanian. In this regard it is considered useful as a stratigraphic datum. This subspecies differs from *B. furtiva* by its much smaller central area and the absence of barlike processes subdividing the perforations. Instead, the membranelike processes which fill the perforations of *B. parca constricta* closely resemble those filling the perforations of *Arkhangelskiella specillata*.”

Subspecies: *A. parcus parcus* (Stradner, 1963) Bukry, 1969, Plate Ij-l.

Same description as the species.

Genus *Broinsonia* Bukry, 1969

Species: *Broinsonia* sp., Plate Im-o.

Specimen that cannot be identified down to species level but can be recognized as belonging to the genus. From Bukry (1969):

“Description: Elliptical coccolith characterized by 2-cycle rim in distal view and 3-tier proximal rim, which is at 3 distinct levels with interelement sutures maintaining same inclination across each tier. Central area comprising single shield divided into quadrants by axial sutures, quadrants perforated in various manners.

Remarks: 1) Distal plate elements are more orthogonal and more regularly arranged than those of *Gartnerago* BUKRY, n. gen. 2) The inner cycle of elements on the distal surface distinguishes *Broinsonia* from *Gartnerago* and *Arkhangelskiella* VEKSHINA. Only *Broinsonia* has a cycle of irregularly margined elements which have a peripheral extension paralleling the outer margin of the cycle. These oddly shaped elements are usually further

modified by having a broad dimple. 3) Perforations are slitlike or circular as in *Arkhangelskiella*. 4) The rims contain fewer elements than *Gartnerago*. 5) In proximal view, *Broinsonia* is not distinguished from *Arkhangelskiella* by rim structure. Central-area perforation or ornamentation is usually distinctive.”

Family: Kamptneriaceae Bown and Hampton, 1997 in Bown and Young, 1997

Genus: *Gartnerago* Bukry, 1969

Species: *G. obliquum* (Stradner, 1963) Noël, 1970, Plate Ip-r and Plate Xc-d.

From Stradner (1963):

“Description: Elliptical coccoliths with simple margin and wide central area, which is decorated with an oblique cross; the longer crossbars lie in direction of the main axis. A varying number of pores perforate the sectors of the central area.”

Personal remarks: The oblique suture is visible when rotating the stage under crossed nicols and with a gypsum plate. The suture has a slight orange-red colour. *G. obliquum* is encountered in samples of Campanian-Maastrichtian age – so the range given by (Young et al., 2016), with LO in Coniacian, is doubtful.

Genus: *Kamptnerius* Deflandre, 1959

Species: *K. magnificus* Deflandre, 1959, Plate Is-t, Plate IIa-c and Plate Xe-f.

From Deflandre (1959):

“Description: Calyptrolithe elliptique. Frange formée de lamelles de calcite jointives à extrémité arrondie, fortement et asymétriquement développée vers l'un des pôles, dressée obliquement sur le bord du fond du calyptrolithe. Largeur de la frange pouvant atteindre et même dépasser la largeur de l'ellipse. Fond du calyptrolithe plus ou moins distinctement marqué de stries qui proviennent de sa structure, formée de lamelles convergeant vers une ligne longitudinale souvent inclinée sur l'axe de l'ellipse. Dimensions du type: longueur totale 19,5 µm; ellipse, longueur 13 µm largeur 11 µm. Autres spécimens: longueur totale 12,5- 19 µm; ellipse, longueur 8,5- 17,5 µm, largeur, 8- 12,5 µm. Remarks: Il n'a été observé que des spécimens en vue frontale ou plus ou moins oblique (figs. 2, 3), et la vue latérale exacte reste à décrire. Les spécimens d'Australie, de plus grande taille, ont une frange proportionnellement

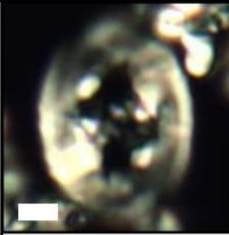
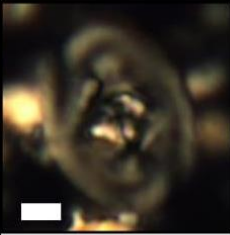
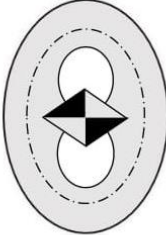
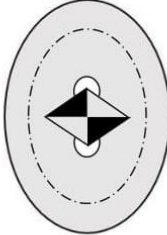
plus étroite. Mais de petites formes d'allure semblable existent dans le Crétacé européen. Les intéressantes variations de ce beau nannofossile seront décrites ultérieurement (1).”

Personal remarks: Ghostly appearance due to the flange. The flange is often missing, but the species is still easily recognized by its thin, but clear rim, and blurry central area.

Order: Eiffellithales Rood et al., 1971

Family: Chiastozygaceae Rood et al., 1973

Genus: Reinhardtites Perch-Nielsen, 1968

Species	<i>R. anthophorus</i>	<i>R. levis</i>
Structural elements		
Openings on side of cross bar	Large	Small or not visible
Light microscope photographs Scale bar = 2 μm		
	<i>R. anthophorus</i> MON1_A	<i>R. levis</i> SK1_B
Structural sketches based on personal observations		

Species: *R. anthophorus* (Deflandre, 1959) Perch-Nielsen, 1968, Plate IId-h.

From Deflandre (1959):

“Description: Embase elliptique relativement épaisse, finement striée sur le bord, portant une hampe cylindrique ou subcylindrique à l'extrémité de laquelle est situé un brge cône pétalé s'ouvrant comme une fleur. L'ombrage révèle que la hampe est finement cannelée (fig. 22) tandis que par transparence (fig. 21) une structure hélicoïdale fine et très peu marquée apparaît.

Le cône terminal est formé par de fortes lamelles de calcite qui peuvent être lobées ou, s'épaississant, tendre vers une forme rhomboédrique. Dimensions: hauteur totale 17-19,7 µm; embase, longueur 11-13 µm, largeur 8-11,5 µm. Remarks: *Rh. anthophorus*, que je ne connais encore que d'une localité, méritait d'être décrit parce qu'il est extrêmement bien caractérisé, facile à reconnaître, et par conséquent susceptible d'être aisément identifié et utilisé."

Personal remarks: *R. anthophorus* must have visible large holes on both sides of the diamond-shaped bride to be recognized. *R. levis* has no holes or very small holes.

Species: *R. levis* Sissingh and Prins, 1977, Plate li-n.

From Sissingh and Prins (1977):

"Diagnosis: A species of *Reinhardtites* characterized by a very broad, smooth plate lining enclosing a broad, rhombical bridge structure, surmounted by a short spine without flaring top part. Description: A well developed rim with radiating rim elements surrounds at its proximal side a low wall. At its distal side it is connected to a broad, smooth plate-lining, leaving sometimes two small openings at both sides of the central bridge structure. In plan view the bridge is broadly rhombical and it extends less far in the direction of the rim than is found in the other species of the genus. The bridge carries a short, broad spine. So far no specimens have been observed, in which the spine terminates in a flaring top part. Derivatio nominis: *levis* (Latin) = smooth.

Size: 8-10.5 µm

Remarks: The species differs from *R. anthophorus* in having a much broader and smooth plate-lining. It differs from *R. aff. anthophorus* in having a bridge structure that extends less far in the direction of the rim."

Personal remarks: The rhombus bridge in the central area has a diamond shape, which is altered in the samples in this thesis, leading to a rounder and more unclear rhombus shape. The overgrown bridge covers the two holes above and below the diamond, so they are difficult to see. The outer rim appears faint. The extinction pattern appears distinctive (V-shape out from the bottom and top of the diamond) when rotating the stage.

Genus: *Tranolithus* Stover, 1966

Species: *T. gabalus* Stover, 1966, Plate IIo-p.

From Stover (1966):

“Description: The coccoliths have an elliptical outline in proximal or distal view and a narrow smooth rim. The central opening is spanned transversely by a relatively wide, slightly distally arched bar, commonly with a small central perforation. Components of the transverse bar and adjacent parts of the rim have the same or nearly the same crystallographic orientation. The curvature of extinction lines across the rim is sinistral in distal view. Length 6-8 μm , width 4-5 μm , height about 1.5 μm . Remarks: Comparison: This species differs from *T. manifestus*, n. sp., m having a narrower nm and one rather than two transverse bars.”

Species: *T. minimus* (Bukry, 1969) Perch-Nielsen, 1984, Plate IIq-t and Plate Xg.

From Bukry (1969):

“Description: The elliptical rim cycle of this small species is composed of 22 to 30 dextrally imbricated elements inclined clockwise. Rim margins are smooth or serrate. The eccentricity of the outline varies from 1.3 to 1.8. The central area is filled by a multi-element central stem flanked by 2 large, flat elements which completely occupy the remaining area. Maximum diameter: 4.8 μm . Remarks: The 2 large central area elements can be enlarged and raised to suggest affinity to *Zygodiscus macleodae* BUKRY.”

Species: *T. orionatus* (Reinhardt, 1966a) Reinhardt, 1966b, Plate IIIa-b and Plate Xh.

From Reinhardt (1966a):

“Description: Eine wallförmige elliptische Randscheibe aus 36 bis 40 dachziegelförmig angeordneten Randblättchen umsäumt eine Area centralis aus Tabulae. Die Tabulae berühren sich längs der Ellipsenachsen und sparen an den 4 Enden der Achsen und im Zentrum je eine Pore aus. Grösse: 5 bis 8 μm .”

Personal remarks: *T. orionatus* can appear very different depending on the alteration. The central area might be closed due to overgrowth. It helps to use the gypsum plate to spot the four bars.

Genus: *Zeugrhabdotus* Reinhardt, 1965

Species: *Z. bicrescenticus* (Stover, 1966) Burnett in Gale et al., 1996, Plate IIIc-d.

From Stover (1966):

“Description: The coccoliths are elliptical in proximal or distal view. The rim is smooth to faintly striate and of medium width. The center of the coccolith has a prominent boss surrounded by an elliptical band of variable width that is not in contact with the boss across the narrow ends of the coccoliths. The central boss appears nearly ortholithic under crossed nicols and is formed of four parts with the crystallographic orientation of components in each part the same or nearly so. The curvature of extinction lines across the rim is sinistral in distal view. Length 6-8 μm , width 4.5-6.0 μm , height 1.5-2.0 μm . Remarks: Comparison: The distinctive, nearly ortholithic central boss and the band of variable width between the rim and central boss are characters that distinguish *Discolithus bicrescenticus* from other species of *Discolithus*. Remarks: The size and shape of the openings between the central boss and the ring which is adjacent to the rim are variable.”

Species: *Z. embergeri* (Noël, 1959) Perch-Nielsen, 1984, Plate IIIe-f.

From Noël (1959):

“Description: Ce discolithe fréquent dans le matériel étudié est elliptique, et présente une bordure lisse. Le plancher présente une ornementation en losange, avec sur la petite diagonale de celui-ci deux perforations (?) circulaires. L'examen de cette forme en lumière polarisée est indiqué fig. 6 a, b, c, d, e. Sur la bordure du discolithe, les fibres de calcite s'éteignent en formant des arcs de cercle. Le comportement du plancher est double: le losange central s'éteint et s'éclaire indépendamment du reste du plancher.

De telles figures renseignent sur la structure du discolithe: le losange central est constitué de fibres de calcite parallèles entre elles; le reste du plancher est formé de fibres rayonnantes qui s'incurvent pour constituer la bordure du discolithe, ainsi que l'indique la coupe théorique 7b. De plus ces fibres de la bordure sont disposées en spirales (fig. 7), ce qui explique les extinctions en arcs de cercle de la bordure. Dimensions: grand axe de l'ellipse 20 μm , petit axe 13 μm . Remarks: Variations: Ce discolithe est de taille variable, 12 à 24 μm pour le grand axe de l'ellipse. L'ornementation du plancher est un peu différente chez certains individus: les côtés du losange étant incurvés (fig. 8). Cette forme bien caractérisée n'avait jamais été signalée.”

Personal remarks: Extremely strong interference colours, orange-red.

Genus: *Ahmuellerella* Reinhardt, 1964

Species: *A. octoradiata* (Górka, 1957) Reinhardt and Górka, 1967, Plate IIIg-h and Plate Xi.

From Górka (1957):

“Description: Elliptique, légèrement allongé, à marge lisse. Aire centrale marquée d'un petit rhombe allongé suivant le grand diamètre de l'ellipse. De chaque angle du rhombe partent deux rayons à extré- mités élargies, n'atteignant pas la marge. Long. 8,8 µm, larg. 7 µm, larg. de la marge 0,8 µm. Remarks: Ne ressemble à aucun discolith connu.”

Genus: *Misceomarginatus* Wise and Wind, 1977

Species: *M. pleniporus* Wise and Wind, 1977, Plate IIIi-j.

From Wise and Wind (1977):

“Description: Diagnosis: A species of *Misceomarginatus* with approximately 20 outer perforations and approximately 8 central perforations. Description: Rim constructed of approximately 70 outer imbricate elements and an inner ring of vertical tabular plates. Two axial and perpendicular fibrous cross bars terminate in the inner ring of rim plates. No spine has been observed. The area central to the diamond-shaped inner framework is constructed of tabular crystals similar to those constructing the outer portion of the central area. Size: Holotype (Figure 1), 9.1 µm X 6.4 µm; Paratype (Figure 2), 8.8 µm X 6.3 µm; Para type (Figure 3), 9.2 µm X 6.8 µm; Para type (Figure 4), 9.2 µm X 6.8 µm; Paratype (Figure 5 left), 8.6 µm X 6.7 µm; Paratype (Figure 6), 9.1 µm X 7.1 µm. Remarks: This species is distinguished from species of *Monomarginatus* by differences in rim construction and in the similarity of design of the inner and outer portions of the central area of this species. *Heteromarginatus wallacei* BUKRY is quite smaller in size, has fewer pores, and a radically different rim structure.”

Personal remarks: A thin and bicyclic rim distinguishes *M. pleniporus* from *N. watkinsii*. A bicyclic rim distinguishes *M. pleniporus* from species of *Monomarginatus*.

Genus: *Neocrepidolithus* Romein, 1979

Species: *N. watkinsii* Pospichal and Wise, 1990, Plate IIIk-l.

From Pospichal and Wise (1990):

“Diagnosis: A large species of *Neocrepidolithus* with an eiffellithid rim constructed of thin rectangular laths imbricated in a clockwise direction. The proximal side is constructed of a thin cycle of elements which form the basal plate. In distal view, the solid central area is composed of blocky elements that form a ridge along the major and minor axis but leave a depression in the center. Description: An elliptical coccolith with a relatively thick outer rim constructed of 50-55 strongly imbricated rectangular laths. The solid central area of the distal side consists of a number of thin overlapping elements. The elements form a ridge along the major and minor axes within the central area. Under cross-polarized light, the rim is birefringent, as is the cross formed by elements of the central area. In plain light, the outline of this cross can also be discerned, and it is quite distinctive in phase contrast light. Remarks: The species is named for Dr. David K. Watkins in honor of his many valuable contributions to this subdiscipline of micropaleontology. In general, most other species of this genus are smaller than *N. watkinsii*, but are found in uppermost Maestrichtian and lower Tertiary sediments. The type species for the genus, *Neocrepidolithus neocrassus* (Perch-Nielsen, 1968; Romein, 1979), is a 4-7 μm form found in Danian sediments. In addition, the height of the rim of the species described here is proportionately less than for other species of the genus. Specimens of *N. watkinsii* are differentiated from species of *Vagalapilla* Bukry (1969) in having the central area completely filled with crystalline elements, whereas the central areas of species such as *Vagalapilla aachena* (Bukry) have open quadrants separated by cross bars. *Neocrepidolithus watkinsii* is, on average, several microns larger than species of *Vagalapilla*.”

Personal remarks: Unicyclic and thick rim.

Genus: *Staurolithites* Caratini, 1963

Species: *S. stradneri* (Rood et al., 1971) Bown and Cooper in Bown, 1998, Plate IIIm-m and Plate Xj.

From Rood et al. (1971):

“Description: Diagnosis: Coccoliths with an eiffellithalid rim and a central cross aligned in the major and minor axes of the ellipse; the short bar of the cross is slightly offset at the center.

Description: The rim of this species is narrow, with a slightly inclined peripheral wall, and consists of about 40 strongly imbricate wedges on the distal side. The bars of the cross are constructed of large overlapping tabulae. The shorter arms of the cross are offset at the center. At the point of juncture between the arms, the cross and the rim, the arms expand slightly in the direction of inclination of the overlapping rim segments. A circular stem arises from the center of the cross. Size: Length 3.2 μm , width 2.4 μm . Remarks: This species is distinguished from other members of the genus by its relatively simple construction and by the offset of the shorter arms at the center.”

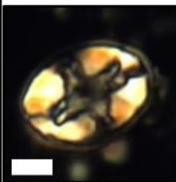
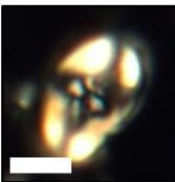
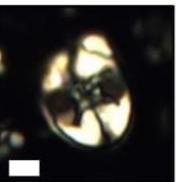
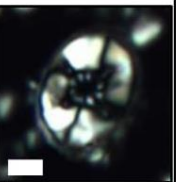
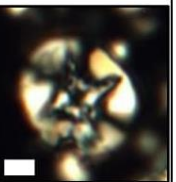
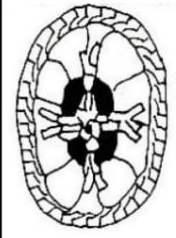


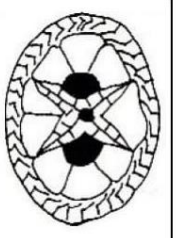
Species: *Staurolithites* sp., Plate IIIo-p.

Specimen that cannot be identified down to species level but can be recognized as belonging to the genus. From Caratini (1963):

J'appelle *Staurolithites* tout corpuscule calcaire constitué d'un anneau circulaire ou elliptique délimitant un espace central creux. Cet espace est occupé par les branches d'une croix dont les extrémités s'appuient sur la partie latérale interne de l'anneau périphérique. Cette croix peut être ornée et différenciée à l'extrême. Mais elle est toujours située dans le même plan que le reste du corpuscule calcaire. C'est en cela que le staurolithe s'oppose au zygolithe ou la structure centrale surmonte le reste du coccolithe. Remarks: En fait, j'aurai pu inclure les types que je désigne par le terme de *Staurolithites* au manipulate déjà existant de *Discolithus* car on peut considérer un staurolithe comme un discolithe percé de quatre perforations relativement étendues, séparées par des septums formant une croix. Mais j'ai déjà fait remarquer combien le parataxon *Discolithus* a tendance à devenir démesuré. Aussi, j'ai pensé que le critère particulièrement caractéristique de la croix barrant l'espace central pouvait servir de base à la définition d'un nouveau manipulate. La terminaison << ites >> marque bien qu'il s'agit d'un genre collectif. On pourra me critiquer pour avoir introduit un taxon supplémentaire que l'on peut considérer comme inutile puisque, je le répète, il était possible de continuer à ranger les staurolithes dans le genre collectif *Discolithus*. Mais je crois que l'avantage qu'il y a à faire éclater ce manipulate *Discolithus* pour les raisons déjà exposées compense largement l'inconvénient qu'entraîne toujours la création d'un terme. D'ailleurs, je me contenterai de rappeler que jadis le genre *Ammonites* BRUGUIÈRE fut longtemps utilisé par les paléontologistes. L'incessante découverte de types nouveaux de Céphalopodes obligea les spécialistes à faire éclater cette unité et à créer des genres dont chacun comprenant bien moins d'espèces fut plus facilement utilisable. C'est pour les mêmes raisons que E. Kamptner a renoncé

à son *Coccolithites* tel qu'il l'avait défini en 1955. Parmi les *Discolithus* déjà décrits, peu de formes répondent à la définition de *Staurolithites*. Quelques discolithes possèdent bien une croix, mais celle-ci « barre une aire centrale ». Puisque l'on parle d'aire, c'est qu'on est vraisemblablement en présence d'une forme possédant un plancher. Dans le doute, j'ai préféré ne pas transférer ces discolithes. Seuls *Discolithus staurophorus* KAMPTNER, 1948 (fig. 10, pl. I) et *D. crux* DEFLANDRE et FERT, 1954 (pl. XIV, fig. 5, texte fig. 55) peuvent être rangés avec certitude dans le nouveau manipulateur. Ils sont donc désignés par les nouvelles combinaisons: *Staurolithites staurophorus* (KAMPTNER) n. comb. *Staurolithites crux* (DEFLANDRE) n. comb. *Discolithus cretaceus* GORKA 1954 (ARCHANGEYSKY 1912) devrait lui aussi figurer désormais dans le manipulateur *Staurolithites*. J'aurai plus loin l'occasion de donner mon opinion sur ce type.”

Family: Eiffellithaceae Reinhardt, 1965

Species	<i>E. eximius</i>	<i>E. lindiensis</i>	<i>E. gorkae</i>	<i>E. parallelus</i>	<i>E. turriseiffelii</i>
Central cross					
Orientation	Axial		Diagonal		
Tips / ends	Bifurcated	Simple	Simple	Bifurcated	Simple
Size	Large	< 8 µm	Small, isolated within the rim	Medium - large	Large, touching the rim
Suture	-	-	-	Yes	-
Light microscope photographs Scale bar = 2 µm					
	<i>E. eximius</i> MOV1_A	<i>E. lindiensis</i> MOV1_A	<i>E. gorkae</i> A5_A	<i>E. parallelus</i> MS1_B	<i>E. turriseiffelii</i> MOV1_A
					
Structural sketches of <i>Eiffellithus</i> species from Perch-Nielsen (1979).					

Genus: *Eiffellithus* Reinhardt, 1965

Species: *E. eximius* (Stover, 1966) Perch-Nielsen, 1968, Plate IIIq-r and Plate Xk.

From Stover (1966):

“Description: The coccoliths are elliptical in proximal or distal view and have a narrow, smooth or faintly striate rim and a base plate. The plate has an axial lozenge-shaped area, whose corners point toward the cardinal areas of the rim, and which is filled by eight more or less triangular pieces. The small calcareous pieces composing the axial cluster are inclined and commonly form either a peaklike structure that extends two or three microns above the base plate, or the base of a stem. The remainder of the base plate consists of a relatively wide band which, under crossed nicols, appears to be formed of indistinctly separated and irregularly shaped pieces. Length 10-12 μm , width 7-9 μm , height 3-6 μm including peak.

Remarks: Comparison: The distinguishing features of the new species include: 1) the narrow rim, 2) the diamond-shaped cluster of eight radial and inclined pieces at the center of the base plate, and 3) the irregularity and indefiniteness of the base plate components adjacent to the rim.

Clinorhabdus eximius differs from *C. turriseiffeli* (DEFLANDRE), new combination, in having a differently oriented axial structure with respect to the longitudinal and transverse axes of the coccoliths. Remark: The narrow rim is commonly incomplete and may be lacking on some specimens. Specimens with striated rims are rare.”

Species: *E. lindiensis* Lees, 2007, Plate IIIs-t.

From Lees (2007):

“Diagnosis: A small species of *Eiffellithus* in which the small, indistinct central cross is axially aligned. The inner cycle fills the central area. Differentiation: This new species is easily distinguished from *E. eximius*, which is much larger, and has a distinctive, bifurcating cross that takes up more of the central area. Furthermore, *E. lindiensis* ranges up into the Maastrichtian. It is distinct from other Late Cretaceous eiffellithids in being small and having an axial cross. Holotype dimensions: L = 4.4 μm , W = 3.08 μm ”.

Personal remarks: Since the original description does not give maximum length, it is defined in this thesis to be smaller than 8 μm and having an axial cross with single tips. This is how *E.*

lindiensis is distinguished from *E. eximius*. The tips of the axial cross overrun the size, in morphological importance, so if a specimen is larger than 8 µm, but do not have a cross with bifurcated tips – it will be counted as *E. lindiensis*. So far, no specimen of *E. lindiensis* larger than 8 µm has been encountered.

Species: *E. gorkae* Reinhardt, 1965, Plate IVa-b and Plate XI.

From Reinhardt (1965):

“Description: Diagnose: Eine Art von *Eiffellithus* mit folgenden Besonderheiten: 3/4 des Radius der Area centralis nimmt die breite, basale Randscheibe ein. An ihrem Innenrand setzen acht Säulchen an und recken sich als Jugum steil empor. Die Area centralis umsäumt ein Wall aus 32- 34 schräg aufeinanderliegenden Eiemmenta petala. Verhältnis der Ellipsenachsen wie 10:6. Länge 5-9 µm.”

Personal remarks: *E. gorkae* usually is smaller than other *Eiffellithus*-species and appears to have more white-grey interference colours, instead of yellow-orange (as is typical for other *Eiffellithus*-species).

Species: *E. parallelus* Perch-Nielsen, 1973, Plate IVc-d.

From Perch-Nielsen (1973):

«Description: Diagnose: Eine Art von *Eiffellithus*, bei der das zentrale X aus Lamellenreihen, die parallel der Diagonalen verlaufen, besteht. Beschreibung: Die Wand besteht aus dachziegelartig angeordneten Lamellen und ist auf der distalen Seite nur als dünner Saum sichtbar. Grosse Platten füllen einen grossen Teil des zentralen Raumes aus. Der Rest wird von einem diagonal angeordneten Kreuz eingenommen, das nur kleine Öffnungen in den Ellipsenbrennpunkten freilässt. Das Kreuz besteht aus feinen Lamellen, die in Reihen parallel der Diagonalen angeordnet sind und so Stützen für den zentralen Fortsatz bilden. Dieser ist rund, hohl und besteht ebenfalls aus feinen Lamellen. Proximal ist die Wand, ein proximaler Kranz und ein diagonales Kreuz sichtbar, das in der Mitte eine Sutur aufweist. Die distalen Platten sind auf der proximalen Seite in kleinere Einheiten aufgelöst.

Remarks: *E. parallelus* unterscheidet sich von *E. turriseiffeli* (DEFLANDRE), 1954 REINHARDT, 1965 durch den Aufbau des zentralen X (taf. 6: 7). Der Unterschied ist auch mit dem Lichtmikroskop leicht feststellbar (taf. 10: 47-50). *E. eximius* (STOVER), 1966 PERCH-

NIELSEN, 1968 hat ein axial orientiertes Kreuz und *E. gorkae* REINHARDT, 1965 (siehe taf. 6: 8) ist kleiner als die neue Art und *E. turriseiffeli* und hat eine sehr einfach gebaute zentrale Struktur sowie einen relativ breiten Rand.”

Personal remarks: Distinguished from other *Eiffellithus*-species by its axial suture within the diagonal cross with bifurcated tips. The least common *Eiffellithus*-species in the samples.

Species: *E. turriseiffelii* (Deflandre in Deflandre and Fert, 1954) Reinhardt, 1965, Plate IVe-f.

From Deflandre and Fert (1954):

“Description: Elliptique, à bord nettement marqué de points correspondant à une structure superficielle striée mal discernable; marge assez étroite; aire centrale apparemment pleine, surmontée d'une corne (brisée) finement cannelée, reliée aux bords par quatre pieds divergents. (Long. 9,4 µm; larg. 7 µm).”

Personal remarks: Distinguished from *E. gorkae* by generally being larger, with stronger interference colours. In addition, the diagonal cross extends until the rim and tends to be thinner, unlike in *E. gorkae*, where the thicker cross tips end within the central area.

Genus: *Helicolithus* Noël, 1970

Species: *H. anceps* (Górka, 1957) Noël, 1970, Plate IVg-h.

From Górka (1957):

“Description: Elliptique, à marge lisse, double. Aire centrale marquée d'un rectangle, dont les angles se prolongent par des rayons plus étroits que la marge. Long. 8 µm, larg. 5,8 µm, larg. de la marge 1 µm. Remarks: Ressemble à *Discolithus litterarius* n. sp., mais en diffère par sa double marge.”

Personal remarks: Unicyclic rim. Sometimes it is difficult to distinguish *H. anceps* from *H. trabeculatus* based on the uni- or bicyclicity of the rim. In these cases, the size determines the species. *H. anceps* > 6 µm, and *H. trabeculatus* < 6 µm.

Species: *H. trabeculatus* (Górka, 1957) Verbeek, 1977, Plate IVi-j.

From Górka (1957):

“Description: Elliptique, à marge lisse. Aire centrale à deux barres formant un X, à bras un peu plus étroits que la marge, s'unissant insensiblement à celle-ci. Long. 4,8 µm, larg. 3,7 µm. Remarks: Ressemble à *Neococcolithes lososnensis* SUJK., qui est cependant plus grand et pourvu de barres larges et arquées.”

Personal remarks: Bicyclic rim.

Order: Stephanolithiales Bown and Young, 1997

Family: Stephanolithiaceae Black, 1968

Genus: *Rotelapillus* Noël, 1973

Species: *R. crenulatus* (Stover, 1966) Perch-Nielsen, 1984, Plate IVk-l.

From Stover (1966):

“Description: Specimens are circular to roughly octagonal in plan view. The rim is of medium width, circular at one end with a finely crenulate margin, and roundly octagonal to hexagonal in outline at the other end with six to twelve (usually nine or ten) short lateral spines. The base is thin (1 µm), circular to hexagonal, and commonly with a small central boss. The rim and base plate are heliolithic. Under crossed nicols, the rim appears to consist of two concentric rings of nearly equal width. The crystallographic orientation of particles in the outer ring of the rim and in the base plate is the same or nearly so (optic C-axes nearly vertical in plan view). Diameter 5-7 µm, height 2-3 µm. Remarks: Comparison: *Stephanolithion crenulatum* differs from *S. bigoti* DEFLANDRE in possessing shorter spines, a more circular outline and a crenulate margin. Remarks: The thin base is lacking on some specimens.”

Personal remarks: Weaker (white-grey) interference colours than *Cylindralithus* sp..

Genus: *Cylindralithus* Bramlette and Martini, 1964

Species: *Cylindralithus* sp., Plate IVm-n.

From Bramlette and Martini (1964):

“Description: Robust, short, nearly cylindrical forms, with some taper to an outer rim, a thin perforated plate forming the base. Appears as a serrate ring in end view, with calcite elements of wall in this usual orientation producing nearly maximum refringence or relief in Canada

balsam, but with thin base rather obscure. Remarks: An apparently related form, but consisting of two parts joined at the base and open at each end, *Coccolithus gallicus* STRADNER, is provisionally assigned to *Cylindralithus*.”

Personal remarks: Stronger interference colours (yellow-orange, even green) than *Rotelapillus* sp..

Order: Podorhabdales Rood et al., 1971 emend. Bown, 1987

Family: Axopodorhabdaceae Wise and Wind, 1977

Genus: *Cribrosphaerella* Deflandre in Piveteau, 1952

Species: *C. ehrenbergii* (Arkhangelsky, 1912) Deflandre in Piveteau, 1952, Plate Ivo-p and Plate Xm.

From Arkhangelsky (1912):

“Description: Coccoliths of this species differ from those of *C. murrayi* by the presence of grooves and dentate margin in the proximal and distal shields. (Translated from Russian).”

Family: Biscutaceae Black, 1971

Genus: *Biscutum* Black and Barnes, 1959

Species: *B. constans* (Górka, 1957) Black and Barnes, 1959, Plate IVq-r.

From Górka (1957):

“Elliptique, allongé, à marge ornée de 19-20 stries transversales. Aire centrale lisse. Long. 5- 9 µm, larg. 4,5- 6 µm, larg. de la marge 1 µm. Remarks: Ressemble à *Discolithus rudis* n. sp., qui se distingue cependant par des perforations de l'aire centrale.”

Family: Cretarhabdaceae Thierstein, 1973

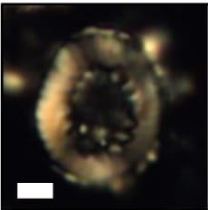
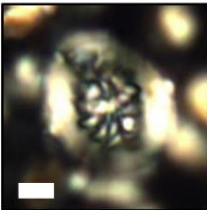
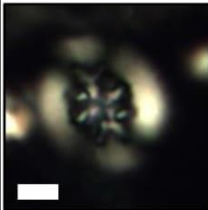
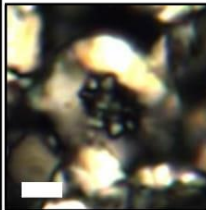
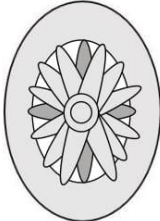

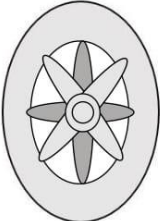

Genus: *Cretarhabdus* Bramlette and Martini, 1964

Species: *C. conicus* Bramlette and Martini, 1964, Plate IVs-t and Plate Xn.

From Bramlette and Martini (1964):

“Description: Elliptical rim has a distinct peripheral groove with basal part smaller, the cone-shaped central area perforated by many pores. Crossbars extend across the long and short axes of the rim, with pointed tips at juncture with rim. The lower part of the stem shows a spiral arrangement, whereas the upper part consists of straight elongate rodlike elements, more apparent under crossed nicols (fig. 6). The spiral part varie3 from most of to only a small part of the length of the stem. Length of basal plate 7- 14 μm , height 15- 25 μm . Remarks: Under crossed nicols, both base and stem are quite distinctive and characteristic of this species.”

Genus: *Retecapsa* Black, 1971

Species	<i>R. surirella</i>	<i>R. crenulata</i>	<i>R. angustiforata</i>	<i>R. ficula</i>
Central area				
Number of bars in each quadrant	4	3	1	-
Central area width	Wide	Wide	Wide	Narrow
Light microscope photographs Scale bar = 2 μm				
	<i>R. surirella</i> MON1_A	<i>R. crenulata</i> MON1_A	<i>R. angustiforata</i> MOV1_A	<i>R. ficula</i> K5_A
Structural sketches based on personal observations				

Species: *R. surirella* (Deflandre and Fert, 1954) Grün in Grün and Allemann, 1975, Plate Va-b and Plate Xo.

From Deflandre and Fert (1954):

“Description: Elliptique à bord finement incisé en éléments de 0,4 à 0,7 μm de large. Aire centrale avec un système de lamelles plus ou moins divergentes, larges d'environ 0,3 μm (Long. 4,8-6 μm ; larg. 3,8-4,6 μm .)»

Personal remarks: *R. surirella* has three bars in each quadrant, and they are more easily observed when rotating the stage and using the gypsum plate.

Species: *R. crenulata* (Bramlette and Martini, 1964) Grün in Grün and Allemann, 1975, Plate Vc-d and Plate Xp.

From Bramlette and Martini (1964):

“Description: Elliptical base has a conspicuous groove around periphery which may be considered a partial separation into two plates, with the proximal side smaller. The relatively broad peripheral part of base is finely striate, and the small central area perforate, with the resulting crenulate appearance of the border between them conspicuous under crossed nicols; the curvature of the extinction lines is sinistral as viewed from the distal side. Central stem with canal has sinistral upward spiral striae, and end of stem broadens to form a calyxlike tip. Length of basal plate 6-11 μm . Height of stem 10-17 μm .

Remarks: The peculiar tip of the stem is similar to that of *Cretarhabdus? anthophorus*, but the spiral striae in the stem of *Cretarhabdus crenulatus* are more conspicuous than in *Cretarhabdus? anthophorus*, and the central area of the base is perforate and quite different otherwise. The base has a relatively small perforate area and a broad outer part, as compared with the base of *Cretarhabdus conicus*.”

Personal remarks: *R. crenulata* has two bars in each quadrant, and they are more easily observed when rotating the stage and using the gypsum plate.

Species: *R. angustiforata* Black, 1971, Plate Ve-f.

From Black (1971):

“Description: A species of *Retecapsa* in which the 4 central windows are nearly circular and have a diameter distinctly smaller than the breadth of the lateral buttresses.

Dimension of holotype: Distal shield 8.0 X 6.7 μm , 27 rays; central area 4.0 X 2.4 μm ; proximal shield 7.0 X 5.4 μm . A single specimen.”

Personal remarks: *R. angustiforata* has one bar in each quadrant. The tips of the bars often appear thinner and sharper than for other *Retecapsa*-species.

Species: *R. ficula* (Stover, 1966) Burnett, 1997, Plate Vg-h and Plate Xq.

From Stover (1966):


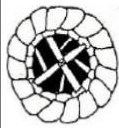






“Description: The coccoliths are elliptical in proximal or distal view and consist of a single plate with a wide rim of approximately 32 ribs. The grooves or striae between ribs are straight and are discernible across most of the rim. The outer margin of the rim is scalloped, the inner margin smooth. The small central opening is floored by a plate constructed of numerous small irregularly shaped calcareous pieces that are closely spaced or have openings between them. The curvature of extinction lines across the rim is sinistral in distal view. Length 6-8 μm , width 5-6 μm , height about 2 μm .

Comparison: The presence of a central structure distinguishes this species from *Cyclolithus solidus*.

Remarks: On some specimens the central structure appears cribrate in bright. field illumination due to openings between the minute pieces. *Coccolithites ficula* may represent a dimorph of *Cyclolithus solidus*. However, the two do not always occur together. For this reason, they are here treated as separate species.”

Family: Prediscosphaeraceae Rood et al., 1971

Genus: *Prediscosphaera* Vekshina, 1959

Species	<i>P. columnata</i>	<i>P. ponticula</i>	<i>P. arkhangel skyi</i>	<i>P. spinosa</i>	<i>P. stoveri</i>	<i>P. cretacea</i>	<i>P. desiderog randis</i>	<i>P. grandis</i>
Structural elements								
Overall shape	Circular		Elliptical					
Cross	-		Axial			Diagonal		
Overall size in um	5-10	max 7.8	large (?)	4-8	4-7	< 9	9-11	11-19
Inner rim cycle	-	-	Broad	-	Broad	-	-	-
Extra bars/cross	-	Secondary bars	-	-	-	-	-	-
Central area	-	-	-	-	Filled	-	-	-
								
Structural sketches of <i>Prediscosphaera</i> species from Perch-Nielsen (1979).								

Species: *P. cretacea* (Arkhangelsky, 1912) Gartner, 1968, Plate Vi-j and Plate Xr-s.

From Arkhangelsky (1912):

“Description: Oval coccoliths consisting of two convex shields. The distal shield shows an oval depression in the central structure from which thin rays diverge towards the margin. These rays produce grooves on the marginal area of the shield. In the central depression the opening is divided by two bars in the form of a cross. The inner shield is grooved or flat in the marginal area. (Translated from Russian).”

Species: *P. desiderograndis* Blair and Watkins, 2009, Plate Vk-l.

From Blair and Watkins (2009):

“Description. This placolith is ellipsoidal in form, has a diagonal cross supporting a robust stem, and two outer shields. The distal shield is composed of 16 non-imbricated elements and appears dark in cross-polarized light. The inner shield is very bright in LM and is approximately half

the width of the distal shield in diameter. Visible sutures divide the dextral and sinistral cross-bars on the diagonal cross. *Prediscosphaera desidero grandis* averages 9.8 µm in length and 8.8 µm in width.”

Personal remarks: *P. desidero grandis* has been observed in samples of Campanian-Maastrichtian age, making it doubtful if the range given by (Young et al., 2016), with last occurrence within the Santonian, is actually true. This species is not used for biostratigraphic analyses in this thesis because of this reason.

Species: *P. arkhangelskyi* (Reinhardt, 1965) Perch-Nielsen, 1984, Plate Vm-n.

From Reinhardt (1965):

“Description: Diagnose: Eine Unterart von Eiffellithus cretaceus mit reduziertem Zentralfortsatz und folgenden Charakteristika: Der distale Ring zeigt 16 Kerben. Er umsäumt wallförmig eine basale Scheibe, welche 3/4 des Zentralfeldes einnimmt. Ihre Seiten verbindet ein Kreuz, aus dessen Zentrum ein kleiner Stab emporstrebt.”

Personal remarks: Very distinctive thick inner rim closing the central area, with curving extinction lines.

Species: *P. spinosa* (Bramlette and Martini, 1964) Gartner, 1968, Plate Vo-p and Plate Xt.

From Bramlette and Martini (1964):

«Description: Elliptical base with crossbars spanning the open central area, and peripheral elements in base with number, shape, and orientation characteristic of the genus, although the bars are parallel to axes of the elliptical base rather than diagonal as in the type species. The central stem is long and slender, apparently formed of four longitudinal elements very slightly twisted in the lower part, and with delicate spines attached at the top. Spines consists of calcite units different from those of stem, as their slightly enlarged base appears separate from the stem under crossed nicols. Length of base 4-8 µm, height of stem 10- 15 µm. Remarks: The stem is quite different from *Deflandrius intercisus*, and the base differs in the parallel rather than diagonal position of crossbars, as related to the axes of the elliptical base.”

Species: *P. stoveri* (Perch-Nielsen, 1968) Shafik and Stradner, 1971, Plate Vq-r.

From Perch-Nielsen (1968):

“Description: Diagnose: Breitelliptischer Coccolith aus zwei ungleichgrossen Randscheiben aus je 16 nebeneinander liegenden Platten. Das Zentralfeld wird durch ein Kreuz in den Ellipsenachsen überbrückt und von sich überlagernden Keilen eingefasst. Beschreibung: Sowohl die grössere als auch die kleinere Randscheibe besteht aus 16 Elementen, die etwas gegeneinander verschoben angeordnet sind und nebeneinander liegen. An ihrem inneren Rand werden sie eingefasst von sich überlagernden Keilen. Auf der einen Seite des Coccolithen scheinen sie sich zum Teil aus den Randelementen der grösseren Scheibe heraus zu entwickeln und teils frei zu liegen. Auf der anderen Seite greifen sie über den kleineren Randring hinweg. Sie bilden eine Art Tubus um das Zentralfeld. Dieses wird von einem Kreuz überbrückt, das aus Latten besteht und oft ausgebrochen ist. Masse des Holotypus: Länge: ca. 5 µm. Breite: ca. 4,5 µm.

Remarks: *D. stoveri* unterscheidet sich von den anderen *Deflandrius*-Arten durch seinen speziellen Aufbau des Zentralfeldrandes, sein kleineres Zentralfeld und durch seine breitelliptische Form. Er wurde nur zögernd zu *Deflandrius* gestellt, da er eine Art Tubus aufweist, der die beiden Randscheiben verbindet, ohne dass die Randscheiben sonst weit voneinander abstehen. Die Zuordnung wird motiviert durch den Fund einer Zwischenform von *D. spinosus* und *D. stoveri*. Sie zeigt einen elliptischen Coccolithen mit zwei Randscheiben aus je 16 Elementen und einem grossen Zentralfeld, an dessen Rand z. T. ebenfalls Keile stehen, die jedoch noch nicht so schlank sind wie diejenigen von *D. stoveri*. *D. stoveri* wurde noch nicht im Lichtmikroskop gefunden und konnte nicht strabtragend beobachtet werden.”

Personal remarks: Usually smaller than *P. spinosa*, and with a thick inner rim that entirely closes the central area. The inner rim usually do not show the curving of extinction lines as for *P. arkhangel'skyi*.

Family: Tubodiscaceae Bown and Rutledge, 1997 in Bown and Young, 1997

Genus: *Manivitella* Thierstein, 1971

Species: *M. pemmatoidea* (Deflandre in Manivit, 1965) Thierstein, 1971, Plate Vs-t and Plate XIa.

From Deflandre in Manivit (1965):

“Description: Coccolithe en ellipse courte et régulière, constitué par un anneau relativement large, de l'ordre du quart au cinquième du petit axe de l'ellipse, fortement ornementé de stries

transversales qui forment une proéminence médiane prenant parfois une apparence perlée. Structure héliolithique bien caractérisée. Longueur: (13) 15 à 18 (20) μm ; largeur: (10) 12 à 14 (15) μm . Les chiffres entre parenthèses concernent des spécimens rares, s'écartant des dimensions habituelles.

Remarks: *Cricolithus pemmatoideus* DEFLANDRE, quoique étant un *nomen nudum*, a été employé déjà par divers chercheurs ayant consulté le Fichier du Laboratoire de Micropaléontologie de l'Ecole Pratique des Hautes Etudes. Cette forme, en effet, souvent rencontrée par G. Deflandre et connue de lui depuis bien des années, a été mise en fiche et photographiée sans avoir fait l'objet d'une publication. Parmi les microphotographies qui la représentent, une très belle épreuve en stéréoscopie a été réalisée par Pierre Bouché. Afin de régulariser la situation de cette intéressante espèce, j'insère une diagnose rédigée par l'auteur du nom.»

Order: Watznaueriales Bown, 1987

Family: Watznaueriaceae Rood et al., 1971

Genus: *Cyclagelosphaera* Noël, 1965

Species: *C. margerelii* Noël, 1965, Plate VIa-b.

From Noël (1965):

“Description: Diagnose: Une espèce du genre *Cyclagelosphaera* répondant très exactement à la définition donnée pour le genre. Remarks: Au point de vue construction générale du coccolithe, le genre *Ellipsagelosphaera* et le genre *Cyclagelosphaera* sont absolument comparables. J'ai différencié les deux genres, sur la forme de leur contour externe, circulaire pour *Cyclagelosphaera*, elliptique pour *Ellipsagelosphaera*, appliquant là l'une des idées directrices de E. Kamptner. Il me semble inutile de donner la description détaillée de la construction de cette espèce puisqu'elle est voisine de celle déjà décrite pour *Ellipsagelosphaera frequens*. Je préciserai seulement quelques points particuliers:

- le disque supérieur de *C. margerelii* est formé de dix-neuf à vingt-cinq lames de calcite de grande taille;

- le tube central détermine une ouverture axiale de petit diamètre, nettement inférieur au tiers du diamètre du coccolithe. Ce tube central-est souvent obturé par des cristaux de calcite qui occupent le fond de la perforation ou bien semblent reposer sur le bord supérieur du tube (figs. 4, 7, 8). Ces cristaux paraissent disposés sans ordre.

- les coccolithes de *C. margereli* dont le tube central est bien dégagé (par exemple fig. 5) sont relativement rares; on pourrait penser qu'il s'agit de formes jeunes.

- comme chez *E. frequens*, le tube central montre, sur sa face tournée à l'intérieur de la lumière, de petites rides horizontales, que l'on peut interpréter comme les limites successives des couches de calcite ayant participé à la formation de ce tube. Par ailleurs, comme je l'ai également signalé pour *Ellipsagelosphaera frequens*, chez *Cyclagelosphaera margereli*, au niveau du Valanginien, les individus montrent un disque supérieur avec une série externe de lames de calcite, nettement décalées les unes par rapport aux autres (figs. 2, 3, 4; fig. 46).

La présence d'un pore central circulaire et de petite taille rappelle *Coccolithus leptoporus* (MURRAY & BLACKMANN) SCHILLER. Mais la structure de ce dernier, figurée par M. Black et B. Barnes est différente de celle observée chez *Cyclagelosphaera margereli*.
Dimensions:"

N° de l'électromicrographie	Nbre lames ext. du disque sup.	Diamètre du coccolithe	Diamètre « lumière centrale »
Oxfordien, Niort.			
N° 1.816 - Holotype (fig. 4)	19	3,1 μ	0,6 μ
N° 1.759 (fig. 5)	23	2,8 μ	0,8 μ
N° 1.812	22	3,2 μ	0,7 μ
Oxfordien, Weymouth.			
N° 93 (fig. 45, fig. 2)	24	4,5 μ	0,95 μ
Portlandien (haut), Kef Talrempt.			
N° 1.613 (fig. 7)	23	4,4 μ	0,9 μ
N° 1.587 (fig. 8)	23	4,4 μ	0,9 μ
N° 1.622	22	4 μ	0,8 μ
N° 1.627	22	4,7 μ	0,9 μ

Genus: *Watznaueria* Reinhardt, 1964

Species: *W. barnesiae* (Black in Black and Barnes, 1959) Perch-Nielsen, 1968, Plate VIc-d and Plate XIb-c.

From Black in Black and Barnes (1959):

“Description: Diagnosis - *Tremalithus* with two nearly circular discs, one slightly smaller than the other, and each consisting of 28 rays (exceptionally 27 or 29). Rays of the smaller disc gently curved, filling the centre, and bluntly pointed at the distal end. Rays of the larger disc not reaching the centre, but radiating from an oval central shield, and squarely truncate at their distal ends. Dimensions of Holotype: 5.5 microns X 4.8 microns. Remarks: Specimens of this species are most easily recognized when lying so that the internal surface is exposed to view, as in fig. 2. In this view, the serrated outline of the smaller disc is seen lying just within the smoother margin of the larger disc. With replicas of suitable density, the continuation of the rays of the larger disc may be traced beneath those of the smaller disc, which they cross obliquely. The rays of the external disc slope steeply towards the circumference, thus giving the central part of the coccolith a substantial elevation.”

Species: *W. fossacincta* (Black, 1971) Bown in Bown and Cooper, 1989, Plate VIe-f.

From Black (1971):

“Description: A species of *Ellipsagelosphaera* with a conspicuous unbridged pore less than twice as long as broad, and a narrow groove marking off an elliptical central area on the proximal side. Size: Distal shield 6.0 x 5.0 μm to 8.5 X 7.3 μm , 28-34 rays; proximal shield 5.0 X 4.1 μm to 7.5 X 5.1 μm , 28-34 rays, central area 2.3 X 1.4 μm to 3.5 X 2.5 μm , pore 1.0 X 0.6 μm to 1.8 X 1.2 μm . Specimens measured, 16.”

Personal remarks: *W. fossacincta* can be distinguished from *W. ovata* by the central area and rim widths. *W. ovata* has a central area width \geq rim width, while *W. fossacincta* has a central area width $<$ rim width.

Species: *W. manivittae* Bukry, 1973, Plate VIg-h.

From Bukry (1973):

“The large placolith *Watznaueria manivittae* n. comb, [new name substituted for *Coccolithus deflandrei* Manivit 1966, p. 268, text-figs. 1 a-c because *Watznaueria deflandrei* (Noel) Reinhardt (ex *Actinosphaera*) has already been transferred to *Watznaueria*], which is common in Upper Jurassic samples from the western Atlantic and Sicily, is also common in Core 94.”

Personal remarks: *W. manivittiae* usually has higher interference colours (yellow-orange) under crossed nicols than the other *Watznaueria* species. In the samples used in this thesis, *W. manivittiae* also seems to be more heavily overgrown than the other *Watznaueria* species.

Informal group: Heterococcoliths inc sedis

Informal group: Placoliths inc sedis

Genus: *Markalius* Bramlette and Martini, 1964

Species: *M. inversus* (Deflandre in Deflandre and Fert, 1954) Bramlette and Martini, 1964, Plate VII-l.

From Deflandre in Deflandre and Fert (1954):

“Description: On a admis, jusqu'à présent, que les placolithes fossiles appartenait à la même espèce que celle qui vit dans nos mers. C'est possible, mais, en attendant une révision générale sérieuse de toutes ces formes, je sépare, sous le nom de *Cyclococcolithus leptoporus* var. *inversus* DEFL. n. v., celles dont les stries ont une courbure inverse et que représentent les figures 4, 5 (Oligocène) et 6, 7 (Oxfordien).”

Personal remarks: The rim appears dark in crossed nicols and is clearly imbricated. The central area is divided into four parts by two sutures, and displays higher birefringence colours; yellow-orange.

9.3.2. Holococcoliths

Genus: *Calculites* Prins and Sissingh in Sissingh and Prins, 1977

Species: *Calculites obscurus* (Deflandre, 1959) Prins and Sissingh in Sissingh and Prins, 1977, Plate VIm-r.

From Deflandre (1959):

“Description: Tétralithe de contour elliptique approché, plus ou moins irrégulier, des échancrures peu profondes séparant les plaquettes; les deux plaquettes opposées du petit axe se touchent sur une courte ligne, ce qui masque souvent le croisillon qui marquerait au centre les lignes de jonction des quatre plaquettes; les deux plaquettes opposées du grand axe semblent donc séparées par cette ligne. Un spécimen, en vue latérale (fig. 28-29) montre une certaine

symétrie qui rappelle celle des pentolithes et implique l'existence d'une face externe et d'une face interne. Dimensions: longueur 6-7 μm , largeur 4,5-5 μm . Remarks: *Tetralithus obscurus* est abondant dans la craie maestrichtienne de Vanves, mais assez rare dans celle de Mioti-Grodno.»

Genus: *Lucianorhabdus* Deflandre and Fert, 1954

Species: *L. arcuatus* Forchheimer, 1972, Plate VI s-t.

From Forchheimer (1972):

“Description: Diagnosis: A species of *Lucianorhabdus* with a massive curved process. The diameter of the basal shield is equal to the width of the process. Description: The massive process with a granulate surface is bent into a “knee” situated at about 3/4 of its length from the basal shield. Six parallel ridges are equidistantly arranged along the whole length. Dimensions: Average length of the longer straight part of the process 15.1 μm ; average length of the shorter straight part 11 μm ; average width 5.5 μm . Remarks: *Lucianorhabdus arcuatus* n. sp. differs from *L. quadrifidus* n. sp. in having a bent and slender process and a basal shield with a diameter equal to the width of the process. Deflandre (1959) illustrated a specimen of *Lucianorhabdus* with a curved process but without a basal shield. However, the process is larger, than in *L. arcuatus* n. sp. Gartner (1968) reported a species of *Lucianorhabdus* with a slender and smooth process and without a basal shield. Both species are reported from the Senonian.”

Species: *Lucianorhabdus* sp., Plate VII a-b.

Specimen that cannot be identified down to species level but can be recognized as belonging to the genus. From Deflandre (1963):

“Description: Baguettes calcaires formées de quatre éléments parallèles accolés intimement, leur jonction apparaissant sous la forme d'une ligne longitudinale par suite de l'orientation optique propre de chaque élément. Forme générale très variable: cylindrique ou subcylindrique, à tendance conique ou globuleuse à une extrémité, ou en forme de champignon, l'ensemble étant droit, ou un peu courbé, plus rarement nettement arqué, exceptionnellement coudé à angle droit. Contour toujours irrégulier, de même que la superficie, laquelle est d'apparence granuleuse ou rugueuse. Coupe transversale de chaque élément sensiblement rhomboïdale, à angle droit à l'intérieur, arrondie vers l'extérieur en quart de cercle ou plus allongée.”

9.3.3. Nannoliths

Order: Braarudosphaerales Aubry, 2013 emend Lees and Bown, 2016

Family: Braarudosphaeraceae Deflandre, 1947

Genus: *Braarudosphaera* Deflandre, 1947

Species: *B. bigelowii* (Gran and Braarud, 1935) Deflandre, 1947, Plate VIIc-d.

From Gran and Braarud (1935):

“Description: Cells isodiametrical, each covered by 12 pentagonal coccoliths, forming a regular pentagondodeka-hedron. Coccoliths flat, relatively thick, touching each other by the margin, which is slightly prominent at the outside. Colour and cilia not seen in the preserved specimens. Diameter 16 μm . Remarks: This species was observed in the surface layers at the most oceanic stations in the Gulf of Maine. Maximum: 680 cells per litre at station 3, 23A, and less abundantly in the bay of Fundy.”

Personal remarks: Górká (1957) described *B. bigelowii* to have a diameter of 8 μm . However, it does not say if this is maximum or minimum. In this thesis, *B. bigelowii* has a diameter ≥ 8 μm .

Informal species: *B. bigelowii* small, Plate VIIe-h.

Description: The same morphology as *B. bigelowii*, but smaller. Górká (1957) described *B. bigelowii* with a diameter of 8 μm . However, it does not say if this is maximum or minimum. In this thesis, *B. bigelowii* small is defined to have a diameter < 8 μm .

Informal group: Nannoliths inc sedis

Family: Microrhabdulaceae Deflandre, 1963

Genus: *Lithraphidites* Deflandre, 1963

Species: *L. carniolensis* Deflandre, 1963, Plate VIIi-j and Plate XIId.

From Deflandre (1963):

“Description: Fusiforme, souvent tronqué et subcylindrique. Holotype: longueur, 26 μm ; largeur, 2,5 μm ”.

Species: *Lithraphidites* sp., Plate VIIIk-n.

Specimen that cannot be identified down to species level but can be recognized as belonging to the genus. From (Deflandre, 1963):

“Description: Bâtonnets calcaires apparemment canaliculés, à coupe transversale cruciforme, formés d'éléments de calcite d'orientation unique.”

Genus: *Microrhabdulus* Deflandre, 1959

Species: *M. belgicus* Hay and Towe, 1963, Plate XIe-f.

From Hay and Towe (1963):

“Description: Diagnosis - A species of *Microrhabdulus* distinguished by evenly spaced cycles of subrhomboidal nodes. Description - An elongate cylindrical rod, about ten times as long as wide, faintly grooved longitudinally, with rings of eight rhomboidal nodes Y_4 micron wide spaced $\%$ micron apart over entire length. Ends truncate.

Remarks: The two previously described species, *Microrhabdulus decoratus* DEFLANDRE and *Microrhabdulus helicoideus* DEFLANDRE, are both smooth, lacking the circlets of nodes characteristic of the new species. Diligent search of preparations of the sample, using an optical microscope with fluorite objectives, has failed to reveal the new species, even though several specimens have been seen and photographed in the electron microscope. The small size of the object, and the minute size of the characteristic nodes, which are at the limit of resolution of the optical microscope, make the new species difficult to find using visible light. In the sample from Folx-les-Caves there are many tiny crystals and carbonate fragments approximately the size and shape of the new species, adding to the difficulty. All objects showing an unusual pattern in polarized light were examined carefully, but none of them resembled the new species. *Microrhabdulus decoratus* DEFLANDRE has been found in the same sample using the light microscope, but has not been identified with the electron microscope. It is very rare in the sample and can be located only because of the spectacular "stadia-rod" pattern that it shows in polarized light. Careful inspection of a number of specimens of *M. decoratus* with phase-

contrast microscopy indicates that the species is smooth, as Deflandre stated, and thus differs from the new species.”

Personal remarks: Only recognized in FEG-SEM so far.

Species: *M. decoratus* Deflandre, 1959, Plate VIIo-p and Plate XIg.

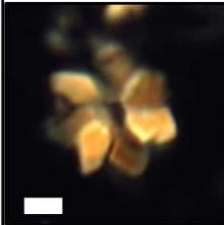

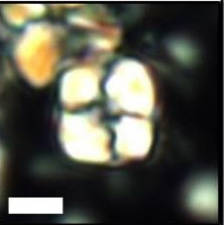
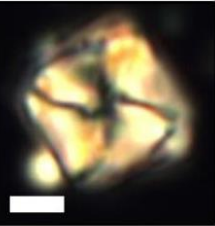




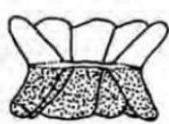



From Deflandre (1959):

“Description: Baguette calcaire cylindrique tronquée aux extrémités, formée par un empilement de manchons dont la calcite est orientée alternativement dans deux sens opposés; chaque manchon est formé de quatre parties, elles-mêmes dédoublées, ce qui se traduit par des faibles stries longitudinales sur la superficie de la baguette; le canal central, étroit, a une forme d'étoile à huit pointes (fig. 4 et 5). En lumière polarisée, nicols croisés et teinte sensible R. 1, en position parallèle ou perpendiculaire à l'axe de polarisation, chaque manchon est bleu d'un côté, jaune de l'autre et l'ensemble donne l'aspect traduit dans les figures 2, 7, 8, par un grisé, et dans les figures 3 et 4, par un contour ombré (pour le bleu). Dimensions - Holotype: longueur 22,8 µm, largeur 1,7-1,8 µm. 17 manchons hauts d'environ 1,3 à 1,4 µm. Autres spécimens: longueur maximale 20- 24 µm, largeur 1,5- 1,8 µm. Nombre de manchons généralement inférieur à 20.

Remarks: Aux figures dessinées à la chambre claire, jusqu'à un grossissement de 5000 (fig. 4), j'ai ajouté une reconstitution (fig. 5) au grossissement de 10.000, réalisée en utilisant les données fournies par des spécimens conservés (dont celui de la fig. 4) et celles obtenues en étudiant des bâtonnets placés verticalement dans le baume du Canada visqueux. Ces dernières conditions, seules, permettent de reconnaître la structure traduite dans les coupes transversales du bas de la figure 4 et du haut de la figure 5. Les ombrages mettent en relief les stries longitudinales dont le bas de la figure 5 explique la genèse. Enfin, des exemplaires favorables ont permis d'observer un fin canalicule à la jonction des éléments des manchons, ce qui explique l'aspect un peu arrondi en lumière polarisée. Je n'insisterai pas d'avantage ici sur ces questions, qui relèvent de l'ultrastructure, me réservant d'y revenir par la suite. Je souligne cependant, qu'il faut éviter de confondre *Microrhabdulus decoratus* avec certaines hampes brisées de *Rhabdolithus* sens. lat. à structure hélicoïdale, que l'on rencontre fréquemment dans la craie. Ces deux types de *Microrhabdulus* se retrouvent fréquemment remaniés, en compagnie d'autres formes sur lesquelles j'espère revenir ultérieurement. Que sont exactement ces baguettes qui, dans certaines craies, sont accompagnées de très nombreux débris de hampes de rhabdolithes non encore étudiés et classés ? J'ai cherché longtemps et vainement des embases de rhabdolithes

susceptibles d'avoir été les compléments des *Microrhabdulus* décrits ci-dessus et d'autres. J'en suis arrivé à la conclusion - provisoire au moins - que les *Microrhabdulus decoratus* et *M. helicoideus*, tels que je les présente, sont entiers.”

Family: Polycyclolithaceae Forchheimer, 1972 emend Varol 1992

Genera	<i>Eprolithus</i>	<i>Lithastrinus</i>	<i>Quadrum</i>	<i>Micula</i>
Structural elements				
Wall elements	Petals (rounded)	Rays (pointy)	Blocks	Blocks
Number of elements	5-9	5-7	4-9	4
Diaphragm	✓	✓		
Diaphragm size	Large	Small - none	-	-
Suture lines	-	-	When 4 elements: axial	Diagonal
Light microscope photographs Scale bar = 2 μm				
	<i>E. moratus</i> K1_B	<i>L. grillii</i> MOV1_A	<i>Q. gartneri</i> MS1_A	<i>Micula</i> sp. A5_A
Top view:				
Side view:				
Structural sketches of <i>Eprolithus</i> , <i>Lithastrinus</i> and <i>Quadrum</i> from Varol (1992), and of <i>Micula</i> from Roth & Bowdler (1979).				

Genus: *Eprolithus* Stover, 1966

Species: *E. moratus* (Stover, 1966) Burnett, 1998, Plate VIIq-r.

From Stover (1966):

“Description: Calcareous microfossils that in plan view appear as a rosette having seven to nine inclined, partly overlapping and twisted segments. The outline of the segments in plan view is lanceolate with slightly rounded or pointed outer margins. Specimens may either lack or have a very small axial pit or opening. Diameter 7-11 μm , height 2-4 μm .

Remarks: Comparison: *Lithastrinus moratus* differs from *L. grilli* STRADNER in having more than six segments and in having the outer margins of the segments less attenuated. Specimens of *L. moratus* also lack pits or depressions along the suture lines separating segments.”

Personal remarks: Distinguished from *L. septenarius* by having a clear diaphragm, and rounded elements.

Genus: *Lithastrinus* Stradner, 1962

Species: *L. grilli* Stradner, 1962, Plate VIIs-t and Plate VIIIa-c.

From Stradner (1962):

“Description: Sternförmige Kalkkörperchen aus 6 stark gedrehten, gegabelten, sich überdachenden Sektoren bestehend. Bei Änderung der Schärfeebene können zwei verschieden orientierte sternförmige Umrissbilder eingestellt werden, von denen das jeweils höher liegende in zentrifugaler Richtung nach rechts gebogene Spitzen zeigt. In der Seitenansicht (Fig. 4) ist die starke Einschnürung des Kalkkörperchens in der Hauptebene zu sehen. Die Durchmesser der beiden sternförmigen Flachseiten sind besonders bei grossen Exemplaren verschieden. Es ist anzunehmen, dass die grössere Flachseite in bezug zur Lage des Zellkernes des Kalkflagellaten in distaler Richtung orientiert war. Die Sektoren lassen an den Unterteilungsflächen auf halber Strecke zwischen dem sehr feinen Zentralkanal und dem Aussenrand schwache Aussparungen erkennen, welche wegen der starken Schräglage der Sektoren jedoch nicht als Fenster erscheinen. Selten. Dimensionen: Durchmesser 7- 11 μm . Höhe 3- 5 μm .

Remarks: Beziehungen: *Lithastrinus grilli* n. sp. ist wegen der polarisationsoptischen Eigenschaften seiner Sektoren, die sich wie Einzelkristalle verhalten, in die engere Verwandtschaft der Familie der Braarudosphaeriden zu stellen. Ob auch Beziehungen zu den aus dem Paleozän beschriebenen Gattungen *Heliolithus* BRAMLETTE & SULLIVAN und *Fasciculiths* BRAMLETTE & SULLIVAN bestehen, ist noch ungeklärt.”

Species: *L. septenarius* Forchheimer, 1972, Plate VIIIId-e.

From Forchheimer (1972):

“Description: Diagnosis: *Lithastrinus* species with seven rays surrounding the central area. *Lithastrinus septenarius* Description: The circular central area composed of seven sectors is proximally and distally surrounded by triangular rays. The average length of the rays about 3.6 μm and the diameter of the central area 2 μm . Dimensions: Average diameter of the specimen including the rays 8.2 μm .

Remarks: *Lithastrinus septenarius* n. sp. differs from *L. grilli* STRADNER, 1962, reported from the Turonian (p. 369, pl. 2, figs. 1-5) in having seven rays. The transmission electron micrographs of *L. Grilli* published by Gartner (1968, pl. 18, figs. 1-2; pl. 20, fig. 17; pl. 22, fig. 26) and Bukry etc. Bukry (1969, p. 43, pl. 21, figs. 3-6) also show six rays, occurring in forms from the Cenomanian - Campanian. Bukry did mention six or seven conical rays arising at each end but as lectotype species he designated a form with six rays illustrated by Stradner (1962, pl. 2, fig. 2). The light microscope micrographs of *L. grilli* illustrated by Manivit (1970, pl. 15, figs. 4-5) from the Turonian show a form with star-shaped outline composed of seven shorter rays.”

Personal remarks: Distinguished form *E. moratus* by having unvisible or very small diaphragm, and more pointy elements (but commonly rounded due to alteration).

Genus: *Quadrum* Prins and Perch-Nielsen in Manivit et al., 1977

Species: *Q. gartneri* Prins and Perch-Nielsen in Manivit et al., 1977, Plate VIIIIf-i.

From Prins and Perch-Nielsen in Manivit et al. (1977):

“Description: Diagnosis: A species of the genus *Quadrum* composed of one or two layers, each consisting of four big, and often high calcite units, separated by sutures, that run more or less perpendicular to the margin on the distal as well as on the proximal surface. The points of bath outer ends of each unit are not clearly protruding.

Description: This more or less cubical species is composed of four columns, between each of which a strongly reduced element may occur, vaguely observable in the light microscope, but invisible in the electron microscope. The cube may be slightly constricted in the middle, but the

points at the outer side of the big units are not clearly protruding. Occasional specimens with only three columns have been found.

Remarks: In the literature this species has often been assigned to *Tetradithus pyramidus* Gardet or *Micula decussata* Vekshina. In the publication of Gardet (1955) the genus *Tetralithus* and thus *T. pyramidus*, the only species she included in the genus, is characterised by two bright and two dark quadrants when viewed under crossed polarised light. This differs markedly from *Quadrum gartneri*, in which the whole body is bright or dark in crossed polarised light, when the nicols are turned.”

Personal remarks: *Q. gartneri* has axial sutures and usually displays weaker interference colours (white-grey).

Species: *Q. eptabrachium* Varol, 1992, Plate VIIIj-k.

From Varol (1992):

“Description: Diagnosis: A species of *Quadrum* having seven ray-like elements in each cycle of the wall.”

Personal remarks: In crossed nicols, *Q. eptabrachium* appears thinner, displaying white and grey colours – in contrast to *L. septenarius* and *E. moratus* that display white and orange colours. It has no diaphragm. *Q. eptabrachium* is also smaller, as (Varol, 1992) stated the holotype to have a maximum diameter of 5.8 μm .

Genus: *Micula* Vekshina, 1959

Species: *M. staurophora* (Gardet, 1955) Stradner, 1963, Plate VIII-o and Plate XIh-i.

From Gardet (1955):

“Description: Nous appelons ainsi une plaque calcaire quadrangulaire de 1 μm d'épaisseur portant à sa partie supérieure une croix à profil légèrement convexe dont les axes coïncident avec les diagonales de la plaque, 3 à 4 μm de côté, 1,5 à 2 μm d'épaisseur. Remarks: Ce discoaster est très différent de ceux figurés jusqu'ici et son attribution à la famille reste douteuse.”

Personal remarks: *M. staurophora* appears to have a “flower” on top of the cube (due to the diagonal depressions) when using the focus knob.

Species: *Micula sp.*, Plate VIIIp-t and Plate IXa-i.

Specimen that cannot be identified down to species level but can be recognized as belonging to the genus and have a diameter from corner to opposite corner larger than 3 μm , are assigned to *Micula sp.* From (Vekshina, 1959):

“Description: Fossil coccoliths in the shape of a parallelogram.”

Personal remarks: A variety of *Micula sp.* were encountered in the samples. I did not feel experienced enough to be sure about the taxonomy of these. Due to this, other species of *Micula* were not used for biostratigraphic analyses.

Informal species: *Micula sp. small*, Plate IXj-m.

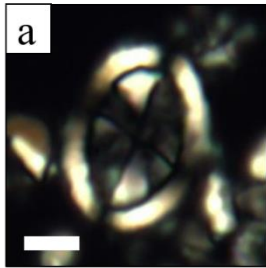
Specimen that cannot be identified down to species level but can be recognized as belonging to the genus and that have a diameter from corner to opposite corner smaller than 3 μm , are assigned to *Micula sp. small*. From (Vekshina, 1959):

“Description: Fossil coccoliths in the shape of a parallelogram.”

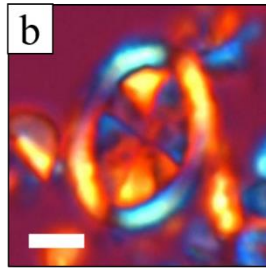
9.4. Appendix 4: Plates

Appendix 4: Plates with photographs taken in the light microscope or the FEG-SEM. First line below each photograph specifies the genus or species name, and the second line specifies in which sample the photograph was taken.

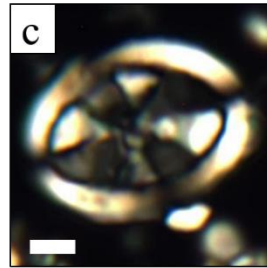
Plate I (white scale bar = 2 μm)



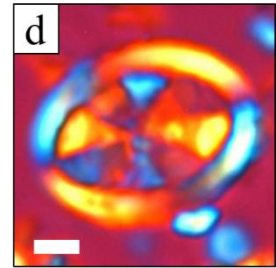
A. confusa (I)
MS1



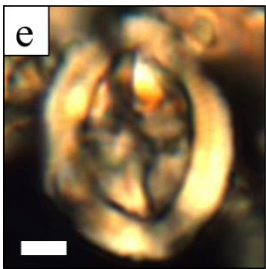
A. confusa (I)
MS1



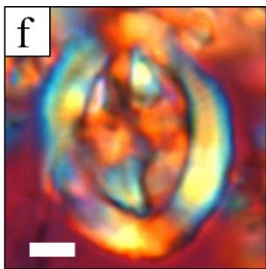
A. cymbiformis (I)
A5



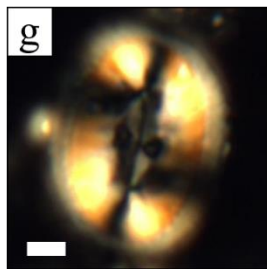
A. cymbiformis (I)
A5



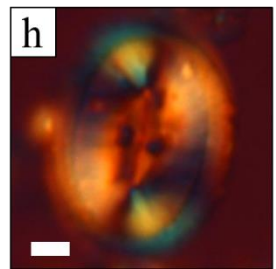
A. maastrichtiensis (I)
TOR4



A. maastrichtiensis (I)
TOR4



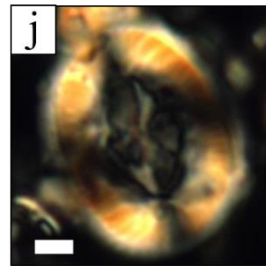
A. p. constrictus (I)
SK1



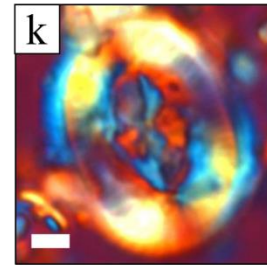
A. p. constrictus (I)
SK1



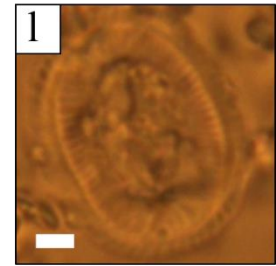
A. p. constrictus (I)
SK1



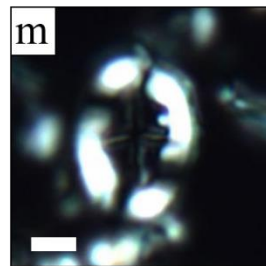
A. p. parcus (I)
MT1



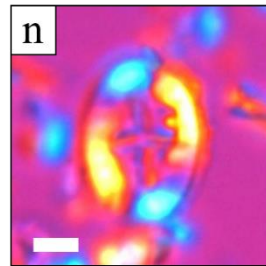
A. p. parcus (I)
MT1



A. p. parcus (I)
MT1



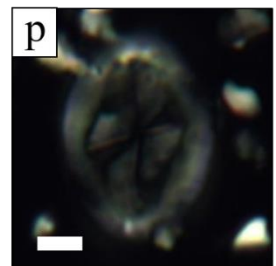
Broinsonia sp. (I)
MS1



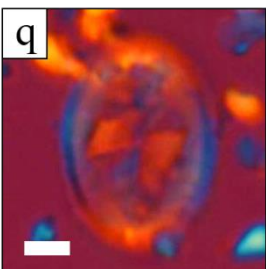
Broinsonia sp. (I)
MS1



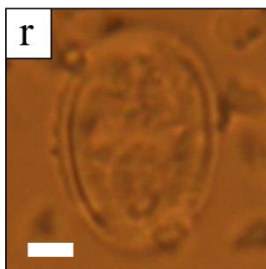
Broinsonia sp. (I)
MS1



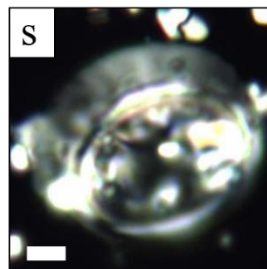
G. obliquum (I)
K1



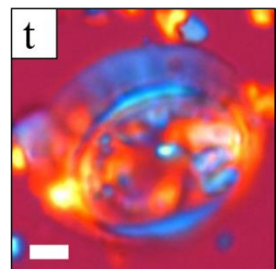
G. obliquum (I)
K1



G. obliquum (I)
K1

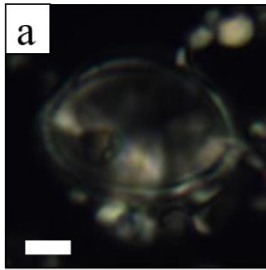


K. magnificus (I)
A5

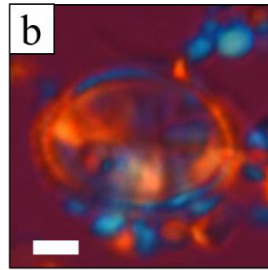


K. magnificus (I)
A5

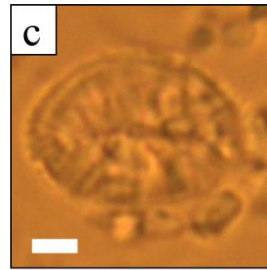
Plate II (white scale bar = 2 μ m)



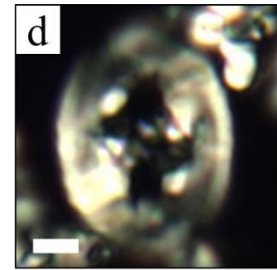
K. magnificus (II)
MT1



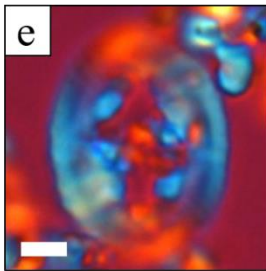
K. magnificus (II)
MT1



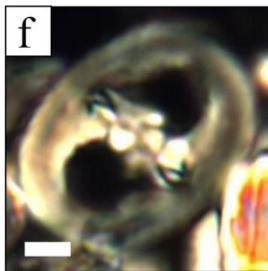
K. magnificus (II)
MT1



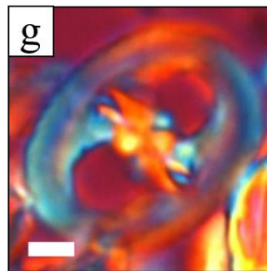
R. anthophorus (I)
MON1



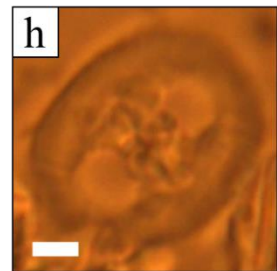
R. anthophorus (I)
MON1



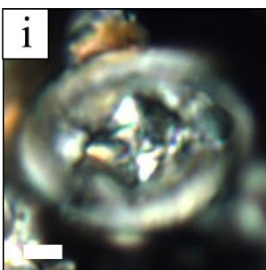
R. anthophorus? (II)
MOV1



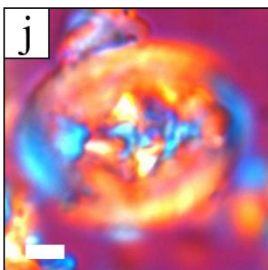
R. anthophorus? (II)
MOV1



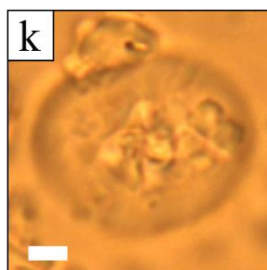
R. anthophorus? (II)
MOV1



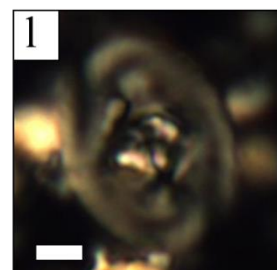
R. levis (I)
MS1



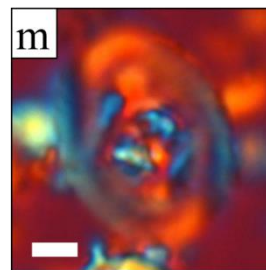
R. levis (I)
MS1



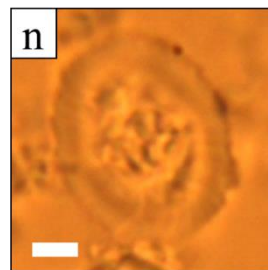
R. levis (I)
MS1



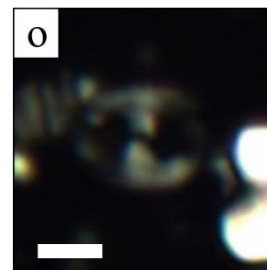
R. levis (II)
SK1



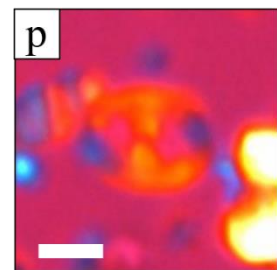
R. levis (II)
SK1



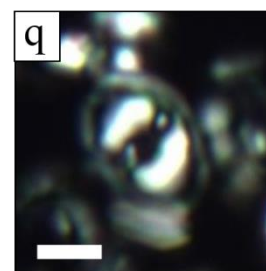
R. levis (II)
SK1



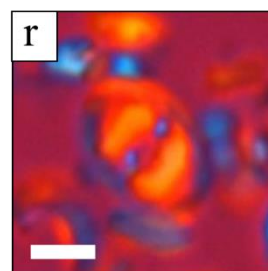
T. gabalus (I)
A5



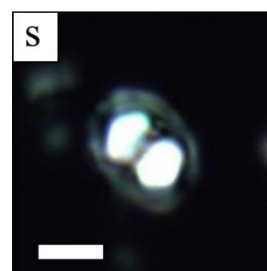
T. gabalus (I)
A5



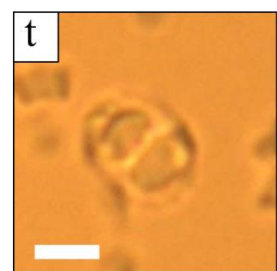
T. minimus (I)
MOV1



T. minimus (I)
MOV1

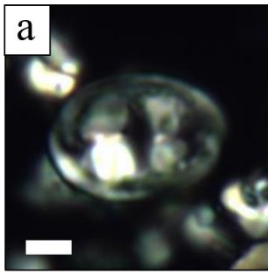


T. minimus (II)
MS1

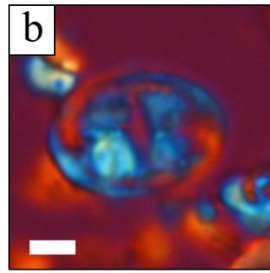


T. minimus (II)
MS1

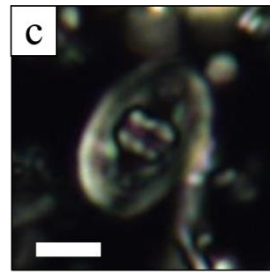
Plate III (white scale bar = 2 μ m)



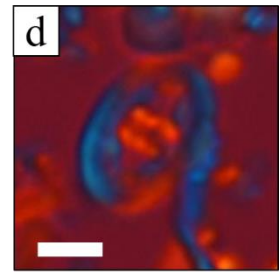
T. orionatus (I)
MS1



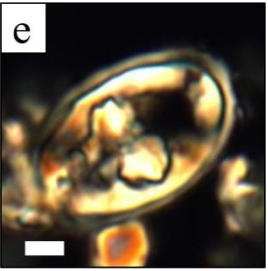
T. orionatus (I)
MS1



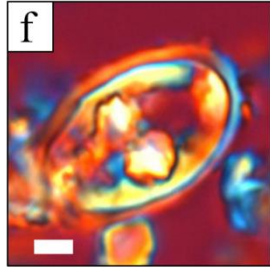
Z. birescenticus (I)
MOV1



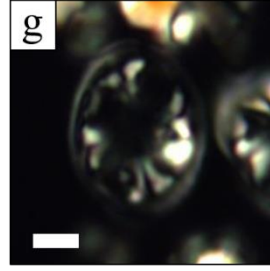
Z. birescenticus (I)
MOV1



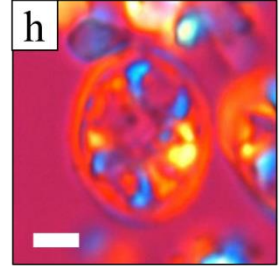
Z. embergeri (I)
K5



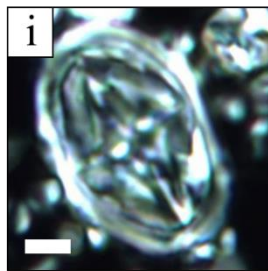
Z. embergeri (I)
K5



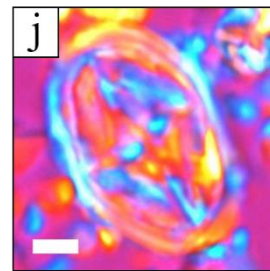
A. octoradiata (I)
A5



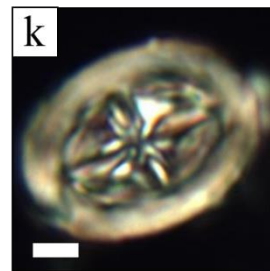
A. octoradiata (I)
A5



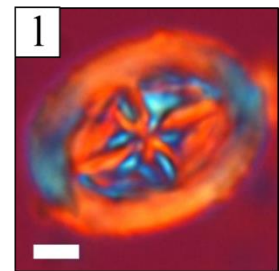
M. pleniporus (I)
MS1



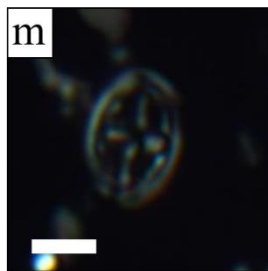
M. pleniporus (I)
MS1



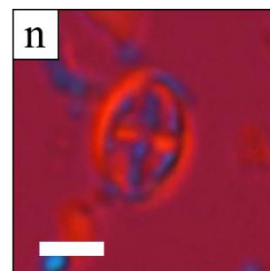
N. watkinsii (I)
L5



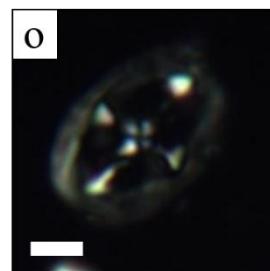
N. watkinsii (I)
L5



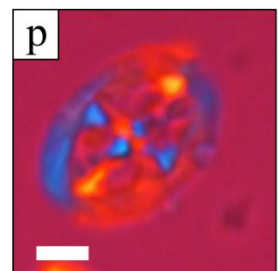
S. stradneri (I)
K1



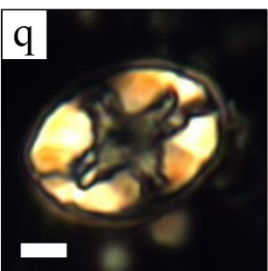
S. stradneri (I)
K1



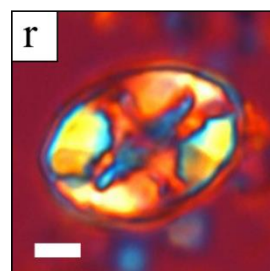
Staurolithites sp. (I)
A5



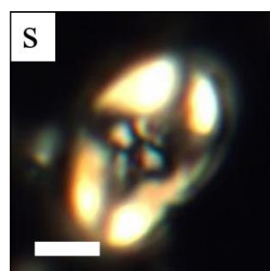
Staurolithites sp. (I)
A5



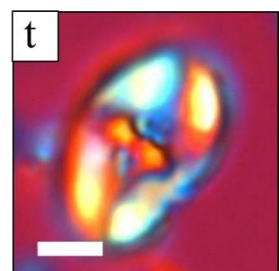
E. eximius (I)
MOV1



E. eximius (I)
MOV1

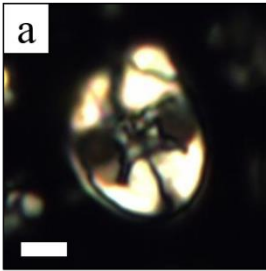


E. lindiensis (I)
MOV1

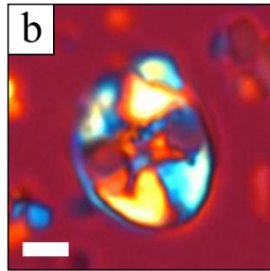


E. lindiensis (I)
MOV1

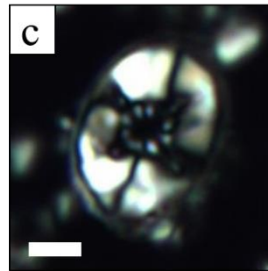
Plate IV (white scale bar = 2 μ m)



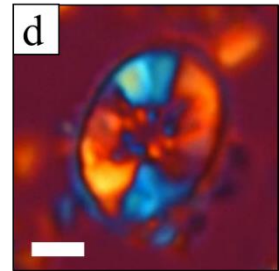
E. gorkae (I)
A5



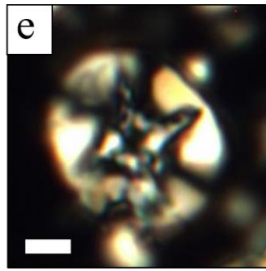
E. gorkae (I)
A5



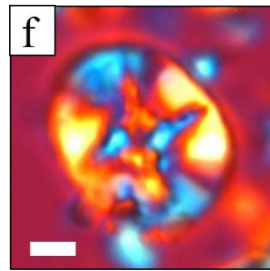
E. parallelus (I)
MS1



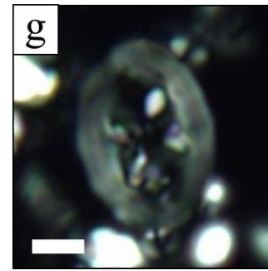
E. parallelus (I)
MS1



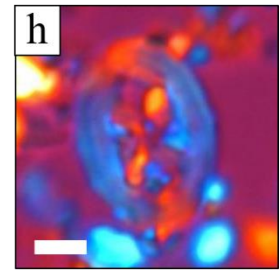
E. turriseiffelii (I)
MOV1



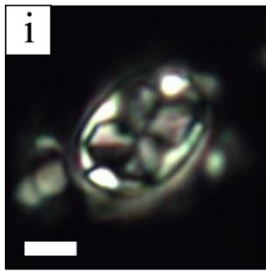
E. turriseiffelii (I)
MOV1



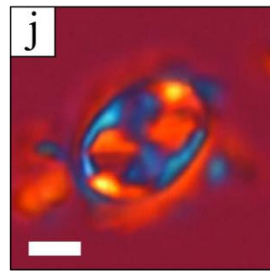
H. anceps (I)
MS1



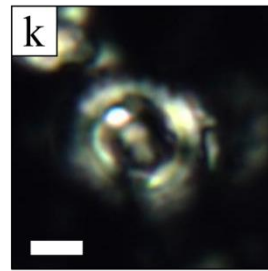
H. anceps (I)
MS1



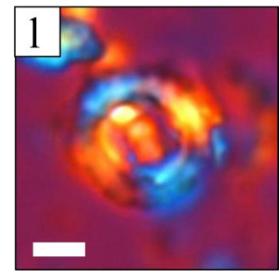
H. trabeculatus (I)
K5



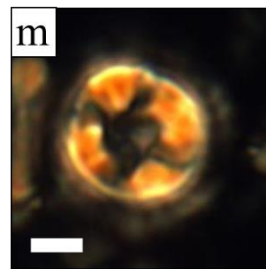
H. trabeculatus (I)
K5



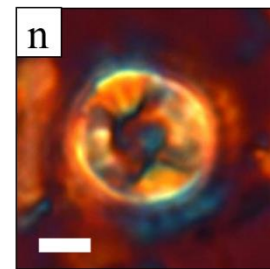
R. crenulatus (I)
MS1



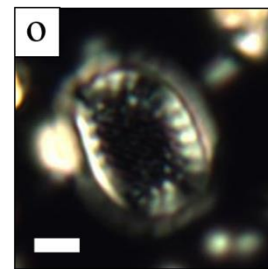
R. crenulatus (I)
MS1



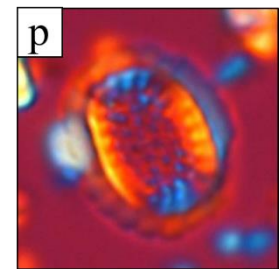
Cylindralithus sp. (I)
MOV1



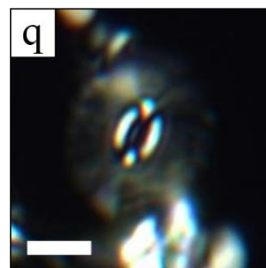
Cylindralithus sp. (I)
MOV1



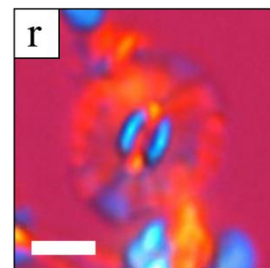
C. ehrenbergii (I)
A5



C. ehrenbergii (I)
A5



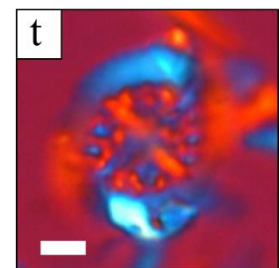
B. constans (I)
MOV1



B. constans (I)
MOV1

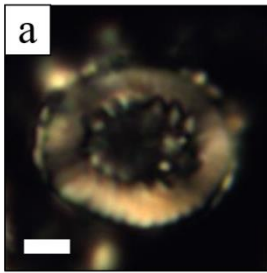


C. conicus (I)
MOV1

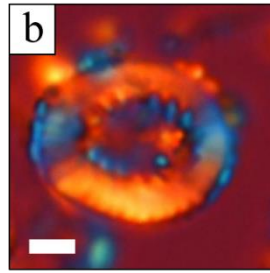


C. conicus (I)
MOV1

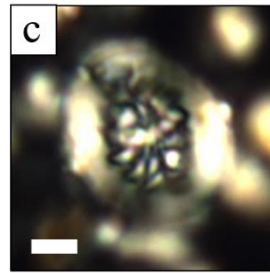
Plate V (white scale bar = 2 μ m)



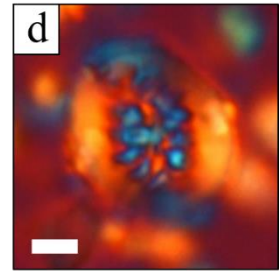
R. surirella (I)
MON1



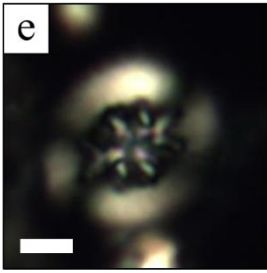
R. surirella (I)
MON1



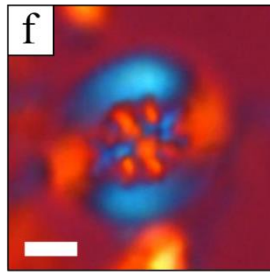
R. cremulata (I)
MON1



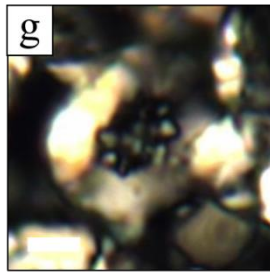
R. cremulata (I)
MON1



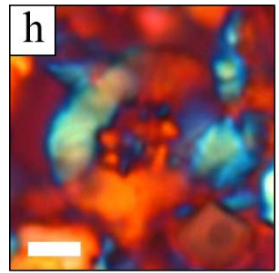
R. angustiforata (I)
MOV1



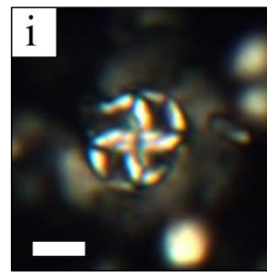
R. angustiforata (I)
MOV1



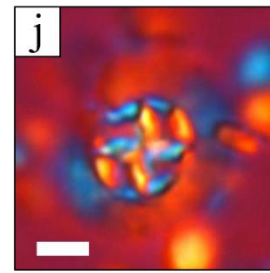
R. ficula (I)
K5



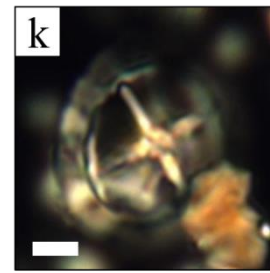
R. ficula (I)
K5



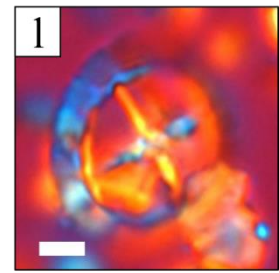
P. cretacea (I)
MOV1



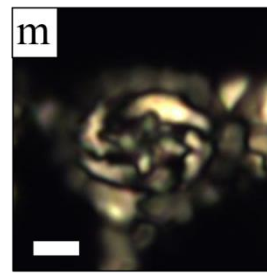
P. cretacea (I)
MOV1



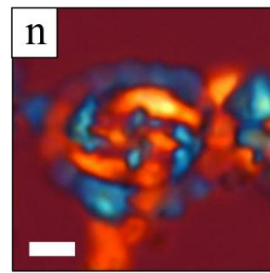
P. desidero grandis (I)
MOV1



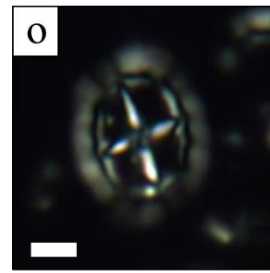
P. desidero grandis (I)
MOV1



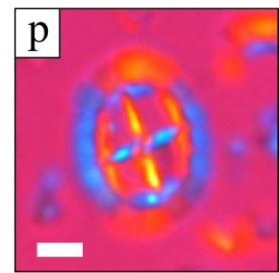
P. arkhangelskyi (I)
MON1



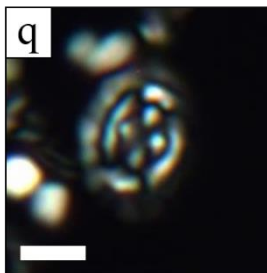
P. arkhangelskyi (I)
MON1



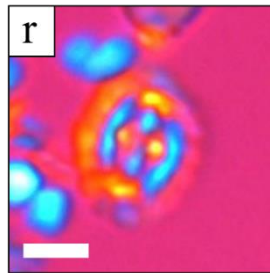
P. spinosa (I)
A5



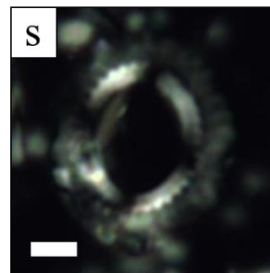
P. spinosa (I)
A5



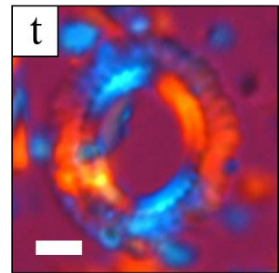
P. stoveri (I)
A5



P. stoveri (I)
A5

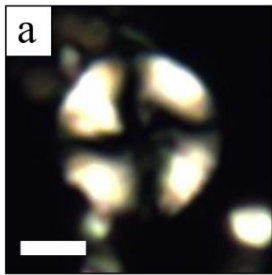


M. pemmatoidea (I)
MS1

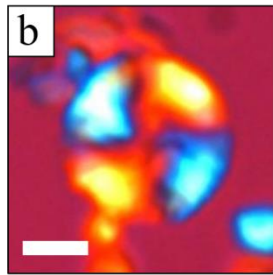


M. pemmatoidea (I)
MS1

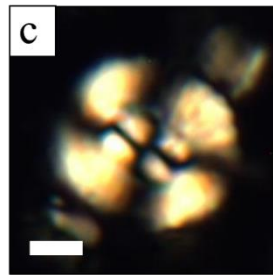
Plate VI (white scale bar = 2 μ m)



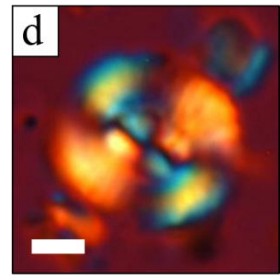
C. margerelii (I)
A5



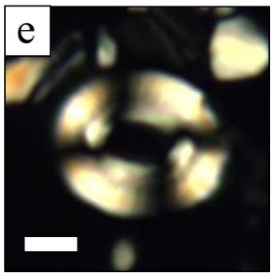
C. margerelii (I)
A5



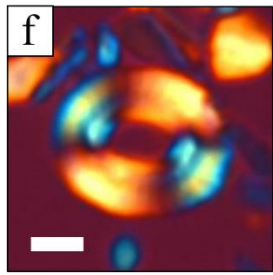
W. barnesia (I)
K5



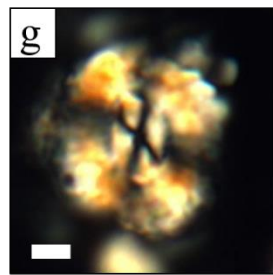
W. barnesia (I)
A5



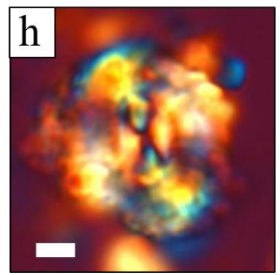
W. fossacineta (I)
MT1



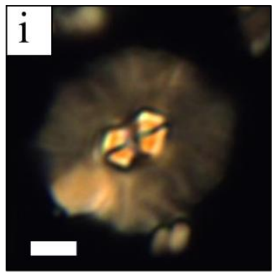
W. fossacineta (I)
MT1



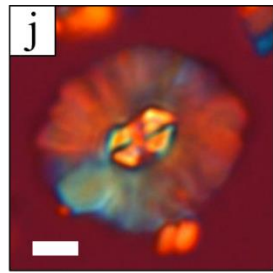
W. manivitia (I)
MS1



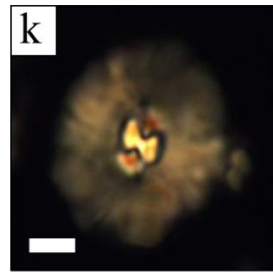
W. manivitia (I)
MS1



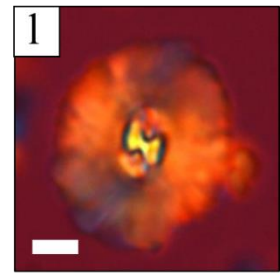
M. inversus (I)
MON1



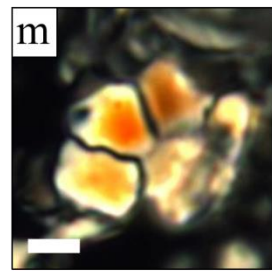
M. inversus (I)
MON1



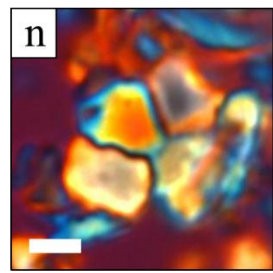
M. inversus (II)
MON1



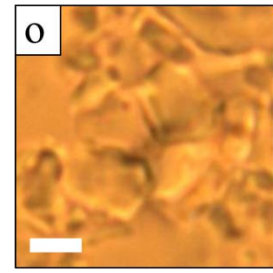
M. inversus (II)
MON1



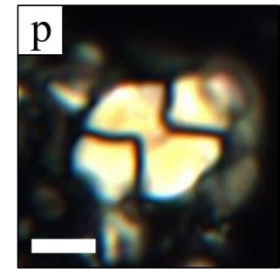
C. obscurus (I)
MT1



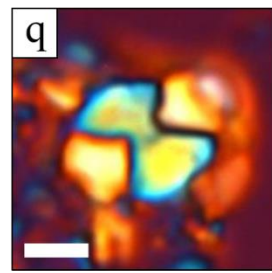
C. obscurus (I)
MT1



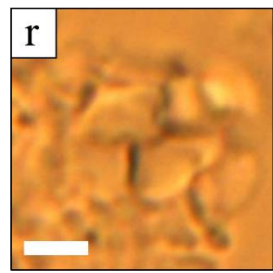
C. obscurus (I)
MT1



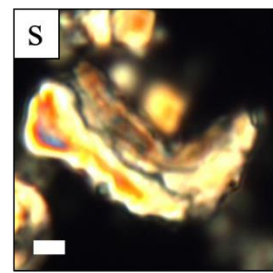
C. obscurus (II)
MT1



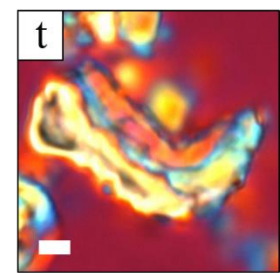
C. obscurus (II)
MT1



C. obscurus (II)
MT1

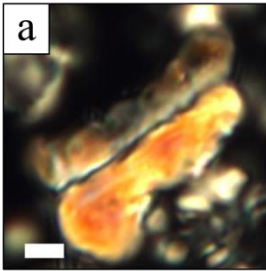


L. arcuatus (I)
L5

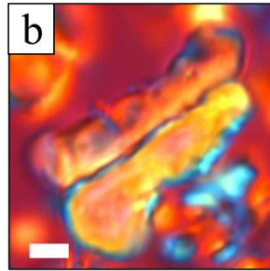


L. arcuatus (I)
L5

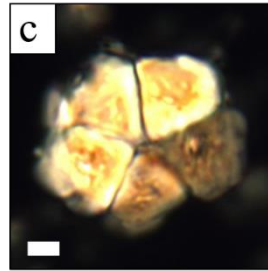
Plate VII (white scale bar = 2 μ m)



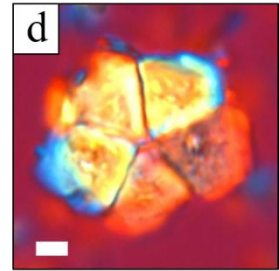
Lucianorhabdus sp. (I)
MOV1



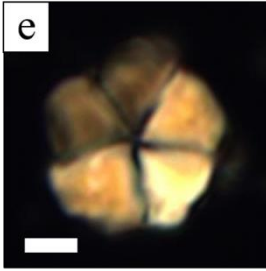
Lucianorhabdus sp. (I)
MOV1



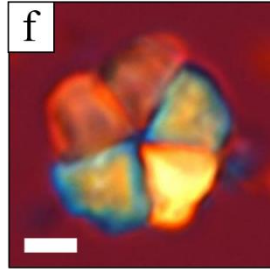
B. bigelowii (I)
MOV1



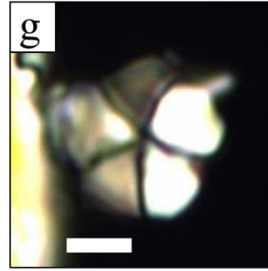
B. bigelowii (I)
MOV1



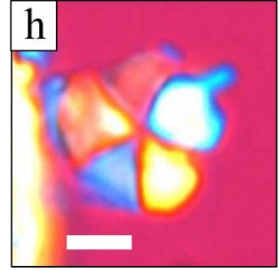
B. bigelowii small (I)
A5



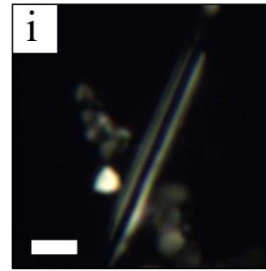
B. bigelowii small (I)
A5



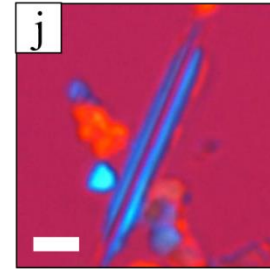
B. bigelowii small (II)
L5



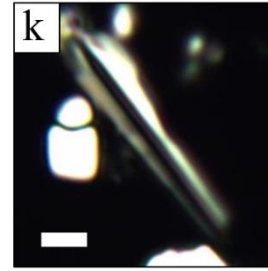
B. bigelowii small (II)
L5



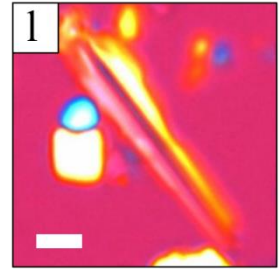
L. carniolensis (I)
K5



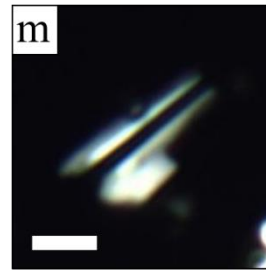
L. carniolensis (I)
K5



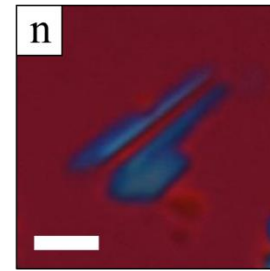
Lithraphidites sp. (I)
A5



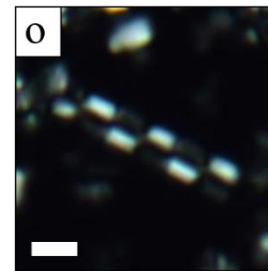
Lithraphidites sp. (I)
A5



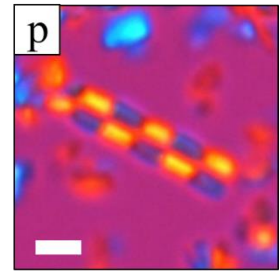
Lithraphidites sp. (II)
A5



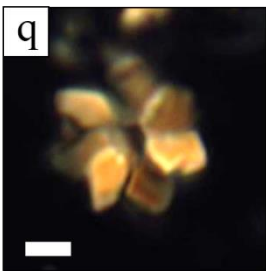
Lithraphidites sp. (II)
A5



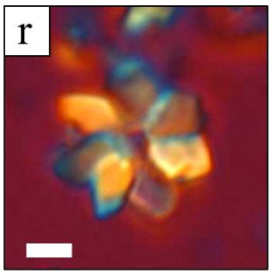
M. decoratus (I)
MS1



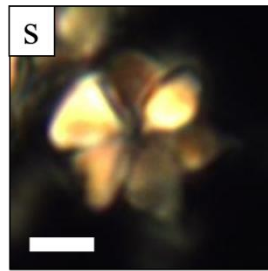
M. decoratus (I)
MS1



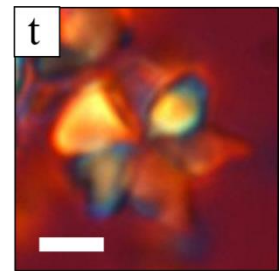
E. moratus (I)
K1



E. moratus (I)
K1

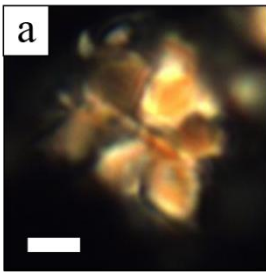


L. grillii (I)
MOV1

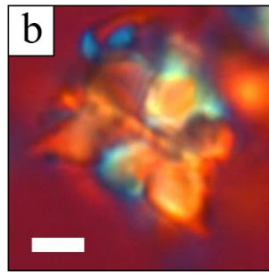


L. grillii (I)
MOV1

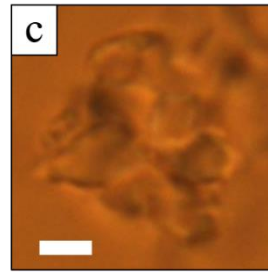
Plate VIII (white scale bar = 2 μm)



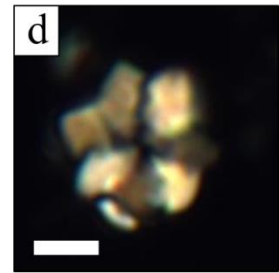
L. grillii side view? (II)
MOV1



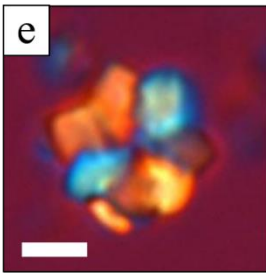
L. grillii side view? (II)
MOV1



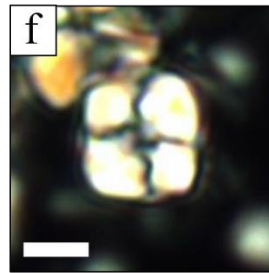
L. grillii side view? (II)
MOV1



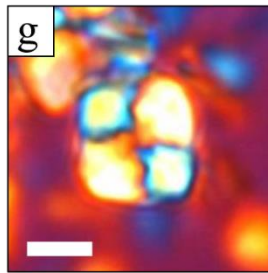
L. septenarius (I)
K1



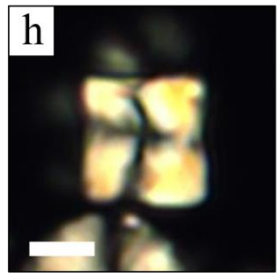
L. septenarius (I)
K1



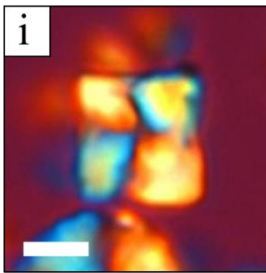
Q. gartneri (I)
MS1



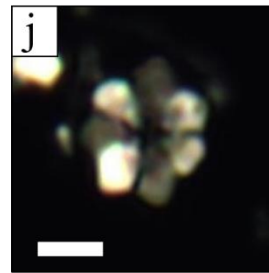
Q. gartneri (I)
MS1



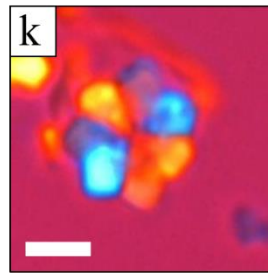
Q. gartneri (II)
K1



Q. gartneri (II)
K1



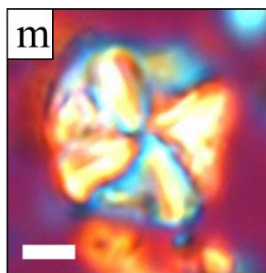
Q. eptabrachium (I)
K5



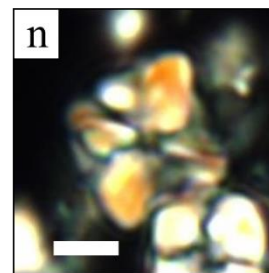
Q. eptabrachium (I)
K5



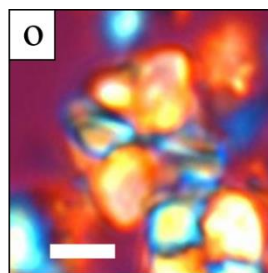
M. staurophora (I)
MS1



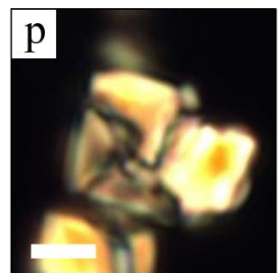
M. staurophora (I)
MS1



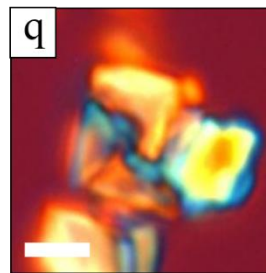
M. staurophora (II)
MS1



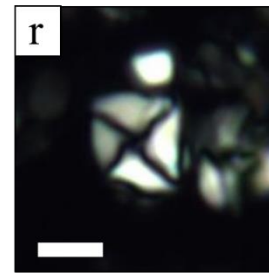
M. staurophora (II)
MS1



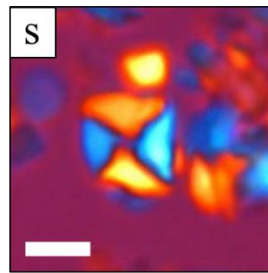
Micula sp. (I)
TOR13



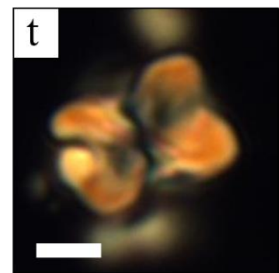
Micula sp. (I)
TOR13



Micula sp. (II)
MS1

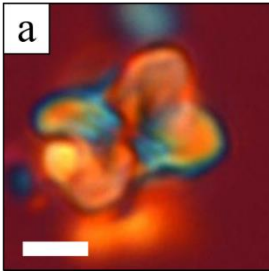


Micula sp. (II)
MS1

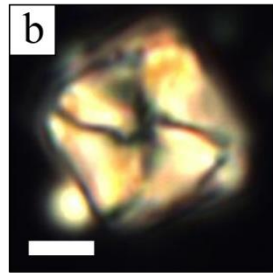


Micula sp. (III)
A5

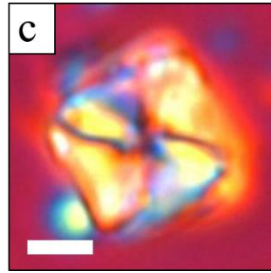
Plate IX (white scale bar = 2 μm)



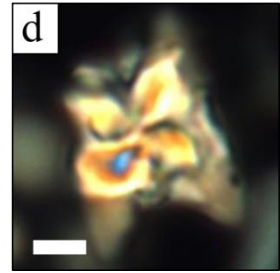
Micula sp. (III)
A5



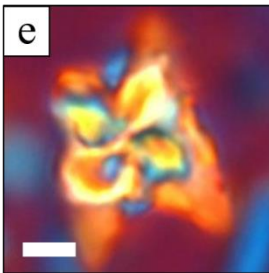
Micula sp. (IV)
A5



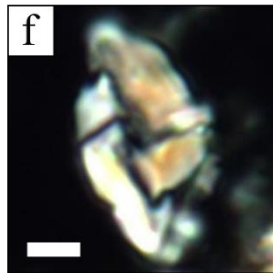
Micula sp. (IV)
A5



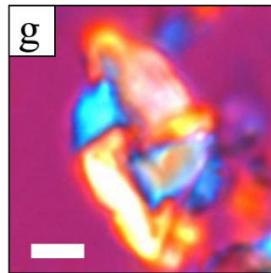
Micula sp. (V)
MS1



Micula sp. (V)
MS1



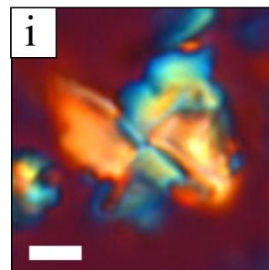
Micula sp. (VI)
MS1



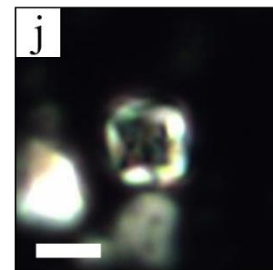
Micula sp. (VI)
MS1



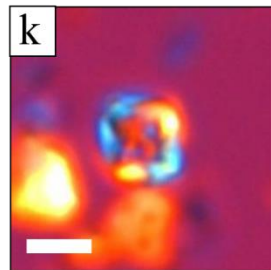
Micula sp. (VII)
MS1



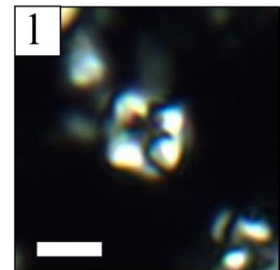
Micula sp. (VII)
MS1



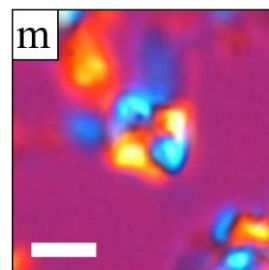
Micula sp. small (I)
MS1



Micula sp. small (I)
MS1

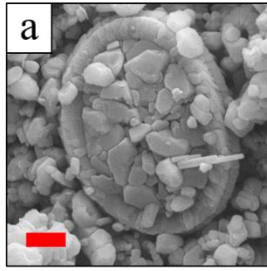


Micula sp. small (II)
MS1

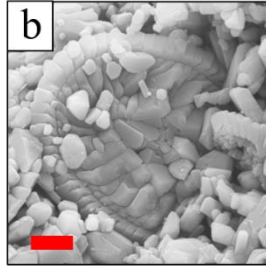


Micula sp. small (II)
MS1

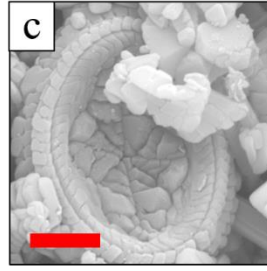
Plate X (red scale bar = 2 μm)



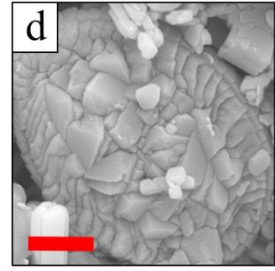
A. cymbiformis (I)
MON1



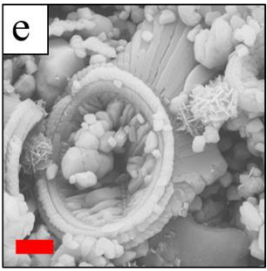
A. p. constrictus? (I)
MT1



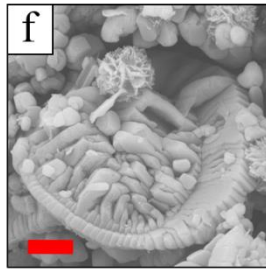
G. obliquum (I)
K1, proximal view



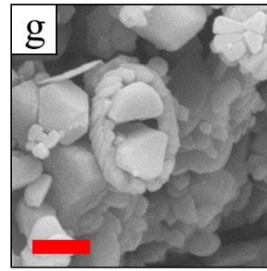
G. obliquum (II)
K1, distal view



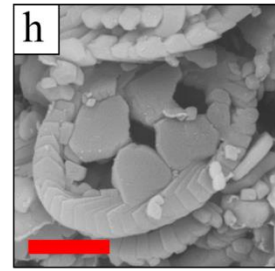
K. magnificus (I)
A1, proximal view



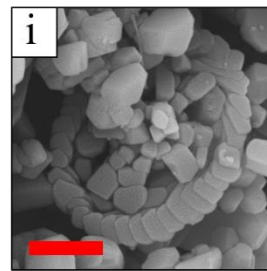
K. magnificus (II)
A1, distal view



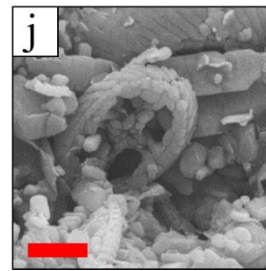
T. minimus (I)
MON1



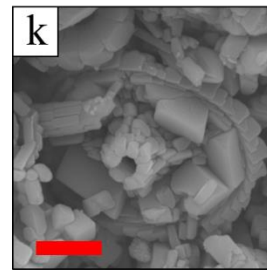
T. orionatus (I)
MOV5



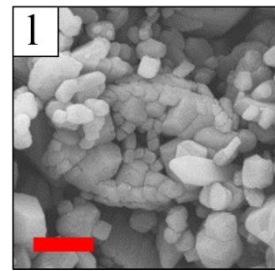
A. octoradiata (I)
SK5



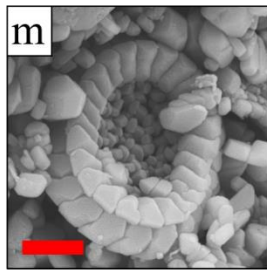
S. stradneri (I)
MOV1



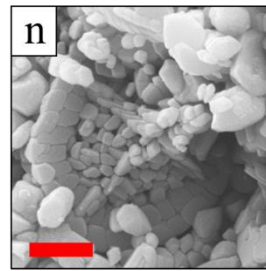
E. eximius? (I)
K1



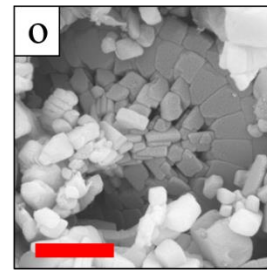
E. gorkae (I)
MT1



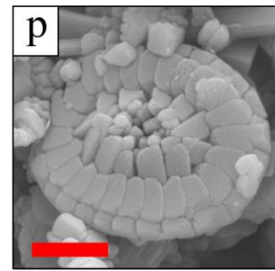
C. ehrenbergii (I)
SK5



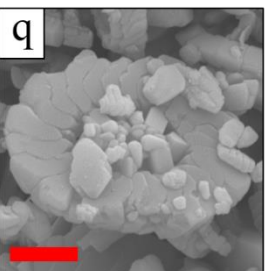
C. conicus (I)
MON1



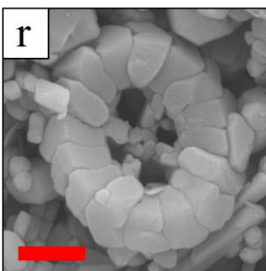
R. surirella? (I)
K1



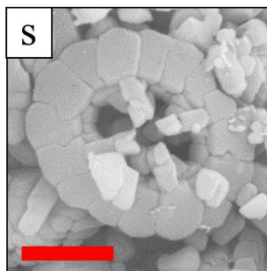
R. crenulata (I)
K1



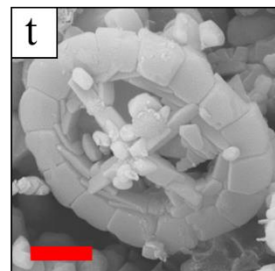
R. ficula? (I)
K1



P. cretacea (I)
SK1, proximal view

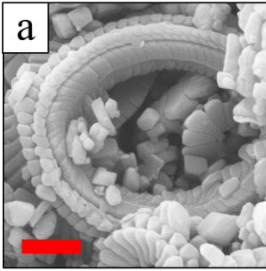


P. cretacea (II)
L1, distal view

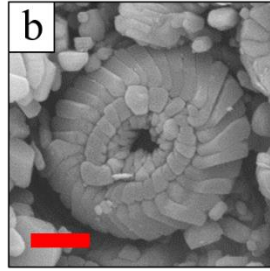


P. spinosa (I)
A1

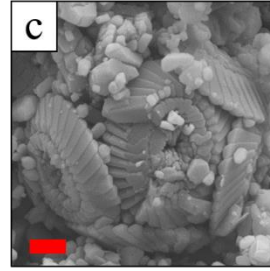
Plate XI (red scale bar = 2 μm)



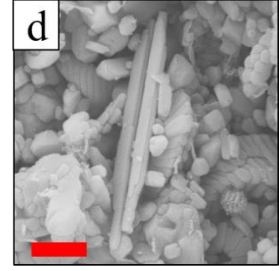
M. pemmatoidea (I)
MON1



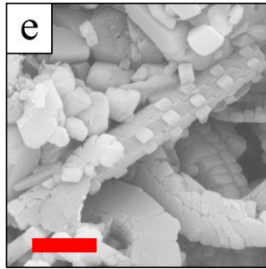
W. barnesiae (I)
MON1



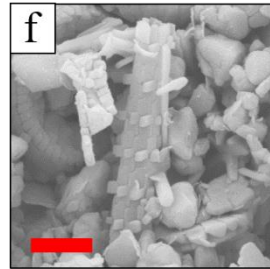
W. barnesiae (II)
MT1, coccosphere



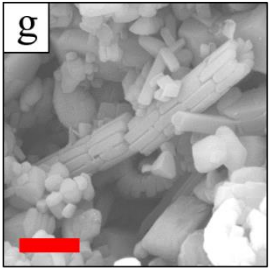
L. carniolensis (I)
L1



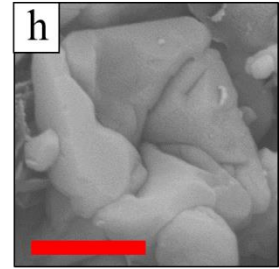
M. belgicus (I)
K1



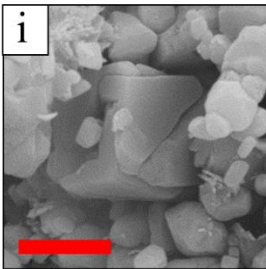
M. belgicus (II)
MOV1



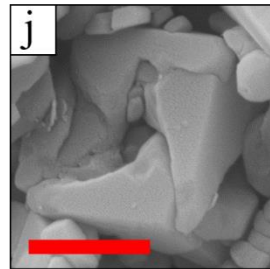
M. decoratus (I)
MON1



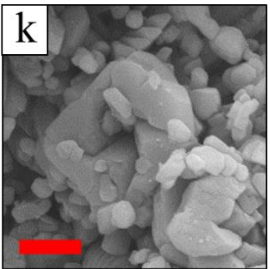
M. staurophora (I)
A1



M. staurophora (II)
A1

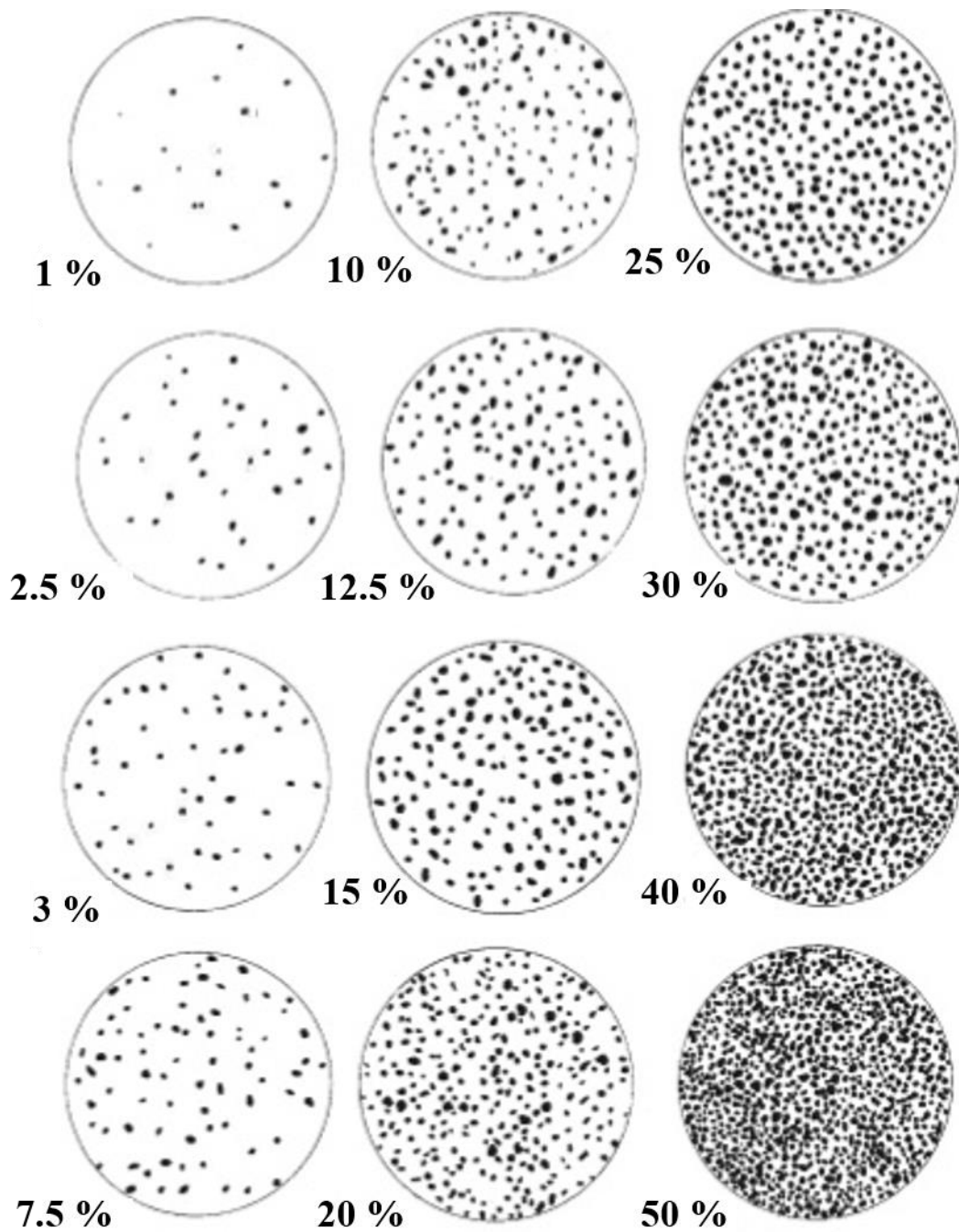


Micula sp. large (I)
MS1



Micula sp. large (II)
MON1

9.5. Appendix 5: Percentage Estimation chart



Appendix 5: Percentage estimation chart from Baccelle and Bosellini (1965).

9.7. Appendix 7: Calcareous Nannofossil Assemblages, Species and Genera in % of Total Count

Sample ID	<i>Watznaueria barnesiae</i>	<i>Biscutum constans</i>	<i>Eiffelithus</i> sp.	<i>Lithraphidites</i> sp.	<i>Lucianorhabdus</i> sp.	<i>Predicocapsa</i> sp.	<i>Helicolithus</i> sp.	<i>Tranolithus orionatus</i>	<i>Cibrosphaerella ebnbergii</i>	<i>Microhabdulus decoratus</i>	<i>Abnuelletta octoradiata</i>	<i>Kampanerius magnificus</i>	<i>Micula</i> sp.	<i>Micula</i> sp. small	<i>Micula stauropora</i>	<i>Calcutites obscurus</i>	<i>Reinhardtites levis</i>	<i>ArKhangei/skielela maastrichtensis</i>	# total count [n]	% <i>Watznaueria barnesiae</i>	% <i>Biscutum constans</i>	% <i>Eiffelithus</i> sp.	% <i>Lithraphidites</i> sp.	% <i>Lucianorhabdus</i> sp.	% <i>Predicocapsa</i> sp.	% <i>Helicolithus</i> sp.	% <i>Tranolithus orionatus</i>	% <i>Cibrosphaerella ebnbergii</i>	% <i>Microhabdulus decoratus</i>	% <i>Abnuelletta octoradiata</i>	% <i>Kampanerius magnificus</i>	% <i>Micula</i> sp.	% <i>Micula stauropora</i>	% <i>Calcutites obscurus</i>	% <i>Reinhardtites levis</i>	% <i>ArKhangei/skielela maastrichtensis</i>	Sample ID	
TOR15	2	3	0	0	0	0	0	0	0	0	0	0	0	0	28	35	177	1	46	300	14.3	21.4	0	0	0	0	0	0	0	0	0	0	21.4	7.14	21.4	0	7.14	TOR15
TOR14	4	0	0	0	2	2	0	0	1	0	0	0	0	0	28	35	177	1	46	300	1.33	0	0	0	0.67	0.67	0	0	0.33	0	0	0	80	59	0.33	0	15.3	TOR14
TOR13	7	3	0	2	26	12	0	0	0	0	1	15	41	137	4	51	301	2.33	0	1	0	0.66	8.64	3.99	0	0	0	0	0.33	64.1	45.5	1.33	0	16.9	TOR13			
TOR12	3	0	0	0	5	1	0	0	0	0	0	10	31	75	1	23	156	1.92	0	0	0	3.21	0.64	0	0	0	0	0	0.64	74.4	48.1	0.64	0	14.7	TOR12			
TOR11	6	0	0	0	7	1	0	0	1	0	0	6	29	71	1	12	137	4.38	0	0	0	5.11	0.73	0	0.73	0	0	1.46	77.4	51.8	0.73	0	8.76	TOR11				
TOR10	6	3	0	22	25	4	0	0	1	0	6	25	26	51	5	117	300	2	1	0	7.33	0	8.33	1.33	0	0	0.33	0	2	34	17	1.67	0	39	TOR10			
TOR9	0	0	0	8	1	0	0	0	0	0	0	9	1	5	4	17	47	0	0	0	17	0	2.13	0	0	0	0	0	0	31.9	10.6	8.51	0	36.2	TOR9			
TOR8	0	16	5	29	2	0	0	0	1	0	4	16	9	10	8	90	192	0	0	0	8.33	2.6	15.1	1.04	0	0.52	0	2.08	18.2	5.21	4.17	0	46.9	TOR8				
TOR7	5	2	16	7	9	4	0	0	0	0	2	15	7	14	10	60	153	3.27	0	1.31	10.3	4.58	5.88	2.61	0	0	0	1.31	23.3	9.15	6.54	0	39.2	TOR7				
TOR6	3	0	0	88	22	17	3	0	1	0	6	22	11	11	15	87	300	1	0	0	29.3	7.33	5.67	1	0	0.33	0	0	2	14.7	3.67	5	0	29	TOR6			
TOR5	0	32	19	8	1	1	0	0	0	0	7	67	15	24	10	90	276	0	0	0	11.6	6.88	2.9	0.36	0	0.36	0	2.54	38.4	8.7	3.62	0	32.6	TOR5				
TOR4	2	2	0	68	23	36	4	2	2	0	11	13	8	13	14	94	300	0.67	0.67	0	22.7	7.67	12	1.33	0	0.67	0	3.67	11.3	4.33	4.67	0	31.3	TOR4				
TOR3	1	1	0	163	11	10	1	0	0	0	4	3	3	7	16	76	300	0.33	0.33	0	54.3	3.67	3.33	0.33	0	0.33	0	1.33	4.33	2.33	5.33	0	25.3	TOR3				
TOR2	11	2	0	115	11	14	1	0	1	0	9	20	5	29	13	62	300	3.67	0.67	0	38.3	3.67	4.67	0.33	0	0.33	0	3	18	9.67	4.33	0	20.7	TOR2				
TOR1	1	0	4	1	1	0	0	0	1	0	15	6	8	5	6	54	1.85	0	0	7.41	1.85	1.85	0	0	1.85	0	0	53.7	14.8	9.26	0	11.1	TOR1					
A1	4	15	21	125	12	0	0	0	14	6	9	7	13	45	1	305	1.31	0	4.92	6.89	0	41	3.93	0	4.59	1.97	2.95	2.3	19	14.8	0.33	0	0	A1				
A5	1	13	37	1	112	6	0	0	13	14	16	14	6	36	0	303	0.33	0	4.29	12.2	0.33	37	1.98	0	4.29	4.62	5.28	4.62	13.9	11.9	0	0	0	A5				
MS1	80	24	10	10	4	59	2	3	1	5	6	0	14	40	20	10	313	25.6	7.67	3.19	3.19	1.28	18.8	0.64	0.96	0.32	1.6	1.92	0	17.3	12.8	6.98	3.19	0	MS1			
M55	57	15	12	4	12	52	1	3	3	7	1	0	2	71	21	7	301	18.9	4.98	3.99	1.33	3.99	17.3	0.33	1	0	1	2.33	0.33	24.3	33.6	6.98	2.33	0	M55			
MS average																		22.2	6.33	3.59	2.26	2.63	18.1	0.49	0.98	0.16	1.3	2.12	0.17	20.8	18.2	6.68	2.76	0	MS average			
SK1	136	12	12	1	4	22	8	1	1	7	5	0	3	17	21	10	302	45	3.97	3.97	0.33	1.32	7.28	2.65	0.33	0.33	2.32	1.66	0	6.62	5.63	6.95	3.31	0	SK1			
SK5	108	14	12	0	7	13	6	3	1	18	2	3	1	4	21	15	302	35.8	4.64	3.97	0	2.32	4.3	1.99	0.99	0.33	5.96	0.66	0.99	8.61	6.95	6.95	4.97	0	SK5			
SK average																		40.4	4.3	3.97	0.17	1.82	5.79	2.32	0.66	0.33	4.14	1.16	0.5	7.62	6.29	6.95	4.14	0	SK average			
MT1	131	33	3	12	2	25	1	0	1	8	6	0	2	13	32	6	308	42.5	10.7	0.97	3.9	0.65	8.12	0.32	0	0.32	2.6	1.95	0	4.87	4.22	10.4	1.95	0	MT1			
MT5	104	35	3	10	8	40	2	1	1	6	3	1	4	17	27	3	303	34.3	11.6	0.99	3.3	2.64	13.2	0.66	0.33	0.33	1.98	0.99	0.33	6.93	5.61	8.91	0.99	0	MT5			
MT average																		38.4	11.1	0.98	3.6	1.64	10.7	0.49	0.17	0.33	2.29	1.47	0.17	5.9	4.92	9.65	1.47	0	MT average			
MON1	66	13	5	8	14	43	2	0	2	7	7	1	1	5	41	36	13	302	21.9	4.3	1.66	2.65	4.64	14.2	0.66	0	0.66	2.32	2.32	0.33	15.6	13.6	11.9	4.3	0	MON1		
MON5	66	22	14	9	7	56	1	2	3	7	7	0	6	26	34	13	305	21.6	7.21	4.59	2.95	2.3	18.4	0.33	0.66	0.98	2.3	2.3	0	10.5	8.52	11.1	4.26	0	MON5			
MON average																		21.7	5.76	3.12	2.8	3.47	16.3	0.5	0.33	0.82	2.31	2.31	0.17	13	11.1	11.5	4.28	0	MON average			
L1	96	21	13	3	14	31	3	0	2	0	3	1	6	29	34	22	311	30.9	6.75	4.18	0.96	4.5	9.97	0.96	0	0.64	0	0.96	0.32	11.3	9.32	10.9	7.07	0	L1			
L5	65	17	13	4	17	37	2	2	2	0	6	3	4	47	35	17	305	21.3	5.57	4.26	1.31	5.57	12.1	0.66	0.66	0.66	0	1.97	0.98	16.7	15.4	11.5	5.57	0	L5			
L average																		26.1	6.16	4.22	1.14	5.04	11	0.81	0.33	0.65	0	1.47	0.65	14	12.4	11.2	6.32	0	L average			
MOV1	63	16	12	28	68	3	25	5	8	11	0	0	0	4	4	0	301	20.9	5.32	3.99	9.3	0	22.6	1	8.31	1.66	2.66	3.65	0	1.33	1.33	1.33	0	0	MOV1			
MOV5	74	17	10	13	6	72	2	18	11	6	14	4	2	5	4	0	300	24.7	5.67	3.33	4.33	2	24	0.67	6	3.67	2	4.67	1.33	2.33	1.67	1.33	0	0	MOV5			
MOV average																		22.8	5.49	3.66	6.82	1	23.3	0.83	7.15	2.66	2.33	4.16	0.67	1.83	1.5	1.33	0	0	MOV average			
K1	115	2	45	2	43	21	30	2	2	2	1	0	1	1	0	0	307	37.5	0.65	14.7	0.65	0	14	6.84	9.77	0.65	0.65	0.65	0.33	0.33	0.33	0	0	0	K1			
K5	116	0	38	3	45	29	38	1	1	0	0	0	1	3	0	0	318	36.5	0	11.9	0.94	0	14.2	9.12	11.9	0.31	0.31	0	0	0.31	0	0.94	0	0	K5			
K average																		37	0.3	13	0.8	0	14	8	11	0.5	0.5	0.3	0.2	0.3	0.2	0.6	0	0	K average			

Appendix 7: Calcareous nannofossil assemblages, species and genera in % of total count.